Autophagy's Roles in the Activation and Ageing of CD4+ T Cells



Dingxi Zhou

Wolfson College

University of Oxford

Thesis submitted for the degree of

Doctor of Philosophy

Hilary 2022

Abstract

Autophagy plays an essential role in the differentiation, homeostasis and renewal of various cell types. Though its molecular machinery has been extensively elucidated, what autophagy specifically degrades remains largely unclear. Here, we created the *Lc3b-APEX2* transgenic mouse model based on the proximity biotinylation technique, which, for the first time, enables us to directly map the proteinaceous content of autophagosomes in any primary cell. Through inserting APEX2, an engineered ascorbate peroxidase, into the endogenous LC3B allele, proteins residing in the autophagosomes can be specifically labelled with biotin and easily purified. After the systemic validation of the mouse model, next, I utilised it to explore the molecular mechanism of why CD4+ T cells, which orchestrate both humoral and cytotoxic immune responses, rely on autophagy to expand when facing antigen-stimuli. We discovered the interleukin-7 receptor alpha (IL-7Rα) as one of the autophagosomal candidates in proliferating CD4+ T cells. Mechanistically, we confirmed that excessive surface IL-7R sequestrate the common gamma chain, impairing the IL-2R assembly and downstream signalling crucial for T cell proliferation. Moreover, we investigated how CD4+ T cells from aged mice, which mimic some of the phenotypes of autophagy-deficient CD4+ T cells, also show several unique changes related to cellular ageing. This study provides proof of principle that key autophagy substrates can be reliably identified with this model to help mechanistically unravel autophagy's contribution to healthy physiology and disease.

Declaration

This thesis is submitted to the University of Oxford in support of my application for the degree of Doctor of Philosophy. The work described herein was performed when I was a graduate student at the Kennedy Institute of Rheumatology, under the supervision of Professor Katja Simon and Dr Luke Jostins. All the work presented in this thesis is the result of my own work unless otherwise stated. No part of my thesis has been accepted or is currently being under submitted for any degree, diploma or certificate or other qualification in the University of Oxford or elsewhere.

Author's Publications

Zhou, D., Borsa, M., & Simon, A. K. (2021). Hallmarks and detection techniques of cellular senescence and cellular ageing in immune cells. *Aging Cell*, *20*(2), e13316.

Zhou, D., Borsa, M., Puleston, D. J., Zellner, S., Capera, J., Sanderson, S., Jostins, L., Behrends, C., Alsaleh, G. & Simon, A. K. (2021). Mapping of the autophagosomal degradome identifies IL-7Rα as key cargo in proliferating CD4+ T-cells. *bioRxiv & in submission.*

Zhou, D., & Borsa, M. (2021). Sensing extracellular ATP boosts memory T cell commitment. *Nature Reviews Immunology*, *21*(8), 473-473.

Acknowledgements

"A day as a teacher, a lifetime as a parent." As this ancient Chinese proverb expresses, my supervisor Professor Katja Simon, not only set an encouraging example of how to be a great scientist and balanced individual but also share her priceless insights and wisdom of life with me. I learnt from her that our life is a challenge, and the only way to achieve success is to embrace uncertainty bravely and the perseverance to give 'another try' after failure. Her steadfast support, and trust in my ability to finish something more than I expected possible, enabled me to cherish my time of life here and pursue new ideas and goals freely every single day. I would like to thank Katja for her boundless generosity, patience, inspiration and care, without which I could not have been where I am right now and made this thesis possible.

A single thread can't make a cord, nor a single tree a forest. I wish to acknowledge all my excellent lab mates, either current or previous ones, for their generous help in my experiment and thesis writing. Particularly, my project could not have been proceeding to where it is right now without the support from Ghada Alsaleh and Mariana Borsa. Xin Ge is a talented student who inspired me to reflect on how to find proper ways to guide others to achieve. I would like to thank Hanlin Zhang, Felix Richter, Houfu Leng, Ana Victoria Lechuga-Vieco, Naj Brown, Klara Piletic, Lin Luo, Tom Riffelmacher, Cristina Dumitru, Sandrine Obba, Alexander Clarke, Daniel Puleston and Sharon Sanderson.

I am particularly thankful to my co-supervisor, Dr Luke Jostins-Dean, and my thesis committee members Professor Alison Simons, Professor Pedro Carvalho and Professor Audrey Gérard, as well as Sir Andrew McMichael, Professor Michael Dustin, Professor Mark Coles, Professor Alex Bullock, Professor Benedikt Kessler, Professor Christian Behrends, Professor

Christopher Goodnow and Professor Roman Fischer, for willing to share their expertise and valuable advice to help my project advance.

I also would like to thank my bosom friends who bring me familiarity in this foreign land. They supported me all along my journey of PhD and encouraged me to overcome various difficulties in my study and life, especially Carl Lee, Jia-Ling Ruan and Zixi Yin, who offered me a great amount of help in both my research and life. My genuine thanks also go to Pengjun Xi, Yitao Zhu, Jingnu Xia, Haoyu Niu, Zihui Su, Jiahe Yang, Linyi Zhu, Guanchen Li, Zhuoyao Chen, Zhu Liang, Wenbo Wang, Fei Gao, Yuxin Mi, Xiaopeng Fu, Ke Zhao, Ying Zhang and Sizhe Lian for their assistance and enjoyable time we spent together.

I want to especially express my heartful appreciation to my parents and other family members, who offered me unconditional love and support all the time ever since I was a kid. Never could I have the opportunity to come to Oxford and finish my degree without them.

Finally, I want to thank the professional and efficient facilities of the Kennedy Institute of Rheumatology, Wolfson College, and other facilities in the university. The China Scholarship Council, the Kennedy Trust, and the UK SPINE are gratefully appreciated for their generous offer of living stipend and tuition fees, which enabled me to study in Oxford without any concern of financial issues.

List of Abbreviations

Abbreviation	Full name
4-OHT	4-hydroxytamoxifen
4EBP1	Eukaryotic translation initiation factor 4E-binding protein 1
8-oxoG	8-oxoguanine
AdH5-OVA	Adenovirus H5-ovalbumin
ADP	Adenosine diphosphate
AKT	Protein kinase B
AMBRA1	Activating molecule in Beclin1-regulated autophagy
AMP	Adenosine monophosphate
AMPK	AMP-activated protein kinase
ANXA7	Annexin A7
AP-1	Activator protein 1
APC	Antigen-presenting cell
APEX2	Engineered ascorbate peroxidase 2
ATG	Autophagy-related
ATP	Adenosine triphosphate
AUTAC	Autophagy-targeting chimaera
BafA1	Bafilomycin A1
Bcl-xL	B-cell lymphoma-extra large
BCL10	B-cell lymphoma/leukaemia 10
Bcl2	B-cell lymphoma 2
BCR	B-cell receptor

BP	Biotin-phenol
c-myc	Myc proto-oncogene protein
C. elegans	Caenorhabditis elegans
CALCOCO1	Calcium binding and coiled-coil domain 1
Ccnd1	Cyclin D1
CD	Cluster of differentiation
CD62L	CD62 ligand
Cdc25a	Cell division cycle 25A
CDK	Cyclin-dependent kinase
CDKN1B	Cyclin-dependent kinase inhibitor 1B
CHIP	Carboxy-terminus of Hsp70-interacting protein
CHX	Cycloheximide
CLP	Common-lymphoid progenitors
CMA	chaperone-mediated autophagy
CNP	2',3'-cyclic nucleotide 3' phosphodiesterase
COVID-19	Coronavirus disease 2019
COX7A2	Cytochrome c oxidase polypeptide 7A2
CTV	CellTrace Violet
CUL3	Cullin 3
DAG	Diacylglycerol
DAMP	Damage-associated molecular patterns
DMSO	Dimethyl sulfoxide
DUSP6	Dual-specific phosphatase 6
E2	E2 ubiquitin-conjugating enzyme

EIF3C	Eukaryotic translation initiation factor 3 subunit
eMA	Endosomal microautophagy
EMB	Embigin
eMI	Endosomal microautophagy
EOMES	Eomesodermin
ER	Endoplasmic reticulum
FAF2	Fas-associated factor family member 2
FIP200	FAK family kinase-interacting protein of 200 kDa
Flag-hKLHL6	Flag-tagged human KLHL6
FOXO1	Forkhead box protein O1
FTH1	Ferritin heavy chain 1
FTL1	Ferritin light chain 1
GABARAP	GABA type A receptor-associated protein
GABARAPL	GABA type A receptor-associated protein-like
GABPα	GA binding protein alpha
GDF	Growth differentiation factor
GFI1	Growth factor independence 1
GPC1	Glypican 1
GSK3	Glycogen synthase kinase 3
H2AC20	H2A clustered histone 20
HDAC1	Histone deacetylase 1
HIV	Human immunodeficiency virus
HNRNPA1	Heterogeneous nuclear ribonucleoprotein A1
HNRNPA2B1	Heterogeneous nuclear ribonucleoprotein A2/B1

HRP	Horseradish peroxidase
HSC70	Heat shock cognate 70
HSP40	Heat shock protein 40
IBD	Inflammatory bowel disease
ICAM1	Intercellular adhesion molecule 1
ICOS	Inducible T-cell costimulator
IFN-γ	Interferon-gamma
IKK	IκB kinase
IL-1R	Interleukin-1 receptor
IL-2R	IL-2 receptor
IL-2Rα	Interleukin-2 receptor alpha
IL-2Rβ	Interleukin-2 receptor beta
IL-7Rα	Interleukin-7 receptor alpha-chain
ILC	Innate lymphoid cell
ILV	Intraluminal vesicle
imMEF	Immortalised embryonic fibroblast
IP_3	Inositol-1,4,5-triphosphate
Irgm1	Immunity-related GTPase family M protein 1
ISR	Integrated stress response
ITAM	Immunoreceptor tyrosine-based activation motif
ITCH	E3 ubiquitin-protein ligase Itchy homolog
ITIM	Immunoreceptor tyrosine-based inhibitory motif
ITK	Inducible T cell kinase
IκB	Inhibitor of NF-κB

JAK	Janus kinase
KEAP1	Kelch-like ECH-associated protein 1
KLHL6	Kelch-like protein 6
KLRG1	Killer cell lectin-like receptor G1
LAMP1	Lysosomal-associated membrane protein 1
LAMP2A	Lysosome-associated membrane protein 2
LANDO	LC3-associated endocytosis
LAP	LC3-associated phagocytosis
LAT	Linker for activation of T cells
LCK	Lymphocyte-specific protein tyrosine kinase
LD	Lipid droplet
LDELS	LC3-dependent extracellular vesicle loading and secretion
LFA-1	Integrin alpha-L
LFQ	Label-free quantitation
LGALS8	Galectin 8
LIR	LC3-interacting region
LSEC	Liver sinusoid endothelial cell
MAIT	Mucosal-associated invariant T
MAP1LC3 (LC3)	Microtubule-associated proteins 1A/1B light chain 3B
MCMV	Murine cytomegalovirus
MHC	Major histocompatibility complex
mTORC1	Mammalian target of rapamycin complex 1
MVB	Multivesicular body

MVE	Multivesicular endosomes
NBR1	Next to BRCA1 gene 1
NCL	Nucleolin
NCOA4	Nuclear receptor coactivator 4
NEDD4	Neuronal precursor cell-expressed developmentally downregulated 4
NF-κB	Nuclear factor kappa-light-chain-enhancer of activated B cells
NFAT	Nuclear factor of activated T cells
NIK	NF-κB-inducing kinase
NK	Natural killer
NKT	Natural killer T
NLRP3	NACHT, LRR and PYD domains-containing protein 3
NRF2	NF-E2-related factor 2
OPP	O-propargyl-puromycin
OPTN	Optineurin
OVA	Ovalbumin
PCA	Principal component analysis
PDCD6IP	Programmed cell death 6 interacting protein
PI_3K	Phosphatidylinositol 3- kinase
PI3P	Phosphatidylinositol 3-phosphate
PIP_2	Phosphatidylinositol-4,5-bisphosphate
PKC	Protein kinase C
PKC-θ	Protein kinase C theta
PLC-γ	Phospholipase C gamma
pMHC-II	Peptides presented by MHC class II

PMSF	Phenylmethanesulfonylfluoride
PRDX3	Peroxiredoxin 3
PRKAR1A	cAMP dependent protein kinase A (PKA) type I-α regulatory subunit (RIα)
PROTAC	Proteolysis-targeting chimaera
PTPN1	Protein tyrosine phosphatase non-receptor type 1
RAB18	Ras-related protein Rab-18
RAB7A	Ras-related protein Rab-7A
RCAN1	Calcipressin-1
ROS	Reactive oxygen species
RPS13	Ribosomal protein S13
S6	40S ribosomal protein S6
SA-β-gal	Senescence-associated beta-galactosidase
SAHF	Senescence-associated heterochromatin foci
SASP	Senescence-associated secretory phenotype
SCAMP3	Secretory carrier-associated membrane protein 3
SERCA	Sarcoplasmic and endoplasmic reticulum Ca(2+)-ATPase 2
SJL	Swiss Jim Lambert
SMAC	Supramolecular activation complex
Smurf1	SMAD-specific E3 ubiquitin protein ligase 1
SQSTM1	Sequestosome 1
STAT5	Signal transducer and activator of transcription 5
T-Atg16l1$^{-/-}$	*CD4cre; Atg16l1$^{flox/flox}$*
T-Atg7$^{-/-}$	*CD4^{cre}*; *Atg7$^{flox/flox}$*
Tat	Trans-activator of transcription

TAX1BP1	Tax1-binding protein 1
TBC1D15	TBC1 domain family member 15
TBK1	TANK-binding kinase 1
TCR	T cell receptor
TFEB	Transcription factor EB
TIRF	Total internal reflection fluorescence
TLR	Toll-like receptor
T_n	Naïve T cell
TNF	Tumour necrosis factor
TNFR	Tumour necrosis factor receptor
TOLLIP	Toll-interacting protein
TSLP	Thymic stromal lymphopoietin
T_{vm}	Virtual memory T cell
Ub	Ubiquitin
ULK1	Unc-51 like autophagy activating kinase 1
UPS	Ubiquitin-proteasome system
UPR	Unfolded protein response
VCP	Valosin containing protein
VPS34	Vacuolar protein sorting 34
WDR18	WD repeat-containing protein 18
WIPI2	WD repeat domain phosphoinositide-interacting protein 2
ZAP70	Zeta chain of T cell receptor-associated protein kinase 70
γ_c	Common cytokine receptor γ chain

Table of Contents

Abstract 1

Declaration 2

Author's Publications 3

Acknowledgements 4

List of Abbreviations 6

Chapter 1: General Introduction – Autophagy and CD4+ T cell activation 2

1.1 Autophagy 2

1.1.1 Macroautophagy 3

1.1.2 Microautophagy and CMV 7

1.2 CD4+ T cell activation 10

1.3 Autophagy's role in CD4+ T cells 16

1.4 Thesis Summary 19

Chapter 2: Materials and Methods 21

2.1 Mice 22

2.2 Genotyping 22

2.3 Preparation of Primary Cells 25

2.4 Cell line generation 27

2.5 Viral vectors and lentivirus production 27

2.6 Bone marrow (BM) chimaera 28

2.7 T-cell adoptive transfer 28

2.8 Proximity Labelling 28

2.9 Proteinase K digestion 28

2.10 Streptavidin-pulldown and on-beads peptide digestion 29

2.11 Mass spectrometry data analysis 30

2.12 Flow cytometry 30

2.13 Lipid droplet staining 32

2.14 SA-β-gal staining **32**

2.15 OPP-Click assay **32**

2.16 IL-7Rα internalisation assay **33**

2.17 Immunoprecipitation **34**

2.18 Western blots **34**

2.19 Immunofluorescence staining and confocal microscopy **35**

2.20 Supported Lipid Bilayer (SLB) preparation and use **36**

2.21 Total Internal Reflection Fluorescence Microscopy (TIRFM) and image analysis **36**

2.22 List of antibodies **37**

2.23 Statistics **39**

Chapter 3. Mapping the autophagosomal content using the *Lc3b-APEX2* mouse model – Introduction **40**

3.1 Introduction **41**

3.1.1 A novel technique to screen for protein-protein interactions 43

3.1.2 Proximity labelling technique to map autophagosomal cargoes 44

Chapter 3. Mapping the autophagosomal content using the *Lc3b-APEX2* mouse model – Results **48**

3.2 Results **49**

3.2.1. Generation and validation of mouse model: genotyping and knock-in site sequencing 49

3.2.2. Expression of the LC3B-APEX2 chimeric protein 51

3.2.3. Enzymatic function of the APEX2-LC3B 53

3.2.4. Examination of biotinylated proteins within different cell fractions 55

3.2.5. Co-localisation of biotinylated proteins with LC3B-APEX2 chimeric protein and LAMP1 57

3.2.6. Proteinase K protection assay 58

3.2.7. Optimisation of the purification of biotinylated proteins 59

3.2.8. Building up the proteomics analysis workflow 61

3.2.9. Applying the proteomics analysis to imMEFs 65

3.2.10. Cell number titration with imMEFs 67

Chapter 3. Mapping the autophagosomal content using the *Lc3b-APEX2* mouse model – Discussion **68**

3.3 Discussion 69

Chapter 4: Characterisation of autophagy and ageing phenotypes in CD4+ T cells – Introduction 73

4.1 Introduction 74

4.1.1 Hallmarks of cellular senescence and cellular ageing 74

4.1.2 Autophagy and ageing 79

4.1.3 Ageing of T cells 82

Chapter 4: Characterisation of autophagy and ageing phenotypes in CD4+ T cells – Results 86

4.2 Results 87

4.2.1. *Atg7*-deficient CD4+ T cells show decreased effector formation in response to pathogens in vivo 87

4.2.2 TCR-transgenic *Atg7*-deficient CD4+ T cells show decreased effector formation in response to TCR-specific antigen in vivo 90

4.2.3. Autophagy-deficient CD4+ T cells show a delayed proliferation in vitro 93

4.2.4. Inducible knock-out of *Atg16l1* in CD4+ T cell impairs its proliferation 97

4.2.5. Different subsets of T cells are altered in the aged immune system 99

4.2.6. Autophagic flux is decreased in aged CD4 T cells 105

4.2.7. T cell activation and proliferation is decreased in aged CD4+ T cells 107

4.2.8. The impaired proliferation in aged CD4+T cells is not due to cellular senescence 109

4.2.9. mTOR signalling pathways are dysregulated in aged T cells 111

4.2.10. The global translation rate is decreased in aged CD4+ T cells 114

4.2.11. Lipid droplets are accumulated in aged CD4+ T cells 116

Chapter 4: Characterisation of autophagy and ageing phenotypes in CD4+ T cells – Discussion 118

4.3 Discussion 119

Chapter 5: Characterisation of autophagic substrates in activated CD4+ T cells and their role for CD4+ T cell proliferation – Introduction 122

5.1 Introduction 123

5.1.1 NF-κB signalling pathway 123

5.1.2. IL-7R signalling pathway 126

Chapter 5: Characterisation of autophagic substrates in activated CD4+ T cells and their role for CD4+ T cell proliferation – Results 132

5.2 Results **133**
5.2.1 Mapping autophagosomal contents in activated pan-T cells. 133
5.2.2 KLHL6 is degraded through autophagy in vitro 137
5.2.3 *Klhl6*$^{-/-}$ T cells do not show an enhanced proliferation upon TCR/CD28-stimuli 140
5.2.4 NF-κB signalling and levels of KLHL6 substrates are not changed in autophagy-deficient CD4+ T cells 142
5.2.5 Autophagosomal content in CD4+ T cells at different time points 144
5.2.6 IL-7R is degraded via autophagy in CD4+ T cells 149
5.2.7 IL-2R, but not IL-7R signalling, is impaired in T-Atg7$^{-/-}$ CD4+ T cells 157
5.2.8 Excessive surface IL-7Rα impairs the assembly of IL-2R via sequestrating γ_c 161
5.2.9 Blocking the IL-7R receptor did not rescue the phenotype of impaired proliferation. 164

Chapter 5: Characterisation of autophagic substrates in activated CD4+ T cells and their role for CD4+ T cell proliferation – Discussion 166

5.3 Discussion 167

Chapter 6: Summary and general discussion 173

6.1 The application of proximity biotinylation technique to study protein degradation 174

6.2 Phenotypes of CD4+ T cells from aged individuals 179

6.3 Applying knowledge of autophagy in T cells to develop novel therapies 182

6.4 Metabolic aspect of T cell activation 184

6.5 Autophagic substrates may, in turn, regulate autophagy level 186

Bibliography 189

List of Figures

Chapter 1: General Introduction – Autophagy and CD4+ T cell activation.....2

Figure 1.1 Autophagy and its core machinery. 5

Figure 1.2 Selective microautophagy. 8

Figure 1.3 Chaperone-mediated autophagy. 9

Figure 1.4 Three major signalling pathways mediating T cell activation.....14

Chapter 3. Mapping the autophagosomal content using the *Lc3b-APEX2* mouse model 40

Figure 3.1 Amino acid sequence of pro-LC3B and knock-in strategy. 47

Figure 3.2 Schematic overview of autophagosome targeting and labelling using APEX2 N-terminally fused to LC3B.....47

Figure 3.3 PCR result of LC3B-APEX2 mouse DNA.....50

Figure 3.4 Confirmation of the genomic sequence of *Lc3b-APEX2* mice.....50

Figure 3.5 Western blot of LC3B-APEX2 chimeric protein. 52

Figure 3.6 Western blot of proximity-labelled splenocytes.....54

Figure 3.7 Western blot of different cell fractions from proximity-labelled imMEFs. 56

Figure 3.8 Confocal microscopy images of proximity-labelled imMEF cells.....57

Figure 3.9 Western blot of imMEFs undergoing proteinase K protection assay.....58

Figure 3.10 Optimisation of autophagosomal cargo purification. 60

Figure 3.11 Schematic overview of three sample groups. 63

Figure 3.12 Building the workflow for statistical analysis of mass-spectrometry data.....63

Figure 3.13 Biotinylated proteins from proximity-labelled imMEFs show high correlcation.64

Figure 3.14 Identification of autophagosomal cargoes in imMEFs.....66

Figure 3.15 Volcano plots of proteins detected from samples with different cell numbers. ...67

Chapter 4: Characterisation of autophagy and ageing phenotypes in CD4+ T cells 73

Figure 4.1 Bone marrow chimaeras show impaired effector formation in T-Atg7$^{-/-}$ CD4+ T cells. 89

Figure 4.2 T-Atg7$^{-/-}$, OT-II mice displayed no sign of lymphopenia or a shift from naïve to memory/effector population at 6-8 weeks old. 91

Figure 4.3 Adoptive transfer experiment shows impaired effector formation in T-Atg7$^{-/-}$, OT-II CD4+ T cells. 92

Figure 4.4 T-Atg7$^{-/-}$ CD4+ T cells display normal upregulation of early-activation markers. 94

Figure 4.5 T-Atg7$^{-/-}$ CD4+ T cells show delayed proliferation in vitro. 94
Figure 4.6 T-Atg7$^{-/-}$ CD4+ T cells display no significant increase of cell death or apoptosis on day 1 and day 3 of activation. 95
Figure 4.7 Divided T-Atg7$^{-/-}$ CD4+ T cells show effective deletion of *Atg7*. 96
Figure 4.8 CD4+ T cells from *Cre-ERT2*+, *Atg16l1*$^{flox/flox}$ mouse model display efficient deletion of *Atg16l1* induced by 4-hydroxytamoxifen (4-OHT). 98
Figure 4.9 *Atg16l1*-deficient CD4+ T cells show impaired proliferation in vitro. 98
Figure 4.10 Aged T cells display a shift from naive to memory/effector populations. 101
Figure 4.11 Aged T cells display an expansion of the virtual memory population. 102
Figure 4.12 Aged T cells display an expansion of the senescent-like population. 103
Figure 4.13 Aged T cells display an expansion of the KLRG1+ population. 104
Figure 4.14 CD4+ T and CD8+ T cells from aged mice show decreased autophagic flux. 106
Figure 4.15 Aged naïve CD4+ T cells showed impaired upregulation of early-activation marker upon TCR-mediated activation. 108
Figure 4.16 Aged naïve CD4+ T cells showed impaired proliferation upon TCR-mediated activation. 108
Figure 4.17 Aged CD4+ T cells did not show increased senescence-associated β-galactosidase (SA-β-Gal) activity. 110
Figure 4.18 mTORC1 signalling declines in aged CD4+ T cells. 112
Figure 4.19 mTORC2 signalling is dysregulated in aged CD4+ T cells. 113
Figure 4.20 Aged CD4+ T cells show a decreased rate of protein synthesis. 115
Figure 4.21 Aged CD4+ T cells showed accumulation of lipid droplets. 116

Chapter 5: Characterisation of autophagic substrates in activated CD4+ T cells and their role for CD4+ T cell proliferation 122

Figure 5.1 Canonical and non-canonical NF-κB signalling pathways. 124
Figure 5.2 IL-7R signalling pathway. 128
Figure 5.3 Proximity labelling and mass-spec analysis of activated pan T cells. 135
Figure 5.4 Declining levels of autophagy may lead to KLHL6 accumulation and attenuated NF-κB signalling in CD4+ T cells. 136
Figure 5.5 Aged CD4+ T cells display attenuated NF-κB signalling. 136
Figure 5.6 KLHL6 interacts with LC3B in vitro. 138
Figure 5.7 KLHL6 is co-localised with autophagosomes in vitro. 139

Figure 5.8 *Klhl6*$^{-/-}$ T cells do not show differences in their numbers or cell proliferation profile. 141
Figure 5.9 Autophagy-deficient CD4+ T cells do not show significant differences in NF-κB signalling when compared to wild-type cells. 142
Figure 5.10 Autophagy-deficient CD4+ T cells do not accumulate KLHL6 substrates. 143
Figure 5.11 Optimisation of sample preparation for proximity labelling in CD4+ T cells. 146
Figure 5.12 Proximity labelling in CD4+ T cells activated for 3 days. 147
Figure 5.13 Proximity labelling in CD4+ T cells activated for 16 hours. 148
Figure 5.14 IL-7Rα is co-localised with autophagosomes in naïve and activated CD4+ T cells. 152
Figure 5.15 IL-7Rα is accumulated in naïve CD4+ T cells upon BafA1 treatment. 152
Figure 5.16 IL-7Rα is accumulated in T-Atg7$^{-/-}$ naïve CD4+ T cells. 153
Figure 5.17 IL-7Rα levels in wild-type or T-Atg7$^{-/-}$ CD4+ T cells activated for 1 or 3 days. 154
Figure 5.18 Quantification of *Il7ra* mRNA expression in splenic CD4+ T cells without activation, activated for 1 day or 3 days. 154
Figure 5.19 IL-7Rα surface level is decreased in naïve CD4+ T cells from aged mice. 155
Figure 5.20 The internalisation rate of IL-7Rα is not changed in T-Atg7$^{-/-}$ naïve CD4+ T cells. 155
Figure 5.21 IL-7Rα surface level is increased in the constitutive and inducible *Atg16l1*-knockout naïve CD4+ T cells. 156
Figure 5.22 Schematic overview of how excessive IL-7Rα may lead to impaired T cell proliferation. 159
Figure 5.23 The amplitude of IL-7R signalling is not changed in T-Atg7$^{-/-}$ naïve CD4+ T cells. 159
Figure 5.24 IL-2R signalling is impaired in autophagy-deficient CD4+ T cells. 160
Figure 5.25 Assembly of IL-2R complex is impaired in the immunological synapse of T-Atg7$^{-/-}$ CD4+ T cells. 162
Figure 5.26 γ_c is sequestrated by the excessive IL-7Rα outside of the immunological synapse. 163
Figure 5.27 Anti-IL-7Rα antibody cannot rescue the impaired proliferation of T-Atg7$^{-/-}$ CD4+ T cells. 165

Chapter 6: Summary and general discussion 173

Figure 6.1 Application of *Lc3b-AP2* transgenic mouse model to investigate the molecular mechanism of how autophagy contributes to CD4+ T cell proliferation, and how they age.175

Chapter 1: General Introduction – Autophagy and CD4+ T cell activation

1.1 Autophagy

Autophagy is a major lysosome-dependent intracellular degradation pathway conserved in most eukaryotic cells. It is classically divided into three subtypes: macroautophagy, microautophagy, and chaperone-mediated autophagy (CMA). They can be distinguished by the feature of their substrates, the mechanisms mediating their cargo trafficking into the lysosome, and the signalling pathways for their regulation[1].

1.1.1 Macroautophagy

Macroautophagy (hereafter referred to as 'autophagy') was first identified in nutrient-deprived yeast[2]. After subsequent studies in mammalian cells, it is now commonly recognised as a crucial regulator of homeostasis in various physiological contexts such as cell metabolism, differentiation, proliferation, survival and cell death, as well as prevention of ageing.

Autophagy activation, through starvation or receptor-mediated signalling, results in the isolation and expansion of a double-membrane vesicle, which sequestrates the cargo material. The double-membrane vesicle is known as an autophagosome, which is then transported to and fuses with the lysosome for cargo degradation and recycling (Figure 1.1). Around 19 core autophagy-related (ATG) proteins form the autophagy machinery and actively orchestrate different steps of autophagy[2]. Most ATG proteins take part in one of two ubiquitin-like autophagy-related protein 8 (*Atg8*) conjugation pathways. Deletion of the key genes involved in both pathways, like *Atg5* and *Atg7*, has been widely used to study autophagy's role in specific cell types under certain circumstances[3].

The activation of ULK1 serine-threonine kinase initiation complex (consisting of ULK1, ATG13, FIP200 and ATG101), which phosphorylates the PI3KC III nucleation complex

(composed of VPS34, Beclin 1, ATG14, AMBRA1 and p115) and triggers the nucleation of the phagophore marks the start of the autophagic process[4,5] (Figure 1.1). The complex facilitates the local PI3P synthesis and the formation of a cup-shaped structure on the ER, called the omegasome[6]. The elongation of the omegasomal membrane is promoted by the ATG9-containing vesicles with several cellular origins that provides membrane material[7]. WIPI2, a protein containing a PI3P binding motif, is subsequently recruited to the omegasomal membrane. Presence of WIPI2 recruits ATG16L1 to the growing structure, which activates the ATG12-ATG5-ATG16L1 complex and is crucial for the generation of the E3 ligase ATG5-ATG12. Lipidation of ATG8 is prepared by the removal of its C-terminal part by the protease ATG4, which allows for its activation by E1-like enzyme ATG7 in an ATP-dependent manner[8]. Activated ATG8 is then conjugated to phosphatidylethanolamine (PE) moiety by the E2-like enzyme ATG3. Finally, ATG8 lipidation is concluded by the E3-like ligase ATG12-ATG5 and inserted into the autophagosomal double membrane. Similarly, ATG12, a core protein in the ATG12-ATG5-ATG16L1 complex, is activated by the E1-like enzyme ATG7 and conjugated to ATG5 with the help of the E2-like enzyme ATG10[8]. After the closure of the autophagosomal membrane, the autophagosome undergoes further maturation and finally fusion with the lysosome.

ATG8 is required during double-membrane expansion and cargo recruitment[3]. Several mammalian homologues of yeast ATG8 protein have been discovered, which are classified into the microtubule-associated protein light chain 3 (LC3), γ-aminobutyric acid receptor-associated protein (GABARAP), and γ-aminobutyric acid receptor-associated protein-like (GABARAPL) subgroups[4]. While LC3/GABARAP family members share sequence and structural similarities, these proteins are mostly likely not redundant due to their preferential tissue expression and autophagy-independent functions[3].

In this study, we focus much of our attention on MAP1LC3 (hereafter referred to as 'LC3'). Cytoplasmic and lipidated LC3 can be distinguished due to their different electrophoretic mobility in SDS-PAGE gels – LC3 is detected at 16-18 kDa in comparison to 14-16 kDa for lipidated LC3 (LC3-PE)[9].

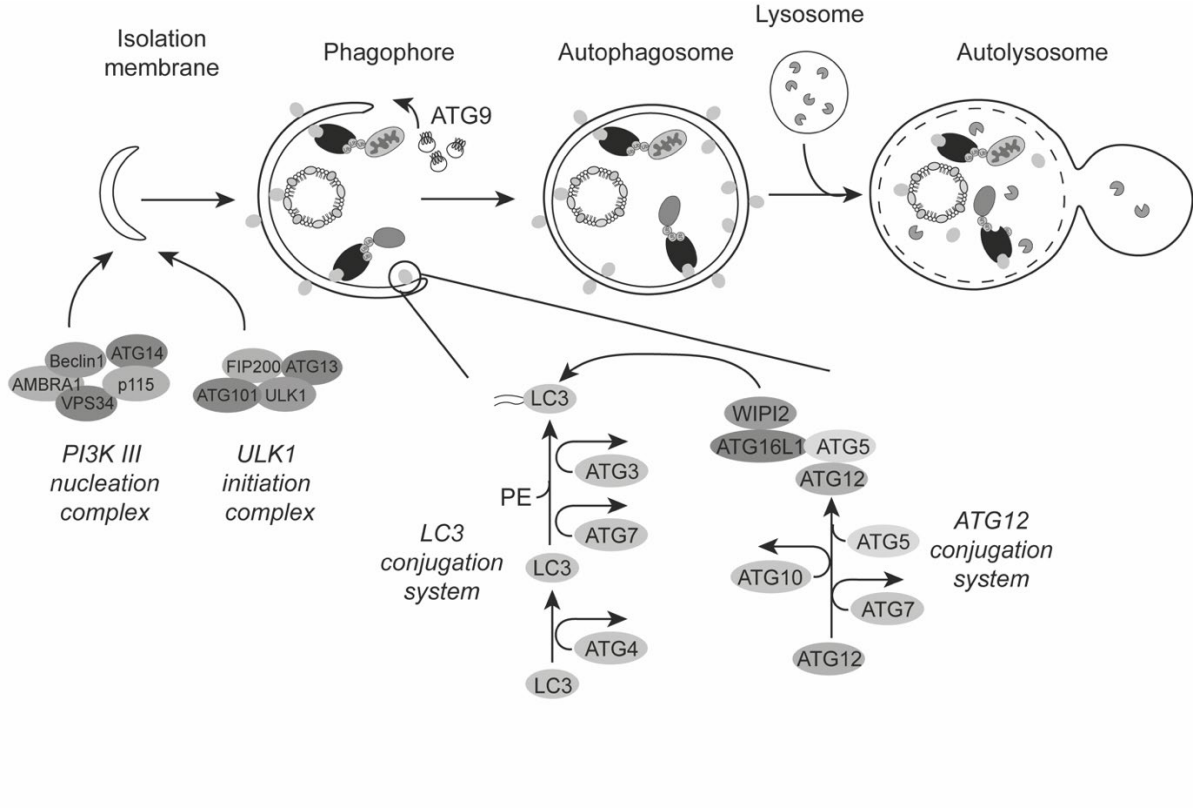


Figure 1.1 Autophagy and its core machinery.

Upon autophagy-inducing stimuli, the ULK1 initiation complex (composed of ULK1, ATG13, ATG101 and FIP200) is activated and further phosphorylates the PI3KC III nucleation complex (composed of VPS34, Beclin 1, ATG14, AMBRA1 and p115), which facilitates the formation of isolation membrane. Further, WIPI2 recruits the ATG12 and LC3 conjugation systems, which trigger two ubiquitin-like reactions, to integrate the lipidated LC3s into the double-membranes of phagophores. Vesicles containing a multi-transmembrane protein ATG9 contribute to the elongation of the phagophore. Autophagy receptors can bind to membrane LC3 and selectively recruit substrates for degradation into the phagophore. After the maturation of the autophagosome, it fuses with lysosomes for cargo degradation. Activating molecule in BECN1-regulated autophagy protein 1, AMBRA1; autophagy-related gene, ATG; FAK family kinase-interacting protein of 200 kDa, FIP200; microtubule-associated protein 1A/1B-light chain 3, LC3; phosphatidylethanolamine, PE; Unc-51 like autophagy activating kinase 1, ULK1; vacuolar protein sorting 34, VPS34; WD repeat domain phosphoinositide interacting 2, WIPI2.

Although autophagy was initially viewed as a non-selective process, recent studies could establish that a large spectrum of cellular cargos can be selectively degraded through the action of receptor proteins. Based on the type of cargo, autophagy has been further grouped into: aggrephagy (aggregated proteins), mitophagy (mitochondria), ER-phagy (endoplasmic reticulum), pexophagy (peroxisomes), nucleophagy (fragments of nucleus), lipophagy (lipid droplets) or xenophagy (intracellular pathogens)[2]. The selectivity of autophagy is conferred by specialized autophagy receptors, which interact with the autophagic substrates and the LC3/GABARAP proteins anchored inside the autophagosomal membrane, via their LC3-interacting region (LIR) motif[10]. P62/SQSTM1 was the first selective autophagy receptor identified. P62 mediates the clearance of poly-ubiquitinated protein aggregates via the autophagic pathway[11]. The types of selective autophagy mediated by several main autophagic receptors have been summarised in Table 1.1. Taken together, cargo specificity during autophagy is achieved through a combination of selective autophagy receptors and ATG8 homologues.

Table 1.1 Autophagic receptors and the types of selective autophagy that they mediate.

Autophagic receptor	Selective autophagy
P62/SQSTM1	pexophagy[12], mitophagy[13], xenophagy[14], aggrephagy[15], lysophagy[16],
NBR1	pexophagy[12], aggrephagy[15]
OPTN	mitophagy[17], xenophagy[18]
TOLLIP	aggrephagy[19]
CALCOCO2/NDP52	mitophagy[17], xenophagy[18],
TAX1BP1	xenophagy[20], aggrephagy[21]

Mammalian target of rapamycin complex 1 (mTORC1) and AMP-activated protein kinase (AMPK) are two major intracellular signalling pathways that regulate autophagy levels in response to nutrient stress. AMPK is activated by an elevated level of ADP and AMP, which indicates a low energy status due to the depletion of cellular ATP[22]. As a positive regulator of

autophagy, AMPK activation promotes autophagy directly through the phosphorylation of key components of the autophagy machinery, including ULK1 and VPS34. At the same time, AMPK activation suppresses the mTORC1 pathway, a negative regulator of autophagy[23-25]. Conversely, amino acid replete cells activate mTORC1 via PI3K-AKT signalling supporting anabolic processes, such as protein translation, lipid and nucleotide synthesis[26-32]. mTORC1 inhibits autophagy by interrupting the interaction between AMPK and ULK1[33]. Moreover, mTORC1-mediated phosphorylation of ULK and ATG13 inhibits the ULK1 complex activity and activation[34]. In addition, it has been shown that mTORC1 can induce the nuclear export of TFEB, a master transcription factor related to autophagy and lysosomal biogenesis[35]. As such, mTORC1 can also suppress the transcription of several key autophagy genes.

However, both autophagy and mTORC1 signalling are required for the full activation and proliferation of T cells[36]. Therefore, there must be an mTORC1-independent mechanism to induce autophagy in activated T cells. Cytokine signalling through IL-2 and other cytokines that use the common gamma chain receptor can boost autophagy in a Janus kinase (JAK)-dependent manner in both activated naïve and effector T cells[37]. This indicates that autophagy is regulated via the integration of distinct signalling pathways in a cell type-specific manner.

1.1.2 Microautophagy and CMV

Microautophagy describes a process during which cytosolic proteins and organelles are directly engulfed by late endosomes/multivesicular bodies (MVBs) through membrane invagination in mammalian cells (Figure 1.2)[38]. This process can lead to either non-selective bulk degradation of cytosolic substrates or to selective degradation of cellular cargo. The latter process requires however some of the same molecular machinery, which is used in autophagy. This was demonstrated by studies showing that microautophagy of the nucleus, lysosome and lipid

droplet fails in cells lacking essential *Atg* genes[39-41]. The use of HSC70 (heat shock cognate protein of 70 kDa, also known as HSPA8) can also promote selective uptake through binding of KFERQ motif-bearing proteins, a mechanism partially shared with CMA[38,42-44]. In addition, a recent study indicates that TOLLIP, a selective autophagy receptor, can drive the selective engulfment of several poly-ubiquitinated proteins into MVBs in an LC3-independent manner[45]. Also, the turnover of synaptic proteins in neurons is mediated by microautophagy[46]. Although the cellular function of microautophagy remains largely unknown, it is proposed to contribute to the quality control of proteins and intracellular membranes, as well as the regulation of some specific cellular processes.

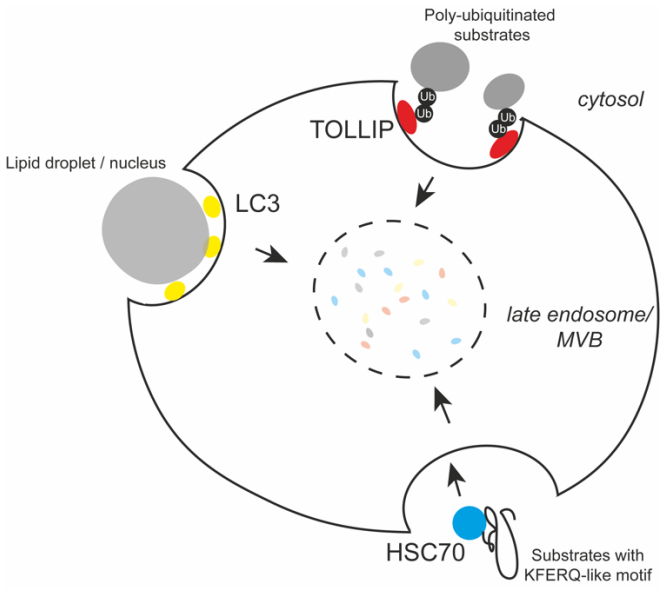


Figure 1.2 Selective microautophagy.

Except for a bulk degradation mechanism which engulfs and degrades cytosolic cargo in small vesicles formed by invagination of late endosomal (or multivesicular body, MVB) membrane, microautophagy can also selectively degrade substrates through recognition and targeting by (1) autophagy receptor TOLLIP, (2) heat shock cognate 70, HSC70 and (3) LC3 and its lipidation machinery.

The third major autophagy pathway is CMA, a process using a distinct cargo recognition and delivery pathway (Figure 1.3). HSC70 recognises proteins containing KFERQ-like motifs as substrates for CMA-mediated degradation[46]. In concert with other co-chaperones (such as

CHIP or HSP40), HSC70 delivers its cargo to the monomeric lysosome-associated membrane protein type 2A (LAMP2), a lysosomal transmembrane protein, which then forms a multimeric complex and translocates the unfolded substrate into the lysosome. CMA plays many roles within the cell, including maintenance of proteostasis, regulation of metabolism, cell cycle and immune response[47]. Although there are functional overlaps with the other two forms of autophagy, the system is not redundant since CMA failures lead to neurodegeneration and cancer, as well as ageing[47].

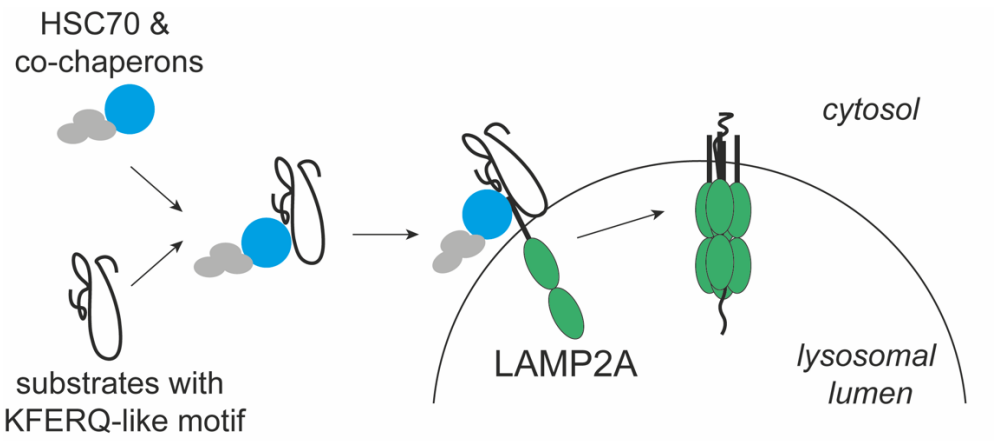


Figure 1.3 Chaperone-mediated autophagy.

Protein substrates bearing KFERQ-like motif are delivered to the lysosomes via a complex composed of chaperone HSC70 and co-chaperones. After binding to the lysosomal LAMP2A, LAMP2A undergoes multimerization and translocate the unfolded substrate into lysosomal lumen for degradation. HSC70, heat shock cognate 70; LAMP2A, lysosome-associated membrane protein 2.

In summary, autophagy (including macroautophagy, microautophagy and CMA) serves as a major cellular degradation pathway. Through removing cellular content in either a bulk or selective manner, it contributes to different physiological aspects. In the following part, I am going to introduce the three signals required for a complete T cell activation and what is known about autophagy's role in this process.

1.2 CD4+ T cell activation

T cell lineages are defined based on their specialised functions, as well as the expression of surface antigens, cytokines and transcription factors[48]. They can be classified into the best-studied conventional CD4+ and CD8+ T cells and some unconventional T cell subsets characterised by the restricted repertoires of T cell receptors (TCR), including γδ T cells, mucosal-associated invariant T (MAIT) cells and natural killer T (NKT) cells. $CD4^+$ T lymphocytes play a central role in mediating both adaptive and innate immune responses through cytokine secretion and receptor-ligand interactions. Most CD4+ T lymphocytes eventually adopt one of several distinct helper T cell phenotypes. During an immune reaction, naïve CD4+ T cells encounter antigen-presenting cells (APCs) and get activated in a 'priming' process. Priming of CD4+ T cells relies on three distinct sequential signals: (1) TCR recognising their cognate antigen in a major histocompatibility complex (MHC)-restricted manner, (2) costimulatory receptors activated by their ligands, and (3) cytokine-amplified differentiation and expansion (Figure 1.4)[49]. In the following part, we will introduce these signals in greater detail.

Conventional T lymphocytes provide a highly effective immune defence against pathogens and aberrant proteins through a diverse pool of TCRs expressed on their surface. The TCR is a heterodimer composed of an α chain and a β chain which together form highly variable domains capable of recognizing a variety of antigen peptides. Recognition of cognate antigen peptides presented by MHC class II (pMHC-II) on APCs via the TCR provides the **first signal** during CD4+ T cell activation. This receptor-ligand interaction promotes the formation of a close membrane contact between APCs and T cells. The pMHC:TCR interaction results in the recruitment of the TCR co-receptor CD3 to the TCRαβ heterodimer promoting a conformational change, which leads to the phosphorylation of CD3 on its immunoreceptor

tyrosine-based activation motifs (ITAMs) through protein tyrosine kinases such as lymphocyte-specific protein tyrosine kinase (LCK)[50-53]. In parallel, CD4, another co-receptor, is recruited to the synapse and is capable of recognizing the pMHC-II molecule upon formation of pMHC:TCR-CD3 complex[54]. CD4 engagement also enhances the targeted delivery of LCK to the complex and subsequent phosphorylation of the ITAM motif on CD3[55]. The phosphorylation of CD3 ITAM promotes the recruitment of the zeta chain of T cell receptor-associated protein kinase 70 (ZAP70), which is exposed to LCK-mediated phosphorylation. The activated ZAP70 then phosphorylates signalling scaffold adaptor proteins, which further activates kinases mediating several signalling cascades including phosphatidylinositol 3-kinase (PI_3K), protein kinase B (AKT), inducible T cell kinase (ITK), linker for activation of T cells (LAT) and protein kinase C (PKC). Protein kinase C theta (PKC-θ) is activated by PI_3K signalling and leads to the nuclear translocation of nuclear factor kappa-light-chain-enhancer of activated B cells (NF-κB), which is required for the transcription of several genes key for T cell activation, like *Il2*[56]. In parallel, ITK and LAT promote phospholipase C gamma (PLC-γ) phosphorylation and activation. This results in the cleavage of the plasma membrane-bound phosphatidylinositol-4,5-bisphosphate (PIP_2) into inositol-1,4,5-triphosphate (IP_3) and diacylglycerol (DAG). Subsequently, DAG triggers the activation of the RAS/MAPK signalling pathway and the nuclear translocation of the transcription factor activator protein 1 (AP-1), which induces the expression of the early-activation marker CD69[57]. IP_3 diffuses into the cytosol and activates its receptor residing on the ER, which triggers the release of ER-stored calcium ions into the cytosol. Increased cytosolic calcium thus activates the nuclear factor of activated T cells (NFAT) in a calcineurin-dependent manner, which is involved with the transcriptional upregulation of another early-activation marker CD25 (or interleukin-2 receptor alpha, IL-2Rα)[58]. These signalling pathways and transcription factors orchestrate the expression of a set of genes necessary for T cell activation.

Apart from the TCR-signalling cascade, stimulation through additional co-stimulatory receptors is an important **second signal** during $CD4^+$ T cell activation. For example, the co-stimulatory receptor CD28 plays a crucial role during naïve T cell priming[59]. The interaction of CD28 with its ligand B7-1 (also known as CD80) or B7-2 (also known as CD86), which are expressed on the surface of APCs, triggers the activation of the PI3K-AKT pathways essential for T cell survival and proliferation. Several downstream targets of PI3K-AKT includes glycogen synthase kinase 3 (GSK3), an NFAT activator, and mTOR, which induces the NF-κB pathway[60]. Both pathways contribute to the production of IL-2, an autocrine cytokine required for CD4+ T cell proliferation. In addition, CD28 signalling can regulate IL-2 level post-transcriptionally by enhancing the stability of the *Il2* transcript[61,62]. Taken together, the induction of PI3K-AKT signalling through co-stimulatory receptors plays an important role in T cell activation, proliferation and function.

Other co-stimulatory receptors, such as CD2, ICOS and CD27 can partially compensate for the loss of function by CD28[63-65]. However, in the absence of CD28 co-stimulatory signalling, T cells cannot be fully activated by TCR-stimuli and become unresponsive to further antigenic stimulation, which is termed anergy[66]. This mechanism may be a preventative process, allowing for the elimination of self-reactive T cells that escaped negative selection in the thymus, since co-stimulatory molecules will not be expressed on APCs in the absence of infection or inflammation.

In addition to TCR- and co-stimulatory signalling, CD4+ T cells rely on cytokines, especially IL-2, as a crucial **third signal** for their activation. IL-2 is a 15.5-kDa glycosylated globular protein first identified as a T cell mitogen and growth factor[67,68]. The main producers of IL-2

are activated CD4+ and CD8+ T cells and it is important for both pro- and anti-inflammatory T cells[69]. Naïve T cells respond poorly to IL-2 since they only express the heterodimeric low-affinity IL-2 receptor (IL-2R), which is composed of a common cytokine receptor γ chain (γ_c, or CD132) and an interleukin-2 receptor beta (IL-2Rβ, CD122)[70]. TCR/CD28-stimulation upregulates the expression of IL-2Rα, which promotes the assembly of the high-affinity IL-2R (IL-2Rα, IL-2Rβ and γ_c). This confers robust downstream signalling from IL-2 in activated T cells, which enables their effective clonal expansion and effector development. The intracellular transduction of IL-2R signalling relies on the JAK family members. JAK1 and JAK3 bind to IL-2Rβ and γ_c, respectively, and undergo mutual phosphorylation[71]. This allows the recruitment of STAT5A and STAT5B transcription factors, which are subsequently phosphorylated and translocate as STAT5 dimers into the nucleus. The target genes of STAT5 mainly involve regulation of the cell cycle in T lymphocytes[72,73]. Moreover, STAT5 regulates the expression of a series of genes related to essential lineage-defining transcription factors, as well as cytokine receptors mediating effector differentiation, in CD4+ T cells[68,72,74,75]. Besides JAK-STAT signalling, IL-2 can also activate the RAS/MAPK and PI3K-AKT-mTOR pathways in T cells, which are also central to T cell activation[71]. Some studies indicate that a lack of IL-2R signalling does not lead to an impaired expansion of antigen-specific T cells in vivo in contrast to previous in vitro reports[76-79]. It is possible that the IL-2-independent expansion of T cells relies on other signals, e.g. the co-stimulatory receptor CD27, to compensate for the lack of IL-2R signalling[80]. Besides, IL-2 promotes programmed cell death of activated T cells upon TCR-mediated restimulation, which may contribute to the contraction of the effector population after clearance of the infection[81].

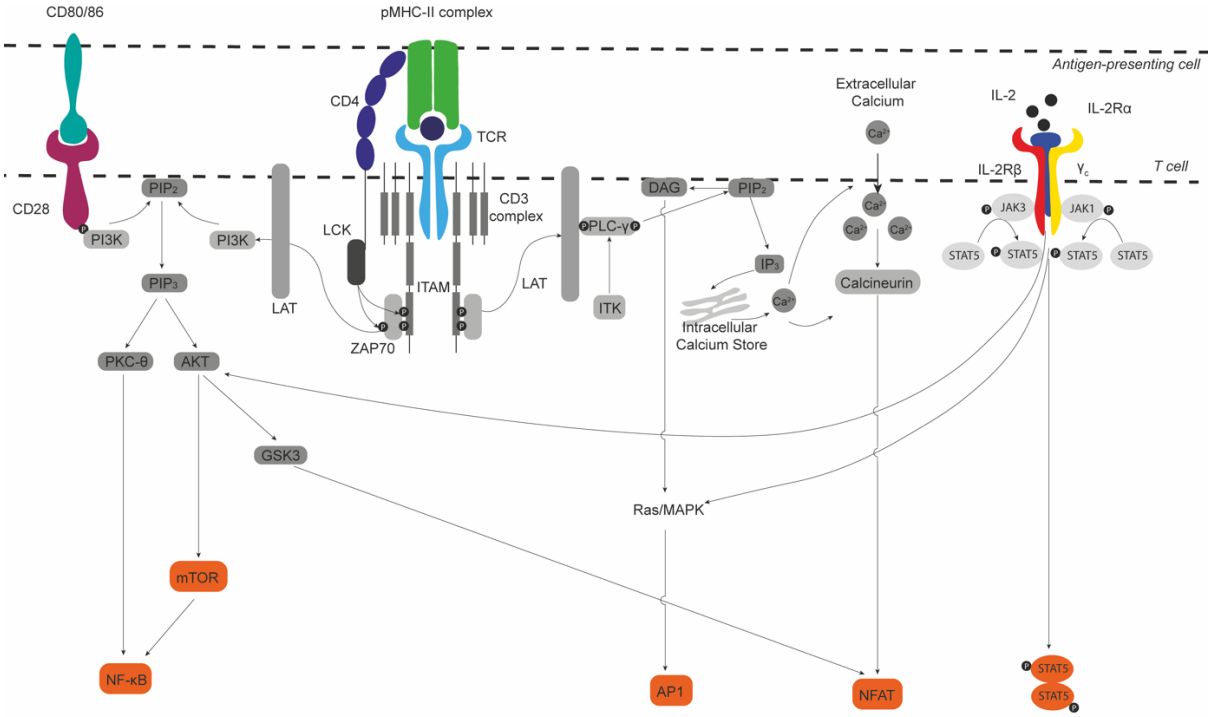


Figure 1.4 Three major signalling pathways mediating T cell activation.

The major signalling components and transcription factors responsible for the transduction of TCR, CD28 and IL-2R signalling pathways, following the recognition of cognate pMHC-II complex. AP-1, activator protein 1; AKT, protein kinase B; DAG, diacylglycerol; GSK3, glycogen synthase kinase-3; IP_3, inositol-1,4,5-trisphosphate; ITAM, immunoreceptor tyrosine-based activation motif; ITK, interleukin-2-inducible T cell kinase; JAK, janus tyrosine kinase; LAT, linker for activation of T cells; LCK, lymphocyte-specific protein tyrosine kinase; mTOR, mechanistic target of rapamycin; NFAT, nuclear factor of activated T cells; NF-κB, nuclear factor kappa-light-chain-enhancer of activated B cells; PLC-γ, phospholipase C-gamma; PKC-θ, protein kinase C theta; PIP_2, phosphatidylinositol-4,5-bisphosphate; PI3K, phosphoinositide 3-kinase; STAT5, signal transducer and activator of transcription 5; TCR, T cell Receptor; Zap70, ζ-chain associated protein kinase of 70 kDa.

Upon pMHC:TCR interaction, surface receptors including TCRs, co-receptors, co-stimulatory receptors and intercellular adhesion molecules, undergo reorganisation and get clustered at the interface between T cells and APCs. This highly dynamic, close-proximity structure is called an immunological synapse or supramolecular activation complex (SMAC) and depends on the actin cytoskeleton. Instead of being uniformly distributed, the surface molecules in the immunological synapses are organised into three distinct compartments: the central (c)SMAC, which is enriched in TCR, co-receptors and co-stimulatory receptors; the peripheral (p)SMAC containing integrin LFA-1 and the cytoskeletal protein talin; the distal (d)SMAC, which is

characterized by a high abundance of CD45 and F-actin[82]. The structure forms the basis of the integration and amplification of signals necessary for T cell activation enabling T cells to achieve high sensitivity to pMHC at single-molecule level[83-86]. Moreover, immunological synapses allow for a directional secretion of cytokine and signalling cascades. As such, it has been shown that IL-2, IL-4 and interferon-gamma (IFN-γ) are preferentially released into the cleft between the CD4+ T cells and APCs, while the secretion of tumour necrosis factor (TNF) and other chemokines occurs in a non-directional manner[87,88]. Importantly, IL-2R signalling is orientated to the T-T interface, which facilitates the capture of secreted IL-2[89]. To mimic the immunological synapse and T cell activation in vitro and recapitulate the SMAC pattern, lipid bilayers containing ICAM1 and pMHC (or anti-CD3) proteins are widely used[90,91].

Following the activation and clonal expansion, naïve CD4+ T cells can further differentiate into several lineages, including T helper (Th)1, Th2, Th17, Th9, regulatory T (Treg) and T follicular helper (T_{FH}) cells. They are characterised by the expression of lineage-specific transcription factors and thus enabling their cytokine production and functions[92]. Environmental cues (in particular the cytokine milieu), intracellular transcriptional networks and corresponding metabolic changes determine the type of T cell differentiation upon TCR-mediated activation[93].

In summary, a complete T cell activation requires sequential signalling through three types of receptors: TCR, co-stimulatory receptors and cytokine receptors. Many of these receptors are polarised as an organised structure at the interface of T cells and APCs, called the immunological synapse, to enhance the signalling. In the next section, I will introduce how autophagy contributes to the maintenance, differentiation and functions of CD4+ T cells.

1.3 Autophagy's role in CD4+ T cells

Autophagy regulates several aspects of adaptive and innate immunity, from maintenance of cellular homeostasis to functions like pathogen clearance and antigen presentation[94,95]. Much of our knowledge on the role of autophagy in T cells comes from CD8+ T cells, but I will focus on the less studied CD4+ T cells[94]. CD4+ T cells rely on both autophagy and CMA to maintain homeostasis, undergo effector expansion and differentiation, as well as memory formation and maintenance.

Autophagy plays a crucial role in the maintenance of peripheral T cell homeostasis. Several transgenic mouse models, whose T cells lack core autophagy genes (*Beclin1*, *Atg3*, *Atg5*, *Atg7*, *Atg16l1* or *Vps34*), display a lymphopenic phenotype in peripheral lymphoid tissues, due to a contraction of both CD8+ and CD4+ T compartments[96-103]. Interestingly, CD8+ T cells are more severely affected by autophagy deficiency compared to their CD4+ counterparts. An enhanced apoptotic level observed in these T cells has been loosely linked to the excessive oxidative stress and unfolded protein response, which is probably caused by impaired turnover of damaged organelles, such as mitochondria and ER[97,104,105]. The enhanced levels of proapoptotic proteins may also be attributed directly to the failure of removing some of these proteins in the absence of autophagy[100,105]. Moreover, naïve T cells exhibit a shift towards a more 'effector/memory phenotype', implicating autophagy in controlling the properties of naïve T cells. It seems plausible that many phenotypes observed in vivo are cumulative effects derived from the failure in maintaining cellular homeostasis in naïve autophagy-deficient T cells over time, such as it was observed in CD8+ T cells[106]. Especially, the inducible, short-term deletion of *Atg3* in T cells in vitro did not affect organelle homeostasis or CD4+ T cell survival[97]. Therefore, the consequences of autophagy's loss ought to be studied before the onset of lymphopenia to exclude any secondary effect on the T cells[107].

Both autophagy and CMA are induced by TCR/CD28-mediated activation and/or common gamma-chain receptor signalling in naïve and effector CD4+ T cells[37,96,105,107]. Studies using mouse models lacking key autophagy genes (*Atg3*, *Atg5*, *Atg7*, *Vps34*, *Becn1*) or CMA genes (*Lamp2a*) clearly demonstrate the importance of autophagy for naïve CD4+ cell proliferation both in vitro and in vivo[96-103]. Cell division is a complex and energy-consuming process requiring high abundance of biosynthetic materials. Autophagy, as a catabolic process, can degrade non-essential macromolecules and organelles, which can instantly provide fuel and building blocks for the synthesis of new macromolecules[108]. Indeed, autophagy guarantees sufficient ATP production through modulating aerobic glycolysis and mitochondrial respiration during effector T cell activation[107]. Moreover, TAX1BP1, an autophagic receptor, mediates the generation of L-cysteines to activate the mTOR signalling pathway, which is responsible for cell growth and proliferation during TCR-mediated activation[109].

Apart from regulating cellular metabolism, autophagy can modulate intracellular signalling pathways related to CD4+ T cell activation via selective degradation. One of the proteins that require autophagy-mediated degradation during T cell activation is the cyclin-dependent kinase inhibitor 1B (CDKN1B), a cyclin-dependent kinase (CDK) inhibitor contributing to cell cycle arrest[102,110]. *Atg7*-deficient naïve T cells fail to downregulate CDKN1B expression upon TCR/CD28-stimuli, indicating an indispensable role of autophagy in T cell proliferation. Moreover, in effector T helper (Th)1 cell, autophagy takes part in the turnover of protein tyrosine phosphatase non-receptor type 1 (PTPN1), a T-cell-anergy-related phosphatase dampening TCR/CD28-signalling[111-114]. In line with this, decreased PTPN1 expression and impaired induction of anergy are observed in autoimmune Th cells with enhanced autophagic flux, while inhibition of autophagy can rescue the phenotype[114]. It indicates that selective

autophagy may serve as a key mechanism to induce autoimmunity. In addition, the CMA-mediated degradation of ITCH, an E3-ubiquitin ligase that promotes the degradation of critical TCR signalling molecules, and RCAN1, a calcineurin inhibitor attenuating NFAT activity, is essential for a sustained TCR-signalling[96]. Diminished proliferation and cytokine production are observed in *Lamp2a*-deficient T cells upon antigenic challenges in vivo. In contrast to the above-mentioned activating roles of autophagy in T cells, autophagy in CD4+ Th2 effector cells can limit the TCR-induced NF-κB activation by selective degradation of B-cell lymphoma/leukaemia 10 (BCL10) in a p62-mediated manner[114]. Overall, we conclude from these studies that autophagy finely tunes CD4+ T cell activation and proliferation through removing key signalling molecules, possibly in a Th subset-specific pattern.

Autophagy also participates in the differentiation and function of effector T cells. Autophagy levels can be influenced through all of these context-specific signals and thus contribute to the acquisition of distinct Th cell functions. A mouse model bearing *Atg16l1*-knockout CD4+ T cells display an expansion of colonic Th2 population and loss of regulatory T cells (Tregs), while no significant change is observed in Th1 or Th17[115]. The loss of Tregs is probably caused by a metabolic shift from mitochondrial respiration to glycolytic metabolism due to the enhanced mTORC1 signalling and c-myc level induced by the impaired autophagy[116]. In contrast, *Atg7*-deficient CD4+ T cells in the liver of a diet-induced hepatic steatosis mouse model are prone to develop features of Th1 and Th17[117]. Moreover, autophagy limits Th9 formation via selectively degrading its master transcription factor PU.1[118].

The formation and maintenance of memory T cells also rely on autophagy[106,119-121]. Murera *et al.* reported that impaired autophagy leads to a dramatic contraction of the CD4+ central memory compartment in vitro, while the energy production in those cells seems to be normal[119].

The authors proposed that compromised survival of CD4+ memory T cells is caused by toxic effects of mitochondrial activity and excessive lipid storage, while another study indicates a metabolic role of autophagy in the maintenance of CD8+ memory population[119,120].

Though many studies indicate that autophagy contributes to different aspects of T cells, the underlying mechanism is still largely elusive. For the TCR-mediated proliferation of CD4+ T cells, it is likely that autophagy is required to selectively degrade a spectrum of molecules at different time points to lift the brake on T cell proliferation, which is finely tuned by multiple signalling pathways. In Chapter 5, I utilised a novel mouse model to map the autophagosomal cargoes of activated CD4+ T cells in unbiased way, and found the autophagy-mediated degradation of IL-7Rα as a new pathway required for CD4+ T cell proliferation.

1.4 Thesis Summary

Autophagy plays an essential role in differentiation, homeostasis and renewal of many immune cells[94]. Moreover, its dysregulation causes a variety of human diseases, including cancer, neurodegeneration, immune deficiencies. However, the autophagic cargo has largely not been elucidated in these contexts. Therefore, there was a need to develop a method that maps autophagic substrates that can be applied to different primary cells. During my thesis project, I generated and validated a mouse model that can identify autophagosomal cargo in a wide range of cell types and validated it in CD4+ T cells. The traditional method to investigate autophagosomal cargoes is lengthy and requires a large number of cells. Moreover, results are compromised by a high false-positive rate due to contaminants from other cellular components. Therefore, we created a mouse model based on the proximity biotinylation technique using LC3B, which can detect protein-protein interaction with high sensitivity and simplify the downstream purification procedures.

After obtaining the *Lc3b-AP2* mouse model, I first validated the expression, enzymatic function and autophagosomal localisation of the LC3B-AP2 protein (Chapter 3). After optimising the protocol of purifying biotinylated autophagosomal proteins adapted to the primary cells, I performed the proximity labelling on immortalised *Lc3b-AP2* MEF cells, which led to the identification of proteins expected as autophagosomal cargoes. Next, I investigated how autophagy contributes to the activation of CD4+ T cells, and how it is related to the age-associated phenotypes (Chapter 4). Based on the observations that autophagy-deficient CD4+ T cells fail to undergo antigen-induced expansion in vivo, I further confirmed that the autophagy-deficient CD4+ T cell proliferated later than their wildtype counterparts upon TCR/CD28-stimuli in vitro. I also aligned the findings with the phenotypes of the aged CD4+ T cells and explored why they displayed compromised autophagy and impaired proliferation. In Chapter 5, I used the *Lc3b-AP2* mouse model to investigate how autophagy contributes to the proliferation of CD4+ T cells mechanistically. I identified IL-7Rα as an autophagosomal cargo during CD4+ T cell activation. Furthermore, I found that the autophagy-mediated degradation of IL-7Rα was required for the assembly of the IL-2R complex and its signalling during $CD4^+$ T cell activation, which is crucial for the expansion of effector T cells. Therefore, I validated a novel mouse model which can help map the autophagosomal proteinaceous cargoes in primary cells. Moreover, I identified a new molecular mechanism related to CD4+ T cell activation, which can be harnessed to treat diseases in which T cells show aberrant levels of autophagic flux.

Chapter 2: Materials and Methods

2.1 Mice

All mice were bred and housed in the animal facilities at the Kennedy Institute of Rheumatology, Oxford. Mice were maintained in filter top cages under SPF conditions and fed *ad libitum*. *Lc3b-APEX2* mice were generated by Cyagen Biosciences Inc. in collaboration with C. Behrends, Munich. For creating this knock-in model, the ATG start codon of mouse endogenous Map1lc3b gene was replaced by the 'APEX2 tag- GGGGSGGGGS linker' using the bacterial artificial chromosomes. Young heterozygotes, male and female each, were crossed to C57BL/6J wildtype mice for colony expansion. Wildtype and heterozygote controls for each experiment were taken from the littermate. The OT-II; $Atg7^{flox/flox}$; $CD4^{Cre}$ mice and their littermate controls OT-II; $Atg7^{flox/wt}$; $CD4^{Cre}$ (interchangeably with OT-II; $Atg7^{wt/wt}$; $CD4^{Cre}$ since no phenotype was observed) were under the breeding of either OT-II; $Atg7^{flox/wt}$; $CD4^{Cre}$ x OT-II; $Atg7^{flox/wt}$; $CD4^{Cre}$ or OT-II; $Atg7^{flox/wt}$; $CD4^{Cre}$ x OT-II; $Atg7^{flox/wt}$; $CD4^{Cre}$. $CD4^{cre}$; $Atg16l1^{flox/flox}$ and *Cre-ERT2*; *Rosa-tdTomato*; $Atg16l1^{flox/flox}$ mice were from Kevin Maloy. Mice around two years old for the ageing experiment were collected from the wildtype female littermate of Gimap line or surplus B6 mice.

All mice were bred on a C57BL/6 background and all procedures were carried out in accordance with Home Office Animals (Scientific Procedures) Act 1986 and as allowed under personal and project licences (PIL: I44DFB4FA; PPL:30/3388). Experimental mice were used at 2-3 months of age unless otherwise specified.

2.2 Genotyping

DNA extraction and PCR

The identification of the mouse genotypes was performed on mouse ear clips. The ear tissue was lysed with 200 µl 50 mM NaOH at 95 ºC for 30 min. After adding 25 µl 1M Tris-base

buffer (pH = 8) for neutrolization, vortex the mixture and centrifuge 5 min at 16000xg at 4 ºC (max speed). The supernatant was used for conducting PCR or stored at -20 ºC.

The PCR reactions were performed with MyTaq™ Red Mix (Applied Biosystems, USA). Primers for the *Lc3b-APEX2*, CD4-Cre and *Atg7 flox*; Cre-ERT2 and Rosa-tdTomato transgenes were as follows:

Map1lc3b-APEX2 PCR

MLCB Fwd: 5'-GTGGGGAACCTCTCAACTGTCAG-3'

MLCB Rev: 5'-GTGGGGAACCTCTCAACTGTCAG-3'

DNA was amplified under the following conditions:

1. 94° C, 3 min
2. 94° C, 30 sec
3. 60° C, 35 sec
4. 72° C, 35 sec
5. 33× cycles from step 2
6. 72° C, 5 min
7. Hold at 12° C

CD4-Cre PCR

CD4 Cre Fwd: 5'-CGATGCAACGAGTGATGAGG-3'

CD4 Cre Rev: 5'-GCATTGCTGTCACTTGGTCGT-3'

Atg7 flox PCR

(WT fwd Primer) 752: 5'-CCATGCTGATGGCTAATGTCTC-3'

(Flox fwd Primer) 753: 5'-CTGCAGGAATTCGATATCATAACTTCG-3'

(Reverse Primer) Atg7-14R: 5'-GTCCAGAGTCCGGTCTCTGGTTG-3'

DNA was amplified under the following conditions:

1. 95° C, 1 min
2. 96° C, 15 sec
3. 65° C, 15 sec
4. 70° C, 10 sec
5. 30× cycles from step 2

6. Hold at 4° C

Cre-ERT2 PCR

Primer Cre1: 5'-AGGTTCGTTCACTCATGGA-3'

Primer Cre2: 5'-TCGACCAGTTTAGTTACCC-3'

Primer IntC500F: 5'-CCTCCGGAGAGCAGCGATTAAAAGTGTCAG-3'

Primer IntC500R: 5'-TAGAGCTTTGCCACATCACAGGTCATTCAG-3'

DNA was amplified under the following conditions:

1. 94° C, 4 min
2. 94° C, 30 sec
3. 60° C, 30 sec
4. 72° C, 1 min
5. 30× cycles from step 2
6. 72° C, 5 min
7. Hold at 4° C

Rosa-tdTomato PCR

oIMR9020: 5'-AAGGGAGCTGCAGTGGAGTA-3'

oIMR9021: 5'-CCGAAAATCTGTGGGAAGTC-3'

oIMR9103: 5'-GGCATTAAAGCAGCGTATCC-3'

oIMR9105: 5'-CTGTTCCTGTACGGCATGG-3'

DNA was amplified under the following conditions:

1. 94° C, 3 min
2. 94° C, 20 sec
3. 61° C, 30 sec
4. 72° C, 30 sec
5. 35× cycles from step 2
6. 72° C, 2 min
7. Hold at 4° C

PCR products were analysed on 2% agarose gel prepared in TAE buffer, which contains 0.01% SYBR® Safe DNA Gel Stain (Invitrogen, Life Technologies). Gels were run at 130V for around 25 min until the bands are fully separated. For Map1lc3b-APEX2 genotyping, the knock-in band is displayed at 347 bp while the wild-type band at 234 bp. For *Atg7* flox genotyping, *Atg7* flox allele displays the band at 160 bp while the wild-type shows at 220 bp. For Rosa-tdTomato genotyping, mutant allele displays the band at 196 bp while the wild-type shows at 297 bp. For Cre-ERT2 genotyping, internal control displays the band at 480 bp while the cre shows at 250 bp.

Tail vein sampling and surface staining

OT-II allele was tested through surface staining on mouse blood samples and flow cytometry. The mice were prewarmed in the warming cabinet at 38 ºC for 5 min, then transferred to the restraint tube and disinfected with 70% ethanol the location for sampling, which is approximately one-third along the length of the tail from the tip. 25G needle was used to puncture the lateral tail vein. Around 50µl blood sample was collected in the Microvette® CB 300 LH capillary tubes (Sarstedt, USA). CD4+ T cells were stained with anti-mouse TCRVα2 monoclonal antibody and identified with flow cytometry.

2.3 Preparation of Primary Cells

Total splenocytes

The mouse spleens were mashed by the rubber plunger end of the 2.5mL syringe (Appleton Woods) against 40m cell strainers (Fisher Scientific), with cold PBS containing 0.1% BSA and 2mM EDTA washing off the cells. After centrifugation at 400xg 4 ºC for 5 min and removal of the supernatant, the pellet was re-suspended with 3mL 1x RBC Lysis Buffer (eBioscience)

and incubate at room temperature with occasional shaking for 4 min. The reaction was stopped by adding 20mL cold PBS. After centrifugation at 400xg 4 ºC for 5 min, the cells were resuspended with PBS (with 2% FBS and 2mM EDTA) and ready for staining or cell sorting.

Mouse pan-T and CD4+ T cell isolation

Mouse T cells and CD4+ T cells were purified from total splenocytes with EasySep™ Mouse T Cell Isolation Kit (Stemcell™ Technology) and EasySep™ Mouse CD4+ T Cell Isolation Kit (Stemcell™ Technology), respectively. The total splenocytes was resuspended in sorting medium (PBS containing 2% FBS and 2mM EDTA) to 100 million/mL and transferred to the Falcon® 5 mL Round Bottom Polystyrene Test Tube (Corning). Mixed with 50μL/mL normal rat serum, cells were then incubated with the Isolation Cocktail for 10 min at room temperature. 75μL/mL Streptavidin RapidSpheres™ was vortex for 30 seconds before adding to the sample. After a period of 2.5 min incubation, sorting medium was topped up to 2.5mL. The Falcon tubes were placed into the magnet and incubated for another 2.5 min. Then solution was carefully transferred to new tubes for further experiment.

T-cell in vitro activation

T cells were cultured in RPMI-1640 Medium (Sigma-Aldrich) contains 10% Fetal Bovine Serum (Sigma-Aldrich), 2% penicillin-streptomycin (Sigma-Aldrich) and 2 mM L-Glutamine (Sigma-Aldrich). For antigen-induced activation, total splenocytes isolated from OT-II mouse spleens were cultured with OVA 323-339 peptide (InvivoGen) and recombinant murine IL-2 (20 ng/ml, PeproTech). For anti-CD3/CD28-induced activation, pan-T or CD4+ T cells were stimulated with Dynabeads Mouse T-Activator CD3/CD28 (Gibco) and recombinant murine IL-2 (20 ng/ml, PeproTech), following manufacturer's instructions.

2.4 Cell line generation

The mouse embryonic fibroblasts (MEFs) were generated according to the protocol3. In brief, *Lc3b-APEX2* homozygous embryos were separated from female uteri on E13.5. After removing the head above eyes and red organs (heart and liver), the rest of the embryos were minced and subjected to 0.25% Trypsin (Sigma) digestion, with intermittent pipetting up and down. Digestion was terminated by MEF culture media (Dulbecco's Modified Eagle Medium, Sigma-Aldrich) supplemented with 10% Fetal Bovine Serum (Sigma-Aldrich), 2% penicillin-streptomycin (Sigma-Aldrich) and 2 mM L-Glutamine (Sigma-Aldrich). Single cells and clusters were transferred onto the T25 flask and incubated with MEF culture media overnight. After replacing the old media and removing the debris, cells were passaged until reaching confluency.

To immortalise the *Lc3b-APEX2* cell line, MEFs were re-seeded to 6-well plates and transduced with the supernatant of the lenti-virus expressing SV40 small and large T antigens overnight. Monoclone immortalised MEFs were selected through dilution cloning and over 10 rounds of passaging.

2.5 Viral vectors and lentivirus production

pLenti CMV/TO SV40 small + Large T (w612-1) was a gift from Eric Campeau (Addgene plasmid # 22298). For packaging the virus, HEK293T cells were transfected with vector and replication-incompetent lenti-viral packaging constructs, harvested after 48-hour post transfection, and viral supernatants filtered through a 0.45 M cellulose acetate filter.

2.6 Bone marrow (BM) chimaera

Bone marrow chimaera was generated similarly as described before4. After erythrocyte lysis, BM cells extracted from a single 8-week-old wild-type or T-Atg7$^{-/-}$ (both CD45.2) were 1:1 mixed with C57BL/6 SJL mouse (CD45.1) in a total volume of 200 µl PBS, with 3 x 10^6 cells each. The mixture was injected intravenously into C57BL/6 SJL CD45.1 recipients 2 hours after being lethally irradiated (450 cGy twice, 4 hours apart.) Followed by an 8-week-reconstitution, BM chimaera was immunised with 1 x 106 PFU MCMV (Smith strain ATCC:VR194).

2.7 T-cell adoptive transfer

For adoptive transfer, 2 x 10^4 purified splenic OT-II T cells from CD45.2 wild-type or T-Atg7$^{-/-}$ mice were intravenously injected into C57BL/6 SJL CD45.1 recipients. After 24 hours, recipient mice were immunised with 1x10^6 IU recombinant adenovirus H5-ovalbumin.

2.8 Proximity Labelling

The proximity labelling based on APEX2 peroxidase was performed as described before. After 30 min biotin-phenol (500 µM, Iris Biotech) treatment at 37 °C, cells were supplemented with H2O2 (1 mM, Sigma-Aldrich) for 1 min and immediately quenched three times with cold quenching solution (10 mM sodium ascorbate, 5 mM Trolox and 1mM sodium azide in DPBS). After 3 times more wash with PBS, the dry pellets of the harvested cells were flash frozen and stored in -80 °C.

2.9 Proteinase K digestion

All steps were performed at 4 °C or on ice unless specified. The pellets of labelled cells were washed and re-suspended in Homogenisation Buffer I (10 mM KCl, 1.5 mM $MgCl_2$, 10 mM

HEPES-KOH and 1 mM DTT adjusted to pH 7.5). After incubating on overhead shaker for 20 min, cell suspension was homogenised with a tight-fitting pestle in Dounce homogeniser (Scientific Laboratory Supplies) with 70 strikes and balances with 1/5 volume of Homogenisation Buffer II (375 mM KCl, 22.5 mM $MgCl_2$, 220 mM HEPES-KOH and 0.5 mM DTT adjusted to pH 7.5). After centrifugation with 600x g for 10 min, clear supernatant containing autophagosomes were transferred to new tubes. For Proteinase K protection assay, supernatant was equally divided into four portions, added with 0.2% Triton X-100 (Merck) and/or 30 µg/mL proteinase K (Roche), or nothing. Following 30 min incubation at 37 °C, PMSF (10mM, Sigma-Aldrich) was administrated to inhibit the proteinase K activity. For mass spectrometry, samples were subjected to 100 µg/mL proteinase K digestion for 1 hour at 37 °C, followed by PMSF treatment. Membrane-protected material was enriched by centrifugation at 17,000x g for 15 min.

2.10 Streptavidin-pulldown and on-beads peptide digestion

The pellets of membrane-protected material were lysed with RIPA buffer containing quenchers (50 mM Tris, 150 mM NaCl, 0.1% SDS, 1% Triton X-100, 0.5% sodium deoxycholate, 1x cOmplete Protease Inhibitor Cocktail (Roche), 1x PhosSTOP (Roche), 10 mM sodium ascorbate, 1 mM Trolox and 1 mM sodium azide), sonicated and centrifuged at 10,000x g for 10 min. The supernatant was incubated with Streptavidin-agarose (Sigma-Aldrich) overnight, which was balanced with RIPA buffer containing quenchers. After 3x wash with RIPA buffer and 3x wash with 3 M Urea dissolved in 50 mM NH4HCO3, beads were incubated TCEP (5 mM, Sigma-Aldrich) at 55 °C for 30 min and shaken at 1000x rpm. Samples were alkylated with IAA (10 mM, Sigma-Aldrich) at room temperature for 20 min and shaken at 1000x rpm, further quenched by DTT (20 mM, Sigma-Aldrich) and washed 2x with 2 M Urea dissolved in 50 mM NH4HCO3. After overnight incubation with trypsin (1 µg/20 µl beads, Promega),

supernatants were collected, plus 2x washes with 2 M Urea buffer. The samples were acidified with trifluoroacetic acid (1%) and underwent vacuum centrifugation to decrease the volume. After being desalted on C18 stage tips (Thermo Scientific), peptides were reconstituted with 0.5% acetic acid and sent for mass spectrometry analysis.

2.11 Mass spectrometry data analysis

MaxQuant (version 1.6.10.43) were used for peak detection and quantification of proteins based on RAW data. MS spectra were searched referred to the manually-annotated UniProt Mus musculus proteome (retrieved 30/03/2020), using the Andromeda search engine with the parameters as follow: full tryptic specificity, allowing two missed cleavage sites, modifications included carbamidomethyl (C) and the variable modification to acetylation (protein N terminus) and oxidation (M), and filtered with a false discovery rate (FDR) of 0.01. Analysis of Label-free quantification intensities of proteins were log2-transformed with Python programming (Version 3.7.6). Missing values were replaced by random values from a distribution a quarter of the width, and -1.8 units of the original sample distributions. Proteins without greater-than-background values in both replicates for at least one condition were removed. Volcano plots were generated using GraphPad Prism software (Version 8.2.1). The $\log_2$(Baf:Ctrl) fold change of each protein is plotted on x versus the $\log_2$(p-value) of each protein plotted on y. Gene ontology analysis was performed with g:Profiler.

2.12 Flow cytometry

To assess the surface receptor level, cells were washed with ice-cold phosphate buffer saline (PBS) and incubated for 20 minutes at 4 °C in the dark, with cold PBS containing Fc block (0.125 g/ml Biolegend) and antibodies. After washing with cold PBS, cells were fixed for 10 minutes at room temperature with 2% Paraformaldehyde and analysed using LSRFortessa™

X-20 Cell Analyzer (BD Biosciences), LSR II Flow Cytometer (BD Biosciences) and Flowjo software (Tree Star). For intracellular staining of IL-7Rα, cells were fixed with Fixation Buffer (BioLegend) in the dark for 20 minutes at room temperature after surface staining, then permeabilised with Intracellular Staining Perm Wash Buffer (BioLegend) and incubated with anti-IL-7Rα antibody 1:100 diluted in Perm/Wash Buffer in the dark for 1 hour at room temperature. Cells were extensively washed with Perm/Wash buffer and resuspended with FACS buffer for further flow cytometry analysis.

To measure cell proliferation profile in vitro, cells isolated from mouse spleens were stained with CellTrace Violet (5 μM, Invitrogen) for 20 min at room temperature in dark. After extensive washing, cells were counted and seeded for activation.

To identify viable cells, cells were stained with LIVE/DEAD Fixable Aqua Stain Kit (1:400, Invitrogen) or LIVE/DEAD Fixable Near-IR Stain Kit (1:1000, Invitrogen) diluted with PBS at 4 °C for 20 min. For apoptosis detection, splenocytes were stained with surface antibody and LIVE/DEAD Fixable Aqua Stain Kit. The cells were stained with Annexin V APC (BioLegend) 1:50 diluted in Annexin V binding buffer (BioLegend). Apoptotic cells were gated on the LIVE/DEAD-negative, Annexin V-positive population.

Tetramer staining was performed similarly as previously described[106]. In brief, before surface staining, cells were incubated with 20ug/ml tetramer in PBS at 37 °C for 30 minutes.

For assessing the phosphor-Stat5 level, cells were fixed with pre-heated 2% PFA for 15 min at 37 °C after the live-dead staining, permeabilised with pre-cooled 90% methanol for more than

4 hours, and stained overnight with the phospho-Stat5 antibody diluted with 0.5% BSA in PBS at 4 °C overnight.

To measure the autophagic flux, cells were treated with Bafilomycin A1 (10 nM) or DMSO for 2 hours before staining. The staining was performed according to the manual of the Guava Autophagy LC3 Antibody-based Detection Kit (Luminex): After surface staining, cells were washed once with Assay Buffer. After permeabilised with 0.05% Saponin, cells were spun immediately and incubated with anti-LC3 (FITC) antibody (1:20 diluted in Assay Buffer) at room temperature for 30 minutes in dark. After extensive washing with Assay Buffer, cells were fixed with 2% PFA and underwent flow cytometry analysis. Autophagic flux was calculated as LC3-II mean fluorescence intensity of (BafA1-Vehicle)/Vehicle.

2.13 Lipid droplet staining

Cells were stained with 10 μM BODIPY (Invitrogen, D3922) diluted in DPBS for 20 min at room temperature, then topped up with PBS, spun down and washed once more with PBS.

2.14 SA-β-gal staining

Before staining, cells were incubated in the culture medium with 10 nM BafA1 for 1 hr, followed by the incubation with 2 mM C_{12}FDG (Invitrogen, I-2904) incubation for 2 hrs at 37 °C, 5% CO_2. After removing the medium, cells were centrifuged and washed twice with 2 mL cold PBS.

2.15 OPP-Click assay

20 μM Click-iT® OPP Reagent (Component A) (from Invitrogen, C10641) were added at the dilution 1:1000 to cell culture medium with cells for 30 min at 37 °C, 5% CO_2. After once

washing with PBS, cells were stained with surface markers and fixed with 4% PFA at room temperature for 10 min. Then, cells were permeabilised with 0.1% Triton X-100 in PBS at room temperature for 10 min. After washing with PBS twice, cells were incubated with 50 µL of Click-OPP reaction cocktail (all components from Invitrogen, C10641: 1x Click-iT OPP Reaction Buffer, Copper Protectant (Component D), 2.5 µM Alexa Fluor picolyl azide (Component B), 1x Click-iT Reaction Buffer Additive, top up with water) for 30 min at room temperature. To terminate the reaction, cells are topped up with PBS, spun down and washed once more with PBS.

2.16 IL-7Rα internalisation assay

IL-7Rα internalisation assay was performed similar as described before[122]. In brief, CD4+ T cells were purified from the spleens of wildtype and T-Atg7$^{-/-}$ mice. After incubating with biotin-conjugated anti-IL-7Rα antibody (BioLegend, A7R34) 1:50 diluted in DPBS on ice for 30 min, cells were extensively washed and fractionated into the following groups (5 x 10^6 cells/group): 90 min on ice, 90, 60 and 30 min at 37 °C, 5% CO_2. After incubation, cells were stained with AF647-Streptavidin (BioLegend), α-CD4 BV605 GK1.5 (1:400), anti-CD44 BV785 IM7 (1:400), LIVE/DEAD Fixable Aqua (Invitrogen) stain for 20 min on ice and fixed with 2% PFA. The % internalised IL-7Rα is calculated as the following equation (MFI: mean fluorescence intensity):

$$\% \text{ internalised IL-7R}\alpha = 100 - \left[\left(\frac{MFI\ sample}{MFI\ 90\ \text{min}\ ice}\right) \times 100\right]$$

2.17 Immunoprecipitation

Cells harvested from 15 cm plates were treated with trypsin and centrifuged down to form the pellet. The pellets were washed once with cold PBS and spun down. Each tube was re-suspended in 2 mL lysis buffer (50 mM Tris pH 7.5, 150 mM NaCl, 0.1% NP40, 1 mM EDTA, 5 mM $MgCl_2$, 10% glycerol, 1mM DTT) with protease inhibitor cocktail. Then samples were then frozen/thawed with dry ice three times, then added into the 1.5 mL tube to centrifuge at full speed for 10 min. Supernatant were collected for pull-down and input. Pull-down samples were mixed with 10 µL anti-FLAG M2 agarose beads (Merck, M8823) washed with lysis buffer (900 µL/tube). The samples were then added into 100 µL 1x loading buffer and boiled at 100 °C with 1000x rpm shaking.

2.18 Western blots

Cells were washed with cold PBS and lysed using RIPA lysis buffer (Sigma-Aldrich) supplemented with cOmplete Protease Inhibitor Cocktail (Roche) and PhosSTOP (Roche). Total protein concentration in supernatant after spinning down the debris was quantified by BCA Assay (23227, Thermo Fisher). Samples were added with 4x Laemmli Sample Buffer (Bio-Rad) and boiled at 100 °C for 5 min, with 20-30 µg protein per sample for SDS-PAGE analysis. 4–20% Mini-PROTEAN TGX Precast Protein Gels (Bio-Rad) with Tris/Glycine/SDS running buffer (Bio-Rad) was used. PVDF membrane (Millipore) transferred with protein were blocked with 5% skimmed milk-TBST. Membranes were incubated overnight with following primary antibodies diluted in 1% skimmed milk, followed by 1-hour room incubation at room temperature with secondary antibodies diluted in 1% milk with 0.01% SDS: IRDye 680LT Goat anti-Mouse IgG (H + L) (Licor, 1:7500), IRDye 680LT Goat anti-Rat IgG (H + L) (Licor, 1:10,000) and IRDye 800CW Goat anti-Rabbit IgG (H + L) (Licor, 1:10,000). Biotinylated proteins were detected by IRDye 680RD Streptavidin (Licor, 1:1000) diluted in 1% milk with

0.01% SDS. Membranes were imaged with the Odyssey CLx Imaging System (Licor). Data were analysed using Image Studio Lite (Licor).

2.19 Immunofluorescence staining and confocal microscopy

For intracellular staining of imMEFs and HeLa cells, cells were seeded on coverslips in tissue culture plates. After reaching 70% confluency, proximity labelled imMEFs (or HeLa cells without treatment) were washed with ice-cold PBS and fixed with 2% paraformaldehyde (Invitrogen) for 10 min, then permeabilised with 0.5% Triton X for 15 min and blocked with PBS containing 0.5% bovine serum albumin (Sigma-Aldrich) for 1 h at room temperature.

For intracellular staining of purified CD4+ T lymphocytes, cells were washed in PBS and transferred on PolyL-Lysine (Sigma-Aldrich) treated coverslips, followed by incubation for 30 min at 37 °C. For intracellular staining, cells were fixed with 2% paraformaldehyde (Sigma-Aldrich) for 10 min and permeabilised with 0.1% Triton X (Sigma-Aldrich) for 10 min, then blocked in PBS containing 2% bovine serum albumin (Sigma-Aldrich) and 0.01% Tween 20 (Sigma-Aldrich) for 1 h at room temperature.

For surface staining of purified CD4+ T lymphocytes, activated cells were washed in PBS and transferred on PolyL-Lysine (Sigma-Aldrich) treated coverslips, followed by incubation for 30 min at 37 °C. After cytokine treatment for 15 min, cells were washed and stained with antibodies at 4 °C for 20 min and fixed with 2% PFA.

After stained with antibodies for 45 min at room temperature and washed, samples were stained with DAPI (1 µg/ml, Thermo Fisher), mounted to slides with SlowFade Gold Antifade Mountant (Invitrogen), and imaged with Zeiss LSM 980 confocal microscope 63x oil

immersion-lens (Zeiss). Data were analysed with ZEN Blue (Zeiss) and ImageJ software. Pearson correlation coefficients were obtained using JACoP pug-in.

2.20 Supported Lipid Bilayer (SLB) preparation and use

Glass coverslips were plasma cleaned and mounted onto six-channel chambers (Ibidi). SLB were prepared as previously described[123], using 1,2-dioleoyl-sn-glycero-3-[(N-(5-amino-1-carboxypentyl) iminodiacetic acid) succinyl]-Ni (NTA-lipids, Avanti Polar Lipids), biotinylated 1,2-dioleoyl-sn-glycero-3-phosphoethanolamine (biotinyl cap PE-lipids, Avanti Polar Lipids) and 1,2-dioleoyl-sn-glycero-3-phosphocholine (DOPC-lipids, Avanti Polar Lipids). Channels in Ibidi chamber were covered with liposome mixture and after a 20 min incubation at room temperature, they were washed and blocked with 3% Bovine Serum Albumin (BSA) and 100 μM $NiSO_4$ for 20 min. After incubation with 10 μg/ml streptavidin, bilayers were incubated with mono-biotinylated 2c11 (anti-mouse CD3 antibody) and his-tagged mouse ICAM1-AF405, to reach a molecular density of 200 molecules/μm^2. Channels were washed and cells were added on the bilayer and incubated at 37°C for 10 min before fixation with 4% PFA. Next, samples were permeabilized with 0.1% Saponin for 10 min and blocked with 100 mM Gly 3% BSA for 30 min. Finally, samples were incubated with primary antibodies in 1% BSA.

2.21 Total Internal Reflection Fluorescence Microscopy (TIRFM) and image analysis

Imaging was performed on an Olympus IX83 inverted microscope equipped with a TIRF module. The instrument was equipped with an Olympus UApON 150 x 1.45 NA objective, 4-line illumination system (405, 488, 561 and 640 nm laser) and Photomertrics Evolve delta EMCCD camera. Image analysis and visualization was performed using ImageJ software. Pearson correlation coefficients were obtained using JACoP pug-in.

2.22 List of antibodies

Name/Target	Company	Clone	Cat#	Dilution
Immunofluorescence				
FITC-LAMP1	BioLegend	1D4B	121605	100
WIPI2 (manually conjugated with AF568)	Sigma	polyclonal	SAB4200399	100
AF647-Streptavidin	BioLegend	n.a.	405237	1000
LC3 (manually conjugated with AF488)	MBL International	polyclonal	PM036	100
APEX (manually conjugated with AF568)	made from Regina Feederle	polyclonal	n.a.	100
IL-7Rα (manually conjugated with AF488)	BioLegend	A7R34	135002	100
IL-2Rα (manually conjugated with AF568)	BioLegend	7D4/CD25	154202	100
γc (manually conjugated with AF647)	BioLegend	TUGm2	132307	100
DYKDDDDK(Flag) Tag Antibody	Cell Signaling Technology	M2	2368T	500
Western blot				
Atg16L1	Cell Signaling Technology	D6D5	8089T	500
CDK2	Cell Signaling Technology	E8J9T	18048T	1000
Roquin 2	Sigma-Aldrich	3F12	MABF288	500
LC3B	Cell Signaling Technology	D11	3868T	1000
APEX (IgG2A)	made from Regina Feederle	polyclonal	n.a.	200
GAPDH	Millipore	6C5	MAB374	10000
β-actin	Cell Signaling Technology	8H10D10	3700T	5000
Cullin 3	Cell Signaling Technology	polyclonal	2759S	1000
DYKDDDDK(Flag) Tag Antibody	Cell Signaling Technology	M2	2368T	1000
ATG9A	Abcam	EPR2450(2)	ab108338	1000
Vimentin	Cell Signaling Technology	D21H3	5741T	1000
Histone H3	Cell Signaling Technology	D1H2	4499T	2000
p62	MBL International	polyclonal	PM045	1000
Flow Cytometry				

BV605 anti-mouse CD4 Antibody	BioLegend	GK1.5	100451	400
AF700 anti-mouse CD3 Antibody	BioLegend	17A2	100215	200
PerCP/Cyanine5.5 anti-mouse CD25 Antibody	BioLegend	PC61	102029	200
APC/Cyanine7 anti-mouse CD62L Antibody	BioLegend	MEL-14	104427	400
PE/Cyanine7 anti-mouse CD69 Antibody	BioLegend	H1.2F3	104511	400
PE anti-mouse CD127 (IL-7Rα) Antibody	BioLegend	A7R34	135009	200
APC anti-mouse CD28 Antibody	BioLegend	37.51	102109	200
BV711 Hamster Anti-Mouse KLRG1	BD Bioscience	2F1	564014	200
PE/Cyanine7 anti-human, mouse, rat CD27	eBioscience	LG.7F9	25-0271-80	200
Phospho-mTOR (Ser2448) Antibody eFluor 450	Thermo Fisher Scientific	MRRBY	48-9718-42	50
Phospho-4EBP1 (Thr36, Thr45) Antibody PE	Thermo Fisher Scientific	V3NTY24	12-9107-42	50
Phospho-S6 (Ser235, Ser236) Antibody APC	Thermo Fisher Scientific	cupk43k	17-9007-42	50
Phospho-Akt (Ser473) (D9E) XP® Rabbit mAb	Cell Signaling Technology	D9E	5315S	50
Phospho-NF-κB p65 (Ser536) (93H1) Rabbit mAb	Cell Signaling Technology	93H1	5733S	50
BV711 Rat Anti-Mouse CD49d	BD Bioscience	9C10	740672	400
BD OptiBuild™ BV650 Rat Anti-Mouse CD122	BD Bioscience	5H4	740509	200
BV421 Rat Anti-Mouse CD132	BD Bioscience	TUGm2	740039	200
Phospho-Stat5 (Tyr694) (C71E5) Rabbit mAb (Alexa Fluor® 647 Conjugate)	Cell Signaling Technology	C71E5	9365S	100
TCR V alpha 2 Monoclonal Antibody (B20.1), APC	eBioscience	B20.1	17-5812-82	400
CD44 Monoclonal Antibody (IM7), eFluor 450, ™	eBioscience	IM7	48-0441-82	200
CD8 alpha Monoclonal Antibody (53-6.7), FITC	eBioscience	53-6.7	MA1-10303	400
20x Anti-LC3 FITC	Luminex	4E12	FCCH100171	20

2.23 Statistics

Data were displayed as mean ± SEM in bar graphs, or mean ± max/min value in box plots. P-values were determined by two-tailed Student's t-test with GraphPad Prism software (Version 8.2.1), with significant statistical differences displayed in the figure legends or graphs.

Chapter 3. Mapping the autophagosomal content using the *Lc3b-APEX2* mouse model – Introduction

3.1 Introduction

Since the term 'autophagy' was coined by Christian de Duve in 1963, the molecular machinery involved in different stages of autophagy was systematically screened in yeast and their mammalian homologs were identified[124,125]. Studies in humans and animals revealed indispensable roles of autophagy in different physiological contexts[126]. Mutations in core autophagy genes and aberrant autophagy levels have been linked to various human diseases, including cancer, infection, myopathies, metabolic, and neurodegenerative disorders. A spectrum of molecules and organelles have been shown to undergo autophagy-mediated degradation, giving rise to different forms of '-phagy' and deepening our understanding of underlying molecular mechanisms[127]. While it has been widely accepted that autophagy maintains cellular homeostasis through the removal of excessive or harmful cellular components and provision of energy and building blocks, it is still elusive what molecules need to be degraded by autophagy in specific cell types and physiological conditions. Therefore, a detailed characterization of autophagosomal cargo in primary cells is urgently needed to better understand the recycling process and in turn provide alternative therapeutic solutions for autophagy-related diseases. Although small molecules which can modulate autophagy activity have been suggested for clinical use[128-130], modulating autophagic flux may make individuals prone to develop other medical complications. Autophagy inhibitors hydroxychloroquine and chloroquine are being used to treat several types of cancers since cancer cells display higher reliance on autophagy than normal cells, however, autophagy inhibition may activate metastatically dormant cancer cells and lead to recurrence[130,131]. Instead, targeting specific autophagic substrates, either through modulating their downstream signalling pathways or diverting the substrates to the proteasomal degradation with proteolysis targeting chimeric (PROTAC) technology, may potentially increase the efficiency of treatment and minimise the side effects[132]. Therefore, profiling of autophagosomal cargo forms the basis for the discovery

of specific druggable targets and can as such open the field of new therapies to treat various types of diseases.

The cellular proteome undergoes constant changes in response to both external and internal stimuli and its remodelling is largely mediated by autophagy[133]. Therefore, the identity of autophagosomal substrates is highly dynamic and obtaining a snapshot of the in vivo autophagosomal substrates is challenging.

Two traditional methods to study autophagy cargoes include (1) subcellular fractionation to purify autophagosomes combined with mass-spectrometry and (2) whole-cell mass-spectrometry to quantitatively detect proteins upregulated in autophagy-deficient cells[133]. Subcellular fractionation to purify autophagosomes relies on extensive gradient ultracentrifugation. To maximise the purification efficiency, it is necessary to optimise the protocol for each specific cell type, which is, in turn, highly time-cosuming[134,135]. Moreover, a relatively large number of cells (100 million) is required due to protein loss during the multiple centrifugation steps[114]. This usually becomes an issue for research in primary cells. Additionally, other cellular components may contaminate the sample and can prevent the discovery of bona fide autophagosomal proteins. On the other hand, identifying proteins accumulated in autophagy-deficient cells by whole-cell mass-spectrometry has its own issues, as loss of autophagy leads to failed differentiation and survival of many cells types, making it difficult to delineate the autophagy degradome in these cells[94]. Moreover, cells may adapt to autophagy deficiency with homeostatic changes. Therefore, the upregulation of some proteins can be due to enhanced transcription or translation rather than impaired degradation, which can confound the proteomics results. For these reasons, a novel method to detect the bona fide autophagosomal cargoes with high specificity and a simplified procedure is urgently needed.

3.1.1 A novel technique to screen for protein-protein interactions

There are two conventional methods to screen for protein-protein interactions: yeast-two hybrid and affinity purification combined with mass spectrometry. Yeast-two hybrid is a powerful tool to map the protein-protein interactome in vivo[136]. However, since it is performed in yeast rather than mammalian cells, the method cannot easily be applied to specific types of proteins, like membrane proteins. Targets of the yeast-two hybrid assay are also limited to stable protein complexes with binary interactions. By contrast, antibody-based affinity purification can enrich the endogenous proteins of interest and their interacting partners in vitro, enabling the screening for complexes composed of multiple subunits[137]. Nevertheless, this method is unable to identify weak or transient interactions, cannot be applied to insoluble protein baits, and its purification efficiency relies on the affinity of antibodies.

Proximity labelling has opened a new era to study molecular interactions. To find binding partners of a protein or proteome within a subcellular organelle, a protein of interest (or a specific protein in the organelle) is genetically fused with engineered enzymes[138]. With the addition of substrates, these enzymes can trigger the biochemical reaction to convert the inert tags (usually biotin or its derivatives) into short-lived, highly reactive species. These can then diffuse from the enzyme's active site and covalently tag neighbouring proteins. Since the labelling radii for enzymes usually fall in a range of 1– 10 nm, only proteins in proximity to the enzyme can be labelled[139]. Moreover, the reactive species are membrane impermeant, which enables the profiling of subcellular proteome to be restricted to proteins that fall within a membrane boundary[140]. After the affinity purification of the tag, the labelled proteins then undergo peptide-sample preparation and mass spectrometry analysis.

Enzymes used for proximity labelling fall into two categories: engineered peroxidases (engineered ascorbate peroxidase 2 - APEX2, horseradish peroxidase - HRP) and biotin ligases (proximity-dependent biotin identification - BioID, BioID2, BASU, TurboID, miniTurbo)[138]. APEX2 can transform inert biotin-phenol into its radical form upon the addition of H_2O_2, which preferentially reacts with electron-rich amino acid residues[140]. By contrast, BioID and TurboID can catalyse ATP and biotin to combine into biotin-5′-AMP, a highly reactive amine, which can diffuse and react preferentially with Lysine residues[141]. The half-life of the reactive species is determined by the local concentration of quenchers in vivo, which is glutathione for APEX, and amines for BioID and TurboID[138]. To further control and fix the reaction time, additional quenchers are administrated, which enables the interrogation of the proteome with high temporal resolution.

Proximity labelling has been applied to dissect signal transduction networks and enzyme-substrate interactions in which protein-protein interactions are transient and cannot be unravelled by traditional methods[138]. The method has also been extended to study insoluble protein complexes (protein aggregates) or structures with low solubility (nuclear structure networks)[142-145]. Proximity labelling has been conducted in several model organisms, including bacteria, yeast, flies, worms, mice, and even human tissue, allowing a direct screening of protein-protein interactions in primary cells ex vivo and in vivo[138].

3.1.2 Proximity labelling technique to map autophagosomal cargoes

As mentioned above, the identification of autophagosomal substrates is particularly important to understanding the role of autophagy. However, the full spectrum of proteins degraded by autophagy remains poorly defined. Autophagosomes can be identified and purified by LC3, an ATG8 homologue. While many of the other autophagy molecules only transiently interact with

autophagosome precursors up to the stage of the mature autophagosome, the lipidated form of LC3 is consistently anchored to the autophagosomal membrane.

Le Guerroué et al. employed the proximity labelling technique to profile potential autophagosomal substrate proteins in the HeLa cell line by overexpressing APEX2 fused with hATG8, an autophagosome-enriched protein[146]. In this study, 6 mammalian hATG8 homologues (LC3A, LC3B, LC3C, GABARAP, GABARAPL1 and GABARAPL2) were genetically tagged with APEX2 and cells stably expressing the constructs underwent proximity labelling and quantitative mass spectrometry analysis. Over a thousand non-redundant biotinylated proteins were identified and displayed a substantial overlap with previously autophagosomal fractionations[147-149]. While candidates upregulated by BafA1-treatment largely overlap across different GABARAPs, LC3 subfamily members show a minimal overlap, indicating a different spectrum of interaction partners across ATG8 homologues. Among all six hATG8 homologues, LC3B-baited candidates displayed the highest reproducibility with the largest number of protein candidates identified, implying that LC3B may mediate the degradation of a broader range of molecules. Therefore, we chose LC3B as the protein bait in our proximity labelling mouse model.

To this end, we designed a transgenic *Lc3b-APEX2* knock-in mouse model based on the published protocol. Why we chose APEX2 was because it was the most efficient enzyme for proximity labelling to date. APEX2 sequence is inserted into the N-terminal end of the endogenous *Lc3b* allele (Figure 3.1) since its C-terminal end is subjected to lipid-conjugation and crucial for its autophagosomal localisation (Figure 3.1)[150]. We also added a flexible GS-linker in between to minimise the steric interference of APEX2 on LC3B. APEX2 genetically fused to LC3B can oxidise biotin-phenol molecules into radicals in the presence of H_2O_2

(Figure 3.2). These highly reactive biotin-phenol radicals further react with proteins in proximity to the APEX2 enzyme inside the autophagosomes. Proteins labelled by the LC3B-APEX2 on the cytosolic side of the autophagosome are removed by proteinase K digestion, while proteins inside are protected by the double-membrane structure. This enables the labelling of autophagosomal cargoes with high specificity and efficiency. Biotinylated proteins are pulled down with streptavidin-based enrichment and analysed by mass spectrometry. For the first time, this model enables us to perform proteomics analysis of the autophagosomal cargo in specific cell types ex vivo.

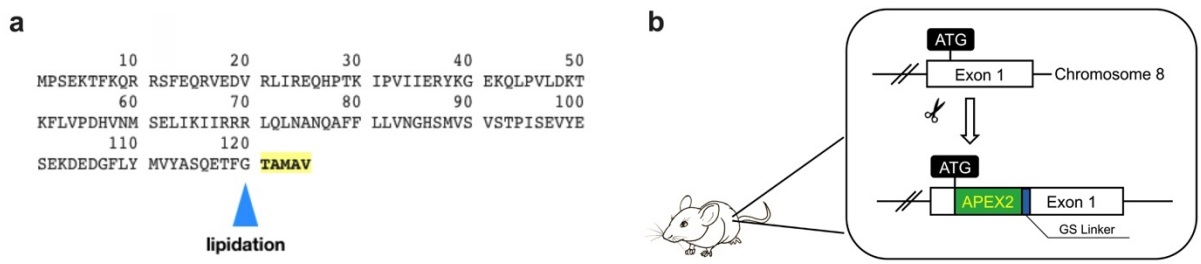


Figure 3.1 Amino acid sequence of pro-LC3B and knock-in strategy.

a) The amino acid sequence of pro-LC3B displayed from N-terminal to C-terminal end. The C-terminal end of pro-LC3B is subjected to ATG4 protease cleavage and lipidation, which is highlighted with the blue arrowhead. b) Schematic overview of the construct for generation of *Lc3b-APEX2* transgenic mouse model. APEX2 sequence and a GS-linker is knocked into the endogenous *Lc3b* locus directly after the ATG-start codon.

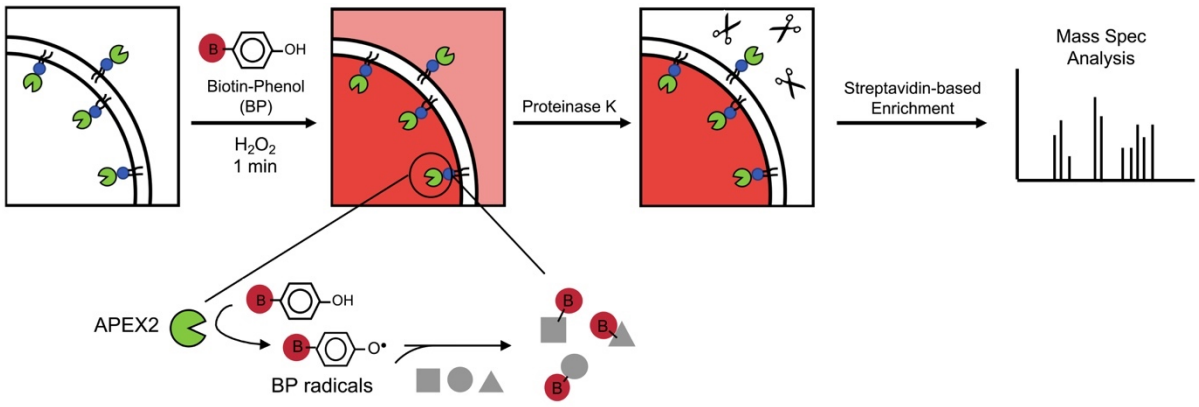


Figure 3.2 Schematic overview of autophagosome targeting and labelling using LC3B-APEX2.

APEX2 can oxidize biotin-phenol (BP) molecules into radicals in the presence of H_2O_2. These highly reactive biotin-phenol radicals further react with electron-rich amino acids. In turn, proteins in proximity to the APEX2 enzyme will be labelled with biotin (B) for further purification. By fusing this enzyme with the autophagosome-specific protein LC3, proteins inside the autophagosome can be labelled with high specificity and efficiency. After the digestion of proteins outside autophagosomes by Proteinase K, biotinylated autophagosomal cargos are pulled down and analysed by mass spectrometry.

Chapter 3. Mapping the autophagosomal content using the *Lc3b-APEX2* mouse model – Results

3.2 Results

3.2.1. Generation and validation of mouse model: genotyping and knock-in site sequencing

For mouse genotyping, we followed the protocol suggested by Cyagen, the company that generated the mouse model. Mouse genome DNA was extracted with hot-shot alkaline lysis and neutralisation. As expected, the LC3B wild-type allele showed bands around 347 bp, and the knock-in allele around 234 bp (Figure 3.3).

Before studying the expression of LC3B-APEX2 chimeric protein, the sequence of the knock-in site was checked to guarantee that there were no mutations in the APEX2 enzyme sequence. Based on the method of purification with proteinase K, DNA from *Lc3b-APEX2* homozygotes was purified and the PCR-amplified region was extracted. As the result show (Figure 3.4), the sequence was consistent with the known sequence of APEX2, GS-linker and endogenous *Lc3b*. After confirming the mouse model at the genomic level, we next proceeded to investigate the protein expression.

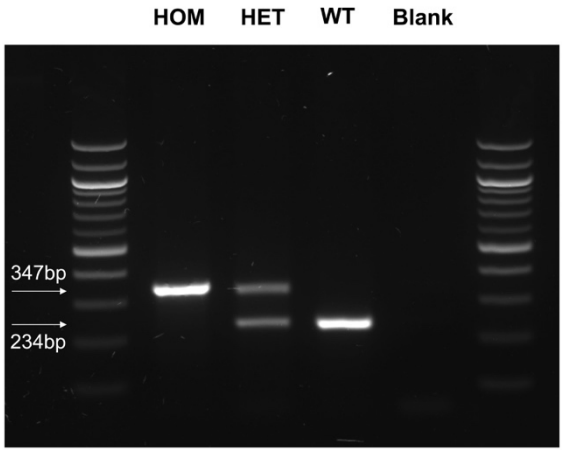


Figure 3.3 PCR result of LC3B-APEX2 mouse DNA.

WT, wild-type; HET, heterozygote; HOM, homozygote. Wild-type LC3B allele shows a band at 234 bp and APEX2-knockin allele displays a band at 347 bp.

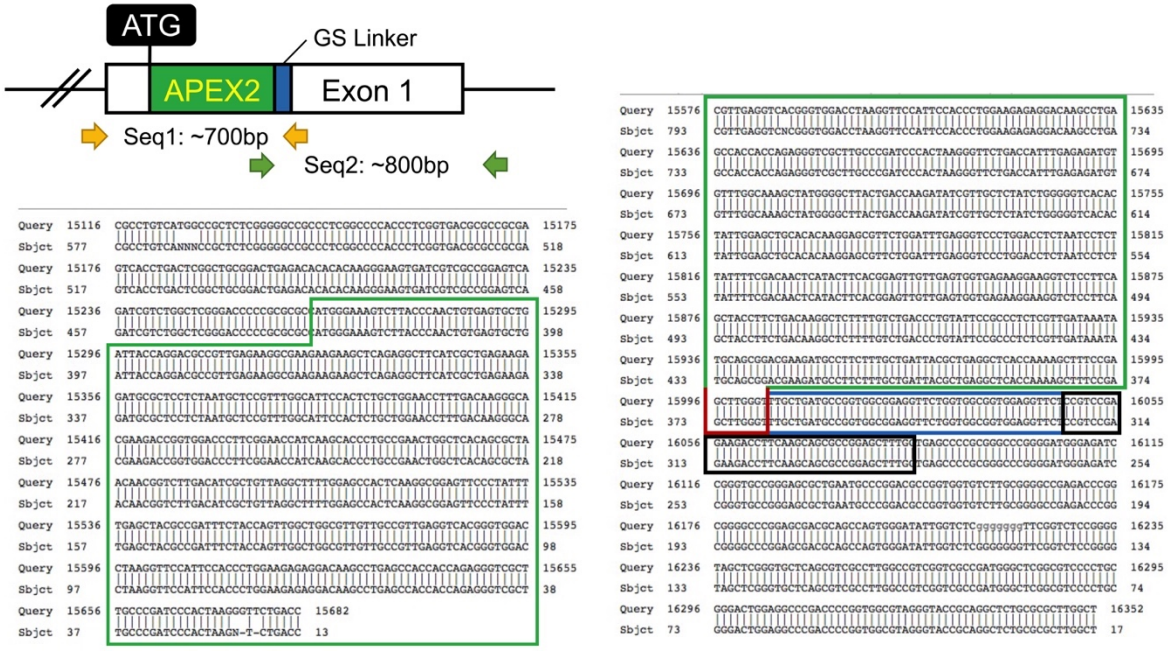


Figure 3.4 Confirmation of the genomic sequence of *Lc3b-APEX2* mice.

Two pairs of primers were designed to cover the whole range of exon 1 region of mouse *Lc3b*. Both sequences were aligned to a gene map provided by the company. The red box indicates APEX2, the blue box indicates GS linker, and the black one includes a part of *Lc3b*.

3.2.2. Expression of the LC3B-APEX2 chimeric protein

Since APEX2 sequence is directly knocked into the endogenous *Lc3b* locus, the *Lc3b-APEX2* homozygotes should express the chimeric protein only with a molecular weight around 44 kDa (LC3B ~ 17 kDa and APEX2 ~ 27 kDa)[151]. As expected, the protein lysate from homozygote mice only showed bands around 44 kDa (Figure 3.5). By contrast, heterozygotes showed two bands, around 17 kDa and 44 kDa, indicating that both the endogenous LC3B protein and the LC3B-APEX2 chimeric protein are expressed.

As introduced above, LC3 has two major isoforms, a cytosol-free LC3-I and a membrane-bound LC3-II, which undergoes a post-translational modification and is conjugated with phosphatidylethanolamine lipid tails when the autophagy machinery is active in the cell. The two isoforms can be distinguished with Western Blotting, since the lipid-conjugated form undergoes faster electrophoresis due to its lipophobic nature, usually displaying a 2 kDa difference[152]. From the membrane, we see that the LC3B-APEX2 protein also displays two bands, indicating that the chimeric protein can be conjugated with lipid tails like the endogenous LC3 protein. When administrating Bafilomycin A1 (BafA1), a drug that stops the autophagosome-lysosome fusion, LC3 is no longer degraded and accumulates in the cell. In immunoblot, both endogenous LC3B-II and LC3B-II-APEX2 signals were increased upon BafA1 treatment, indicating that the chimeric protein is also degraded by the autophagic flux and therefore localised in the right compartment, the autophagosome. In conclusion, we validated that the LC3B-APEX2 chimeric protein is expressed and functional in our mouse model.

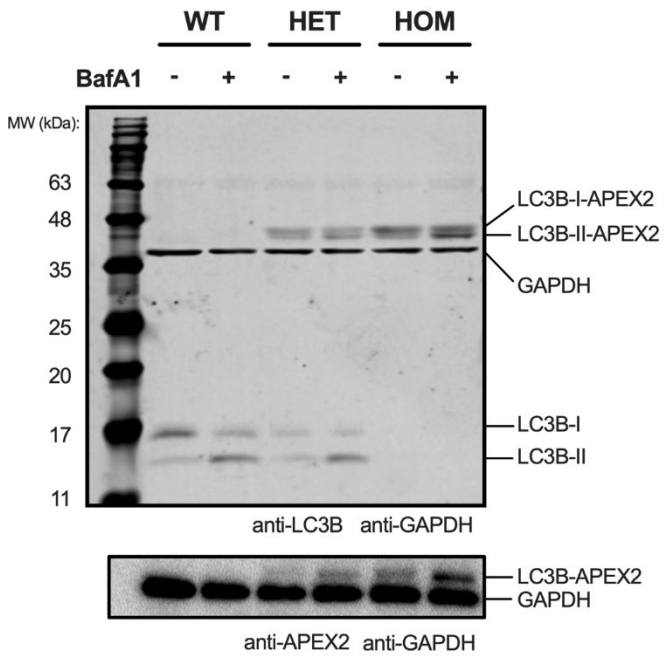


Figure 3.5 Western blot of LC3B-APEX2 chimeric protein.

Western blot was performed on whole cell lysate of total splenocytes from wild-type, heterozygous, and homozygous mice, with or without 10 nM BafA1 treatment for 2 hours. LC3B (upper) and APEX2 (lower) is indicated at the expected sizes. The experiment was repeated as biological triplicates with similar results.

3.2.3. Enzymatic function of the APEX2-LC3B

In contrast to HRPs, whose enzymatic activity is hugely impacted by the local chemical environment, the engineered APEX and APEX2 peroxidases can be applied to cell compartments with a large range of pH and ionic strength[140]. However, we were unsure whether its enzymatic activity remains intact in our in vivo model. To check enzymatic function of the protein, splenocytes from both wild-type and homozygote animals were activated with LPS for three days to enhance the autophagic flux[153]. Cells from homozygotes treated with both biotin phenol and H_2O_2 displayed the strongest biotin bands (Figure 3.6). As Figure 3.6 shows, some biotin bands consistently appear in both wild-type cells or when lacking one or both substrates. Four endogenously biotinylated proteins were identified in mammalian cells, including propionyl-CoA carboxylase (72 kDa), 3-methylcrotonyl-CoA carboxylase (75 kDa), pyruvate carboxylase (130 kDa), and acetyl-CoA carboxylase (220 kDa), mainly enriched in mitochondria[154]. Molecular weights of the observed bands (pointed with arrows in Figure 3.6, around 75 kDa, 135 kDa and 245 kDa ladder) are consistent with the size of these proteins, which implied the identities of the observed bands as these known endogenously biotinylated proteins. In contrast, wild-type cells supplemented with both biotin-phenol and H_2O_2 and homozygote cells supplemented with H_2O_2 also displayed a diffuse range of biotin signal which was less strong. This is probably due to the presence of biotin derivatives and intracellular peroxidases in the culture system and was also seen in the previous in vitro study by Le Guerroué et al.[146]. In the following steps, these contaminating bands can be controlled for by using BafA1 to ensure identification of autophagosomal cargo only. We proceeded to the next step to create immortalised embryonic fibroblasts (imMEFs) from these mice to validate that our strategy can be applied to this cell type.

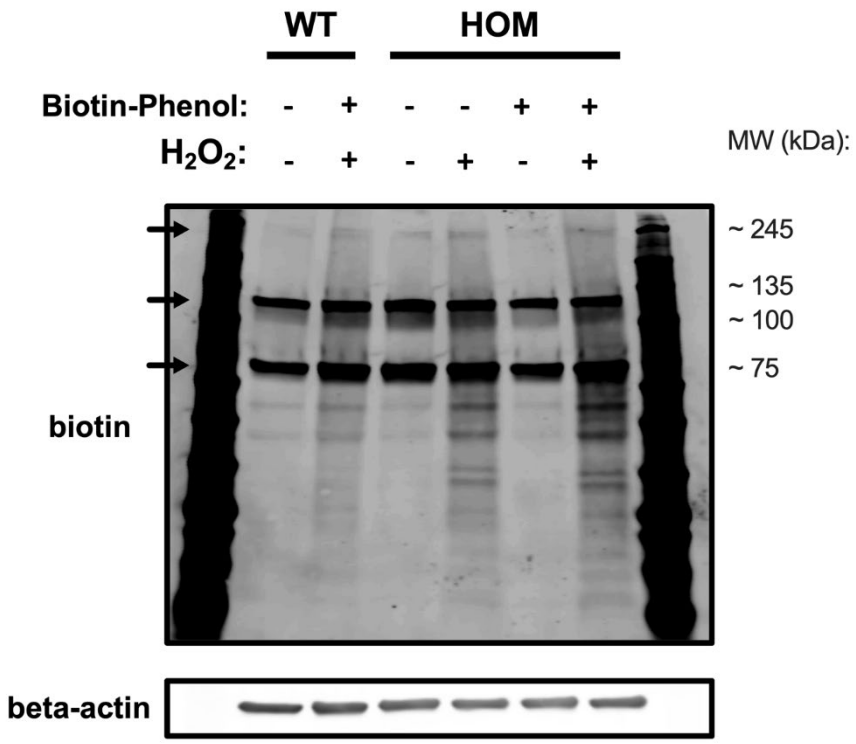


Figure 3.6 Western blot of proximity-labelled splenocytes.

Total splenocytes from wild-type or homozygous mice were activated with 10 μg/mL LPS for 3 days. Cells were labelled with biotin-phenol and/or H_2O_2. The experiment was repeated three times in total with similar results. Arrows indicate the bands of endogenously biotinylated proteins. MW: molecular weight.

3.2.4. Examination of biotinylated proteins within different cell fractions

To identify in which cell fractions the biotinylated proteins are enriched, we performed cell fractionation on proximity-labelled imMEFs and analysed the fractions on a western blot. The imMEFs were generated from *Lc3b-APEX2* homozygous embryos according to published protocols and immortalised with lentivirus expressing SV40 small and large T antigens[155]. As Figure 3.7a shows, the LC3 signal is enriched in the cytoplasmic fraction as LC3-I and the organelle fractions as LC3-II, consistent with the cellular localisation of its two isoforms. LC3 was originally discovered as a microtubule-associating protein in rat brain[156]. Although the LC3 signal is absent from the cytoskeletal fraction, the biotin signal indicates strong labelling of endogenous proteins in both organelle and cytoskeletal fractions (Figure 3.7b). It is likely that there is very little LC3 attached to the cytoskeleton (a) which can be, however, amplified by biotin labelling (b). As expected, a strong signal can be found in the organelle membrane fraction, further implying that the LC3B-APEX2 protein performs its enzymatic role in this cellular compartment.

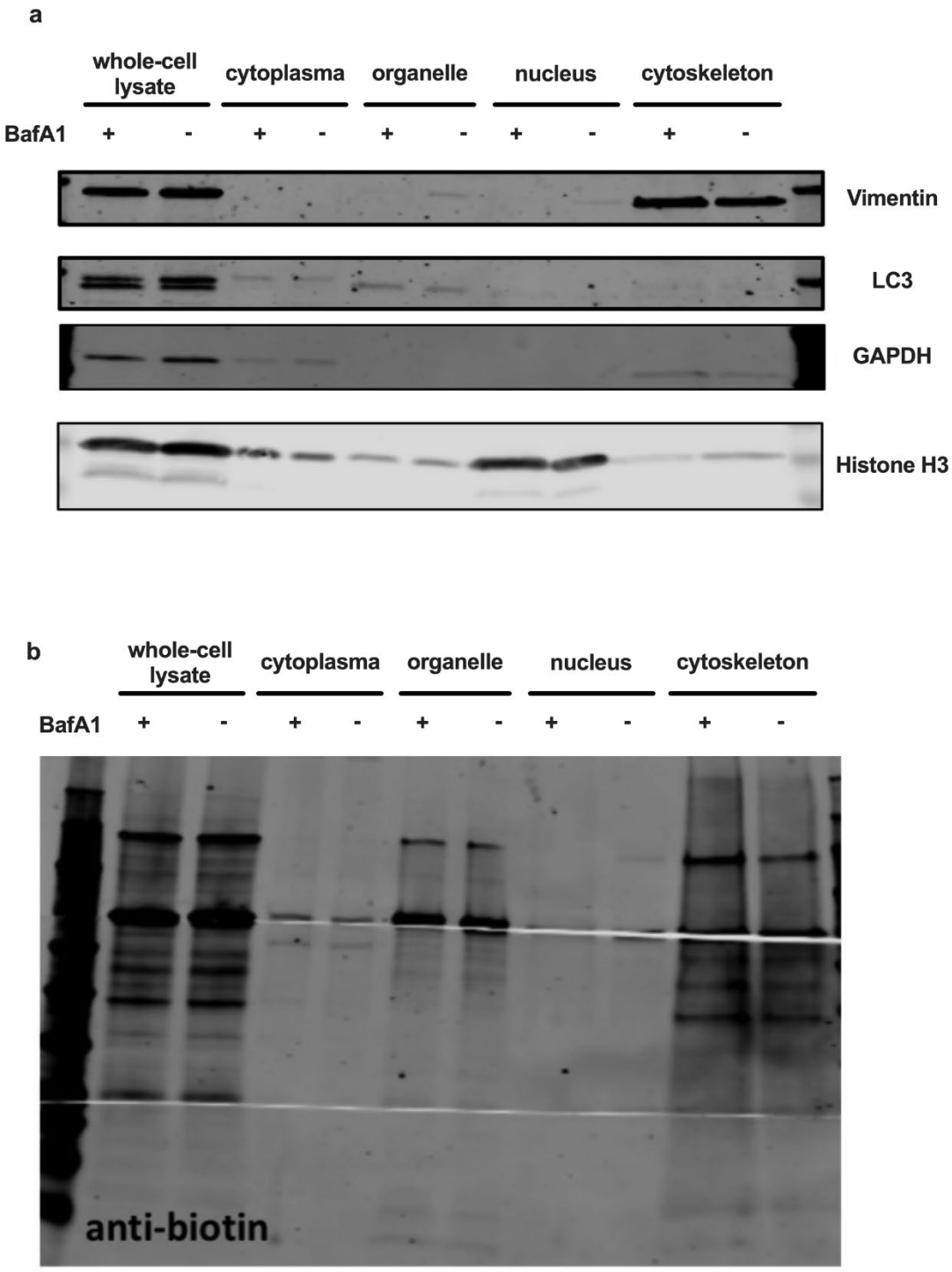


Figure 3.7 Western blot of different cell fractions from proximity-labelled imMEFs.

a) imMEFs were incubated with BafA1 (100 nM) or DMSO for 2 hours before fractionation. Vimentin is a cytoskeleton marker, Histone H3 is a nuclear marker, and GAPDH is a cytosolic marker. All these markers are expressed in the whole cell lysate and further enriched in different cell fractions. b) Streptavidin blot showing biotinylated proteins in each cell fraction.

3.2.5. Co-localisation of biotinylated proteins with LC3B-APEX2 chimeric protein and LAMP1

To validate whether biotinylated proteins are enriched in the targeted compartment, we performed proximity labelling in imMEFs followed by staining the cells with anti-APEX2, biotin and LAMP1 for confocal imaging. As Figure 3.8 shows, biotin-positive puncta are co-localised with the LC3B-APEX2 containing compartment, indicating that APEX2 protein can effectively label proteins in LC3B-APEX2-enriched structures. Upon BafA1 treatment, biotin-positive puncta appear partially colocalised with the lysosomal marker LAMP1, indicating that mature autophagosomes containing the LC3B-APEX2 complex reach the lysosomal compartment.

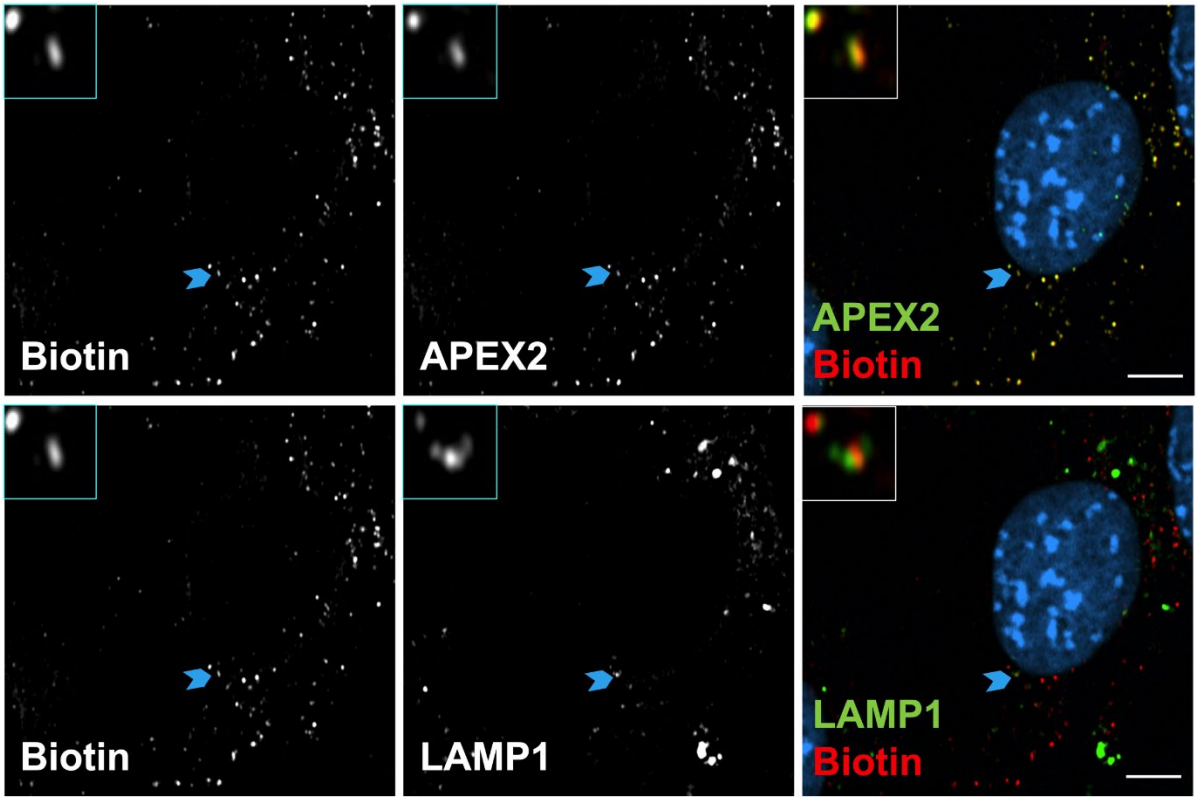


Figure 3.8 Confocal microscopy images of proximity-labelled imMEF cells.

ImMEFs made from the *Lc3b-APEX2* mouse model were treated with 100 nM BafA1 or DMSO for 2 hours. Cells were proximity-labelled and stained for biotin, APEX2 and LAMP1. Light blue arrows indicate colocalization events with magnifications at the upper-left corners. Scale bar: 5 μm.

3.2.6. Proteinase K protection assay

To validate whether the LC3B-APEX2 chimeric protein is anchored to an autophagosomal inner membrane, a prerequisite to label luminal proteins, we performed the proteinase K protection assay. Proteinase K can digest proteins outside and on the surface of the autophagosome, while the substrates residing inside the autophagosomal lumen are protected by its double-membrane structure[157]. Upon treatment with Triton-X, a strong detergent able to break the membrane, Proteinase K gains access to the autophagosomal lumen and degrades proteins inside. Homogenates extracted from proximity-labelled imMEFs were divided into four equal parts and incubated with proteinase K and/or Triton-X, or either. Compared to untreated or Triton-X-only controls, bands of p62, APEX2 and biotinylated proteins were partly preserved when the sample was treated with proteinase K only (Figure 3.9). On the other hand, ATG9A, a multi-span transmembrane protein, was completely removed by proteinase K digestion. Administration of both proteinase K and Triton-X completely degraded all proteins. These results confirmed the intraluminal localisation of LC3B-APEX2 protein and the protective effect of autophagosomal membranes upon proteinase K-digestion.

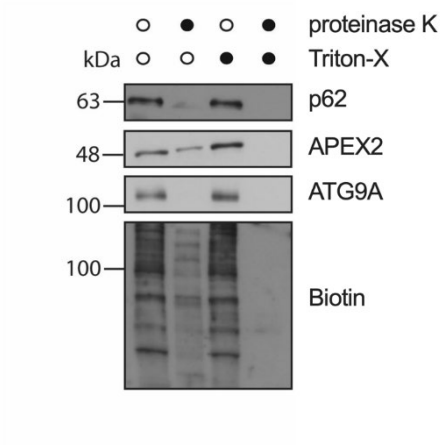


Figure 3.9 Western blot of imMEFs undergoing proteinase K protection assay.

Homogenates from imMEF were labelled, then left untreated or incubated with proteinase K, Triton-X, or both, and protein levels were assessed by immunoblotting. Courtesy of Susanne Zellner.

3.2.7. Optimisation of the purification of biotinylated proteins

We further optimised the protocol of autophagosomal cargo purification. As Figure 3.10a shows, the purification follows three main steps: (1) homogenising cells to release organelles, (2) removing proteins outside the autophagosomes with proteinase K and enriching the autophagosomes, and (3) pulling down biotinylated proteins with streptavidin-agarose beads. To test the pull-down efficiency, we split the whole cell lysate of imMEF cells, with one half being incubated with streptavidin beads and then eluted with loading buffer, while the other half was directly assessed by a western blot (Figure 3.10b). The intensities of biotinylated bands between the two conditions mentioned above were similar, indicating a high pull-down efficiency. Next, we titrated the concentration of PMSF, a proteinase K inhibitor. The original protocol recommended we stop the proteinase K activity with 10mM PMSF, which is much higher than the usual working concentration of 0.1-1mM. When supplemented in excess amount, PMSF precipitates after being centrifuged at 4 °C, leading to the formation of a loose and fragile pellet along the tube wall, rather than a solid pellet at the bottom of the tube, which makes the removal of the supernatant without disturbing the pellets containing the autophagosomes more difficult. We observe that 1mM PMSF is enough to inhibit the proteinase K activity (Figure 3.10c). More importantly, the compacted pellets formed under this condition retain more autophagosomal proteins (image not shown). Therefore, 1 mM PMSF was used in the following proximity labelling experiments. Next, we proceeded to trypsin digestion of samples for mass spectrometry. Figure 3.10d shows that the samples with trypsin digestion displayed no biotin signal, which means that the proteins were completely digested into small peptides. Figure 3.10e indicates that biotinylated proteins were enriched in fraction A (cell debris) and fraction E (elutes from the beads), while fraction B and fraction C showed very low biotin signals.

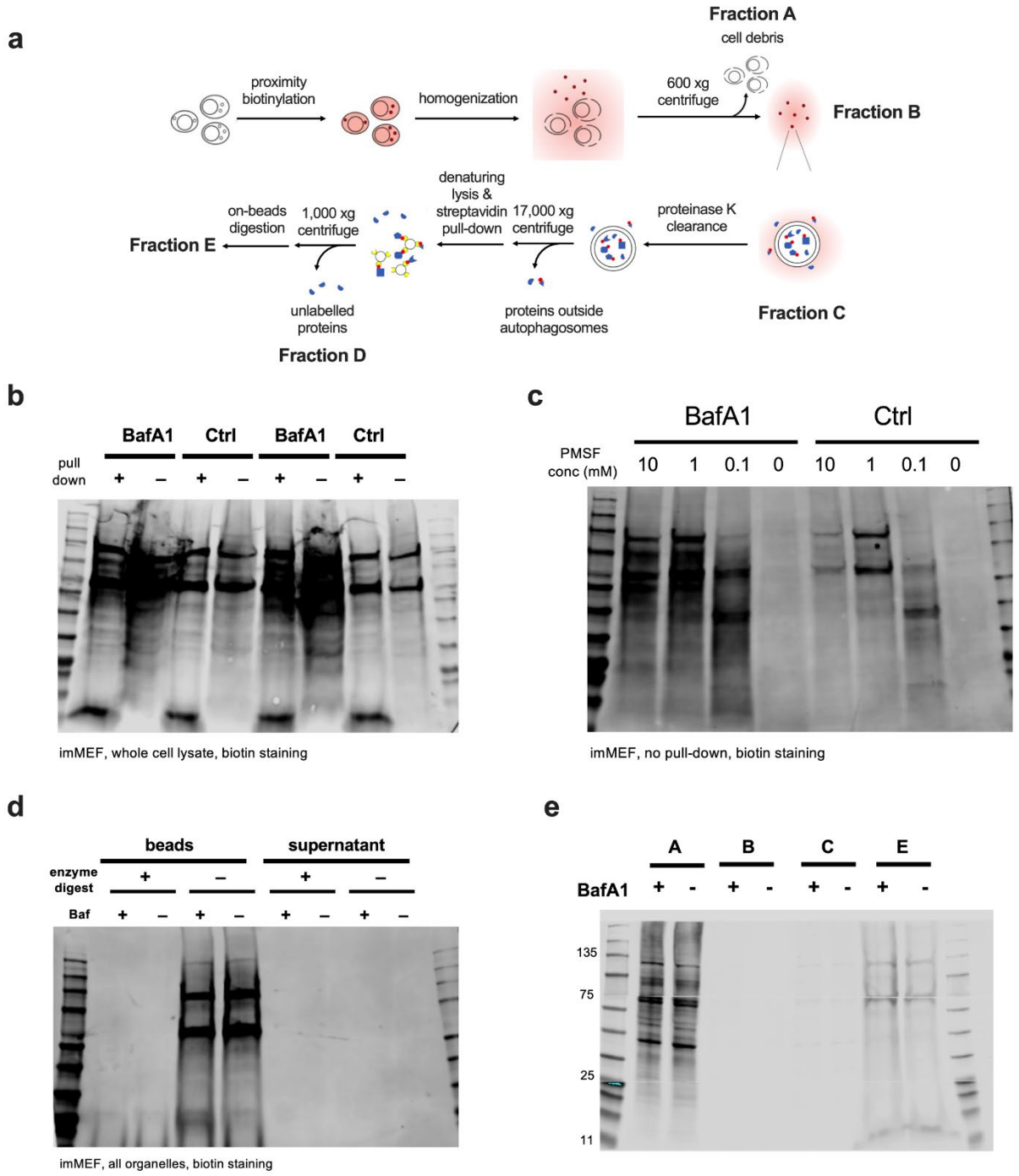


Figure 3.10 Optimisation of autophagosomal cargo purification.

a) Schematic overview of steps to purify autophagosomal cargoes. b) Western blot showing the efficiency of enriching biotinylated proteins by streptavidin beads. c) Western blot demonstrating how different concentrations of PMSF inhibit proteinase K and enrich the autophagosomes. d) Western blot showing the efficiency of trypsin digestion. e) Western blot of biotin labelling of different fractions collected during the autophagosomal cargo purification.

3.2.8. Building up the proteomics analysis workflow

To validate whether the *Lc3b-APEX2* mouse model can be applied to map the cellular autophagosomal contents, we utilised imMEFs and profiled their cargo candidates during basal housekeeping autophagy. Prior to proximity labelling, cells were treated with 100 nM BafA1 (Baf) or DMSO (Ctrl) to ratiometrically quantify the proteins being upregulated when autophagosomes accumulate in the cells without being degraded in the lysosomes (Figure 3.11). In order to identify and exclude proteins resistant to proteinase K during later analysis, a control group (Rapi) utilised MS-compatible *Rapi*Gest, a Triton-X substitute, during proteinase K treatment.

Based on the optimised protocol which maximises the efficiency of autophagosomal biotinylated protein enrichment, samples under 3 conditions (Baf, Ctrl, Rapi), with four biological replicates per group each, were sent for mass-spectrometry analysis. Raw mass spectrometry data underwent analysis using the MaxQuant suite to identify and quantify proteins. A total of 706 non-redundant proteins were identified referring to the Swiss-Prot, a reviewed- and manually annotated database of mouse proteins.

To perform the analysis of ProteinGroup data generated by MaxQuant, a workflow based on Python programming was designed for filtering and statistical analysis (Figure 3.12a). Proteins identified as 'only identified by site (only by a peptide carrying a modified residue, which is less reliable without application of specific enrichment method)', 'reverse (reversed sequence of naturally existed proteins)' and 'potential contaminant' were filtered out[158]. Moreover, proteinase K-resistant proteins and proteins only identified once among all eight samples (Baf and Ctrl) were filtered out. Since the original LFQ intensity displayed a skewed distribution (Figure 3.12b), a log-based normalisation was applied to transform data to a normal distribution.

2D principal component analysis showed a clustering of the samples within each group (Figure 3.12c). Pearson's correlation coefficient also displayed a high correlation between the samples within each group (Figure 3.12d and Figure 3.13), with Baf and Ctrl groups correlating better compared to the Rapi group. Since mass spectrometry has its limit for detection, low-abundant peptides may turn out as missing values, affecting the downstream statistical analysis through the introduction of large variation[159]. Therefore, 'imputation' is necessary to replace the missing values with a random small value. These random numbers are attributed based on the optimised parameters to fit a distribution, where missing values had been measured. Pairwise comparison between Baf and Ctrl was performed with a two-tailed Student's t-test.

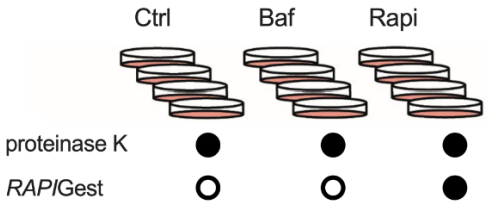


Figure 3.11 Schematic overview of three sample groups.

Ctrl and Baf groups were only treated with proteinase K, while Rapi group was treated with both proteinase K and *RAPI*Gest.

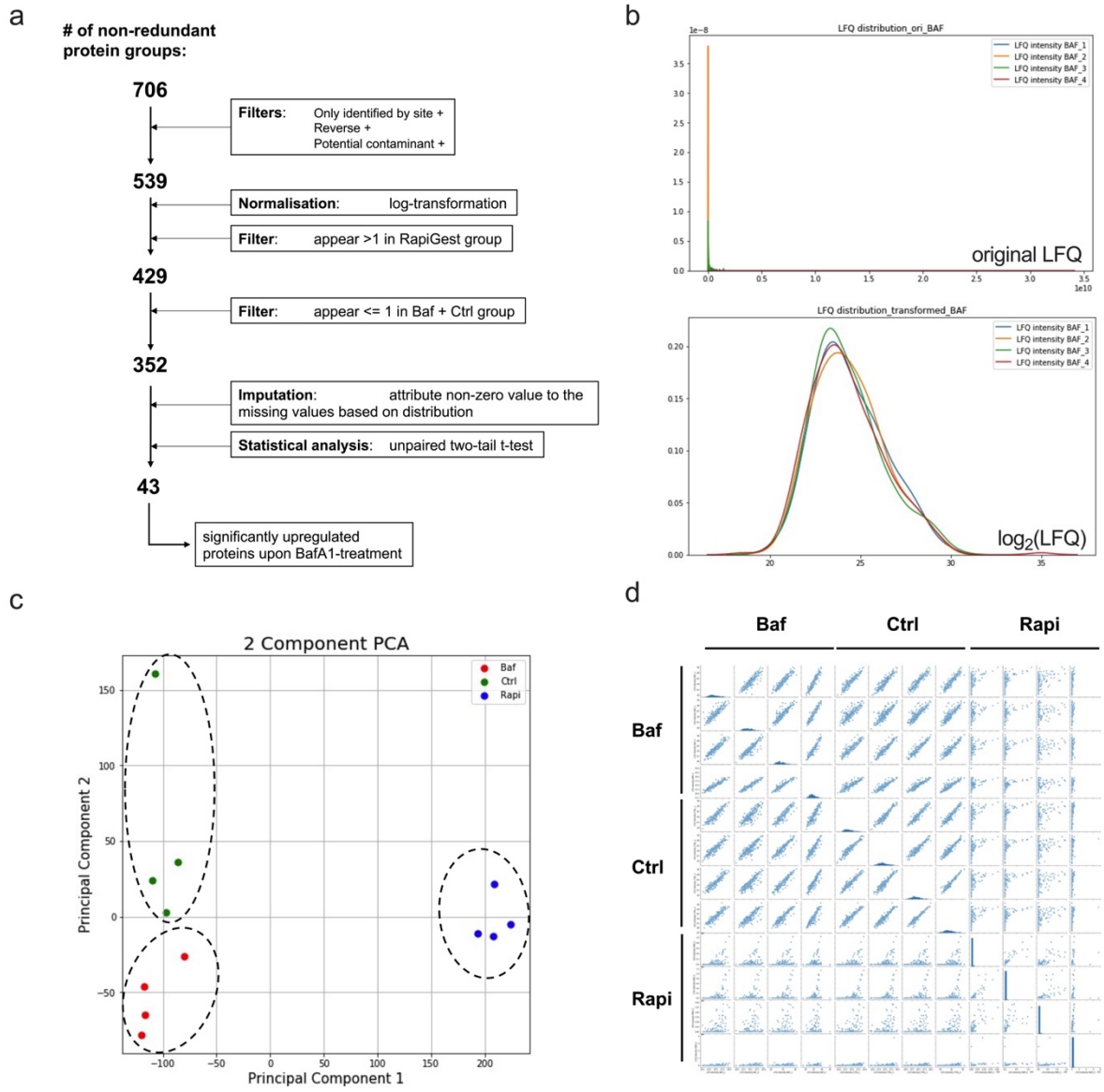


Figure 3.12 Building the workflow for statistical analysis of mass-spectrometry data.

a) Flow chart of the proteomics analysis. b) Distribution plots of original label-free quantitation (LFQ) intensity (upper) and log-transformed one (lower). c) Plot of principal component analysis (PCA) to show clustering of samples in Baf (red), Ctrl (green) and Rapi (blue) groups. d) Scatter plots showing a correlation of protein LFQ intensities between each sample in Baf, Ctrl and Rapi groups.

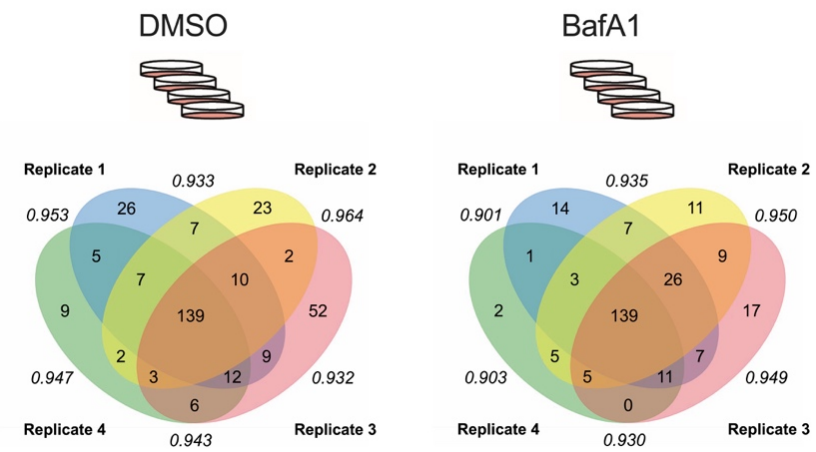


Figure 3.13 Biotinylated proteins from proximity-labelled imMEFs show high correlcation.

Venn diagram showing overlap of total proteinase K-protected and biotinylated proteins identified across four biological replicates in DMSO- and BafA1-treated groups. Pearson's correlation coefficients of two replicates are displayed.

3.2.9. Applying the proteomics analysis to imMEFs

According to the statistical analysis, 43 proteins were sensitive to BafA1-mediated upregulation and thus recognised as candidates of autophagosomal cargoes. These candidates can mainly be categorised into the following four groups: (1) LC3 homologue (GABARAPL2); (2) selective (or putative) autophagy receptors (SQSTM1/p62, NBR1, CALCOCO1[160], NCOA4[147]); (3) known autophagy substrates (KEAP1[161], FTL1 and FTH1[162]); and (4) autophagy regulators engulfed by autophagosomes (TBK1[163], PRKAR1A[164], LGALS8[165,166], TBC1D15[167], NEDD4[168], VCP[169], ANXA7[170]). Even at basal state, several types of selective autophagy occur inside imMEFs – mitophagy (mitophagy regulators - TBC1D15 and ANXA7, and mitochondrial protein - COX7A2[171]), ferritinophagy (NCOA4, FTL1 and FTH1), lysophagy (LGALS9, LGALS8, VCP), and probably lipophagy (RAB18 – a protein residing on lipid droplet[172]), indicating that macroautophagy is important in maintaining the cellular organelle homeostasis. Interestingly, our analysis discovered some genes that were enriched in distinct LC3-positive compartments, including SCAMP3 and RAB7A that localise to endosomes[173,174], and PDCD6IP which is involved in the exosome biogenesis, and promotes exosome secretion[175,176]. This discovery is consistent with the APEX labelling of hATG8s and autophagic receptors.

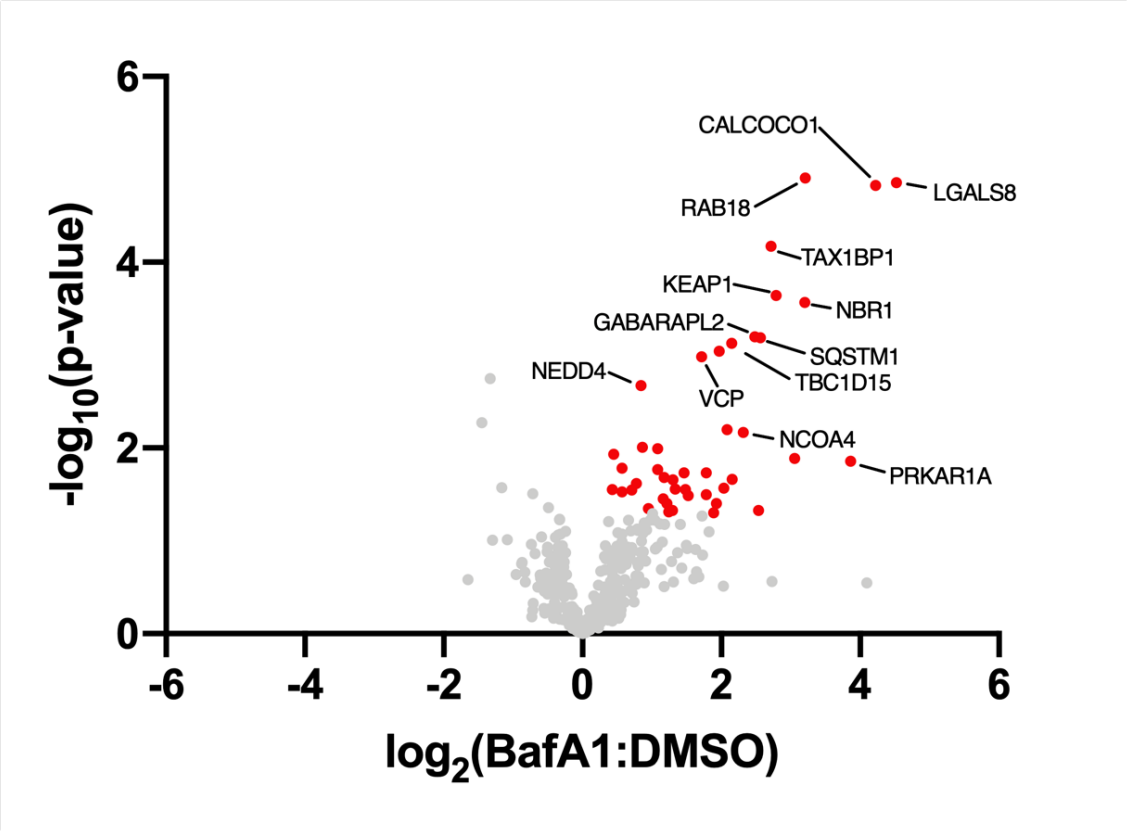


Figure 3.14 Identification of autophagosomal cargoes in imMEFs.

Volcano plot showing proteins labelled by APEX2-LC3B in imMEFs. Proteins significantly upregulated in BafA1-treated samples are highlighted in red ($p<0.05$ by Student's t test, n=4 biological replicates, experiment has been repeated three times).

3.2.10. Cell number titration with imMEFs

We next examined how the cell number affects total amount of candidates being identified. Two autophagy-related proteins, TAX1BP1 and SQSTM1, were significantly increased in BafA1 group across four experimental replicates (Figure 3.15), with the total cell number ranging from 0.125 million to 8 million. However, we noticed that the more cells we started with, the more significantly upregulated candidates we obtained, indicating that a larger cell number correlates with a better yield.

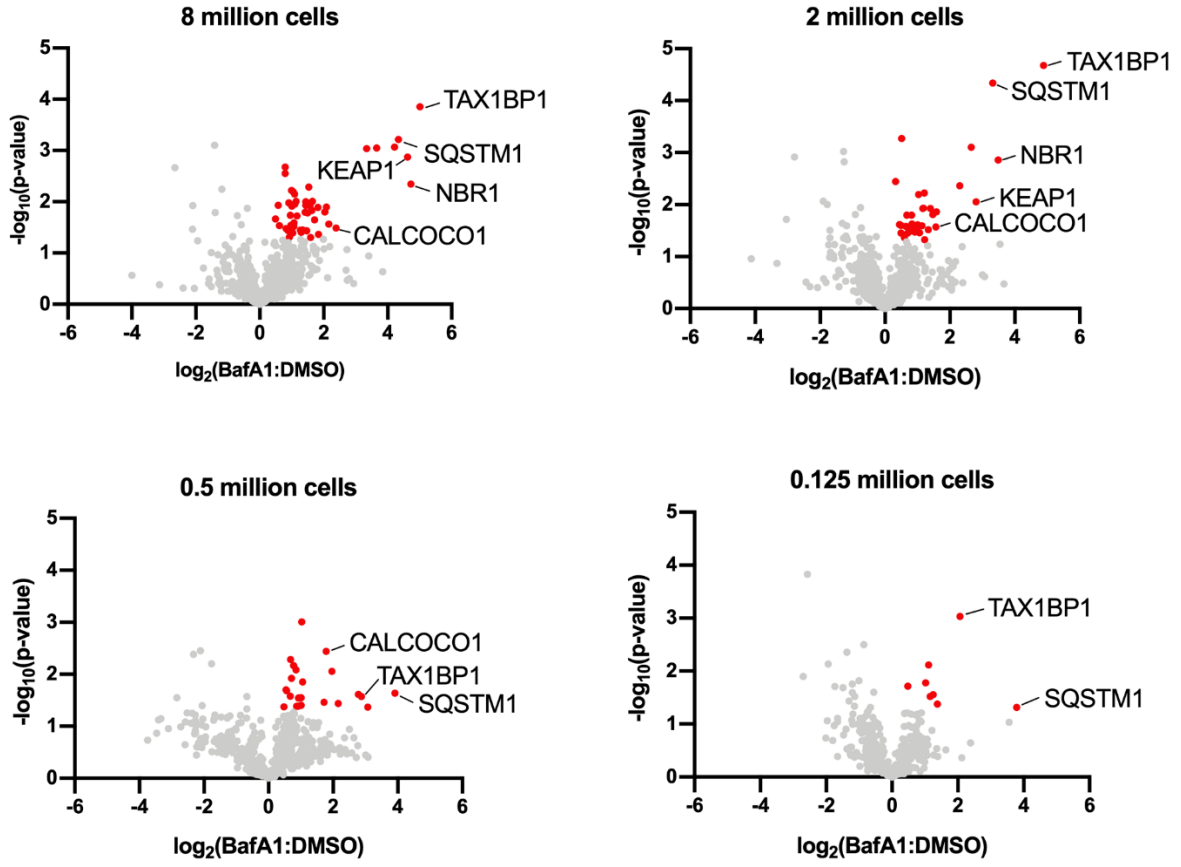


Figure 3.15 Volcano plots of proteins detected from samples with different cell numbers.

Biotinylated proteins from samples starting with different numbers of imMEFs were analysed with mass spectrometry. Proteins significantly upregulated in BafA1-treated samples are highlighted in red ($p<0.05$ by unpaired two-tailed Student's test, n=3 biological replicates per group).

Chapter 3. Mapping the autophagosomal content using the *Lc3b-APEX2* mouse model – Discussion

3.3 Discussion

Lc3b-APEX2 model is the first transgenic mouse model which addresses screening of autophagosomal contents with a proximity labelling technique. Unlike other traditional methods, our one-size-fits-all protocol due to its simplicity requires minor optimisations when applied to a different cell type. According to the previously published protocol, substrate incubation and labelling time may need to be adjusted to maximise the labelling efficiency while reducing non-specific labelling[151]. Since LC3 is ubiquitously expressed in different cell types and involved in both formation of autophagosomes as well as in the recruitment of autophagy substrates, our mouse model allows for the identification of autophagy degradome in different types of primary cells under various physiological conditions. As such it allows the establishment of an autophagosomal degradome atlas in a high throughput manner.

Here, we used LC3 as a bait protein to perform the proximity labelling of autophagosomal cargoes. Cellular localisation and functions of LC3 molecules are diverse. Lipid-conjugated LC3 not only resides on autophagosomes but also on single-membrane vesicles, including phagosomes, endosomes, and multivesicular endosomes (MVEs)[177]. Emerging evidence suggests that autophagy machinery contributes to several non-degradative processes including LC3-associated phagocytosis (LAP), LC3-associated endocytosis (LANDO), and endosomal microautophagy (eMI). LAP is crucial for phagocytotic cells to clear pathogens and damage-associated molecules and is facilitated by the insertion of LC3 onto phagosome membranes[178]. LANDO is an endocytic pathway with machinery that is independent of LAP. It has been shown to facilitate a receptor-mediated uptake of extracellular β-amyloid[179]. However, LC3 is conjugated to the cytosolic membrane surface of these vesicles in both LAP and LANDO. While the proteins associated with these structures may be labelled initially, they will be removed during a subsequent proteinase K digestion.

By contrast, eMI, triggered by nutrient starvation, mediates the turnover of cytosolic components and membrane proteins[39,180]. LC3 molecules are delivered to the limiting membrane of MVEs and undergo intraluminal budding to carry cargoes into the cisternae of the MVEs in the form of intraluminal vesicles (ILVs). The cargoes in ILVs are degraded upon MVE-lysosome fusion. Since ILVs are protected from proteinase K by MVE outer membrane and since BafA1-treatment inhibits the lysosome, there is a possibility that some candidate proteins identified in our model belong to the eMI pathway.

The other role of LC3 unrelated to autophagy is LC3-dependent extracellular vesicle loading and secretion (LDELS)[181]. In this non-canonical EV secretion pathway, LC3-positive ILVs bypass the conventional EV pathway via endoplasmic reticulum and Golgi apparatus and are released as EVs through the fusion of MVEs and plasma membrane. Cargoes included in the EVs have been identified as RNA-binding proteins and small non-coding RNAs. As with eMI, proteins found in LDELS can also be identified with our proximity labelling protocol. Therefore, the *Lc3b-APEX2* mouse model can be used to screen cargoes in multiple subcellular structures other than autophagosomes when combined with specific inhibitors of these pathways, which broadens the application of the model. An advanced method to increase the spatial specificity is a split proximity labelling enzyme[182]. These enzymes are composed of two inactive fragments, which can be brought together by LC3 and another membrane specific marker of a target compartment. The use of this technique may help to further distinguish proteome within different LC3-positive compartments.

BafA1 is a small molecule inhibiting pump activities of V-ATPase and Ca^{2+}-transporting ATPase ATP2A/SERCA[183]. It can disrupt the autophagic flux by impairing the lysosomal

acidification and autophagosome-lysosome fusion. The compound has been widely used in the field to inhibit autophagy at a late stage. However, evidence shows that BafA1-treatment leads to a lysosomal dysfunction and damage, and induces autophagy-mediated clearance of damaged lysosomes, metabolic changes, or even apoptosis[184-186]. This is consistent with our discovery that proteins involved in lysophagy (Lgals9, Lgals8, Vcp) were highly upregulated in BafA1-treated groups. To prevent a shift in cellular proteome and status and to minimise BafA1 impact on cells, it is important to optimise its concentration and time of incubation. Moreover, BafA1 has been shown to promote exosome release in different cell lines[187,188]. Since exosomes are also LC3-bound vesicles, the proteins inside exosomes can also be targeted through proximity labelling, similar to autophagosomal cargoes[181]. This may explain why we observed some proteins downregulated in BafA1 group. When one of the major degradation pathways is blocked, cells need to get rid of unnecessary, or even harmful, materials in a quick manner to maintain cellular homeostasis. Therefore, diverting the cargo to exosomes when lysosomal degradation is inhibited might be physiologically meaningful. As intracellular contents that are directly released outside of cells are recognised as damage-associated molecular patterns (DAMPs) and can induce excessive innate immune responses, which is why cells may have evolved a system to package cargo within membranes and 'dump' them outside[189].

Our strategy of creating a mouse model may lead to some biased results. Here, we chose LC3B as the bait molecule based on empirical knowledge from HeLa cells. However, it remains unclear how individual ATG8 subfamilies contribute to different types of autophagy. Knocking out a specific type of ATG8 in mice does not lead to a significant functional loss, indicating their functional redundancy, however, different ATG8 subfamily members vary in their binding affinities towards autophagy adaptors and receptors[190,191]. In addition, different cell

types may preferentially utilise specific types of Atg8s. It is important to check whether LC3B is involved in autophagy before utilising the LC3B-APEX2 model to map autophagosomal cargoes in the cell type of interest.

We chose APEX2 for proximity labelling because it was the most efficient enzyme to date which allowed labelling with a high temporal resolution (minutes of reactions by APEX2 compared to days of reaction by BioID)[192-195]. Since autophagy is a highly dynamic process, controlling the reaction time to capture a snapshot of the autophagosomal proteome increases the reliability of the technique. However, several caveats of the enzyme may hinder its more extensive application. First, biotin phenol radicals generated by APEX2 preferentially react with electron-rich amino acids residues, which means that only proteins with certain exposed amino acids on the surface can be labelled and these include Tyr, Trp, His and Cys[140]. Besides, a key chemical to trigger the biochemical reaction, H_2O_2, is highly toxic, which limits its use in ex vivo studies. Cells may undergo remarkable changes after isolation, which makes the result liable to artificial effects. Instead, an enhanced version of the biotin ligases, TurboID or miniTurboID, utilising the non-toxic biotin and shortening the reaction time to 10 minutes may broaden the application of in vivo proximity labelling to more organisms[141].

In summary, the successful validation of the mouse model and the results in imMEFs faithfully recapitulate the LC3B-APEX2 transfected HeLa data. In chapter 5 we will therefore be testing this novel technology in primary cells directly obtained from the transgenic mouse model.

Chapter 4: Characterisation of autophagy and ageing phenotypes in CD4+ T cells – Introduction

4.1 Introduction

4.1.1 Hallmarks of cellular senescence and cellular ageing

In this chapter, I am investigating the role that autophagy plays in preventing the ageing of T cells. Ageing describes the progressive deterioration of organs and tissues in an organism as a result of the passage of time. It has been listed as the top risk factor of numerous diseases, including cardiovascular diseases, cancers, neurodegeneration and type-2 diabetes[196]. As population ageing becomes the dominant demographic trend in the current century, human society is facing an unprecedented challenge. Moreover, the ongoing COVID-19 pandemic informed us that elderly people, especially with compromised immune systems and co-morbidities, are among the most affected. It is an urgent need to understand biological ageing and develop effective anti-ageing therapies. The advance of geroscience is of considerable help. With its assumption that the underlying mechanisms of ageing and age-related diseases are largely overlapping and shared across cell types, it provides us with an important insight into ageing and unravels several interconnected 'pillars' promoting ageing. The immune system is not an exception. Its age-associated dysregulation and deterioration, so-called '**immunosenescence**', describes immune system-wide changes over the lifetime of an individual. As for the cellular changes in individual immune cells, we will term them as markers for '**immune cell senescence**'. And here, based on the previous studies in the immune system, I will give a brief introduction to these markers categorised into **cellular senescence** and **cellular ageing**.

Cellular senescence refers to a state in which cells undergo irreversible cell cycle arrest[197]. It plays a crucial role in tissue remodelling, wound healing and tumour suppression during development[198]. However, senescent cells accumulate in aged organisms since they are resistant to apoptosis and evade immunosurveillance[199,200]. Due to their ability to induce

chronic sterile inflammation, termed 'inflamm-ageing', senescent cells contribute to the development of age-associated phenotypes and diseases, while interventions to eliminate or modulate this cell population can largely alleviate, or even reverse, their negative effects. The most common hallmarks to detect cellular senescence include the activation of $p16^{INK4a}$ and p53 pathways, telomere attrition, senescence-associated secretory phenotype (SASP), enhanced senescence-associated beta-galactosidase (SA-β-gal) activity and senescence-associated heterochromatin foci (SAHF)[201].

The most direct inducer of cellular senescence is the activation of two pathways inhibiting the cyclin-dependent kinases, the **$p16^{INK4a}$/pRB** and the **p53/$p21^{CIP}$** pathways. When facing stresses like DNA damages or oncogene activation, these two pathways are activated, leading to a growth arrest at the initial stage of cellular senescence[201]. While **telomere attrition**, another marker for cellular senescence, may explain why senescent cells stop proliferating. Over repeated cell divisions, telomeric DNA shortens and inflicts unrepairable DNA breaks and consistent DNA damage response due to the limit of the replication machinery[202]. Studies have shown that this can activate the **$p16^{INK4a}$/pRB and p53/$p21^{CIP}$** pathways and further lead to a cell cycle arrest of senescent cells[203].

Moreover, senescent cells can secrete a plethora of pro-inflammatory cytokines, chemokines, growth factors and proteases, termed **SASP**[204]. It leads to enduring inflammation and probably the degeneration of the local niche during ageing. The SASPs released by accumulating senescent cells during ageing is believed to cause systemic inflamm-ageing and ageing at the organismal level[205,206].

Senescent cells also display the condensation of pericentromeric satellite heterochromatin, a structural change of chromosomes termed '**SAHF**'. These heterochromatic DNA domains can silence the expression of proliferation-promoting genes in senescent cells, therefore, enhancing the irreversible arrest of cell cycles. The structure is usually associated with the expression of **γ-H2AX**, a minor histone H2A variant that is formed de novo upon DNA damage[207]. This molecule has been widely served as a readout for DNA double-strand breaks, as well as genomic instability and telomere dysfunction[208,209].

Besides, SA-β-gal activity, as a readout for lysosomal health, has been widely used to detect cellular senescence. The enhanced activity of lysosomal beta-galactosidase, whose optimal pH is far lower than the pH required for detection, is observed in senescent samples both in vitro and in vivo[210]. It may reflect an impaired renewal of lysosomes and accumulation of damaged ones during cellular senescence. Both $p16^{INK4a}$ expression level and SA-β-gal activity are commonly applied as markers to define the senescent cells.

Different from cellular senescence which has age-specific pleiotropic effects (wound healing during youth and disrupting tissue homeostasis during ageing), some cellular changes reflect the dysfunction in certain physiological aspects during ageing and exert an overall negative impact[211]. Here, we considered these cellular changes not directly linked with senescence as **hallmarks for cellular ageing**, including accumulation of organelles (dysfunctional mitochondria, lipid droplets), DNA lesions and disturbed protein homeostasis (proteostasis).

Aged cells frequently display an accumulation of dysfunctional mitochondria, which is caused by the decreased rate of mitochondrial protein synthesis and the failed removal of the damaged mitochondria[212,213]. As a consequence, inefficient energy production cannot support the key

physiological pathways and functions. Moreover, the disrupted electron transport chain generates massive reactive oxygen species (ROS) during oxidative respiration of damaged mitochondria[214]. Combined with the imbalance of cellular oxidant/antioxidant ratio, aged cells favour the production of oxidants and **excessive ROS** that compromise cell homeostasis and function[215]. Therefore, the accumulation of impaired mitochondria and upregulated ROS are used as biomarkers for cellular ageing. The enhanced ROS production further leads to **DNA lesions**. 8-oxoguanine (8-oxoG) is a common DNA lesion resulting from the ROS-mediated oxidation of guanine. This form of DNA damage accumulates in various mammalian tissues during ageing[216].

The **accumulation of lipid droplets (LDs)** has also been linked with ageing. LDs are spherical organelles that serve as reservoirs for intracellular neutral lipids. Except for its role in providing building blocks for membrane structure and energy metabolism, the organelle also affects physiological processes such as inflammation and insulin signalling, whose dysregulation are linked to the onset of ageing[217-219]. Other evidence supporting the immune-modulatory role of LDs comes from diseases. In response to inflammation and stress, macrophages generate LDs and display phenotypes related to cellular senescence ($p16^{INK4a}$ and SASP)[220]. These foamy cells enriched with LDs exert a deleterious effect throughout all stages of atherosclerosis. Similarly, microglia from aged brains accumulate LDs and represents a dysfunctional and pro-inflammatory state, which potentially contribute to neurodegenerative diseases[221]. It is not known whether the adaptive immune cells also increase their LD storage during ageing and whether it is linked to their dysfunction, thus worth further investigation.

Disturbed proteostasis is another key hallmark of ageing. Three interconnected arms of the proteostasis network include protein synthesis and folding, maintenance of conformational

stability, and protein degradation[222]. The advance of transcriptome and proteome analysis, as well as direct functional tests, indicate that alterations in all three components contribute to the decline of proteostasis during ageing. In nematodes, the rates of global protein synthesis display a reduction with ageing[223-225]. The attenuating protein translation is closely related to a decrease in both cytosolic and mitochondrial ribosomes and the inhibition of translation initiation factor 2α activity mediated by unfolded protein response (UPS) and integrated stress response (ISR)[226,227]. Besides, the altered translation of specific proteins, like TFEB, whose translation rate is mainly determined by the hypusination of EIF5A to facilitate the translation of its hard-to-read regions, is mediated by pathways irrelevant to the global mechanism[228]. Interestingly, the **nutrient-sensing mTOR** signalling pathway, which can enhance protein translation, was widely reported to be upregulated in several tissues, and pharmacological inhibition of the pathway delays ageing[229]. However, downregulation of mTOR signalling components was also observed in some tissues, further complicating the link between mTOR activity and ageing[230]. Therefore, tissue-specific screening of mTOR signalling pathways and protein translation levels can deepen our understanding of the role of mTOR in proteostasis and ageing.

The intracellular protein catabolism can remove misfolded or damaged proteins under various forms of cellular stress. The activity of both major components, the **ubiquitin-proteasome system** and **autophagy**, declines progressively across multiple tissues during ageing, leading to the formation of toxic protein aggregates[124,231]. Enhancing both pathways was shown to be beneficial to the extension of lifespan in organisms[232-234]. However, not much is known about these cellular senescence and ageing hallmarks in aged T cells and whether they are related to autophagy. Therefore, I will display these two aspects measured in the aged T cells in the result section below.

4.1.2 Autophagy and ageing

The diverse catabolic substrates of autophagy indicate its broad functions in different physiological and diseases conditions, including ageing. Mounting evidence indicated that autophagy levels decline across different tissues and animal species during ageing, mainly characterised by the reduced expression of key *Atg* genes, decreased rate of autophagolysosomal fusion and diminished lysosomal proteolytic function[235-238]. Similarly, reduced levels of autophagy were observed in different human tissues, closely linked to the onset of multiple age-associated diseases[239-241]. Our lab has shown that basal autophagic flux is dampened in adaptive and innate immune cells from aged mice and in human cells[106,228,242,243]. Since autophagy is crucial for the maintenance of memory CD8+ T cells and memory B cells, autophagy deficiency incurs impaired memory formation, further leading to compromised vaccine efficacy and increased incidence of infection in elderly people.

Beyond the correlation of decreased autophagy level and progression of ageing, the modulation of autophagy can determine a causal role for declining autophagy levels in ageing. Several organisms, including yeast, *C. elegans* and *Drosophila*, displayed shortened lifespan when their essential autophagy genes were genetically inactivated[235,244,245]. The global knock-out of *Becn1*, *Atg5*, *Atg7*, *Atg9a* and *Atg13* leads to embryonic or postnatal death in mice, indicating the essential role of autophagy during development[3]. Mice with conditional deletion of autophagy in specific cell types are viable, although they develop several progeroid phenotypes which recapitulate age-associated diseases in humans. For example, loss of autophagy in the central nervous system leads to massive neuronal death and neurodegeneration-like behavioural abnormalities[246]. The formation of ubiquitin-containing inclusion bodies in neurons mirrors the phenotypes observed in human neurodegenerative diseases. The dysfunction of autophagy in skeletal muscles leads to atrophy and myopathy[247]. During human

ageing, hematopoietic stem cells display impaired self-renewing, as well as myeloid skewing and lymphoid deficiency[248]. Our lab found that deletion of autophagy in hematopoietic stem cells leads to a reduced stem cell pool, lymphopenia and atypical myeloproliferation[249]. Besides, *Atg7*$^{-/-}$ macrophages show reduced innate immune function and elevated basal inflammation[243]. Moreover, loss of autophagy in CD8+ T cells and B cells leads to impaired immune memory formation, coinciding with the age-associated decline of adaptive immunity in human[106,228]. Taken together, cells from the hematopoietic lineage with autophagy deficiency reflect an aged phenotype.

In line with the deleterious effect of autophagy-deficiency in longevity, overexpressing *Atg* genes is linked to delayed ageing in *Drosophila* and mice[235,250]. Overexpression of AMPK, a positive regulator of autophagy, in *C. elegans* and *Drosophila* can also prolong their lifespan through enhancing autophagy level[251]. Moreover, the life-extending effect of *daf-2*, *glp-1*, *eat-2* and *clk-1* mutations in *C. elegans* all rely on autophagy since their role for longevity is disrupted when autophagy genes are knocked out[245,252-256]. In addition, many anti-ageing drugs exert their effect through enhancing autophagy. Rapamycin, an mTOR signalling inhibitor that boosts autophagy, can slow down many forms of age-dependent changes in mice even when treated late in life[257,258]. A natural polyamine called spermidine can promote longevity through enhancing TFEB translation and further boosting autophagy[228,259]. Another metabolite, NAD^+, can stimulate autophagy via mTOR inhibition and deacetylation of several *Atg* genes[260,261]. Several of its precursors have been shown to increase lifespan or improve healthspan in *C. elegans*, *Drosophila* and mice[262-265]. Other anti-ageing interventions, including exercise and calorie restriction, act via an autophagy-dependent mechanism[266]. In summary, it appears that autophagy induction is largely beneficial to prevent ageing.

Mechanistically, decreased autophagy may lead to the ageing phenotypes due to following reasons:

1) Loss of proteostasis: The accumulation of bulk protein aggregates during ageing is linked with several neurodegenerative diseases and muscular dystrophy[267]. Since protein aggregates are mainly degraded by autophagy, genetic and pharmacological autophagy induction can effectively decrease protein aggregates in aged cells and further enhance proteostasis and promotes longevity in several animal models[250,256,268-271].
2) Failure in energy provision and macromolecule turnover: By mediating the bulk degradation of certain macromolecules (glycogen, lipid droplets and nucleic acids) to replenish nutrients, selective autophagy (respectively glycophagy, lipophagy, and RNA- and DNA-autophagy) can produce energy and promote protein synthesis. Although other cytosolic enzymes can break down these macromolecules, autophagy facilitates a more rapid integrated response during states of stress. In contrast, declined autophagy during ageing may lead to the accumulation of macromolecules, which can impair cellular function and tissue homeostasis. For example, a defect in autophagy is companied by abnormal glycogen inclusions in neurons of patients with Lafora disease[272]. Hepatocytes show an autophagy-dependent accumulation of lipid droplets, which predispose elderly people to steatosis[273]. Therefore, autophagy prevents ageing by regulating macromolecule availability and ensuring a healthy metabolism.
3) Accumulation of damaged organelles: Damaged subcellular organelles need to be timely removed by autophagy to guarantee the integrity of cellular functions. For instance, damaged mitochondria with disrupted respiratory chain can generate excessive ROS and induce oxidative stress, and defective mitophagy is linked with neurodegeneration[274]. Additionally, immediate clearance of damaged lysosomes is even more urgent as lysosomes with broken membranes can release hydrolases into the cytosol, leading to

pyroptosis and caspase-independent cell death[184]. The quality surveillance of subcellular organelles by autophagy is essential in the prevention of ageing and its related diseases.

4) Systemic inflammation led by the innate immune system: autophagy may control inflamm-ageing by inhibiting the pro-inflammatory macrophages and degrading the NLRP3 inflammasome[275,276].

Taken together, autophagy's health benefits make it a popular target to understand the ageing process and unravel more therapeutic interventions of age-associated diseases.

4.1.3 Ageing of T cells

During organismal ageing, the immune system is also prone to dysregulation and deterioration. The combination of the overall changes during this process is termed '**immunosenescence**', where both innate and adaptive immune cells undergo remarkable changes[201]. Here, I will focus on T cells. Accumulating evidence indicates that both absolute number and relative frequency of naïve T cells are decreased during ageing, which leads to a lymphopenic phenotype[201]. The decline in naïve T cell production is largely due to thymic involution which starts after the onset of adulthood[277]. With a shrinking repertoire of antigen-specific cells, the aged immune system shows a compromised ability to fight novel pathogens and establish memory response, while antigen-experienced cells, or effector T cells, featured by high expression of CD44 and low levels of CD62 ligand (CD62L), undergo homeostatic proliferation and increased oligoclonality to replenish the shrinking pool[201]. The past and persistent infections also lead to an increased frequency of the effector population over the lifetime. These overall changes lead to a shift from naïve to memory/effector populations for both CD4+ and CD8+ T cells during ageing.

A substantial population of antigen-inexperienced T cells with memory phenotypes expands during ageing. In mice, these T cells are referred to as virtual memory T cells (T_{vm}) and characterised by high expression of CD44 and low expression of CD49d[278]. Compared to the conventional naïve T cell (T_n), T_{vm} cells are low in proliferative capability and display several hallmarks linked to senescence, including upregulated γ-H2AX, exhaustion markers, cell-cycle inhibitors and anti-apoptotic Bcl-2[278]. Their innate-like functional properties and response to self-antigens also imply their role in inflamm-ageing and autoimmune diseases[279]. The development of T_{vm} occurs in the periphery, relying on the cytokine (IL-15 or IL-4, depending on the genetic background of the mice) and the transcription factor eomesodermin (EOMES)[280,281]. Though CD8+ T_{vm} cells are relatively well-defined, it is still elusive whether CD4+ T cells also adopt these memory-like features during ageing.

The frequency of two terminally-differentiated T lymphocytes is increased during ageing. Relatively undifferentiated T cells are characterised by their surface expression of CD28 and CD27[282]. CD28 is an essential co-stimulatory receptor on T cells. When binding to either CD80 or CD86 on antigen-presenting cells, it can induce the 'second signal' during T cell activation, which is indispensable for the clonal expansion of naïve T cells, cytokine production and the prevention from apoptosis and exhaustion[60,283]. CD27 belongs to the TNFR family. When binding to CD70, CD27 transduces the downstream signalling to promote the survival of activated T cells through its pro-metabolic and anti-apoptotic effects[284]. During ageing, relatively undifferentiated T cells gradually downregulate the surface expression of CD28 and CD27 due to repetitive activation and turn into the highly differentiated CD28- CD27- population. The CD28- CD27- T cell enters the end-stage differentiation and displays the characteristics of replicative senescence, together with a decline in its telomerase activity and phosphor-Akt (Ser473) level[282,285]. An increase in this population is observed in both CD4+

and CD8+ compartments during ageing. The surface expression of another molecule, the killer cell lectin-like receptor G1(KLRG1), has also been linked with aged T cells[286,287]. KLRG1 is a co-inhibitory receptor that contains an immunoreceptor tyrosine-based inhibitory motif (ITIM) in its cytoplasmic domain. When binding to cadherins, it induces the downstream signalling to recruit SHIP-1 and SHP-2, two phosphatases to dampen the TCR signalling[288]. These two sets of molecules are linked with each other since the blockade of KLRG-1 on CD8+ CD27- CD28- T cells can restore their proliferation.

Interestingly, most of the ageing-associated populations mentioned above are better defined and investigated in CD8+ T cells than in their CD4+ counterpart. Since naïve CD8+ T cells experience a more striking loss during ageing than CD4+ T cells, and CD4+ T cells are responsible for a much wider range of functions to assist both adaptive and innate immunity, I hypothesised that these two major types of T lymphocytes may behave quite distinctly during ageing[277]. It is therefore worth investigating whether the changes described in CD8+ T cells happen to CD4+ lymphocytes. Therefore, I conducted a comparative study of both populations based on previous studies on CD8+ T cells.

In addition to a global change of phenotypic changes, there are also age-related functional changes in T cells. During antigen-induced activation, aged naïve T cells display a declined response to mitogen and TCR signalling, featured by impaired upregulation of early-activation markers, decreased proliferation, as well as altered cytokine secretion[278,289]. Moreover, the formation of long-term memory cells is disrupted[106,278]. Our lab confirmed that aged CD8+ T cells were unable to recall robust memory response, consistent with the phenotype of an autophagy-deficient model[106]. Enhancing autophagy with spermidine can recover the phenotype. In line with the phenotypes of aged naïve CD4+ T cells, some studies indicate that

the defects of autophagy-incompetent CD4+ T cells appear even earlier during the primary activation with decreased proliferation[97,101,105,107,290]. One possible explanation is that the aged cells are senescent, thus have lost the capacity to re-enter the cell cycle upon TCR activation. However, $p16^{INK4a}$+ T cells display a minor increase, albeit significant, during ageing (less than 1%), which cannot explain why most aged T cells experience a remarkable proliferation defect[291]. Probably, $p16^{INK4a}$ promoter activation does not reflect its mRNA level due to the marked stability of $p16^{INK4a}$ transcript[201]. Therefore, it is necessary to combine other senescent markers, like the p53-p21 pathway, which is less understood in the immune population, and SA-β-gal activity, to conclude whether the impaired proliferation of aged CD4+ T cells is due to the cellular senescence. Another hypothesis is that autophagy can selectively degrade certain molecules to unleash the brake on T cell activation, which is impaired by the decline in autophagy during ageing. Therefore, next, I examined the ageing phenotypes and aligned them to the phenotypes of autophagy-deficient CD4+ T cells.

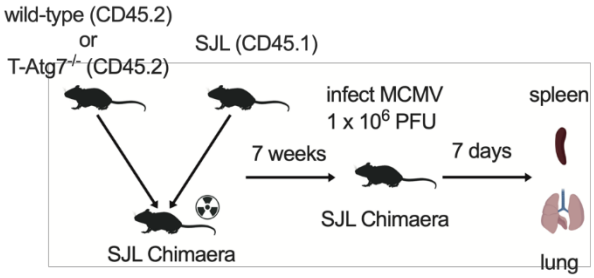
Chapter 4: Characterisation of autophagy and ageing phenotypes in CD4+ T cells – Results

4.2 Results

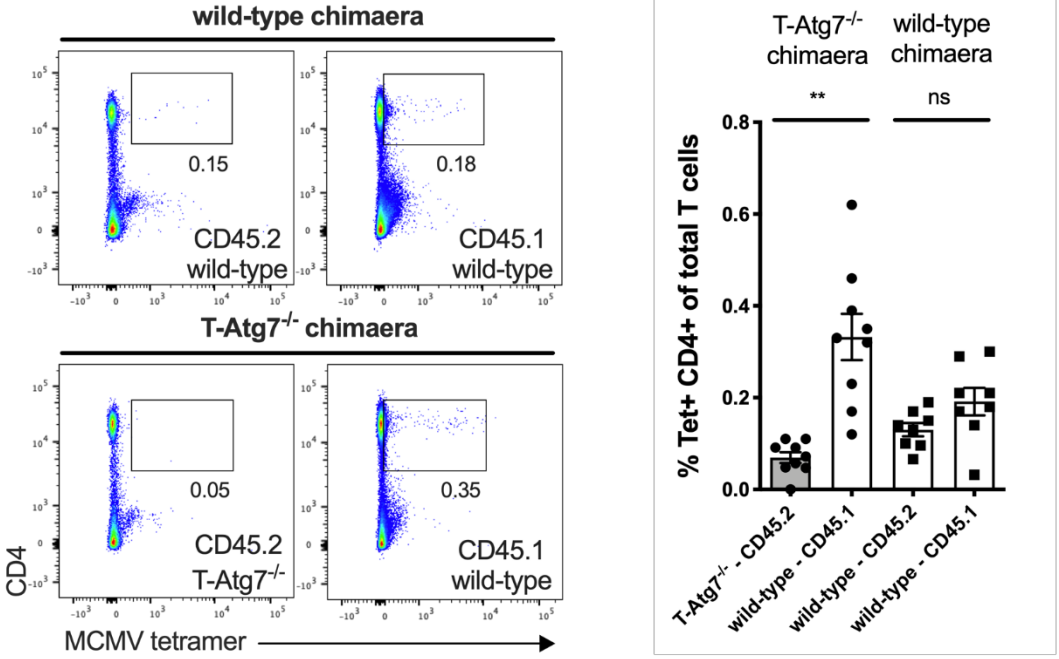
4.2.1. *Atg7*-deficient CD4+ T cells show decreased effector formation in response to pathogens in vivo

It has been reported that aged naïve CD4+ T cells are not able to proliferate normally. Therefore, we examined whether autophagy-deficient phenotype in CD4+ T cells mimics the aged phenotype. This was done before the start of my PhD by Dr Daniel Puleston and Dr Sharon Sanderson. We used a mouse model conditionally deleting *Atg7*, an essential autophagy gene, in both CD4+ and CD8+ T lymphocytes (*CD4*^{cre}; *Atg7*$^{flox/flox}$, hereafter as T-Atg7$^{-/-}$). Since the expression of Cre under the control of CD4 enhancer and promoter sequences is initiated at the very late double-negative stage of T-cell development, the deletion rate of loxP flanked genes usually reaches more than 90% efficiency by the double-positive stage[292]. With the same mouse model, our lab has discovered that the formation of memory CD8+ T cells was dramatically impaired when lacking autophagy[106]. Here we address the role of autophagy in the effector formation of CD4+ T cells. In order to rule out the effects of autophagy-deficiency in antigen-presenting cells expressing CD4, we generated bone marrow chimaeras with bone marrow cells 1:1 mixed of SJL wild-type controls (CD45.1+) with wild-type littermate controls or T-Atg7$^{-/-}$ mice (both are CD45.2+) (Figure 4.1a). After 7 weeks challenged by murine cytomegalovirus (MCMV), the MCMV-specific CD4+ T cells in both spleen and lungs were stained with MHC class II tetramers and evaluated by flow cytometry on day 7-9, which is the peak time for effector T cell formation[293]. The percentage of CD45.2+ MCMV-specific T-Atg7$^{-/-}$ cells was significantly decreased compared to that of CD45.1+ wild-type cells in both spleen and lungs (Figure 4.1b and c).

a



b **Spleen**



c **Lung**

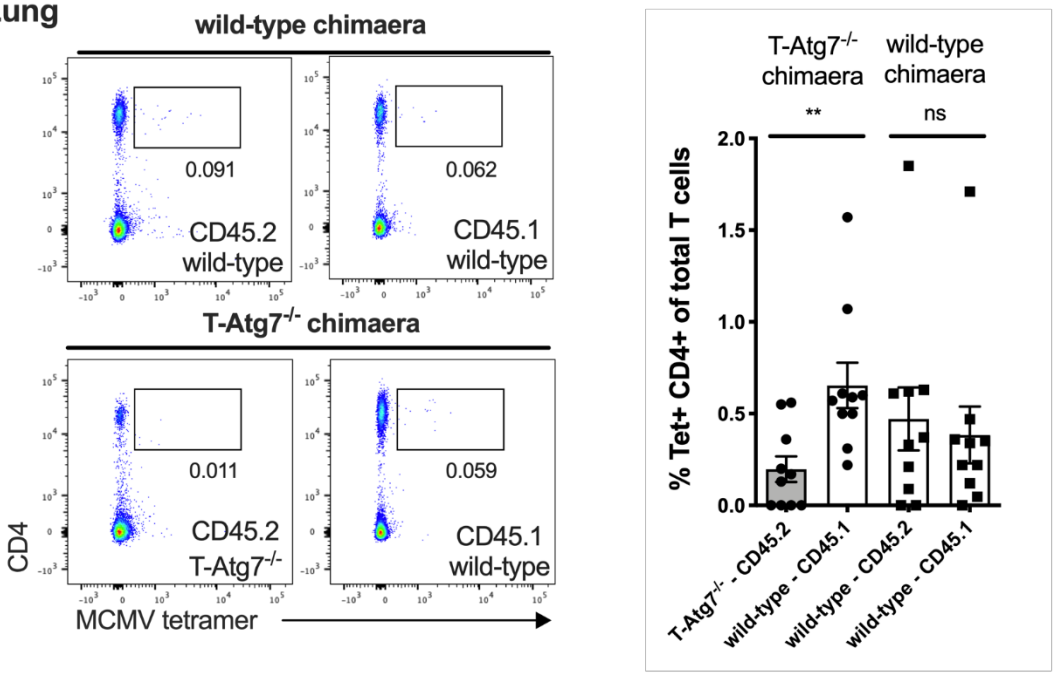


Figure 4.1 Bone marrow chimaeras show impaired effector formation in T-Atg7$^{-/-}$ CD4+ T cells.

a) Experimental set-up to generate the bone marrow (BM) chimaeras. CD45.1+ hosts were lethally irradiated and reconstituted with a 1:1 mix of BM from CD45.1+ wild-type with either CD45.2+ T-Atg7$^{-/-}$ or CD45.2+ wild-type. After 7 weeks of reconstitution, the hosts were infected with 1x10^{6} PFU mouse cytomegalovirus (MCMV) intravenously (i.v.). Cells from both spleens and lungs were collected and analysed on day 7 post-infection. Dot plots display MCMV-specific CD4+ T cells from the spleen (b, left) and lungs (c, left) of CD45.2+ wild-type or T-Atg7$^{-/-}$ donors and CD45.1+ donors. Bar graphs indicate the percentage of Tet+ CD4+ T cells within CD45.2+ CD19- or CD45.1+ CD19- population in the spleen (b, right) or lungs (c, right) as mean ± SEM (n=9 mice per group). All statistics by Mann-Whitney paired two-tailed U-test, p**<0.01, ns: not significant. Results are representative of three independent experiments. The experiment was performed by Sharon Sanderson.

4.2.2 TCR-transgenic *Atg7*-deficient CD4+ T cells show decreased effector formation in response to TCR-specific antigen in vivo

To further confirm that the expansion of the effector population in autophagy-deficient CD4+ T cells is impaired upon antigenic stimulation, we crossed the *CD4^{cre}; Atg $^{flox/flox}$* mice with the mouse model transgenic for OT-II T-cell receptor, which specifically recognises ovalbumin[294]. In the *CD4^{cre}*; *Atg $^{flox/flox}$;* OT-II mice, we observed neither CD4+ T cell lymphopenia nor a shift from naïve (CD62L^{+} CD44^{low}) to effector/memory population (CD62L^{-} CD44^{high}) in the spleens of naïve 6-8-week-old mice (Figure 4.2a and b).

To further confirm the compromised effector formation of autophagy-deficient CD4+ T cells upon antigenic stimulation, next, we transferred splenic CD4+ T cells from either wild-type or T-Atg7$^{-/-}$ mice of CD45.2+ background into CD45.1+ host mice. 24 hrs after the T cell transfer, the host mice were challenged with recombinant adenovirus H5-ovalbumin (AdH5-OVA) to activate the OT-II transgenic T cells (Fig. 4.3a). The expansion of the T-Atg7$^{-/-}$ effector population was significantly impaired in both spleen and blood on day 9 (Figure 4.3b and c), consistent with our observation above that the endogenous CD4+ T cells failed to proliferate in response to MCMV.

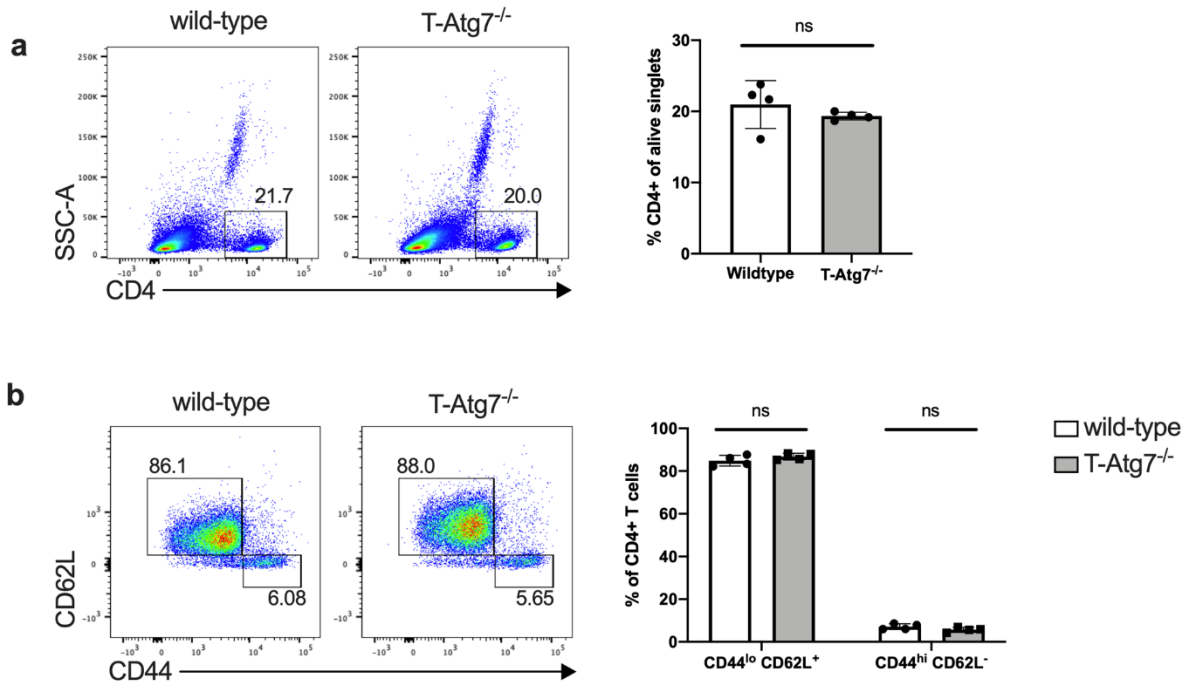


Figure 4.2 T-Atg7$^{-/-}$, OT-II mice displayed no sign of lymphopenia or a shift from naïve to memory/effector population at 6-8 weeks old.

a) Dot plots (left) of CD4+ lymphocytes from the spleens of wildtype or T-Atg7$^{-/-}$ mice. Bar graph (right) indicates the percentage of the gated population among total splenocytes as mean ± SEM (n=4 mice per group). b) Dot plots (left) showing different CD4+ T cell subsets, including naïve (CD62L^{+} CD44^{lo}) and effector (CD62L^{-}, CD44^{hi}) T cells, from the spleens of wildtype or T-Atg7$^{-/-}$. Bar graph (right) indicates the percentage of each subset among total CD4+ T cells as mean ± SEM (n=4 mice per group). All statistics by unpaired two-tailed Student's t-test, ns: not significant. Results are representative of three independent experiments.

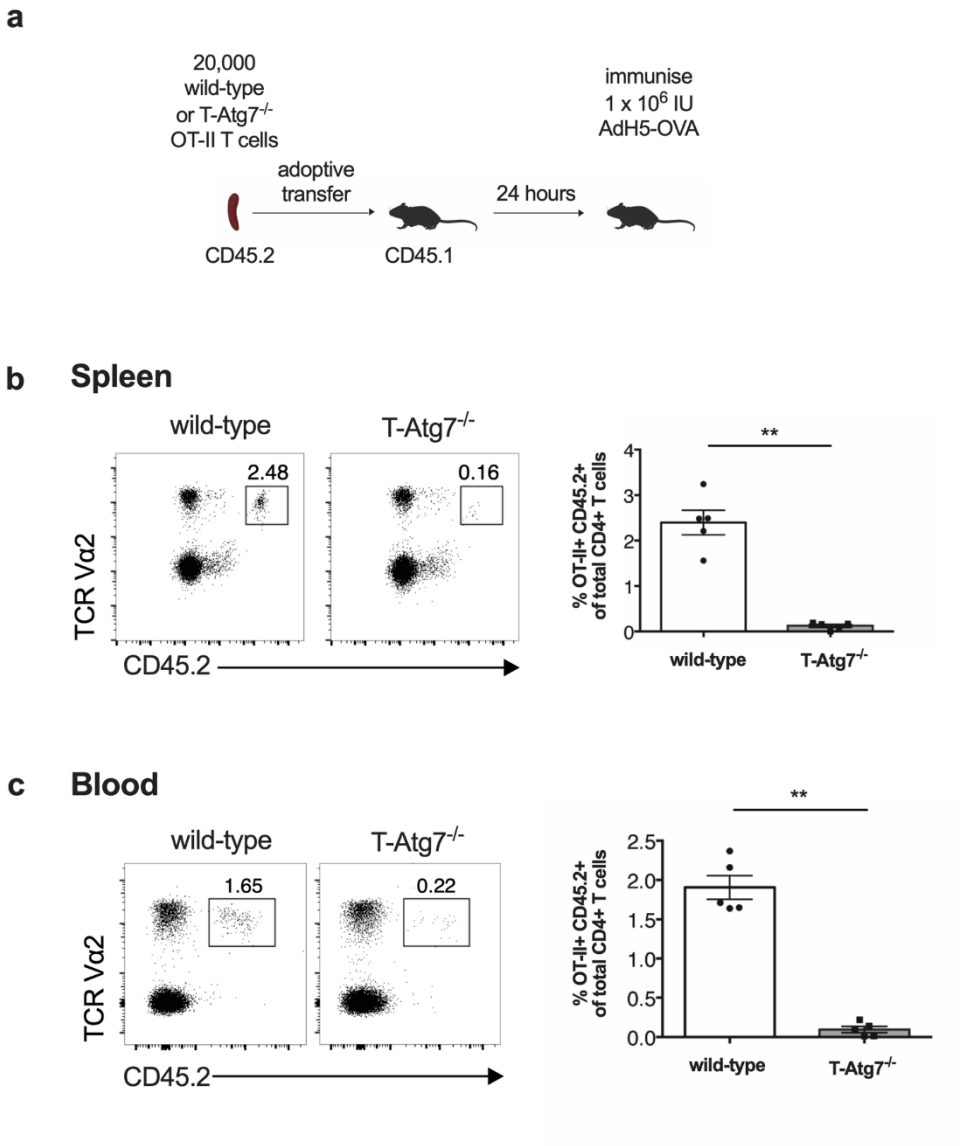


Figure 4.3 Adoptive transfer experiment shows impaired effector formation in T-Atg7$^{-/-}$, OT-II CD4+ T cells.

a) Experimental set-up for the adoptive transfer experiment. 2 x 10^4 OT-II CD4+ T cells from either CD45.2 Wildtype or T-Atg7$^{-/-}$ mice were adoptively transferred into CD45.1 recipient mice. 8 days after the immunisation with 1x10^6 IU recombinant adenovirus H5-ovalbumin (AdH5-OVA), the OT-II CD4+ cells in the spleens and blood of the recipient mice were detected by flow cytometry. Dot plots are gated on CD45.2+, TCR Vα2+ in recipient mice's spleen (b, left) and blood (c, left). Bar graphs depict the percentage of the gated population within the total CD4+ T cell population in the spleen (b, right) or blood (c, right) as mean ± SEM (n=5 mice per group). All statistics by unpaired two-tailed Student's t-test, p**<0.01. Results are representative of three independent experiments. The experiment was performed by Daniel Puleston.

4.2.3. Autophagy-deficient CD4+ T cells show a delayed proliferation in vitro

To understand the underlying mechanism of why antigen-specific CD4+ T cells do not expand in vivo, we dissected the proliferation profile via in vitro TCR-activation. The proliferation profile was obtained by flow cytometry after activating OT-II CD4+ T cells isolated from wild-type or T-Atg7$^{-/-}$ with ovalbumin at different time points. Results indicate that the upregulation of two early-activation markers, CD69 and CD25, was not changed in T-Atg7$^{-/-}$ CD4+ T cells on day 1 activation compared to wild-type (Figure 4.4), suggesting a normal TCR-signalling and priming[295].

However, the proliferation of T-Atg7$^{-/-}$ CD4+ T cells was significantly delayed compared to their wild-type counterpart on days 3 and 7 of activation (Figure 4.5). The impaired expansion cannot be attributed to the excessive apoptotic level or cell death since the frequency of Annexin V+/LD-NIR- and LD-NIR+ CD4+ T cells did not show significant differences between wild-type and autophagy-deficient cells on day 1 or 3 of activation (Figure 4.6).

On day 10, T-Atg7$^{-/-}$ CD4+ T cells caught up and all cells divided similarly to wild-type (Figure 4.5). To exclude the preferential proliferation (and escape) of CD4+ T cells with incomplete *Atg7* knockout, we measured *Atg7* mRNA expression by qRT-PCR on day 7 in sorted T cells that had undergone a maximum number of detectable cell divisions (i.e. that diluted the cell dye to the maximum) (Figure 4.7a). Indeed, in proliferated CD4+ T cells from T-Atg7$^{-/-}$; OT-II mice, the *Atg7* mRNA was undetectable (Figure 4.7b). Our discovery of delayed proliferation in response to antigen further confirms and extends the results of other autophagy-knockout models that demonstrated an impaired CD4 expansion in response to non-specific stimulation[97,101,105,107,290].

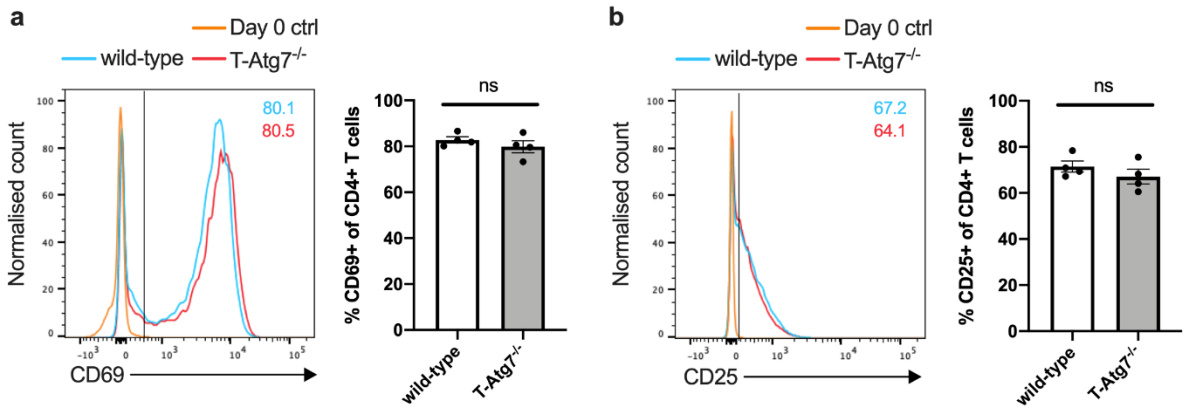


Figure 4.4 T-Atg7$^{-/-}$ CD4+ T cells display normal upregulation of early-activation markers.

Histograms showing the expression level of two early-activation markers, CD69 (a, left) and CD25 (b, left), in TCR-transgenic OT-II CD4+ T cells from wild-type (blue) or T-Atg7$^{-/-}$ (red) mice activated with ovalbumin (1mg/ml) for 1 day. Non-activated negative control (Day 0 ctrl, orange) was included. Bar graphs indicate the percentage of CD69+ (a, right) and CD25+ (b, right) populations among the total CD4+ T cells (n=4 mice per group) as mean ± SEM. Statistics by unpaired two-tailed Student's t-test, ns: not significant. Results are representative of two independent experiments.

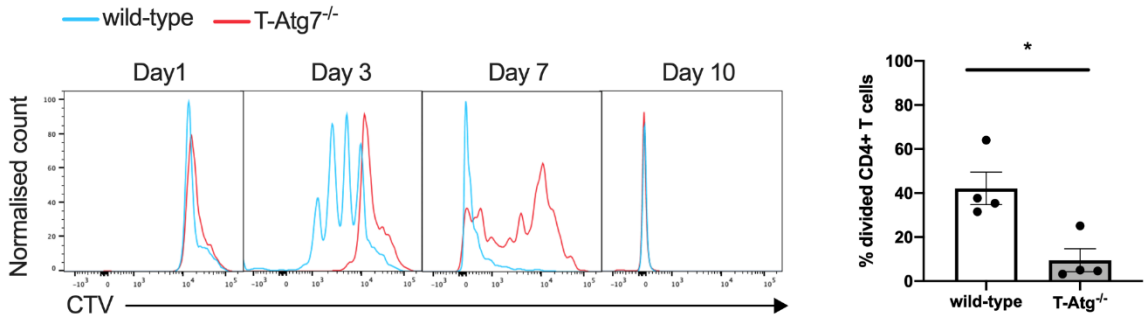


Figure 4.5 T-Atg7$^{-/-}$ CD4+ T cells show delayed proliferation in vitro.

Histograms to show the proliferation profile of wild-type (blue) or T-Atg7$^{-/-}$ (red) CD4+ T cells by days of activation. Total splenocytes containing TCR-transgenic OT-II CD4+ T cells were stained with CellTrace Violet (CTV) and cultured with ovalbumin (1 mg/ml) and murine IL2 (20 ng/ml) for 1, 3, 7 and 10 days. Bar graph (right) indicates the percentage of divided cells (CTV^{lo}) among total CD4+ T cells on day 3 as mean ± SEM (n=4 mice per group). Statistics by unpaired two-tailed Student's t-test, *p<0.05. Results are representative of four independent experiments. Results in collaboration with Ghada Alsaleh.

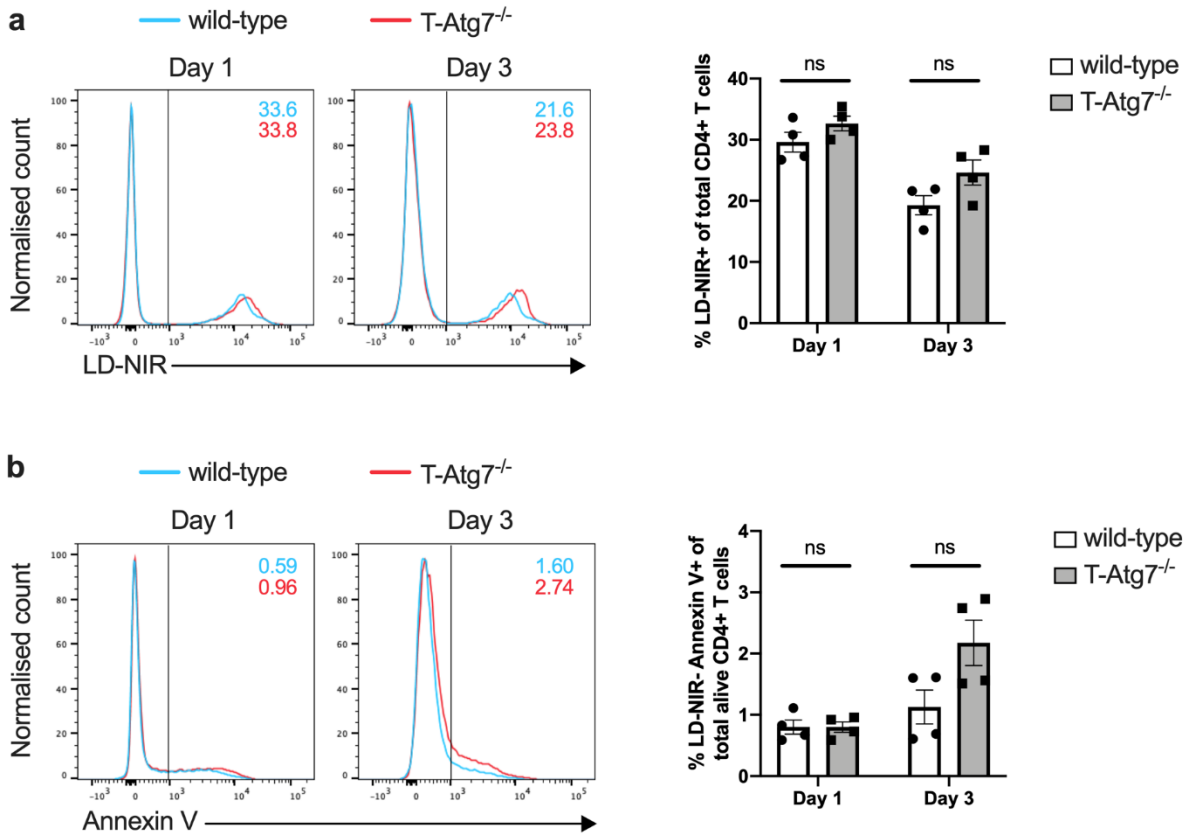


Figure 4.6 T-Atg7$^{-/-}$ CD4+ T cells display no significant increase of cell death or apoptosis on day 1 and day 3 of activation.

a) Histograms (left) showing the expression level of cell death markers in TCR-transgenic OT-II CD4+ T cells from wild-type (blue) or T-Atg7$^{-/-}$ (red) mice activated with ovalbumin (1 mg/ml) for 1 or 3 days. Bar graphs (right) indicate the percentage of Dead+ populations among total CD4+ T cells (n=4 mice per group) as mean ± SEM. b) Histograms (left) showing the expression level of apoptotic markers in TCR-transgenic OT-II CD4+ T cells from wild-type (blue) or T-Atg7$^{-/-}$ (red) mice activated with ovalbumin (1mg/ml) for 1 or 3 days. Bar graphs (right) indicate the percentage of Annexin V+ populations among total CD4+ T cells (n=4 mice per group) as mean ± SEM. Statistics by unpaired two-tailed Student's t-test, ns: not significant. Results are representative of two independent experiments.

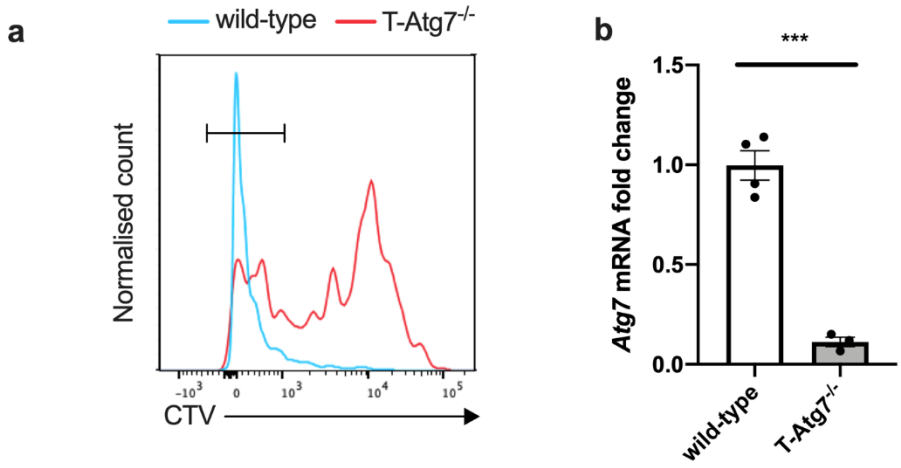


Figure 4.7 Divided T-Atg7$^{-/-}$ CD4+ T cells show effective deletion of *Atg7*.

a) Divided (CTV^{lo}) CD4+ T cells activated for 7 days were sorted (black bar indicates the gating strategy) and the *Atg7* mRNA level was quantified with qRT-PCR. b) Bar graph shows the fold change in *Atg7* mRNA of T-Atg7$^{-/-}$ divided CD4+ T cells normalised to their wild-type counterparts (n=3-4 mice per group) as mean ± SEM. Statistics by unpaired two-tailed Student's t-test, ns: not significant. Result in collaboration with Ghada Alsaleh.

4.2.4. Inducible knock-out of *Atg16l1* in CD4+ T cell impairs its proliferation

To further confirm that the impaired CD4+ T cell proliferation is due to the lack of autophagy, rather than a secondary effect of long-term adaptation to the loss of autophagy during differentiation in vivo, *Atg16l1*$^{flox/flox}$ mice were crossed to mice expressing inducible Cre and tdTomato fluorescent reporter, Ai14. The mouse model utilises the second-generation tamoxifen-inducible Cre, Cre-ERT2. The Cre recombinase is fused to a mutant form of estrogen receptor, which can be activated by ER antagonists 4-hydroxytamoxifen (4-OHT) but not by endogenous estrogen[296,297]. When binding to 4-OHT, the fusion protein is translocated into the nucleus inducing DNA recombination at the loxP site.

To confirm that the inducible Cre can effectively delete the *Atg16l1* allele when administrated with 4-OHT, CD4+ T cells were purified from the spleens of Cre-ERT2-positive (*Cre-ERT2*+), *Atg16l1*$^{flox/flox}$ mice and activated for three days with or without the presence of 500 nM 4-OHT (Figure 4.8a). Western blot shows that the ATG16L1 protein level was significantly reduced in CD4+ T cells treated with tamoxifen compared to those treated with vehicles (Figure 4.8b). Moreover, around 90% of 4-OHT-treated CD4+ T cells were tdTomato-positive (Figure 4.8c), indicating the high deletion efficiency in vitro.

Consistent with our observation in the constitutive *Atg7*$^{-/-}$ model, on day 3 of activation, the average cell division of 4-OHT-treated CD4+ T cells from *Cre-ERT2*+; *Atg16l1*$^{flox/flox}$ mice is significantly delayed compared to its vehicle-treated counterpart (Figure 4.9a). The minor but still significant decrease might be due to the late onset of the *Atg16l1* deletion compared to the constitutive knockout model. This significantly impaired proliferation was not due to the side effect of 4-OHT since no difference was observed in cell division between 4-OHT-treated and

vehicle-treated CD4+ T cells from Cre-ERT2-negative (*Cre-ERT2-*); *Atg16l1*$^{flox/flox}$ (Figure 4.9b).

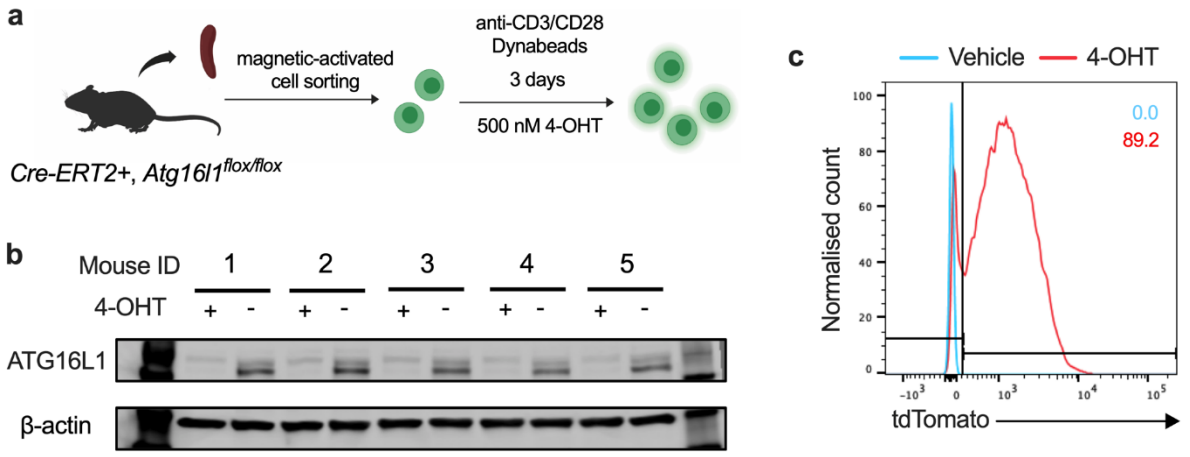


Figure 4.8 CD4+ T cells from *Cre-ERT2*+, *Atg16l1*$^{flox/flox}$ mouse model display efficient deletion of *Atg16l1* induced by 4-hydroxytamoxifen (4-OHT).

a) Experimental set-up for inducible knock-out of *Atg16l1* in the CD4+ T cells from the *Cre-ERT2*+, *Atg16l1*$^{flox/flox}$ mouse model. b) Western blot to show the ATG16L1 protein level in *Cre-ERT2*+, *Atg16l1*$^{flox/flox}$ CD4+ T cells treated with vehicle or 4-OHT during a 3-day activation. c) Histogram shows tdTomato expression level in *Cre-ERT2*+, *Atg16l1*$^{flox/flox}$ CD4+ T cells, with a Rosa-tdTomato reporter, treated with vehicle (blue) or 4-OHT (red) during a 3-day activation.

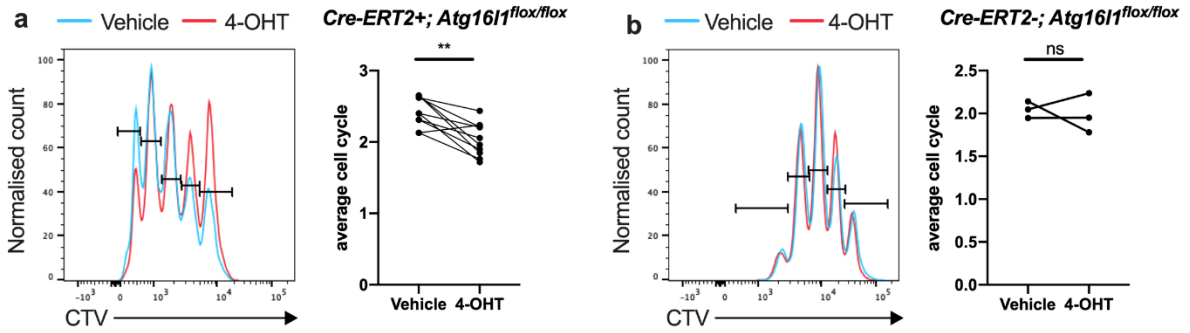


Figure 4.9 *Atg16l1*-deficient CD4+ T cells show impaired proliferation in vitro.

a) Histogram (left) showing proliferation profile of splenic CD4+ T cell from *Cre-ERT2*+, *Atg16l1*$^{flox/flox}$ mice. Cells were stained with CellTrace Violet (CTV), treated with vehicle (blue) or 4-hydroxytamoxifen (4-OHT, red) and activated for 3 days. Bar graph (right) indicates the average cell division of total tdTomato+ CD4+ T cells (n=10 mice per group). b) Histogram (left) shows proliferation profile of splenic CD4+ T cell from *Cre-ERT2*-, *Atg16l1*$^{flox/flox}$ mice undergoing 3-day activation, as a control to exclude the effect of 4-OHT treatment. Bar graph (right) indicates the average cell division of total CD4+ T cells (n=3 mice per group). All statistics by unpaired two-tailed Student's t-test, p**<0.01, ns: not significant. Results are representative of two independent experiments.

4.2.5. Different subsets of T cells are altered in the aged immune system

In this next set of experiments, I investigated the changes of CD4+ T cells in the aged immune system, and how they are related to a diminished autophagy level. Before moving into the cellular changes of aged T cells, I first checked the different populations of T cells in both young (3 months) and old (2 years) mice. The frequency of CD8+ T cells was significantly decreased among total splenocytes, while the CD4+ T cells displayed no difference (Figure 4.10a). It is consistent with a previous report that the aged CD8+ T cell populations undergo a more severe contraction than CD4+ T cells[298]. Moreover, both CD4+ and CD8+ lymphocytes showed a decreased naïve population and an increased effector population (Figure 4.10b and c), indicating a shift from naïve to memory/effector population in both cell types.

Next, I checked whether the CD4+ T cell population displays an increased frequency of age-related surface markers, similar to what has been described for CD8+ T cells[299]. For antigen-inexperienced virtual memory population (T_{vm}) characterised by the high expression of CD44 and low levels of CD49, an increase in its frequency was apparent in CD4+ (and CD8+ T cells) during ageing, as well as an increase of the antigen-experienced memory population (T_{mem}) and a decrease in naïve T cells (T_n) (Figure 4.11). Therefore, CD4+ T cells can develop memory-like features analogous to CD8+ T_{vm}, at least in the terms of cellular markers.

Within the $CD44^{hi}$ antigen-experienced effector/memory population, I observed a significant increase of CD27- CD28- population in both aged CD4+ and CD8+ T lymphocytes, indicating an expansion of these terminally differentiated subsets (Figure 4.12). The phenotype is also observed in human T cells during ageing[300]. It is worth noticing that the CD27- CD28- population is present at a much higher frequency even in young CD4+ effector/memory

compartment than in CD8+, implying the stability of memory of CD4+ T cells is lower than that of its CD8+ counterparts since both co-stimulation receptors promote the survival[301].

The frequency of the KLRG1+ population was also increased in both antigen-experienced CD4+ $CD44^{hi}$ and CD8+ $CD44^{hi}$ populations during ageing, while CD8+ T cells shows a much higher frequency (Figure 4.13). It might be linked with the dramatic decrease in the cytolytic activity of CD8+ T cells during ageing[302].

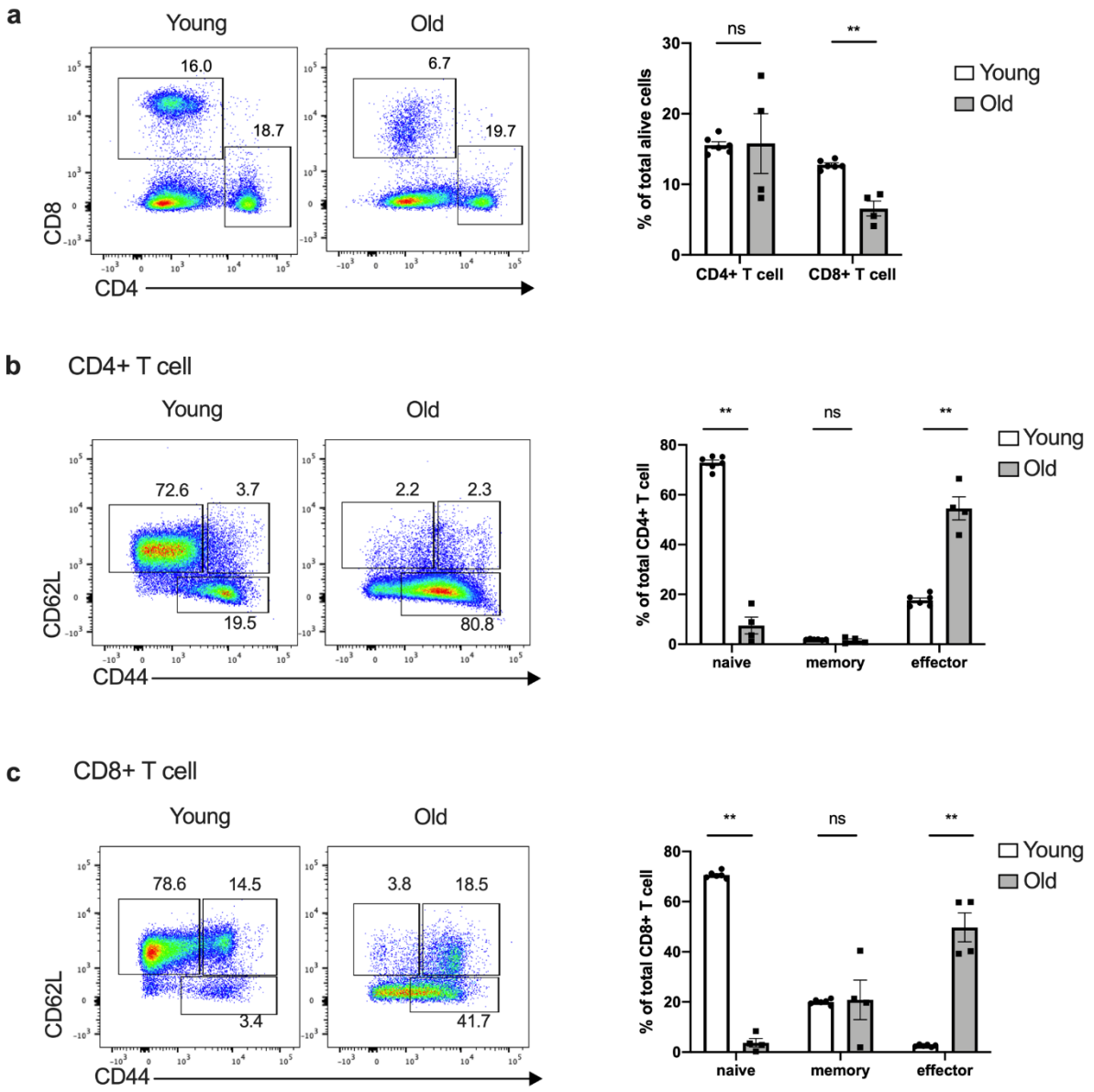


Figure 4.10 Aged T cells display a shift from naive to memory/effector populations.

a) Dot plots (left) of CD4+ and CD8+ T lymphocytes from the spleens of young (3 months) and old (2 years) mice (n = 4-6 mice per group). Bar graph (right) indicates the percentage of the gated population among total splenocytes. Dot plots show different CD4+ (b, left) and CD8+ (c, left) T cell subsets, including naïve (CD62L+ CD44^{lo}), memory (CD62L+, CD44^{hi}) and effector (CD62L-, CD44^{hi}) T cells, from the spleens of young (3 months) and old (2 years) mice (n=4-6 mice per group). Bar graphs indicate the percentage of each subset among total CD4+ (b, right) and CD8+ (c, right) T cells as mean ± SEM. All statistics by unpaired two-tailed Student's t-test, **p<0.01, ns: not significant. Results are representative of three independent experiments.

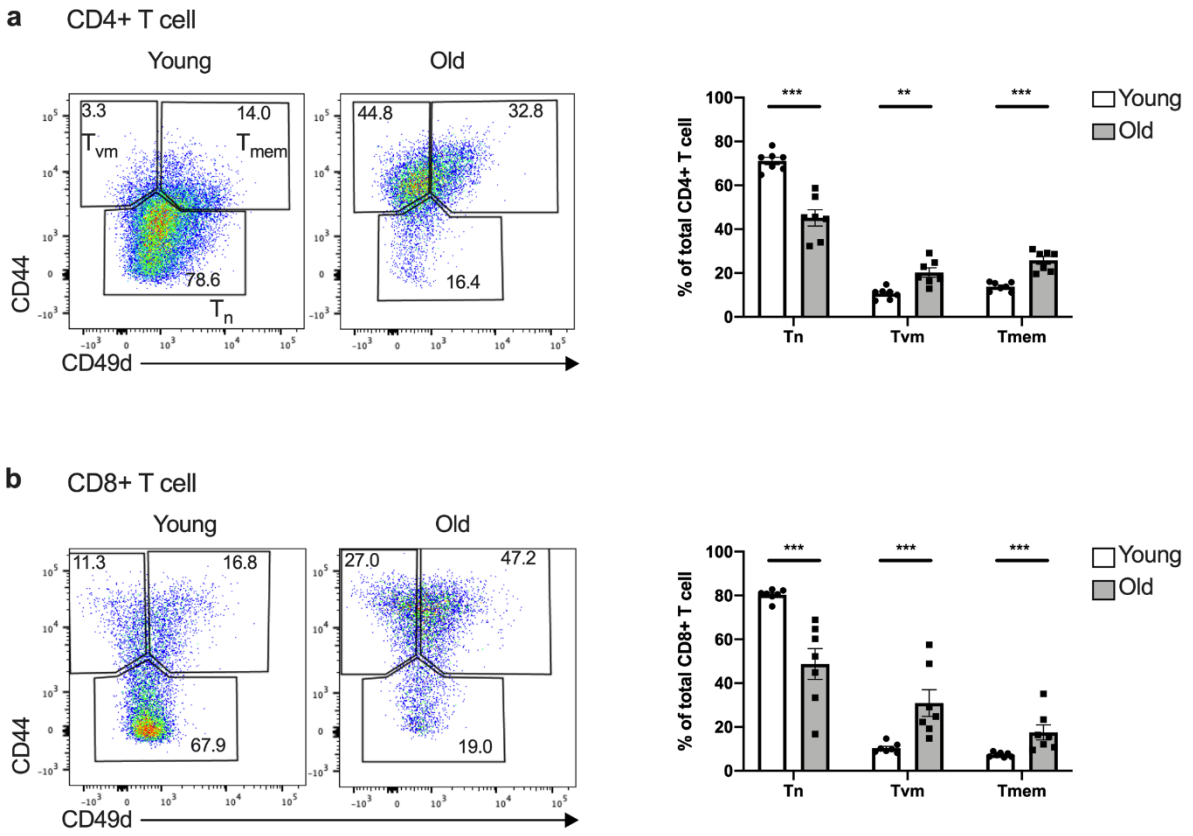


Figure 4.11 Aged T cells display an expansion of the virtual memory population.

Dot plots of different CD4+ (a, left) and CD8+ (b, left) T cell subsets, including naïve (T_n, $CD44^{lo}$), memory (T_{mem}, $CD44^{hi}$, $CD49^{hi}$) and virtual memory (T_{vm}, CD62L-, $CD44^{hi}$) T cells, from the spleens of young (3 months) and old (2 years) mice. Bar graphs indicate the percentage of each subset among total CD4+ (a, right) and CD8+ (b, right) T cells as mean ± SEM (n=7 mice per group). All statistics by unpaired two-tailed Student's t-test, **p<0.01, ***p<0.001. Results are representative of three independent experiments.

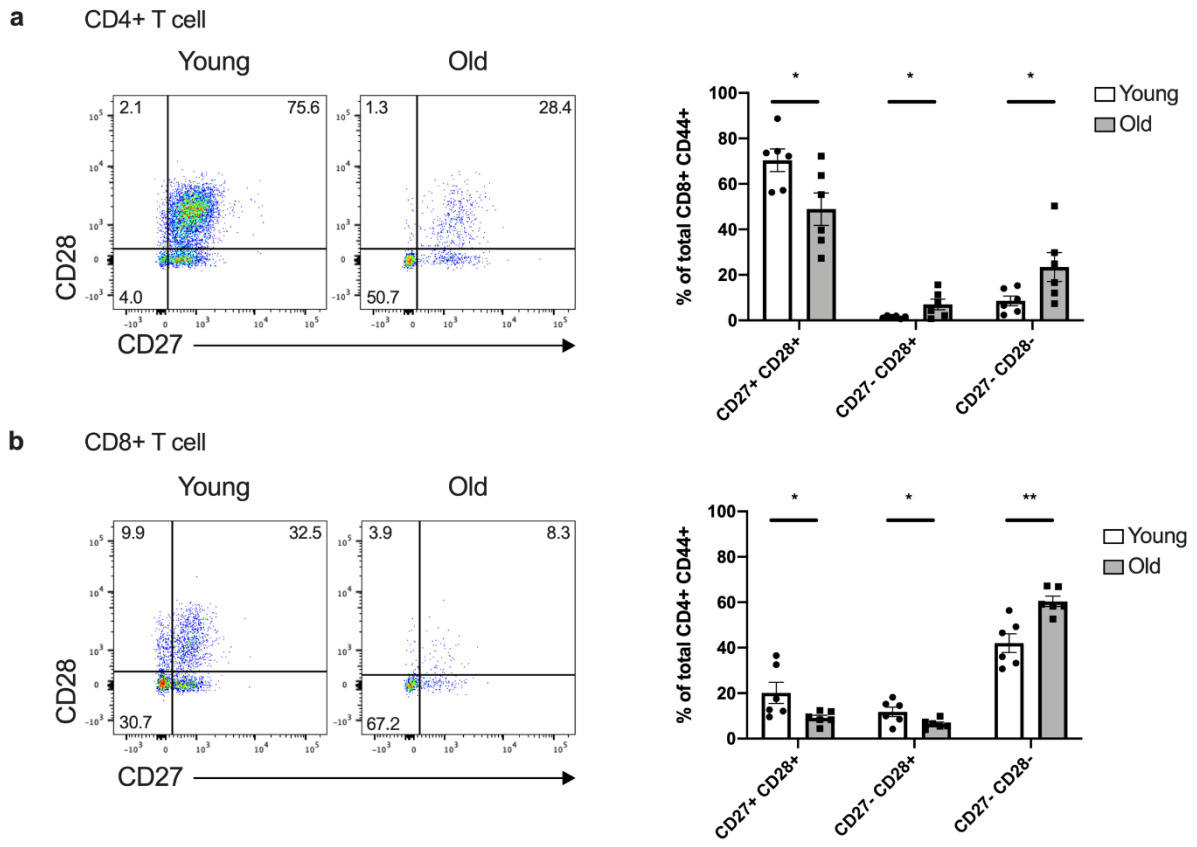


Figure 4.12 Aged T cells display an expansion of the senescent-like population.

Dot plots of different CD8+ CD44^{hi} (a, left) and CD4+ CD44^{hi} (b, left) T cell subsets, including CD27+ CD28+, CD27- CD28+, and CD27- CD28- T populations, from the spleens of young (3 months) and old (2 years) mice. Bar graphs indicate the percentage of each subset among total CD8+ CD44^{hi} (a, right) and CD4+ CD44^{hi} (b, right) T cells as mean ± SEM (n=6 mice per group). All statistics by unpaired two-tailed Student's t-test, *p<0.05, **p<0.01. Results are representative of three independent experiments.

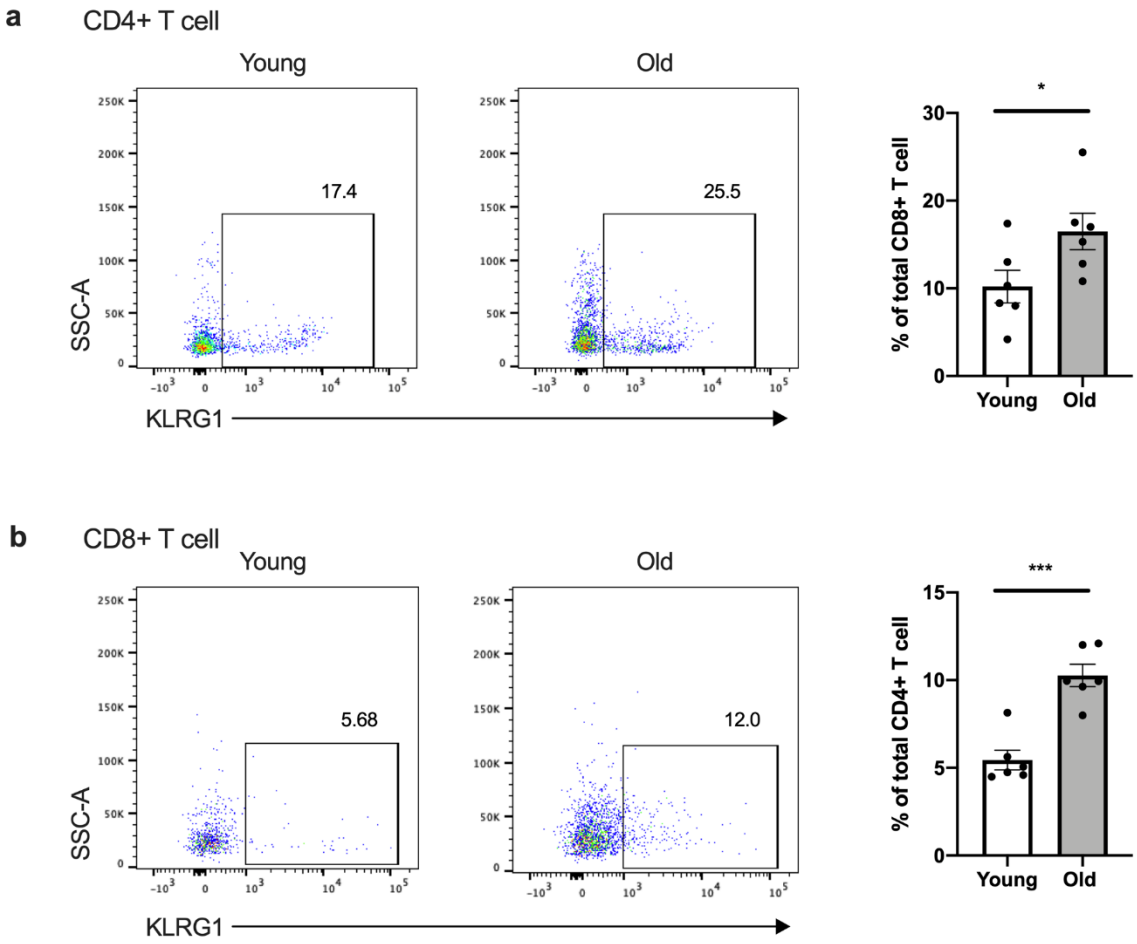


Figure 4.13 Aged T cells display an expansion of the KLRG1+ population.

Dot plots showing KLRG1+ populations in CD8+ (a, left) and CD4+ (b, left) T cell from the spleens of young (3 months, blue) and old (2 years, red) mice. Bar graphs indicate the percentage of KLRG1+ population among CD8+ CD44^{hi} (a, right) and CD4+ CD44^{hi} (b, right) T cells as mean ± SEM (n=6 mice per group). All statistics by unpaired two-tailed Student's t-test, **p<0.01. Results are representative of three independent experiments.

4.2.6. Autophagic flux is decreased in aged CD4 T cells

Aged cells usually show compromised autophagy[303]. Here, I utilised a newly-developed autophagy detection kit based on LC3-II flow cytometry staining to confirm that the autophagy flux declines in different subsets of aged CD4+ T cells[242]. Cells were treated with BafA1, a lysosomal V-ATPase inhibitor that prevents the acidification of lysosomes and further blocks the autophagosome-lysosome fusion. Upon BafA1-treatment, the membrane-bound LC3-II is increased in CD4+ T cells from both young (3 months) and old (2 years) (Figure 4.14a) due to the accumulation of autophagosomes. Note that aged CD4+ T cells displayed a significantly higher basal LC3-II level, reflecting the impaired autophagosome-lysosome fusion and consequently the accumulation of LC3-II positive autophagosomes in aged cells. Autophagic flux was calculated as LC3-II geometric mean fluorescence intensity (BafA1-Vehicle)/Vehicle. While the autophagic flux was similarly high in different young CD4+ T cell subsets, a significant decrease of autophagic flux in all populations was observed during ageing (Figure 4.14b). The naïve CD4+ T cell was the most affected population, which may hint at a more severe functional deficit. During ageing, the autophagic flux was also decreased in CD8+ T cells, but the reduction was more homogenous across different subsets (Figure 4.14c).

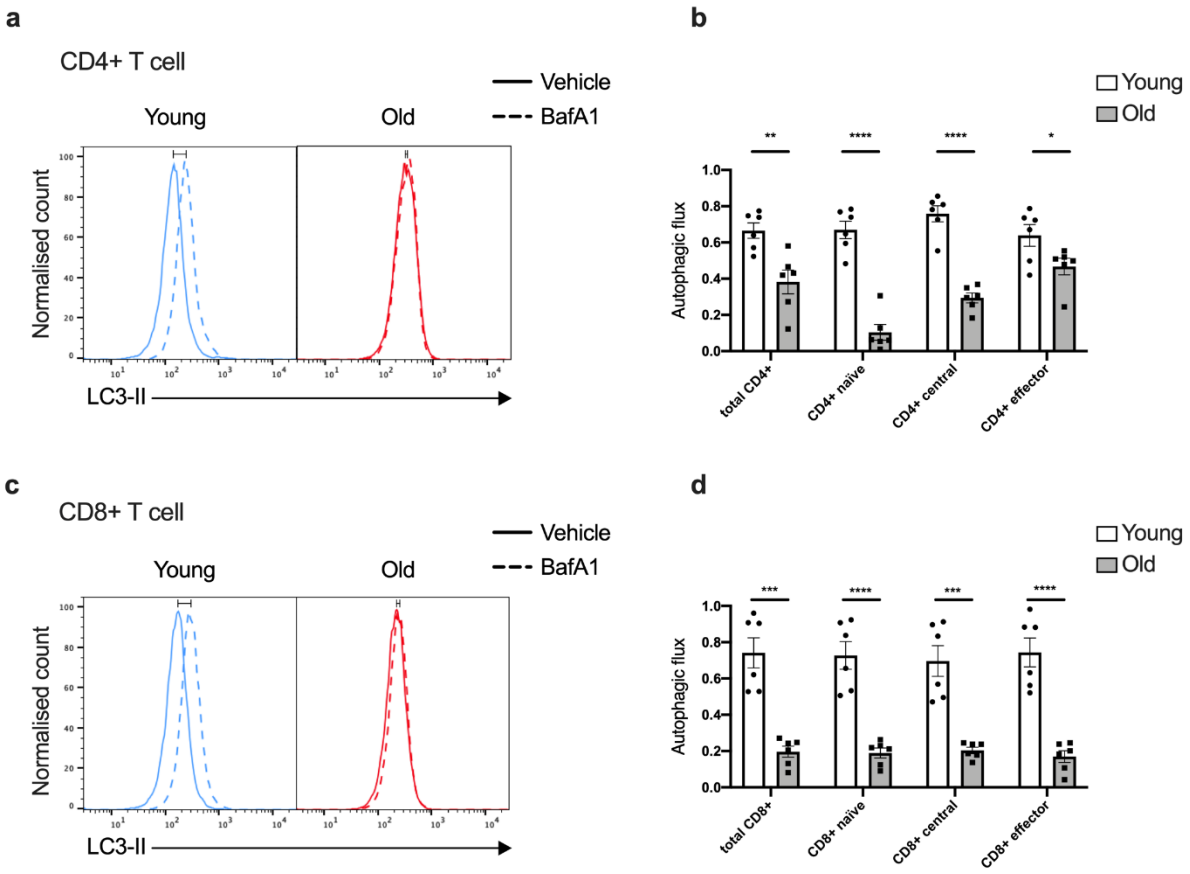


Figure 4.14 CD4+ T and CD8+ T cells from aged mice show decreased autophagic flux.

a) Representative LC3-II plots of CD4+ T cells isolated from the spleen of young (3 months, blue) and old (2 years, red) mice, cultured in complete RPMI media for 2 hours, with (solid) or without (dotted) BafA1. Cytosol-free LC3-I was washed away by 0.05% Saponin, leaving the membrane-bound LC3-II stained with conjugated antibody and measured by flow cytometry. Bar graphs indicate the autophagic flux in different CD4+ (b) and CD8+ (c) T cell subsets from young (3 months) and old (2 years) mice as mean ± SEM (n = 6 mice per group), which was calculated by the LC3-II geometric mean fluorescent intensity (BafA1 - Vehicle)/Vehicle. Statistics by unpaired two-tailed Student's t-test, p*<0.05, p**<0.01, p***<0.001, p****<0.0001. The result is representative of two independent experiments.

4.2.7. T cell activation and proliferation is decreased in aged CD4+ T cells

We found that autophagy-deficient CD4+ T had a proliferation defect and aged CD4+ T were with an impaired autophagic flux. Therefore, I checked whether aged CD4+ T cells mimic the proliferation profile of autophagy-deficient CD4+ T cells. Because the T cell pool in the aged immune system is dominated by effector and memory populations, and to compare the activation and proliferation of young and old naïve CD4+ T cells, I purified the splenic CD44- CD4+ T cells via flow sorting. Consistent with a previous report, at day 1 post-activation, the CD25+ population in aged mice is significantly lower than in their young counterpart (Figure 4.15)[304]. This is the opposite of what we observed in T-Atg7$^{-/-}$ CD4+ cells where the early-activation markers were not changed (Figure 4.4). Some studies report that the impaired early activation of naïve CD4+ T cells during ageing might be due to the alterations in membrane raft and defective one-carbon metabolism[305]. The perturbations of TCR signal transduction appears in CD4+ T cells during ageing but not when loss of autophagy, due to the alteration in the membrane lipid composition or the accumulation of phosphatases. In contrast, the proliferation profile on day 3 indicates a significant decrease of cells undergoing divisions (Figure 4.16), which is similar to the proliferation defect of autophagy-deficient CD4+ T cells. In summary, these results confirm that the CD4+ T cell with impaired autophagy partly mirrors the ageing phenotypes.

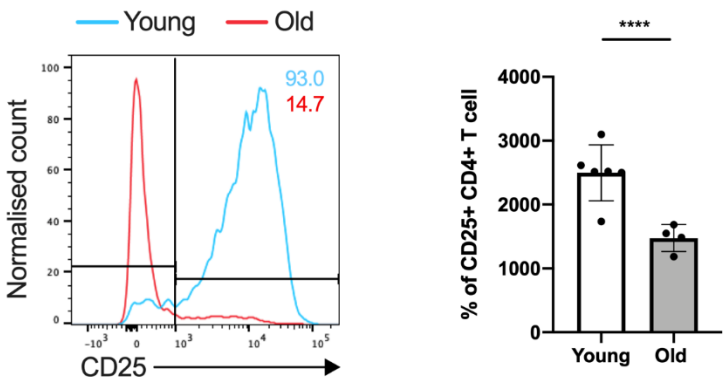


Figure 4.15 Aged naïve CD4+ T cells showed impaired upregulation of early-activation marker upon TCR-mediated activation.

Histogram (left) showing CD25 expression level in CD4+ T cell activated for 24 hours, from young (3 months, blue) and old (2 years, red) mice. Bar graph (right) indicates the percentage of CD25+ CD4+ T cells as mean ± SEM (n = 4-6 mice per group). Statistics by unpaired two-tailed Student's t-test, p****<0.0001. The result is representative of two independent experiments.

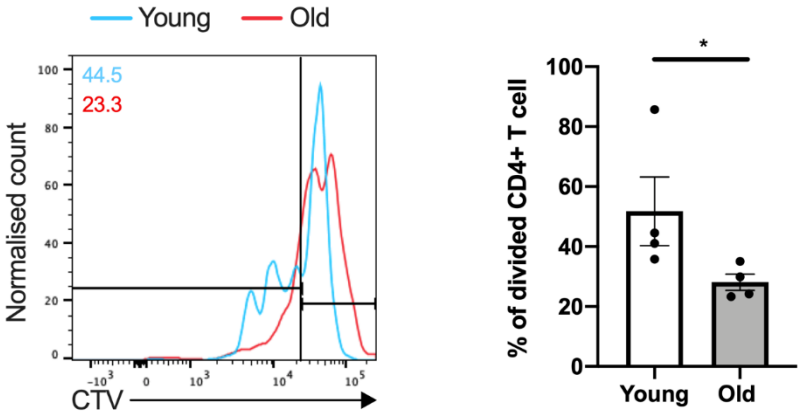


Figure 4.16 Aged naïve CD4+ T cells showed impaired proliferation upon TCR-mediated activation.

Histogram (left) showing the proliferation profile of flow-sorted CD44- CD4+ T cells stained with CellTrace Violet and activated for 3 days, from young (3 months, blue) and old (2 years, red) mice. Bar graph (right) indicates the percentage of divided CD4+ T cells as mean ± SEM (n = 4-6 mice per group). Statistics by unpaired two-tailed Student's t-test, p*<0.05. The result is representative of two independent experiments.

4.2.8. The impaired proliferation in aged CD4+T cells is not due to cellular senescence

The impaired proliferation of aged CD4+ T cells might be linked with cellular senescence, a term that refers to the irreversible cell cycle arrest state and recapitulates ageing[197]. I checked two common markers for detecting cellular senescence, $p16^{INK4a}$ expression and enhanced senescence-associated β-galactosidase (SA-β-Gal) activity. I tried several commercial antibodies for $p16^{INK4a}$. However, there are no validated antibodies for murine $p16^{INK4a}$ to date (personal communication, Professor Michelle Linterman). Using a reporter system, a paper published in 2019 showed no dramatic increase of $p16^{INK4a}$-expressing peripheral T cells during ageing[291]. Therefore, I continued to examine the other senescent marker, the SA-β-Gal activity.

To measure SA-β-Gal activity, I used C_{12}FDG (5-dodecanoylaminofluorescein di-β-D-galactopyranoside), a galactosidase substrate that is covalently linked to a 12-carbon lipophilic moiety[306]. After entering the cell and being cleaved by galactosidase, its fluorescent product can be integrated into and retained by the intracellular membrane structure. I performed the C_{12}FDG staining on both young and old CD4+ T cells treated with BafA1 to increase the lysosomal pH. In line with the $p16^{INK4a}$ result, there was no significant increase in SA-β-Gal activity in naïve, memory or effector CD4+ population during ageing (Figure 4.17). In summary, cellular senescence may not explain the defects of activation and proliferation in aged CD4+ T cells.

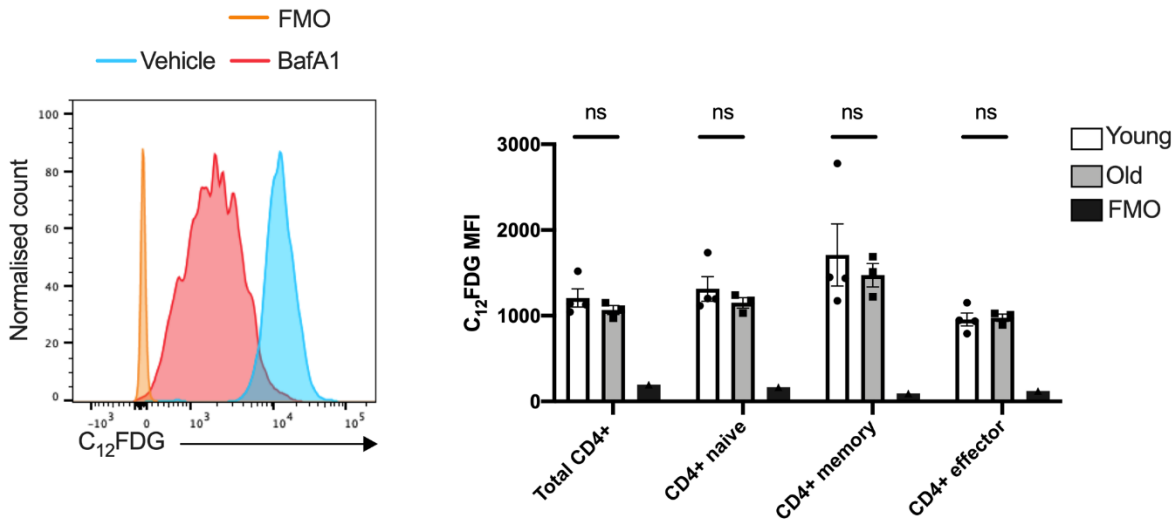


Figure 4.17 Aged CD4+ T cells did not show increased senescence-associated β-galactosidase (SA-β-Gal) activity.

a) The lysosomal beta-galactosidase displays peak activity of hydrolysing the beta-galactosides between pH 4.0 and 4.5 in functional lysosomes (Vehicle, blue). In senescent cells, due to the accumulation of the enzyme, such activity is detectable at pH 6.0 when cells are treated with Bafilomycin A1 (BafA1, red), but non-senescent cells show lower signal. b) Bar graph indicating the SA-β-Gal activity in different CD4+ T cell subsets treated with BafA1 for 2 hours prior to the C_{12}FDG staining as mean ± SEM, from young (3 months) and old (2 years) mice (n=3-4 mice per group). All statistics by unpaired two-tailed Student's t-test, ns: not significant. The result is representative of two independent experiments.

4.2.9. mTOR signalling pathways are dysregulated in aged T cells

mTOR forms part of two distinct complexes, mTORC1 and mTORC2, which act as the major regulator of growth and is the link between the availability of nutrients in the environment and the control of most anabolic and catabolic processes. The inhibition of TOR activity has beneficial effects during ageing, including autophagy induction. To test whether decreased autophagy in aged CD4+ T cells is due to altered upstream signalling pathways, I investigated mTORC1 signalling (directly suppresses autophagy) and mTORC2 signalling (suppresses autophagy indirectly, through activation of mTORC1) (Figure 4.18 and 4.19). As expected, when T cells are treated with Torin 1, an inhibitor for both signalling pathways, the staining for phosphorylated Tor, 4EBP1 and pS6, as well as phosphorylated Akt at Ser473 site, displays a shift to the left (Figure 4.18a, b and c, left; Figure 4.19, left). Interestingly, basal mTORC1 signalling, which is indicated by the reduced levels of phosphorylated S6 and 4EBP1, undergoes a small but significant decrease in CD4+ T cells during ageing, (Figure 4.18b and c, middle). By contrast, mTORC2 signalling, indicated by the phosphorylation status of Akt on its Ser473, was increased in aged naïve CD4+ T cells, but decreased in the effector population (Figure 4.19, middle). Upon TCR-mediated activation, aged CD4+ T cells failed to upregulate both mTORC1 and mTORC2 signalling pathways to the same extent as their young counterparts (Figure 4.18a, b and c, right; Figure 4.19, right). These results reflect that the decreased autophagy levels in aged CD4+ T cells are caused by multiple factors rather than the change of a single upstream signalling pathway. These data also show that intrinsic deficits of aged CD4+ T cells lead to impaired metabolic sensing during activation.

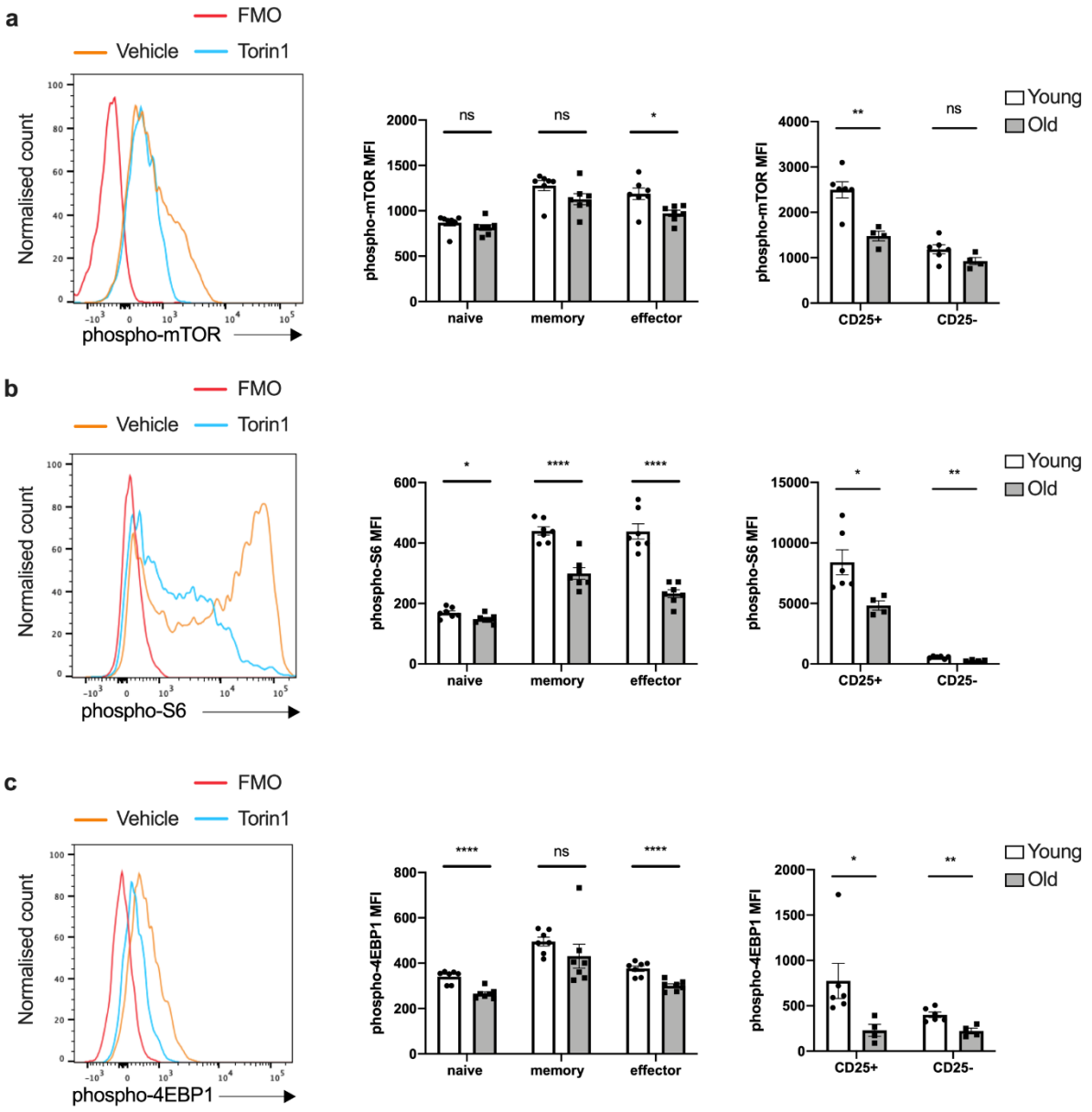


Figure 4.18 mTORC1 signalling declines in aged CD4+ T cells.

Representative plot of phosphorylated-mTOR (a, left), phosphorylated-S6 (b, left), and phosphorylated-4EBP1 (c, left) staining. Both FMO control (orange) and the negative control treated with Torin 1 (an mTOR inhibitor, blue) showed a lower signal compared to the vehicle-treated sample (red). Bar graphs indicate the phosphorylated-mTOR (a, middle), phosphorylated-S6 (b, middle), and phosphorylated-4EBP1 (c, middle) levels in different CD4+ T cell subsets at the basal level as mean ± SEM. Bar graphs indicate the phosphorylated-mTOR (a, right), phosphorylated-S6 (b, right), and phosphorylated-4EBP1 (c, right) level as mean ± SEM in CD4+ T cells activated for 24 hours, gated by CD25 expression level. All statistics by unpaired two-tailed Student's t-test, with n=4-6 mice per group. p*<0.05, p**<0.01, p****<0.0001, ns: not significant. The results are representative of two independent experiments.

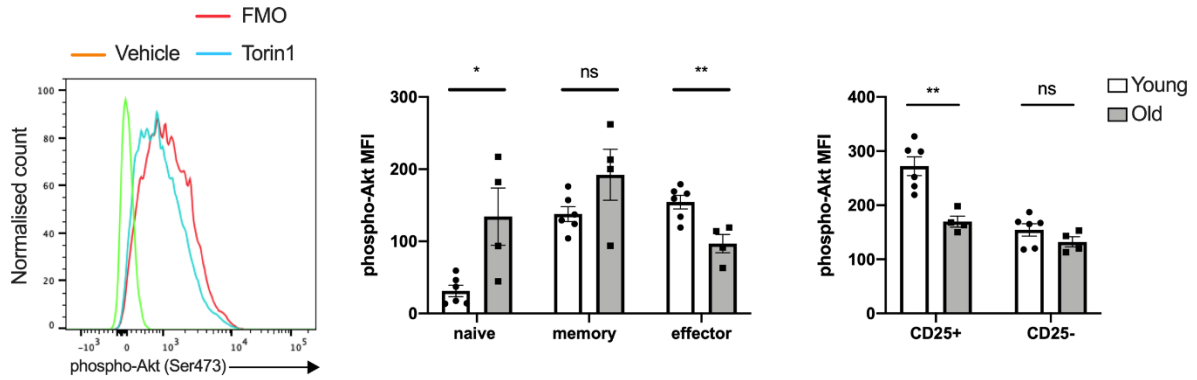


Figure 4.19 mTORC2 signalling is dysregulated in aged CD4+ T cells.

Representative plot (left) of phosphorylated-Akt (Ser473) staining, downstream of mTORC2. FMO control (orange) and negative control treated with Torin 1 (an mTOR inhibitor, blue) showed a lower phosphorylated-mTOR level compared to the vehicle-treated sample (red). Bar graph (middle) indicates the phosphorylated-Akt (Ser473) level in different CD4+ T cell subsets at the basal level as mean ± SEM. Bar graph (right) indicates the phosphorylated-Akt (Ser473) level as mean ± SEM in CD4+ T cells activated for 24 hours, gated by CD25 expression level. All statistics by unpaired two-tailed Student's t-test, with n=4-6 mice per group. p*<0.05, p**<0.01, ns: not significant. The results are representative of two independent experiments.

4.2.10. The global translation rate is decreased in aged CD4+ T cells

The result above shows downregulation of basal mTORC1 signalling in aged CD4+ T cells, which may imply that the cells are deprived of amino acids and therefore overall protein synthesis rate may be decreased[307]. Translation has been found reduced in many tissues from old mice[308,309]. To determine the protein synthesis rate in T cells, I used O-propargyl-puromycin (OPP)-Click assay, which allows cells to incorporate the OPP into de novo synthesised peptides, as it can be detected by the flow cytometry via fluorophores conjugated to the OPPs, which is triggered by the 'Click' reaction (Figure 4.21a). The amount of incorporated OPP reflects the protein synthesis rate. Administration of a translation elongation inhibitor, cycloheximide, should reduce the OPP level and was used as a positive control of my assay (Figure 4.21b, left). Among all CD4+ T cell subsets, the global translation rate displayed a significant decrease compared to the young cells (Figure 4.21b, right), which is consistent with the decreased mTORC1 signalling that I found in these subsets during ageing.

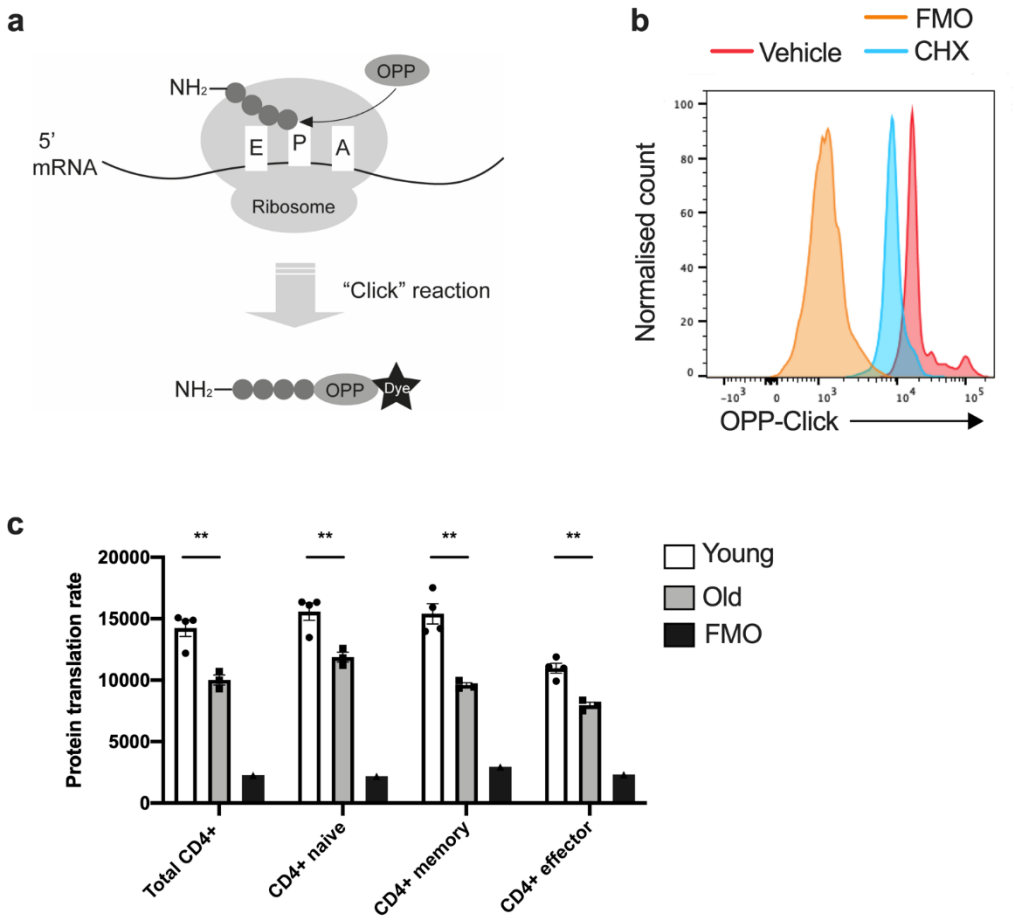


Figure 4.20 Aged CD4+ T cells show a decreased rate of protein synthesis.

a) Schematic overview of the OPP-Click assay measuring protein synthesis rate. O-propargyl-puromycin (OPP) is integrated into the peptides which are newly synthesised. Then Click reaction can conjugate the fluorophore to OPP for detection by flow cytometry b) Representative OPP-Click plot (left) of CD4+ T cells freshly isolated from the mouse spleen and incubated in the complete RPMI media. The protein translation rate was measured by OPP-Click assay (red). Cycloheximide (CHX), a protein translation inhibitor, was administrated to the cells for 2 hours as a positive control (blue). An FMO negative control (orange) was included. Bar graph (right) indicates the comparison of different CD4+ T cell subsets from young (3 months) and old (2 years) mice as mean ± SEM (n=3-4 mice per group). All statistics by unpaired two-tailed Student's t-test, p**<0.01. The results are representative of two independent experiments.

4.2.11. Lipid droplets are accumulated in aged CD4+ T cells

Lipid droplets serve as storage organelles that regulate systemic energy homeostasis. They consist of a hydrophobic core of neutral lipids and a phospholipid monolayer shell decorated by several types of proteins[310]. Lipolysis and lipophagy are two catabolic pathways to release the free fatty acids sequestered in the lipid droplets to facilitate metabolic changes and membrane biogenesis[311]. Dysregulation of either pathway may lead to an accumulation of the lipid droplets and predispose the individuals to disease, including obesity, non-alcoholic fatty liver disease, cardiovascular disease[310]. To examine whether the quantity of lipid droplets changes in aged T cells, which displayed decreased autophagy level and dysregulated metabolism, we performed staining using a hydrophobic fluorescent dye called BODIPY, which can bind to the neutral lipids enriched in lipid droplets. My data show that the lipid droplets levels were significantly upregulated in all CD4+ T cells subsets of aged mice (Figure 4.21). This observation is consistent with a previous report in *Atg5*-knockout CD4+ T cells, suggesting lipophagy's role in CD4+ T cell metabolism[119].

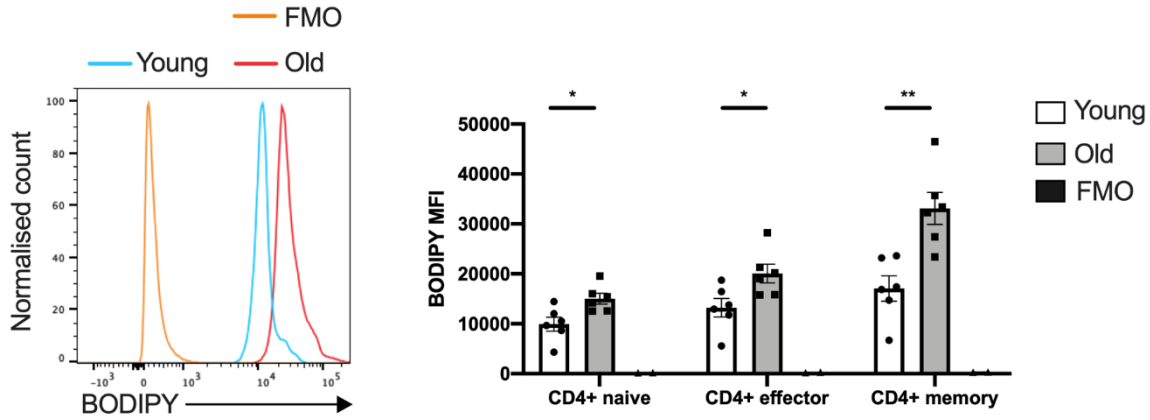


Figure 4.21 Aged CD4+ T cells showed accumulation of lipid droplets.

a) Histograms showing the BODIPY staining in CD4+ T cells from young (3 months, blue) and old (2 years, red) mice, with FMO staining as a control (orange). BODIPY is commonly used to detect intracellular neutral lipids enriched in lipid droplets. b) Bar graph showing the lipid droplet level in different CD4+ T cell subsets from young (3 months) and old (2 years) mice as mean ± SEM (n=6 mice per group). All statistics by unpaired two-tailed Student's t-test, p*<0.05, p**<0.01. The results are representative of two independent experiments.

In summary, I found that one of the classical markers for **cellular senescence**, SA-β-Gal activity, was not changed in aged T cells. For hallmarks of **cellular ageing**, I observed a disrupted proteostasis (typified by a decline in autophagic flux and protein synthesis rate) and an accumulation of lipid droplets across all T cell subsets from aged mice. The decreased autophagy level seems irrelevant to mTOR signalling since I observed an age-associated decrease of both mTORC1 and mTORC2 signalling either pre- or post-activation, except for naïve T cells from aged mice which display an increased mTORC2 signalling.

Chapter 4: Characterisation of autophagy and ageing phenotypes in CD4+ T cells – Discussion

4.3 Discussion

In this chapter, I have applied flow cytometry-based techniques to detect the hallmarks of cellular senescence and cellular ageing in immune cells (techniques are summarised in my review)[201]. However, due to the COVID-19 pandemic, my access to the aged mice was limited. Not all markers were systematically screened and linked to the functional changes of different subsets of the T cells during ageing. To fully understand the cellular changes of the aged T cells, further studies need to be conducted to detect the onset of expression of the different biomarkers over the lifetime of the mouse, thereby establishing a longitudinal atlas that will represent the 'depth' of ageing, i.e. being positive for several biomarkers would indicate a deeper ageing phenotype.

My previous lab members found that autophagy-deficient CD4+ T cells fail to form the effector population upon two forms of antigenic stimulation. Based on their research and previous studies with different mouse models lacking autophagy, I further extend the observation that the T-Atg7$^{-/-}$ CD4+ T cells showed delayed proliferation compared to the wild-type cells[97,101-103,105,107,290,312]. Excluding that the phenotype is due to incomplete gene knockout or excessive cell death, the late onset of the cell cycle in T-Atg7$^{-/-}$ CD4+ T cells is likely caused by a delayed degradation of some molecular 'brakes' on proliferation, which need to be degraded by autophagy initially, and later by some compensatory pathways, such as UPS. Therefore, to find the molecules needed to be degraded by autophagy to lift the 'brake', in the next chapter, I utilised the *Lc3b-APEX2* mouse model to investigate the autophagosomal cargoes of the activated CD4+ T cells.

To some extent, CD4+ T cells from aged mice mimic the autophagy-deficient counterparts, since both of them have impaired autophagy and proliferation. However, unlike T-Atg7$^{-/-}$

CD4+ T cells whose TCR/CD28-signalling is intact, cells from aged mice had a priming issue. Indeed, some studies indicate that the TCR signalling is impaired in aged T cells due to inefficient ROS production and a change in membrane property to form rafts necessary for the signal transduction[313]. Moreover, in naïve CD4+ T cells, the expression of miR181a is reduced during ageing, leading to the overexpression of its target dual-specific phosphatase 6 (DUSP6)[314]. Since DUSP6 can dephosphorylate ERK, it attenuates the ERK signalling pathway during T cell activation and disrupts the forward feedback loop in TCR signalling[315]. Also, it can explain the impaired induction of mTOR activity after T cells are activated. A similar mechanism may not apply to the autophagy-deficient CD4+ T cells, thus explaining their different phenotypes. To align the phenotypes of these two cell populations, it is important to consider that autophagy-deficient mice used here entirely lack autophagy (from the thymic stage of development onwards), while autophagy levels gradually decline in aged cells. Long-term cellular homeostasis may therefore lead to distinctive adaptive states. It is possible that knocking-down autophagy rather than deleting it entirely may simulate the process of ageing better. Moreover, multiple factors contribute to cellular ageing. Identifying each factor's contribution to age-associated functional changes can help to fill the gap in our understanding of ageing.

To explore whether the impaired proliferation of aged T cells is due to the cellular senescence, I checked the SA-β-Gal activity, which showed no significant change in CD4+ T cells during ageing. However, to make sure that cellular senescence is not a factor leading to age-associated changes in T cells, it is necessary to systemically screen for other senescent markers as well, such as telomere length, SASPs and protein levels of p53 and γ-H2AX[201]. Moreover, due to the heterogeneous expression level of each marker in different T cell subsets, and the

immunosenescence-related population shift, the screening needs to be performed at single-cell resolution for a cell-type-wise comparison in young and old immune systems.

For the markers of immune cell ageing, as expected, I observed the disturbed proteostasis typified by a decline in autophagy and global translation rate. Interestingly, in contrast to the previous studies in other cell types, the basal level of the mTORC1 signalling was significantly decreased in most T cell subsets from aged mice, whereas elevated mTORC2 signalling, which involves the control of cell metabolism, may contribute to the defects of aged naïve CD4+ T cells. The pathway can boost glucose uptake and glycolysis while suppressing oxidative phosphorylation (OXPHOS)[316]. Since naïve T cells are metabolically quiescent and primarily rely on OXPHOS, enhanced mTORC2 activity may lead to their metabolic change and probably affect their maintenance as well as response upon antigenic stimulation during ageing[317]. Besides, I observed an accumulation of lipid droplets in aged CD4+ T cells, similar to a previous finding in autophagy-deficient T cells[119]. It is still elusive whether this is due to a decreased degradation of the organelle (via lipophagy, CMA or lipolysis), or their increased formation in response to the inflammatory environment, and how LDs are linked to the age-associated phenotypes of CD4+ T cells[318-320]. Further investigation into the metabolic status of naïve CD4+ T cells during ageing is required to make a solid conclusion.

Initially, I planned to use the *Lc3b-APEX2* model to investigate the autophagosomal cargoes in young and aged CD4+ T cells, to see whether autophagy mediates the degradation of a different set of proteins in T cells during ageing. However, the ageing of the *Lc3b-APEX2* mice was interrupted by the COVID-19 pandemic. Instead, in the next chapter, I investigated the autophagosomal proteome during CD4+ T cell proliferation, a process that we found was delayed in the absence of autophagy.

Chapter 5: Characterisation of autophagic substrates in activated CD4+ T cells and their role for CD4+ T cell proliferation – Introduction

5.1 Introduction

In chapter 1, I introduced three major signalling pathways essential for T cell activation and proliferation, which are mediated by TCRs, co-stimulatory receptors and IL-2Rs. Here, driven by the proximity labelling results in CD4+ T cells, I will introduce two molecules that are also key for the maintenance and function of T cells, and their signalling pathways, the transcription factor NF-κB and the cytokine receptor IL-7R.

5.1.1 NF-κB signalling pathway

Nuclear factor kappa-light-chain-enhancer of activated B cells (NF-κB) is a family of inducible transcription factors evolutionarily conserved in most eukaryotic cells. Through forming homo- or heterodimers to initiate the transcription of target genes, the NF-κB proteins contribute to a collection of cellular processes, including immune and inflammatory responses, as well as cellular growth and apoptosis[321]. The family is composed of five structurally-related members – NF-κB1 (or p50), NF-κB2 (or p52), RelA (or p65), RelB and c-Rel. These proteins share a common Rel homology domain which facilitates their dimerization and binding to DNA[322].

NF-κB activity in vivo is under tight control to allow fine regulation of its downstream inflammatory cascade. Based on the differences in external triggering stimuli, and which transcription dimers are recruited, NF-κB signalling can be categorised into canonical and non-canonical pathways. The activation of the canonical NF-κB pathway relies on the signals transduced through the antigen receptors (T-cell receptors and B-cell receptors), pattern-recognition receptors (e.g. Toll-like receptors, NOD-like receptors), or pro-inflammatory cytokine receptors[323] (Figure 5.1). In unstimulated cells, members of the canonical IκB (inhibitor of NF-κB, including IκBα, IκBβ, and IκBε) family sequestrate the transcription

complex in the cytoplasm and inhibit the signalling. When cells receive environmental stimuli, the IκB kinase (IKK) complex is activated and its IKKβ subunit phosphorylates the IκB protein, which allows its K48-linked ubiquitination, which culminates in its proteasome-mediated degradation. Followed by the removal of IκB proteins, the NF-κB complex translocates into the nucleus and initiates the expression of target genes. In contrast, several tumour necrosis factor receptors (TNFRs) account for the activation of the non-canonical pathway and relay signals to the NF-κB-inducing kinase (NIK)[324] (Figure 5.1). IKKα in the IKK complex triggers the partial degradation of the non-canonical IκBs, p100 and p105 (precursors of NF-κB2 and NF-κB1, respectively). The well-orchestrated events result in the nuclear localisation of the major dimer RelB/p52.

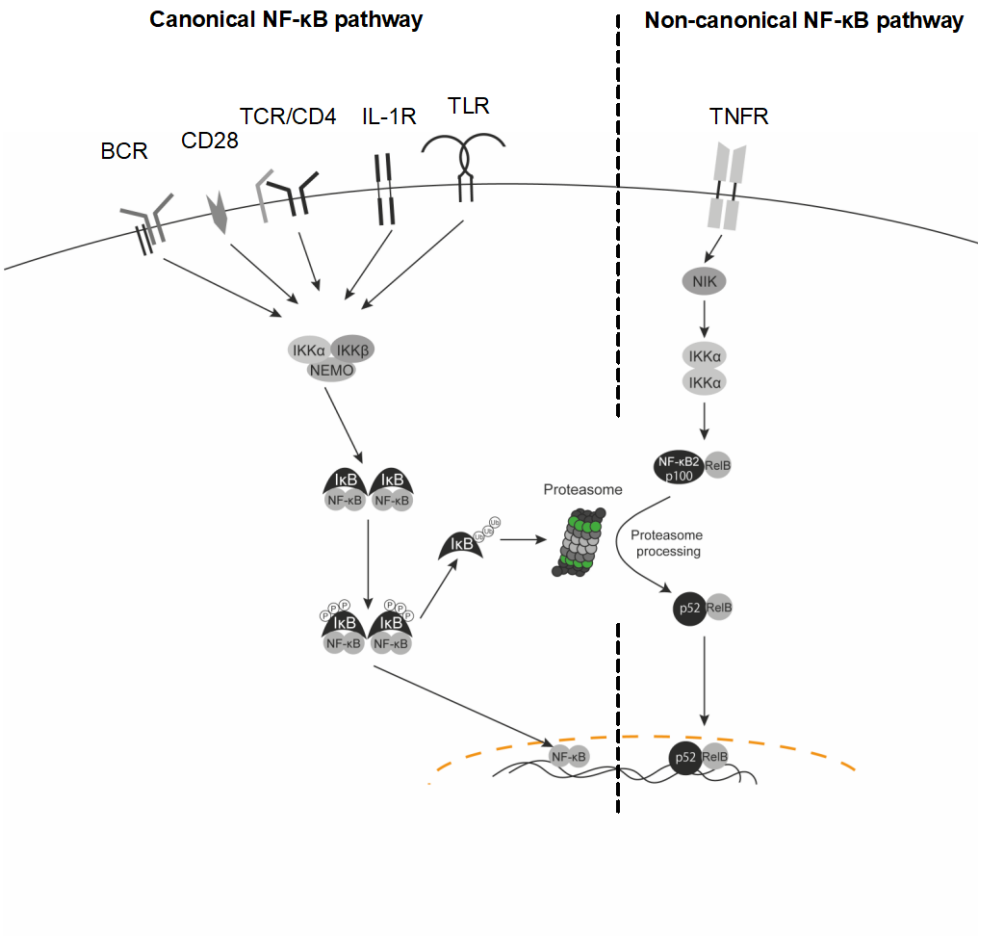


Figure 5.1 Canonical and non-canonical NF-κB signalling pathways.

The activation of B-cell receptor (BCR), co-stimulatory receptor CD28, T-cell receptor (TCR), interleukin-1 receptor (IL-1R) and/or toll-like receptor (TLR) can induce the canonical NF-κB

signalling pathway. IκB kinase (IKK) complex can phosphorylate inhibitor of NF-κB (IκB), which facilitates its further polyubiquitination and degradation by the proteasome. The NF-κB complex enters the nucleus and initiates the transcription. For the non-canonical pathway, NF-κB-inducing kinase (NIK) relays the signal from the tumour necrosis factor receptor (TNFR) and activates the IKKα dimer. IKKα triggers the partial degradation of the non-canonical IκBs by the proteasome and facilitates the nuclear translocation of the NF-κB complex.

NF-κB activity is further regulated by post-translational modifications, one of which is the phosphorylation of p65 at the serine 536 residue[325-327]. When the NF-κB complex containing p65 binds to IκB, the site is deeply embedded between the interface of IκB and p65. Accompanied by IκB removal, the serine 536 site gets exposed to the cytosol and is phosphorylated by the casein kinase 2, which further facilitates NF-κB's DNA-binding and dimerization capacities. Combined with flow cytometry, the phosphorylated p65 level has been widely used to measure NF-κB activity in different cell types, including T cells[328].

Accumulating evidence has shown a critical role of the NF-κB signalling pathway in inflammasome activation and pro-inflammatory cytokine production in innate immune cells[329]. Furthermore, NF-κB regulates different aspects of adaptive immunity. In T cells, NF-κB signalling guides the survival and maturation of newly-generated T cells in the thymus[330]. The activation of mature naïve T cells by TCR/CD28-dependent activation also requires NF-κB signalling and contributes to the production of IL-2, a crucial cytokine needed for autocrine T cell activation and proliferation[331,332]. Simultaneously, c-Rel-mediated expression of the anti-apoptotic protein B-cell lymphoma-extra large (Bcl-xL) is crucial for T cell survival during activation[333]. Moreover, the differentiation of CD4+ naïve T cells into various effector subpopulations also relies on NF-κB signalling, through both intrinsic and extrinsic mechanisms[334]. In CD8+ T cells, NF-κB plays a pivotal role in maintaining the long-term memory T cells[335].

Due to its essential role in mediating inflammation, keeping NF-κB activity under control is crucial for the maintenance of tissue homeostasis. During ageing, the homeostasis of NF-κB signalling is gradually lost, characterised by chronic inflammation and oxidative stress. NF-κB signalling is increased in multiple tissues from aged mice, including heart, liver and brain[336-338]. Furthermore, overexpressing NF-κB in cultured cells has been shown to promote senescence, which may be mechanistically explained by the fact that several of its target genes are SASP[339]. While there is accumulating evidence of strong crosstalk between signalling pathways involved in ageing and the NF-κB signalling pathway, including reports of elevated NF-κB activity in aged human T cells, further exploration is still needed to identify how NF-κB signalling is related to the ageing phenotypes of T cells, and whether autophagy plays a role in this[340].

5.1.2. IL-7R signalling pathway

Interleukin-7 (IL-7) is a soluble globular cytokine with a molecular weight of 25 kDa. It is mainly produced by thymic epithelial and mesenchymal cells, as well as stromal cells in the bone marrow and endothelial cells in lymph nodes, which reflects its essential role in the development and maintenance of lymphocytes[341]. *Il7* mRNA expression is also detectable in non-lymphoid tissues, including skin, intestine and lung. The IL-7 receptor (IL-7R) is a heterodimer that consists of an interleukin-7 receptor alpha-chain (IL-7Rα) and a common gamma chain (γ_c). Since the receptor of IL-7 shares the γ_c with other receptors that sense IL-2, IL-4, IL-9, IL-15, and IL-21, these cytokines form the common cytokine receptor γ chain family[342]. Besides, IL-7Rα is also shared by the thymic stromal lymphopoietin (TSLP) receptor. TSLP is a distant paralogue of IL-7 and is crucial for thymocytes and B-cell lymphopoiesis, as well as in allergic diseases[343]. The TSLP receptor is a heterodimer consisting of IL-7Rα and a

unique TSLP-receptor chain. As IL-7R and TSLP receptors share a subunit, this implies they also exhibit overlapping downstream signalling pathways and functions.

IL-7 binding can enhance the dimerization of IL-7Rα (or CD127) and γ_c (or CD132), which activates downstream signalling pathways, among which the JAK/STAT pathway is most thoroughly studied one (Figure 5.2). The dimerised IL-7Rα and γ_c can recruit JAK1 and JAK3 respectively[344,345]. Followed by the mutual phosphorylation of both kinases, JAK3 can further phosphorylate the CD127 on its tyrosine 449 residue to recruit and phosphorylate the transcription factor STAT5, leading to the active heterodimer composed of STAT5A and STAT5B[346]. The phosphorylated STAT5, in turn, disassociates from the receptor, dimerises in the cytosol and translocates into the nucleus to initiate the transcription of downstream genes. Additionally, IL-7 is also responsible for inducing the MEK/ERK and PI3K/AKT cascades, which, altogether with JAK-STAT signalling, facilitate the expression of a series of genes related to cell survival and homeostatic proliferation, including cyclin D1 (*Ccnd1*), B-cell lymphoma 2 (*Bcl2*), and cell division cycle 25A (*Cdc25a*) [347-349]. Since these downstream signalling pathways compete with each other, it remains to be investigated which pathway takes leading roles in different physiological and disease contexts[350].

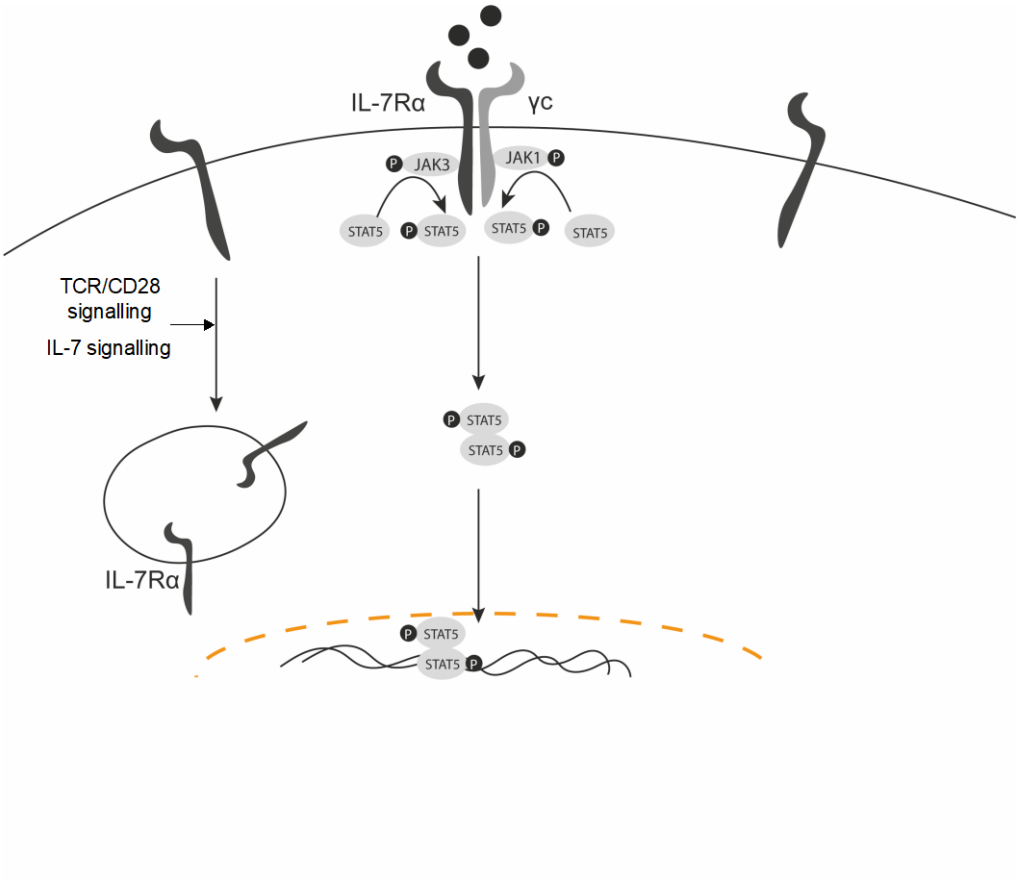


Figure 5.2 IL-7R signalling pathway.

IL-7 receptor (IL-7R) is a heterodimer composed of the IL-7Rα chain and the common gamma chain (γ_c). When binding to IL-7, IL-7R can recruit and trigger the phosphorylation of JAK1/3 and STAT5, sequentially, which facilitates the translocation of phosphorylated STAT5 dimer into the nucleus to transcribe genes. The IL-7Rα is internalised when cell receives stimulation through TCR, CD28 or IL-7R.

Due to the limited availability of endogenous IL-7, IL-7R signalling is tightly regulated via the expression of its receptor at both mRNA and protein levels to maximize the total number of cells being supported. The transcription factor, ETS-1, can bind to and activate the *Il7r* promoter in peripheral T cells. Loss of ETS-1 leads to a decreased IL-7R expression and a lymphopenic phenotype in both CD4+ and CD8+ T cells, indicating its role in IL-7R-signalling-dependent homeostatic proliferation[351]. Another transcription factor maintaining IL-7Rα expression in peripheral naïve T cells is forkhead box protein O1 (FOXO1). By contrast, TCR or cytokine stimulation deactivates FOXO1, which downregulates *Il7r* mRNA level[352-

[354]. Moreover, IL-7-stimulation can repress *Il7r* expression via transcriptional suppressor GFI1 in CD8+ T cells, but not in CD4+ T cells, indicating a distinct regulation of the gene expression in two types of T lymphocytes[354]. In addition, effector CD8+ T cells can recruit the histone deacetylase HDAC1 onto the *Il7r* promoter and facilitate GFI1-mediated suppression, whereas GABPα binding reverses the process in CD8+ memory precursors[355]. At the protein level, IL-7Rα found on the cell surface constantly undergoes clathrin-mediated endocytosis and recycling when IL-7 is absent[356]. The receptor is rapidly internalised and degraded by proteasomes and lysosomes upon IL-7 binding[356,357]. It was reported that VPS34 contributes to the recycling of the internalised IL-7Rα from MVBs, and *Vps34*-deficient T cells display a decreased surface expression of this receptor[312]. Some exogenous proteins, such as the soluble human immunodeficiency virus (HIV) Tat protein, targets surface IL-7Rα on CD8+ T cells for proteasome-mediated degradation, which compromises the CD8+ T cell survival, proliferation and function[358].

The roles of IL-7R signalling in the development and maintenance of the entire lymphoid compartment are supported by the phenotypes found in IL-7- and/or IL-7R-deficient mice[359-361]. In the bone marrow, IL-7R expression starts in common-lymphoid progenitors (CLPs), which gives rise to T cells, B cells and natural killer (NK) cells[362]. Both pre-B and pro-B cells, rather than mature B cells, rely on IL-7 for lymphopoiesis[363]. Additionally, IL-7R signalling is critical for the generation of bone marrow-derived group 2 and group 3 innate lymphoid cells (ILCs)[364,365]. The development of lymphoid progenitors into several lymphoid lineages in the thymus also requires IL-7. Besides, the survival, proliferation and differentiation of T cells at the double-negative stage is modulated by high surface expression levels of IL-7Rα[366,367]. Evidence supports that the robust IL-7R signalling at this stage favours the generation of γδ over αβ T cell lineages[368]. Once entering the double-positive stage, T cells lose the surface IL-

7Rα expression completely, which enables effective removal of T cells responding to self-antigens via apoptosis[369]. Mature T cells that successfully pass the negative selection can re-express the IL-7Rα in a TCR-dependent manner, and emigrate into the periphery to replenish the naïve T cell pool[370].

In the periphery, both naïve and memory T cells require IL-7R signalling to promote their survival, metabolism and homeostatic proliferation[371-373]. IL-7 is critical for the priming of CD4 primary responses to antigens[361,374]. Upon cognate antigen recognition by T cells, the transcription of *Il7r* is antagonised by the TCR and IL-2R signalling pathways, while IL-2Rα expression is upregulated aiming to amplify IL-2R signalling[375,376]. This transition uncouples the T cells from IL-7R-mediated homeostatic proliferation to turn on IL-2R-mediated expansion characteristic of the effector responses. At the resolution phase, the effector T cell pool undergoes a substantial contraction, which is accompanied by down-regulation of IL-2Rα. However, a small subset of antigen-specific T cells can re-express IL-7Rα and become precursors for long-term memory cells[377]. Though widely observed in conventional T cells, the reason why IL-2Rα and IL-7Rα display opposing expression patterns remains elusive. This chapter contains results that may explain these observations.

Given its multiple key physiological roles, dysregulation of IL-7R signalling has been implicated in several diseases. T- and B-cell acute lymphoblastic leukaemia are characterised by hyperactivation of IL-7R signalling, which induces the survival and proliferation of leukemic cells[378,379]. Excessive IL-7Rα and IL-7 levels are also found in autoimmune diseases, including diabetes, multiple sclerosis, rheumatoid arthritis and inflammatory bowel diseases[380-383]. By contrast, administration of exogenous IL-7 to patients with immune deficiencies and severe infections can rescue their lymphopenia phenotype[384-387]. Moreover, during ageing, IL-

7Rα expression level is decreased in both naïve and CD45RA+ effector memory CD8+ T cells, without any significant change in γ_c level[388]. On the other hand, higher *Il7r* gene expression in nonagenarians is linked with a reduced mortality rate[389]. Finally, IL-7 therapy is effective to boost the naïve and memory T cell homeostasis in aged macaques[390].

In the following part, I will present the results related to these two pathways, based on the autophagosomal candidates obtained from activated *Lc3b-APEX2* T cells.

Chapter 5: Characterisation of autophagic substrates in activated CD4+ T cells and their role for CD4+ T cell proliferation – Results

5.2 Results

5.2.1 Mapping autophagosomal contents in activated pan-T cells.

To better understand the underlying molecular mechanism of how lack of autophagy leads to impaired CD4+ T cell proliferation, I investigated the autophagic degradome by applying the LC3B-APEX2 system to proliferating pan-T cells. We first purified pan-T cells from the *Lc3b-APEX2* mouse model and activated them with anti-CD3/CD28 Dynabeads for 3 days prior to proximity labelling (Figure 5.3a). This was also useful as T cell number increases exponentially after a 3-day activation with enhanced autophagy level. Both larger numbers of cells and higher autophagy activity would potentially allow the identification of a higher number of autophagy targets. After activation, cell viability was superior to 80% and T cell purity was higher than 83% (Figure 5.3b). As expected, the early-activation marker, CD25 (IL-2Rα), was fully upregulated at day 3 post-activation (Figure 5.3c). Moreover, we confirmed that the LC3B-APEX2 protein was expressed in activated T cells, and LC3B-II level (as a measurement of autophagic flux) was increased upon BafA1 treatment (Figure 5.3d). The proximity labelled cells (around 10 million cells per sample) were purified and sent for mass spectrometry. A total of 356 proteins were identified, with high reproducibility as shown by the Pearson's correlation coefficient between each biological replicate (Figure 5.3e, left). Gratifyingly, SQSTM1/p62, an autophagic receptor, was increased in BafA1-treated samples, although not quite reaching statistical significance (Figure 5.3e, right). Among the seven significantly upregulated proteins, H2A clustered histone 20 (H2AC20) and WD repeat-containing protein 18 (WDR18) are mainly located in the nuclei[391,392]; Glypican 1 (GPC1) is a cell surface proteoglycan enriched on cancer-related exosomes[393]; Peroxiredoxin 3 (PRDX3) and 2',3'-cyclic nucleotide 3' phosphodiesterase (CNP) are two mitochondrial proteins involved in antioxidant responses and mitochondrial permeability, respectively[394,395]. However, we first focused our attention on a

candidate that had the potential to play a role in T cell survival and activation/proliferation: Kelch-like protein 6 (KLHL6).

KLHL6 is an E3-ligase that labels its substrates with ubiquitin, thereby facilitating their proteasome-mediated degradation (Figure 5.4a). Previous research showed that a loss-of-function mutation in KLHL6 leads to the hyperactivation of NF-κB signalling in B cell lymphoma (Figure 5.4b). One of KLHL6's substrates, Roquin 2, is an mRNA decay factor, which can destabilise the mRNA of A20 (TNFAIP3), an NF-κB suppressor. I hypothesised that KLHL6 is accumulated in autophagy-deficient CD4+ T cells and inhibits NF-κB signalling (Figure 5.4b), which is crucial for the proliferation of T cells. Interestingly, I found that the level of phosphorylated p65, the major active form of NF-κB transcription factor in T cells, was significantly decreased in CD4+ T cells from aged mice, either without activation or after 24-hour activation (Figure 5.5, middle and right). Therefore, I went on to validate whether KLHL6 is an autophagosomal cargo in CD4+ T cells.

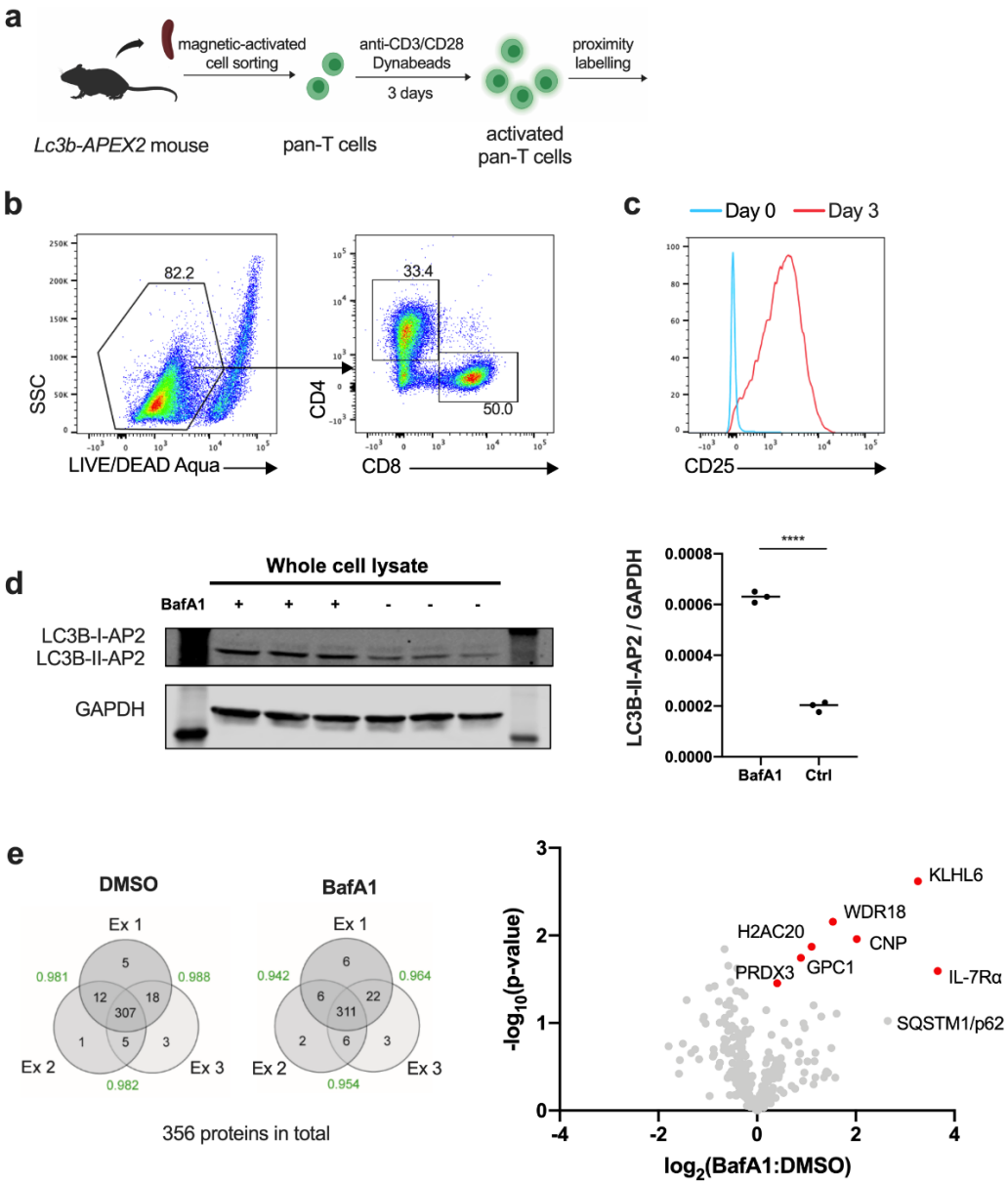


Figure 5.3 Proximity labelling and mass-spec analysis of activated pan T cells.

a) Experimental set-up: splenic total T cells purified from LC3B-APEX2 mice were activated with anti-CD3/CD28 Dynabeads for 3 days. After removing the beads, cells were proximity-labelled and autophagosomal biotinylated proteins were enriched for mass-spectrometry analysis. b) Dot plots display the survival rate and the purity of total T cells on day 3 post-activation. c) Histogram depicting the surface expression of CD25 gated on live total T cells at day 0 (prior to activation) and day 3 post-activation. d) Venn diagrams depicting proteinase K-protected, biotinylated proteins identified in activated total T cells with more than two spectral counts across three biological replicates (Ex) in both DMSO- and BafA1-treated groups. Pearson's correlation coefficients of two replicates are displayed. e) Volcano plot of proteins from (a) labelled by LC3B-APEX2 in activated CD4+ T cells. Proteins significantly upregulated in response to BafA1 treatment are highlighted in red, $p < 0.05$ by unpaired two-tailed Student's t-test (n=3 biological replicates per group), with each replicate combining T cells from two mice. (e) analysis provided by courtesy of Susanne Zellner.

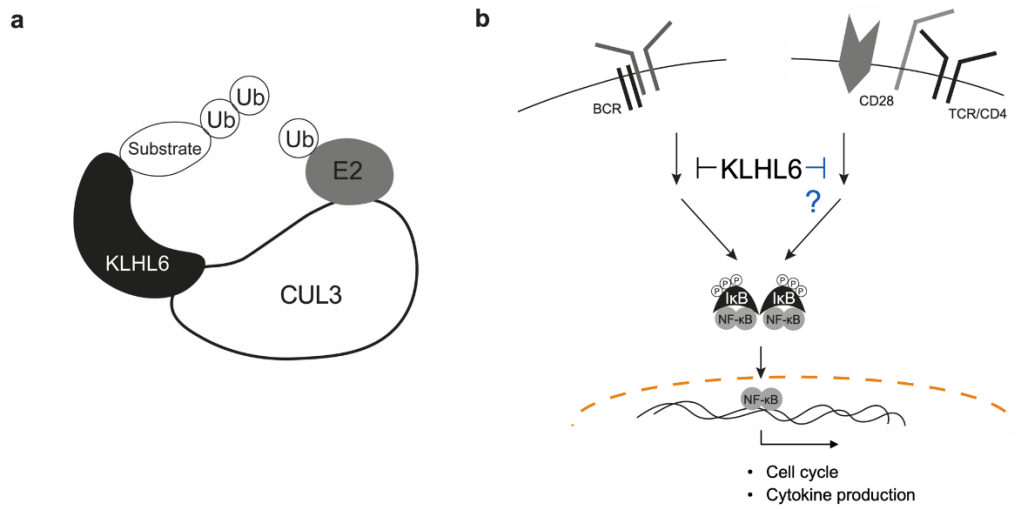


Figure 5.4 Declining levels of autophagy may lead to KLHL6 accumulation and attenuated NF-κB signalling in CD4+ T cells.

a) Schematic overview of how human KLHL6 performs the role of E3 ligase. The assembly of KLHL6 with cullin3 forms a cullin-RING ubiquitin ligase. KLHL6 recruits the substrates for proteasomal degradation and transfers the ubiquitin loaded on E2 ligase to the substrates. Ub, ubiquitin; CUL3, cullin 3; E2, E2 ubiquitin-conjugating enzyme. b) Schematic overview of how KLHL6 may inhibit TCR-mediated upregulation of NF-κB signalling in CD4+ T cells. Previous studies suggest that KLHL6 attenuates BCR-induced NF-κB signalling in normal B cells and B cell lymphoma. Since TCR- and co-receptor-signalling can also boost NF-κB signalling in T cells, which is crucial for the proliferation and secretion of cytokines, I hypothesised that autophagy-deficient CD4+ T cells have higher KLHL6 protein levels that inhibit the NF-κB signalling.

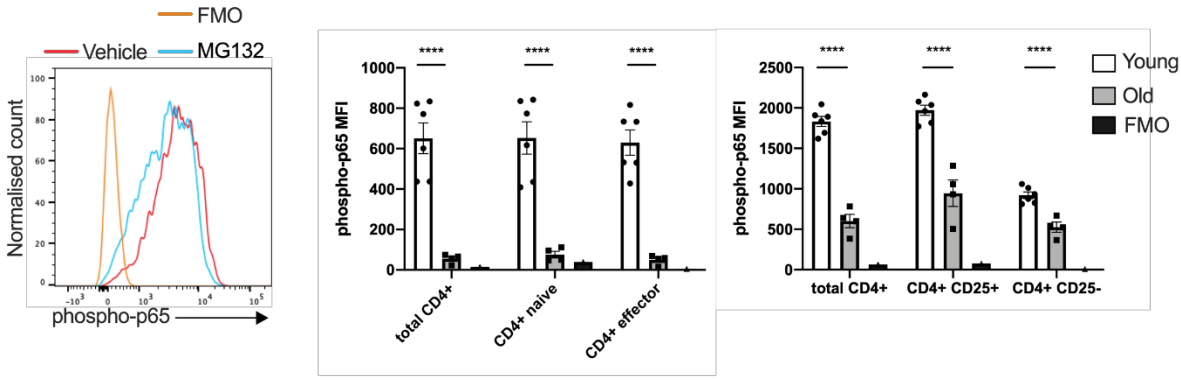


Figure 5.5 Aged CD4+ T cells display attenuated NF-κB signalling.

Representative plot (left) of phosphorylated-p65 staining, a major activated form of NF-κB transcription factors in T cells. FMO control (orange) and negative control treated with MG-132 (blue), a proteasome inhibitor which prevents the degradation of IκB, show lower phosphorylated-p65 compared to the vehicle-treated sample (red). Bar graphs showing phosphorylated-p65 levels in different CD4+ T cell subsets at basal level (middle) or in CD4+ T cells activated for 24 hours (right, gated by CD25 expression level) as mean ± SEM. All statistics by unpaired two-tailed Student's t-test (n=4-6 mice per group). p****<0.0001. The results are representative of two independent experiments.

5.2.2 KLHL6 is degraded through autophagy in vitro

A database, called iLIR (http://repeat.biol.ucy.ac.cy/iLIR/), can be used to assess potential LC3-interacting region (LIR) protein domains based on its sequence[396]. Analysis of the KLHL6 protein sequence shows it contains a LIR motif (Figure 5.6a, indicated by the magenta rectangle). Since there is no available commercial antibody to detect murine KLHL6 in primary cells, to validate whether KLHL6 is an autophagic cargo experimentally, I overexpressed Flag-tagged human KLHL6 (Flag-hKLHL6) in cell lines and determined whether KLHL6 interacts with LC3. I performed co-immunoprecipitation in HEK cells transfected with Flag-hKLHL6. Figure 5.6b showed that LC3B, as well as a KLHL6 binding partner – CUL3, were co-immunoprecipitated with Flag-hKLHL6, indicating that LC3B indeed interacts with hKLHL6. By contrast, the negative controls, either transfected with Flag-tagged eGFP construct or untransfected, did not show any CUL3 or LC3B bands in the immunoprecipitated samples, ruling out the possibility that the interaction between hKLHL6 and LC3B was due to non-specific binding. Moreover, confocal imaging of HeLa cells transfected with Flag-hKLHL6 displayed an enhanced co-localisation of LC3B-containing compartment with hKLHL6 upon BafA1 treatment, reflected by a significant increase in the Mander's coefficient (Figure 5.7). Taken together, I validated that hKLHL6 can be degraded by autophagy in our overexpression system in vitro. However, protein overexpression may change the cellular status and boost autophagy to remove them in bulk[397]. Therefore, I moved on to see whether KLHL6 is potentially degraded by autophagy in primary T cells.

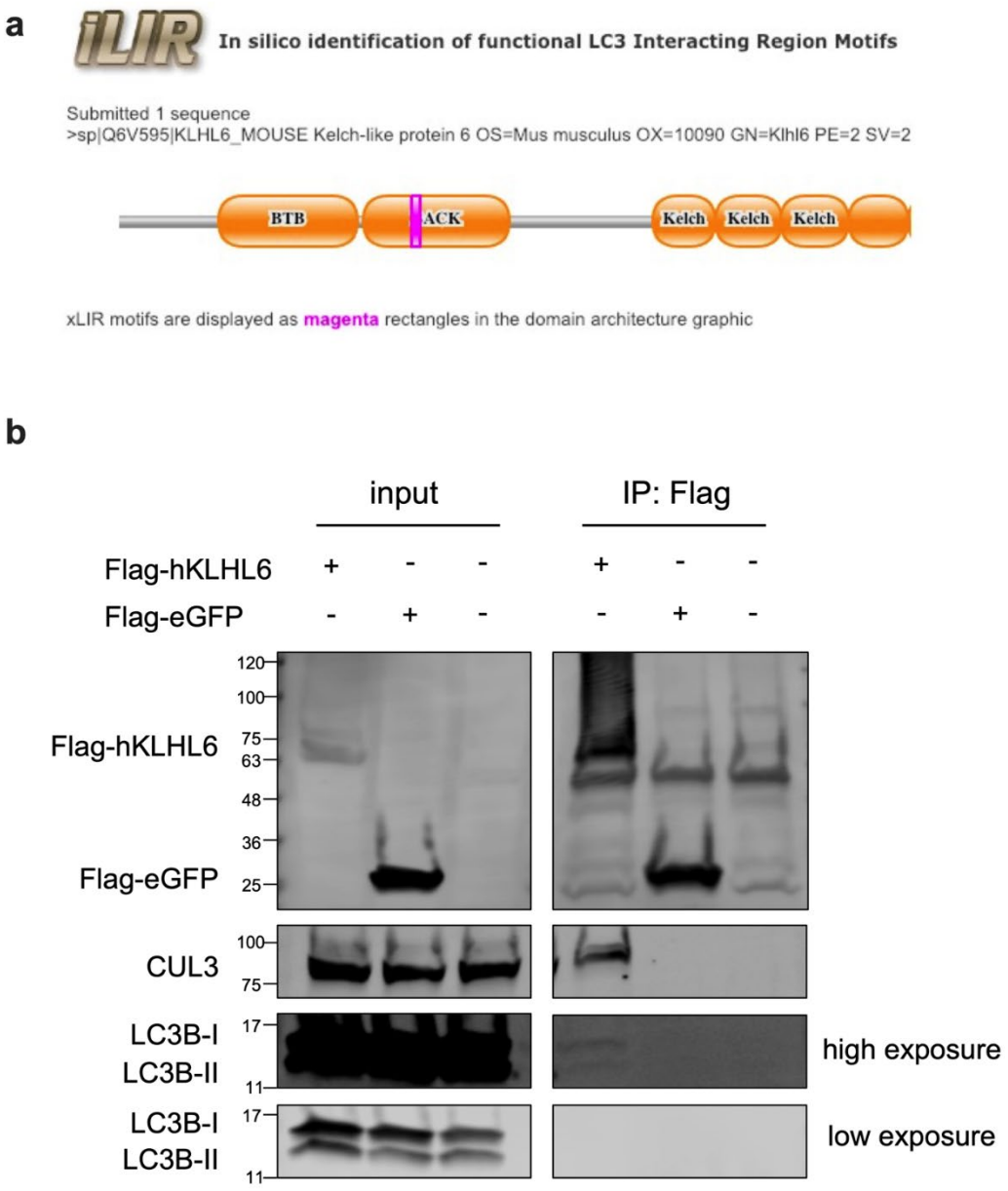


Figure 5.6 KLHL6 interacts with LC3B in vitro.

a) Result from the iLIR database showing that KLHL6 contains a potential LC3-interacting region (LIR) motif (magenta) in the ACK domain. b) An immunoprecipitation experiment was performed to examine the interaction between Flag-hKLHL6 fusion protein and endogenously expressed LC3B in HEK 293T cells. Cells transfected with Flag-eGFP and non-transfected cells were used as controls. The experiment was repeated twice with one representative experiment shown here.

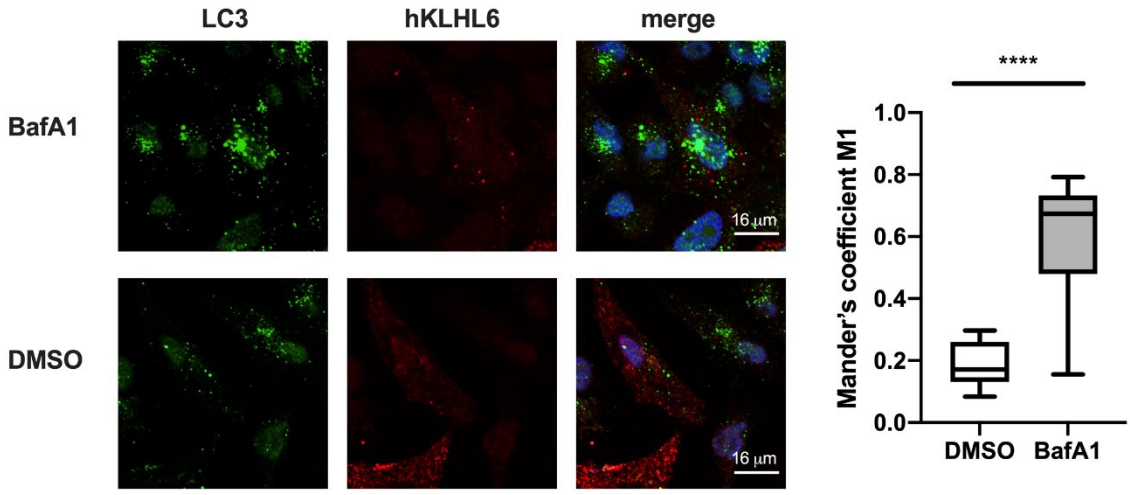


Figure 5.7 KLHL6 is co-localised with autophagosomes in vitro.

a) Confocal imaging of LC3 and KLHL6 in HeLa cells overexpressing Flag-KLHL6. HeLa cells were transfected with Flag-hKLHL6 construct and incubated with BafA1 or DMSO, then stained with LC3 and Flag antibodies, followed by the staining of secondary antibodies conjugated with fluorophores. b) Box graph showing Mander's coefficient M1, which describes how well LC3 is co-localised with hKLHL6 (n=20 cells per group). Data are represented as mean ± max and min values, with unpaired two-tailed Student's t-test, p****<0.0001.

5.2.3 *Klhl6*$^{-/-}$ T cells do not show an enhanced proliferation upon TCR/CD28-stimuli

To confirm whether KLHL6 levels affect CD4+ T cell proliferation, I decided to check whether the NF-κB signalling and proliferation capacity are affected in CD4+ T cells isolated from a global *Klhl6*$^{-/-}$ mouse model[398]. This was done in collaboration with Professor Christopher Goodnow and Dr Etienne Farquhar. Consistent with previous reports, here they show that knocking-out *Klhl6* impairs the survival and differentiation of transitional B cells in bone marrow, both absolute numbers and frequencies of mature B cells in the periphery being significantly decreased in *Klhl6*$^{-/-}$ mice when compared to their wild-type counterparts (Figure 5.8a and b, left)[399]. Regarding T cells, using our protocols and antibody panels, *Klhl6*$^{-/-}$ mice did not show any significant differences in absolute numbers, indicating that the increased frequency of T cells observed in these mice is due to the reduced numbers of B cells. When analysing CD4+ and CD8+ T cell subsets separately, our collaborators could neither observe any differences in their absolute numbers or frequencies (Figure 5.8 a and b, middle and right), suggesting that *Klhl6* is dispensable for the development and/or survival of T cells.

To further investigate KLHL6's role in T cell proliferation, our collaborators measured the level of NF-κB signalling and proliferation profile in CD4+ T cells activated for 3 days. The cells undergoing two or more rounds of cell cycle showed a slight but significant increase in phosphorylated p65 level (Figure 5.8c). However, the proliferation was even delayed, rather than enhanced, in *Klhl6*$^{-/-}$ CD4+ T lymphocytes (Figure 5.8d). Overall, this implies that KLHL6 is either inhibitory or dispensable for the development and proliferation of CD4+ T cells.

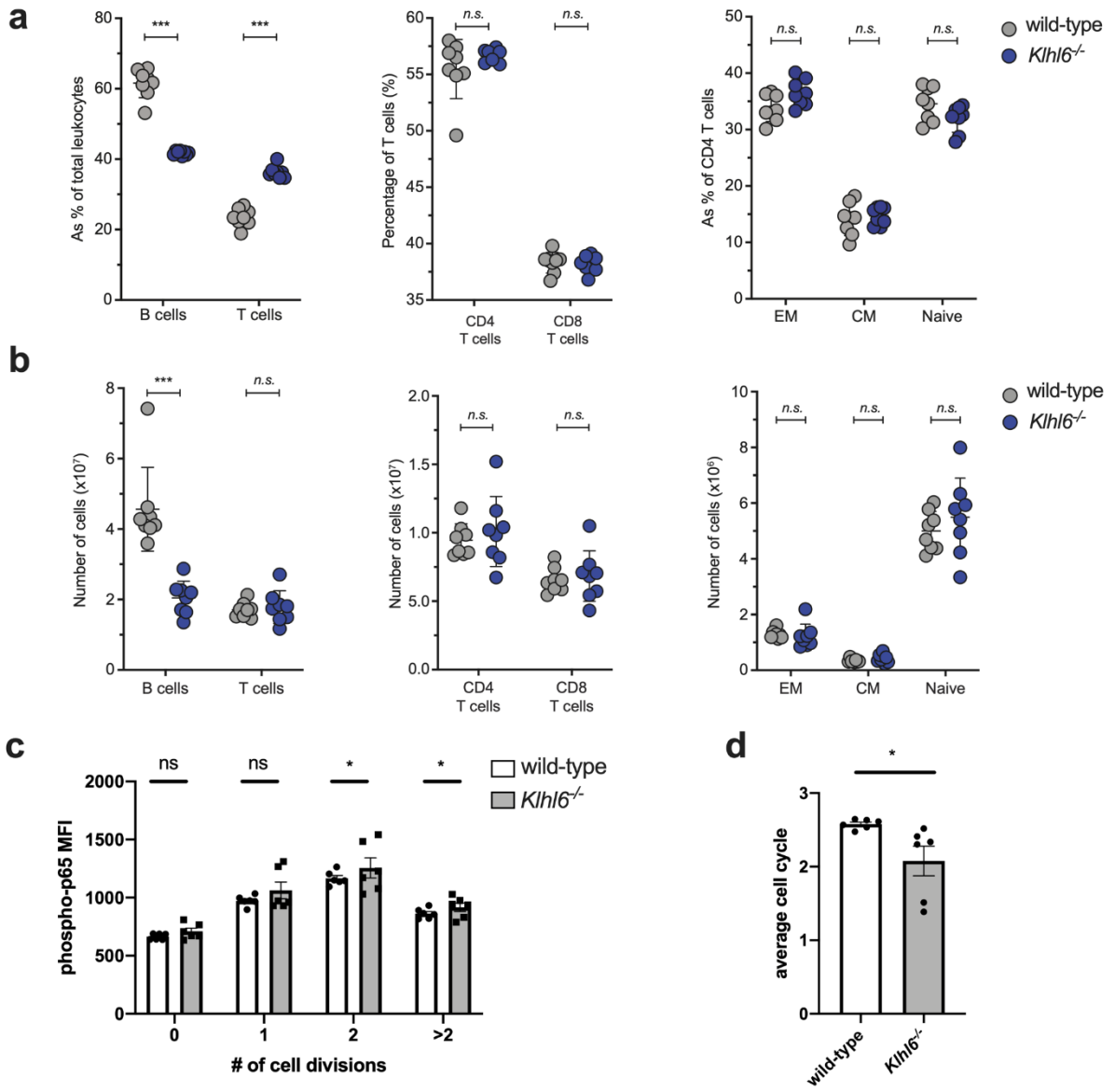


Figure 5.8 *Klhl6*$^{-/-}$ T cells do not show differences in their numbers or cell proliferation profile.

Scatter plots showing the comparison of frequency (a) and absolute number (b) of different lymphocyte populations from wild-type or *Klhl6*$^{-/-}$ mice. All statistics were performed with unpaired two-tailed Student's t-test (n=7-8 mice per group), p***<0.001, n.s.: not significant. c) Bar graph indicating the comparison of phosphor-p65 level in CD4+ T cell from wild-type or *Klhl6*$^{-/-}$ mice activated for 3 days, based on the number of cell divisions. d) Bar graph indicating the average cell division of CD4+ T cells undergone after 3 days of activation. T cells were stained with CellTrace Violet and activated with anti-CD3/CD28 Dynabeads in vitro for 3 days. Both statistics are unpaired two-tailed Student's t-test (n=6 mice per group), p*<0.05, ns: not significant. In courtesy of Etienne Farquhar.

5.2.4 NF-κB signalling and levels of KLHL6 substrates are not changed in autophagy-deficient CD4+ T cells

Our previous results showed that NF-κB signalling is decreased in cells from aged animals (when autophagy is known to be impaired) and that hKLHL6 interacted and co-localised with LC3B in vitro. However, when we measured NF-κB signalling in autophagy-deficient CD4+ T cells, we discovered that phosphorylation of p65 was not affected, as we could not observe any significant differences when compared to wildtype cells. This was observed both for basal levels of p-p65 (Figure 5.9, left) or its expression after activation (Figure 5.9, right). Furthermore, the expression of Roquin 2 and CDK2, two known downstream substrates of KLHL6, did not decrease in activated CD4+ T cells from the inducible *Atg16l1*-knockout model (Figure 5.10). These data indicate that, although being an autophagy target, KLHL6 expression is not changed in autophagy-deficient CD4+ T cells.

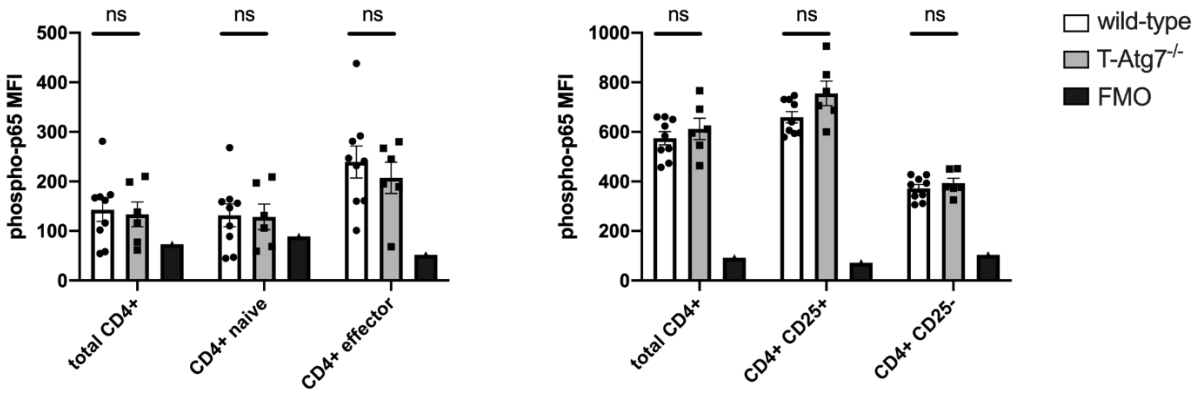


Figure 5.9 Autophagy-deficient CD4+ T cells do not show significant differences in NF-κB signalling when compared to wild-type cells.

Bar graph (left) showing p-p65 expression in different CD4+ T cell subsets isolated from T-Atg7$^{-/-}$ mice or wild-type littermate controls as mean ± SEM. Bar graph (right) showing the p-p65 expression as mean ± SEM in CD4+ T cells (gated on CD25 expression level) from T-Atg7$^{-/-}$ mice or wild-type littermate controls 24 hours post-activation. All statistical analysis was performed by unpaired two-tailed Student's t-test (n=4-6 mice per group), ns: not significant. The results are representative of two independent experiments.

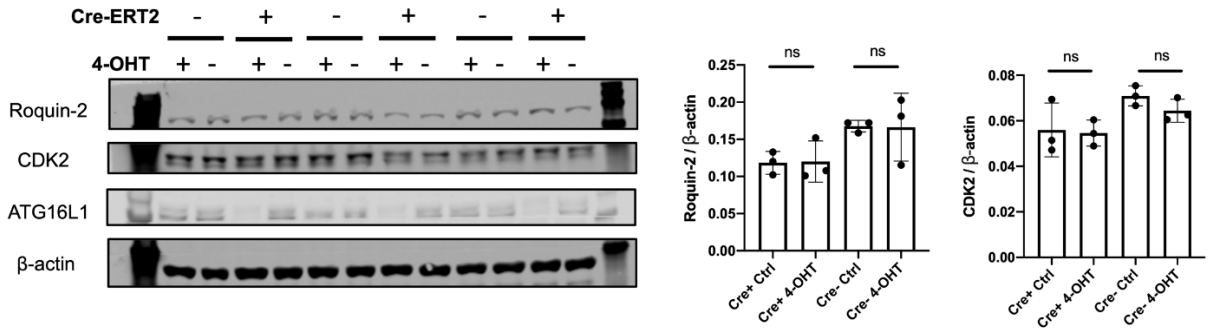


Figure 5.10 Autophagy-deficient CD4+ T cells do not accumulate KLHL6 substrates.

a) Western blot of whole-cell lysates of CD4+ T cells from *Cre-ERT2*+, *Atg16l1*$^{flox/flox}$ or *Cre-ERT2*-, *Atg16l1*$^{flox/flox}$ treated with 4-hydroxytamoxifen (4-OHT) or vehicle and activated in vitro and for 3 days. b) Bar graphs show the levels of Roquin (left) and CDK2 (right) in different samples, normalised to actin level (n=3 mice per group). All statistical analysis was performed by paired two-tailed Student's t-test, ns: not significant.

5.2.5 Autophagosomal content in CD4+ T cells at different time points

Since autophagosomal cargoes may differ substantially between CD4+ and CD8+ T cells, to explore what autophagy degrades specifically in CD4+ T cells and obtain a list of candidates genuinely related to its proliferation, we performed proximity biotinylation on CD4+ T cells rather than on pan-T cells isolated from the *Lc3b-APEX2* mouse model. Based on our previous results that showed a positive correlation between cell numbers and the discovery of autophagosomal candidates, we activated splenic murine CD4+ T cells for 3 days, which promoted their expansion and provided us with sufficient numbers of CD25+ activated CD4+ T cells (Figure 5.11a). At this time point, cells had undergone three rounds of cell division on average as shown in Figure 4.5. Most importantly, activated CD4+ T cells exhibited a peak of autophagic activity between days 2 and 3 (Figure 5.11b), which supports this is an appropriate time point to investigate the role of autophagy in CD4+ T cell proliferation. Therefore, we decided to activate CD4+ T cells from the *Lc3b-APEX2* model in vitro with anti-CD3/CD28 Dynabeads for 3 days, followed by proximity labelling.

Similar to the results obtained from pan-T cells, the mass-spectrometry analysis of activated CD4+ T cells showed high reproducibility between biological replicates, calculated by the Pearson's R-value (Figure 5.12a). Among total 112 proteins protected from proteinase K-treatment and enriched by streptavidin beads, seven candidates were significantly upregulated in samples treated with BafA1 (Figure 5.12b). These included again interleukin-7 receptor alpha (IL-7Rα), RAB8A, a small Rab GTPase indispensable for exocytic trafficking of post-Golgi vesicles to the plasma membrane[400]; embigin (EMB), a surface protein widely expressed in the haematopoietic system which may mediate cell-cell interactions[401]; nucleolin (NCL), a protein mainly localised in nucleolus[402]; ribosomal protein S13 (RPS13) and eukaryotic translation initiation factor 3 subunit (EIF3C), two proteins associated with ribosomes; and

Fas-associated factor family member 2 (FAF2), a protein located on both ER and lipid droplet[403]. Interestingly, KLHL6 was not identified again. We decided to focus on one of the candidates, IL-7Rα, which was found repeatedly increased among 3 out of 4 biological replicates with the highest fold change (Figure 5.3e & Figure 5.12c). The TCR/CD28-signalling-mediated downregulation of IL-7Rα expression is in line with our data, which suggests that IL-7Rα might be degraded in an LC3B+ compartment during T cell activation[376]. While I did not expect to find IL-7Rα as an autophagic substrate, as its signalling is not directly related to the CD4+ T cell effector formation, I nevertheless investigated how autophagic degradation of this receptor contributes to T cell proliferation regulation.

To investigate whether the autophagosomal degradome at earlier activation stages differs from the 3-day activated samples, I also performed the proximity labelling in CD4+ T cells activated for 16 hours, a time point before the onset of cell proliferation, with 4 million cells per biological replicate[404]. I found 102 non-redundant proteins, however, the correlation between each sample was not as high as the one found in previous experiments (measured again by the Pearson's R-value), especially for the BafA1-treated group (Figure 5.13a). We interpreted this as a probable result of the heterogeneity of each biological replicate. Only four proteins were found to be significantly upregulated upon BafA1 treatment: nucleolin (NCL), heterogeneous nuclear ribonucleoprotein A1 (HNRNPA1) and heterogeneous nuclear ribonucleoprotein A2/B1 (HNRNPA2B1) – three nuclear proteins, and α-tubulin, the major component of microtubules. This may indicate that low-autophagy levels at the 16 hours post-activation prevents us from finding more candidates.

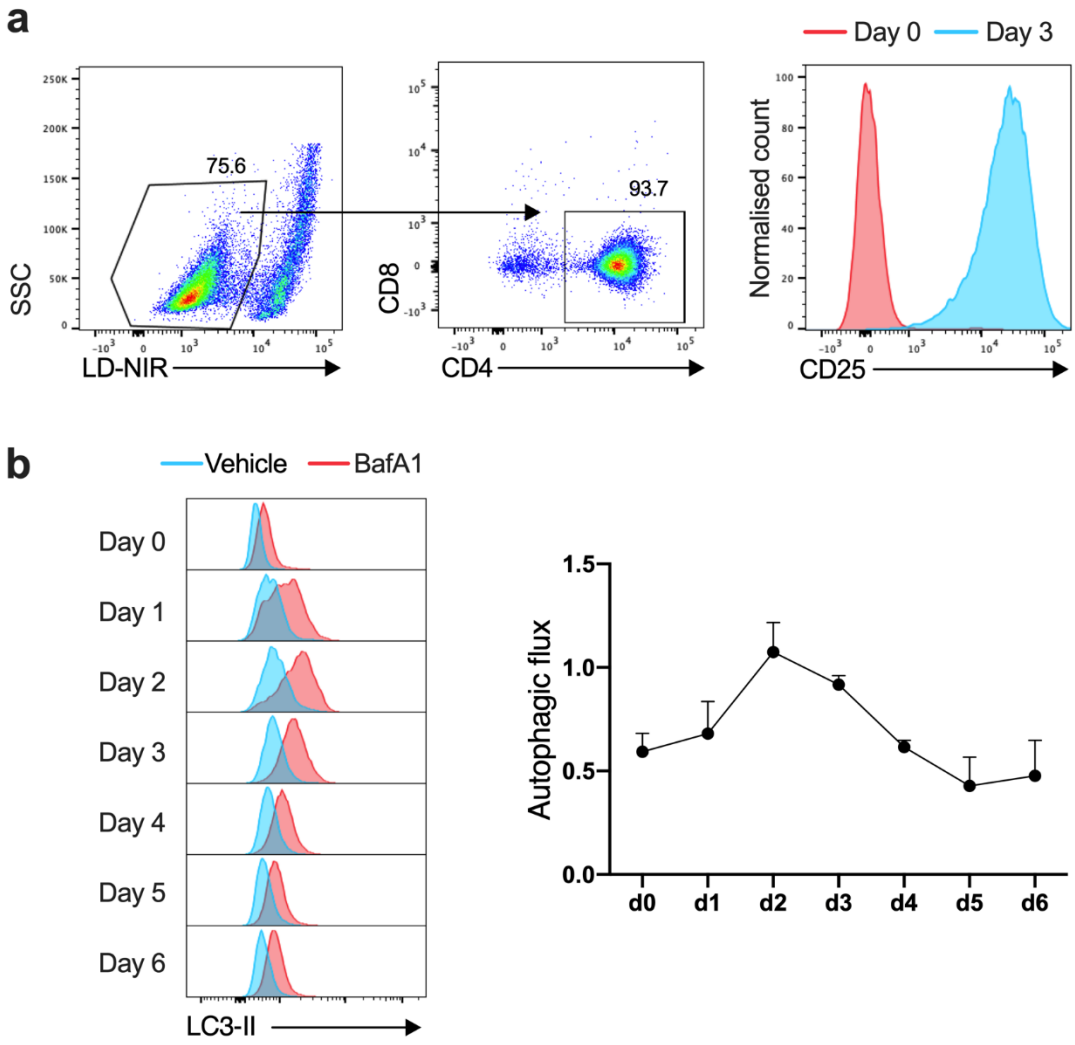


Figure 5.11 Optimisation of sample preparation for proximity labelling in CD4+ T cells.

a) Dot plots (left) displaying the survival rate and the purity of CD4+ T cells at day 3 post-activation. Histogram (right) depicts the surface level of CD25 on live CD4+ T cells at days 0, 1 and 3 post-activation. b) LC3-II histograms (left) of activated CD4+ T cells on corresponding days, which were treated or not with BafA1 for 2 hours before staining. Autophagic flux (right) was calculated by the LC3-II geometric mean fluorescent intensity (BafA1 - Vehicle)/Vehicle, n = 3 mice. Data are represented as mean ± SEM.

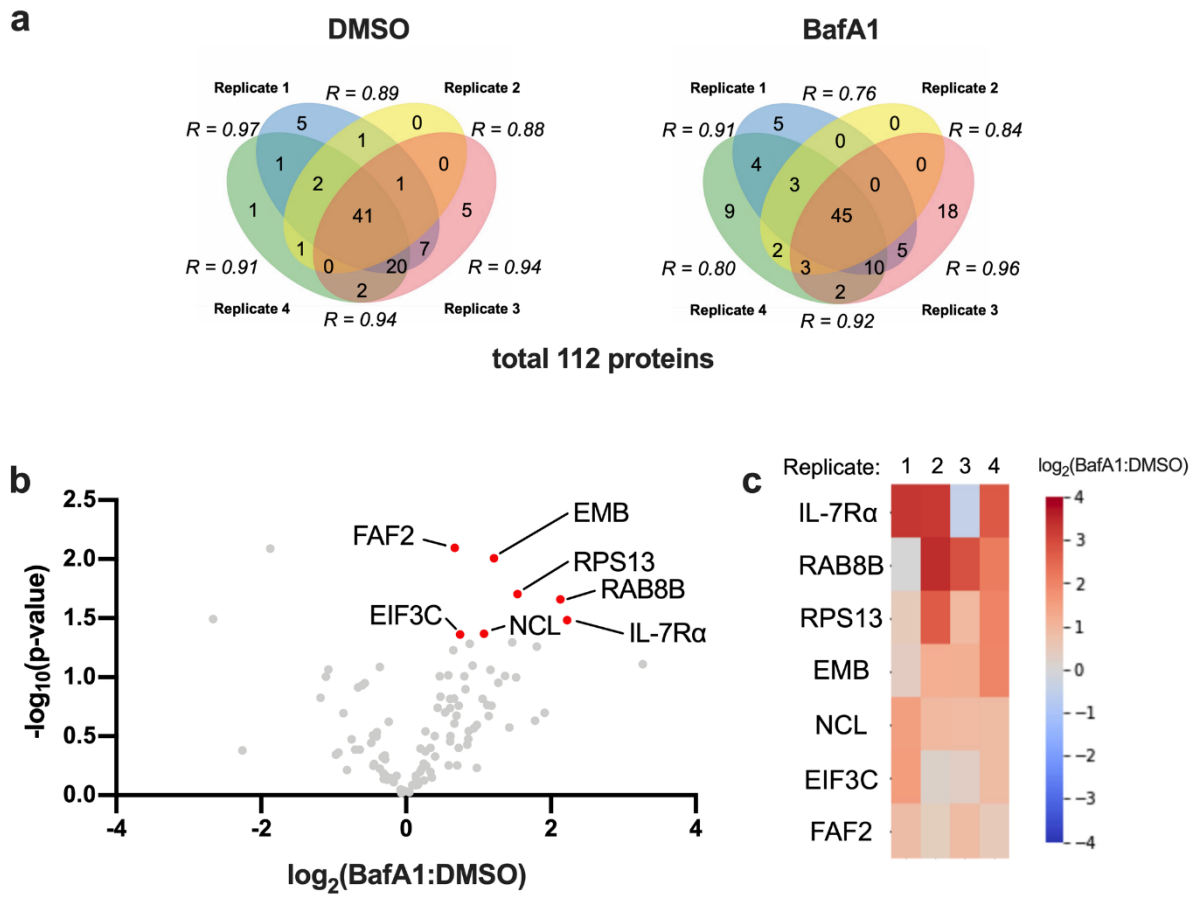


Figure 5.12 Proximity labelling in CD4+ T cells activated for 3 days.

a) Venn diagrams depicting proteinase K-protected, biotinylated proteins identified in CD4+ T cells activated for 3 days with more than two spectral counts across four biological replicates in both DMSO- and BafA1-treated groups. Pearson's correlation coefficients of two replicates are displayed in italic. b) Volcano plot of proteins from (a) CD4+ T cells activated for 3 days and labelled by LC3B-APEX2. Proteins significantly upregulated in response to BafA1 treatment are highlighted in red, $p<0.05$ by unpaired two-tailed Student's t-test (n=4 biological replicates per group), with each replicate combining T cells from two mice. c) A $\log_2$(BafA1/DMSO) heat map of the BafA1-upregulated candidates. The red colour indicates an upregulation in BafA1-treated samples, while blue represents a decrease.

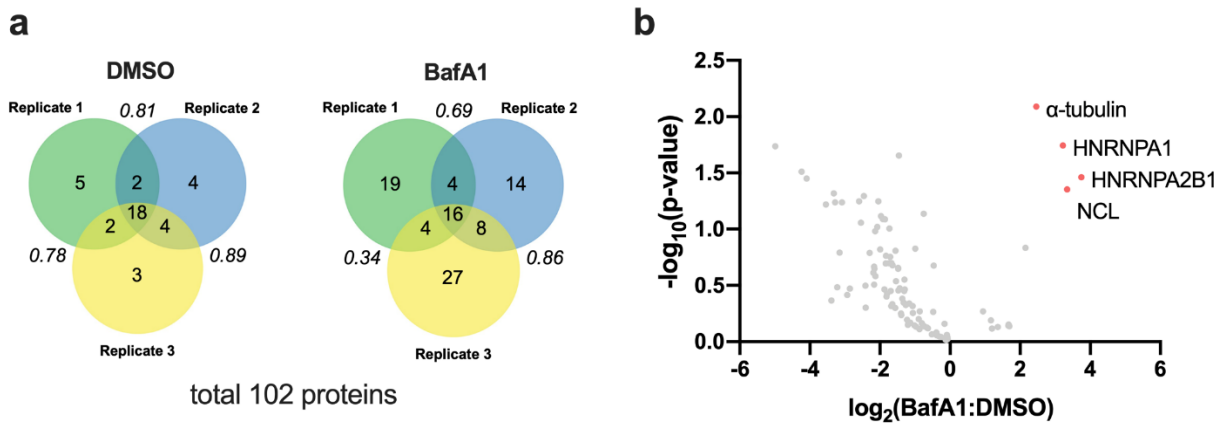


Figure 5.13 Proximity labelling in CD4+ T cells activated for 16 hours.

a) Venn diagrams depicting proteinase K-protected, biotinylated proteins identified in CD4+ T cells activated for 16 hours with more than two spectral counts across four biological replicates in both DMSO and BafA1 treated groups. Pearson's correlation coefficients of two replicates are displayed in italic. b) Volcano plot of proteins from (a) 16-hour activated CD4+ T cells labelled by LC3B-AP2. Proteins significantly upregulated in response to BafA1 treatment are highlighted in red, $p<0.05$ by unpaired two-tailed Student's t-test ($n=3$ biological replicates per group), with each replicate combining CD4+ T cells from two mice.

5.2.6 IL-7R is degraded via autophagy in CD4+ T cells

IL-7R signalling is crucial for the homeostatic maintenance of peripheral T cells and the function of other cell types. During TCR-mediated activation, IL-7Rα is gradually lost from the cell surface due to enhanced endocytosis and degradation, and its gene expression is also suppressed[77]. Of relevance, the trafficking of IL-7Rα relies on intracellular vesicles, which might also be LC3-positive compartments. To determine whether IL-7Rα is indeed found in autophagosomes, we performed immunostainings on both naïve and 3-day-activated CD4+ T cells. Confocal imaging showed that the IL-7Rα was colocalised with two autophagosomal markers, LC3B and WIPI2, to some degree, in BafA1-treated CD4+ T cells with or without activation (Figure 5.14). WIPI2 is an early autophagosomal marker dispensable for the LC3-associated phagocytosis (LAP)[178]. Therefore, we confirmed that the IL-7Rα is a bona fide autophagosomal cargo.

To confirm whether IL-7Rα is indeed degraded by autophagy, I checked whether it is accumulated in wild-type cells treated with the autophagy inhibitor BafA1. After a 12-hour incubation with BafA1, the whole-cell level of IL-7Rα was significantly upregulated in purified naïve CD4+ T cells (Figure 5.15), indicating that autophagy indeed mediates the degradation of this molecule.

To see whether the genetic deletion of autophagy leads to a similar phenotype, I determined the IL-7Rα expression in splenic CD4+ T cells from T-Atg7$^{-/-}$ mice. As Figure 5.16a and b show, IL-7Rα exhibited a significant upregulation at both surface and whole-cell levels in T-Atg7$^{-/-}$ naïve T cells, but not in the effector population. TCR-mediated activation of wild-type and Atg7$^{-/-}$ CD4+ T cells revealed that IL-7Rα expression is higher in autophagy-deficient cells at day 1 post-activation, but this difference disappears at day 3 (Figure 5.17). This might

explain why autophagy-deficient CD4+ T cells start to proliferate after 3 days of activation. qRT-PCR analysis showed that the increased expression of IL-7Rα protein was not caused by enhanced transcription of *Il7ra* (Figure 5.18). When analysing naïve CD4+ T cells from aged mice, we observed a down-regulated expression of surface IL-7Rα level (Figure 5.19). This is in contrast to what we found in autophagy-deficient CD4+ T cells, but is consistent with a previous report showing that naive CD8+ T cells from aged mice show significantly decreased *Il7ra* mRNA expression[388].

Previous studies showed that some key autophagy genes, like *Atg7* and *Atg5*, control the internalisation of surface receptors[122,405]. To address whether the accumulation of IL-7Rα in autophagy-knockout CD4+ T cells is caused by decreased internalisation, we measured the amount of biotin-conjugated IL-7Rα at the cell surface over time. We confirmed that the surface expression of IL-7Rα was higher in T-Atg7$^{-/-}$ naïve CD4+ T cells in comparison to their wild-type counterparts, but could not observe any differences in the rate of receptor internalisation, represented by the percentage of internally trafficked IL-7Rα (Figure 5.20).

To confirm that autophagy-deficient T cells obtained from other tissues also show an increased surface expression, naïve CD4+ T cells from the colon of *CD4^{cre}; Atg16l1$^{flox/flox}$* (T-Atg16l1$^{-/-}$) mice were stained for surface level of IL-7Rα showing similar results (Figure 5.21a). Using *Atg16l1*-deficient mouse models in addition to the *Atg7*-deficient one that we used above, I ensured that the observed phenotype is mediated by an autophagy-dependent mechanism[178]. To rule out an adaptation effect caused by the long-term deficiency in autophagy, I utilised an inducible autophagy-knockout model, and confirmed a similar, albeit milder, phenotype (Figure 5.21b). This *Cre-ERT2*+; *Atg16l1$^{flox/flox}$* mice with tdTomato reporter were fed with a single dose of tamoxifen. After 1 week, around 15% of total CD4+ T cells were still tdTomato-

negative (Figure 5.21c), suggesting that those CD4+ cells remained autophagy-proficient after tamoxifen-feeding. In line with the results from two constitutive autophagy-knockout models, surface IL-7Rα level was significantly increased in tdTomato-positive naïve, but not in the effector T cell populations (Figure 5.21d).

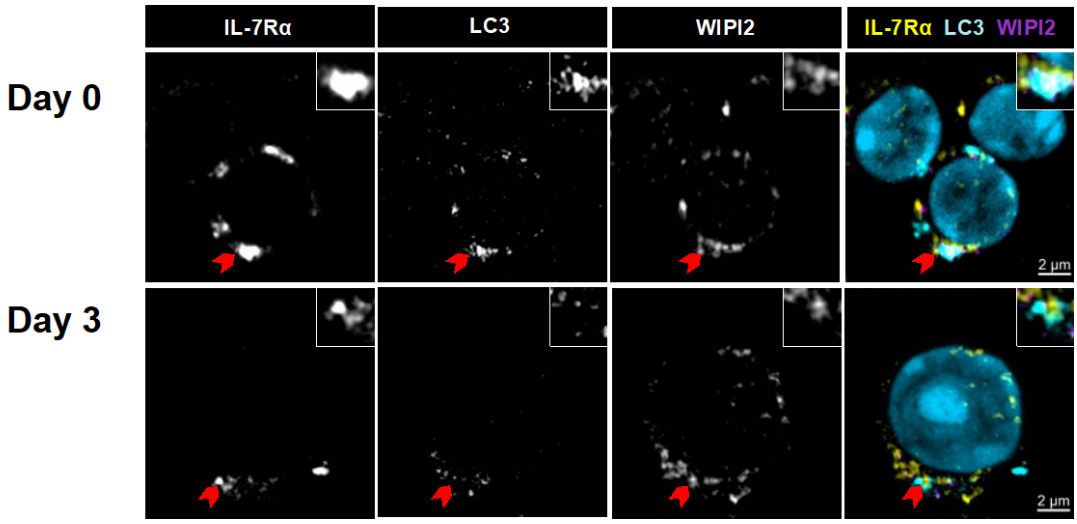


Figure 5.14 IL-7Rα is co-localised with autophagosomes in naïve and activated CD4+ T cells.

Confocal imaging of IL-7Rα, LC3 and WIPI2 in wild-type CD4+ T cells without activation or activated for 3 days. Red arrows indicate colocalization events, whose magnifications are displayed at the upper-right corners. These experiments were repeated as biological triplicates with similar results.

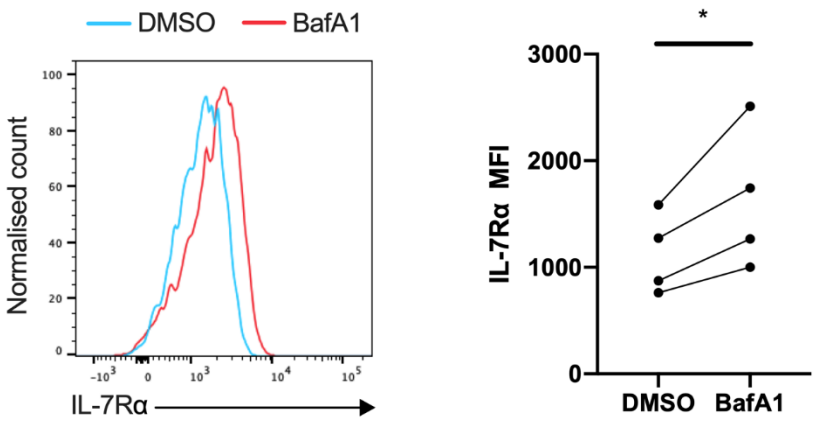


Figure 5.15 IL-7Rα is accumulated in naïve CD4+ T cells upon BafA1 treatment.

Histogram (left) of IL-7Rα at whole-cell level (surface + intracellular), gated on splenic naïve CD4+ T cells purified from wild-type. Dot and line graph (right) show the whole-cell level of IL-7Rα as geometric mean fluorescent intensity (MFI) in purified naïve CD4+ T cells treated with or without BafA1 for 12 hours. All values are represented as mean ± SEM with paired two-tailed Student's t-test (n=4 mice per group), p*<0.05.

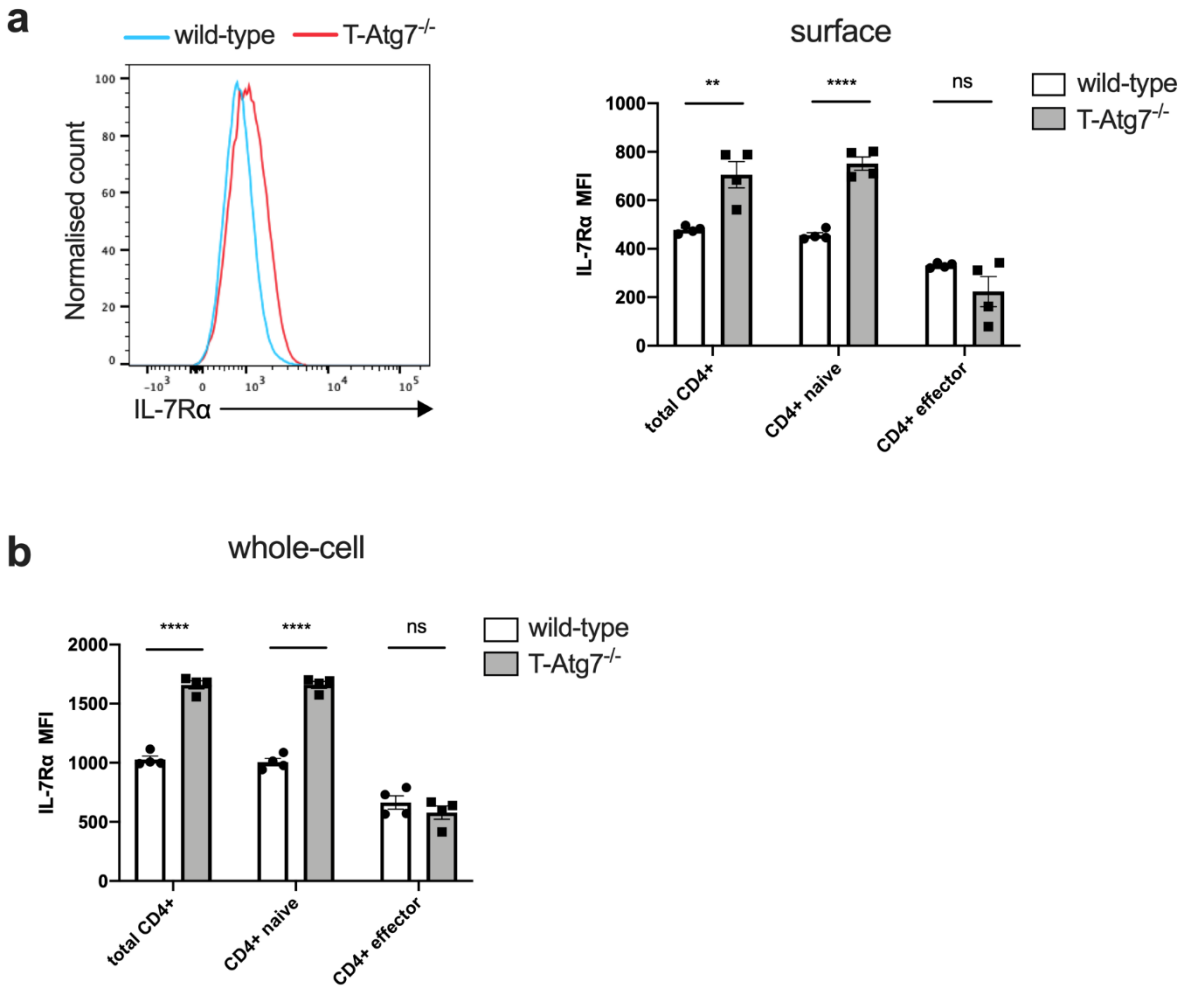


Figure 5.16 IL-7Rα is accumulated in T-Atg7$^{-/-}$ naïve CD4+ T cells.

a) Histogram (left) of IL-7Rα surface level, gated on splenic CD4+ T cells from wild-type or T-Atg7$^{-/-}$ mice. Bar graphs show the surface (a, right) or whole-cell (b) level of IL-7Rα as geometric mean fluorescent intensity (MFI) in total CD4+ T cell, naïve CD4+ T cell (CD62L+ CD44^{lo}) or effector CD4+ T cell (CD62L- CD44^{hi}). Quantitative analyses are representative of four independent experiments. All values are represented as mean ± SEM with unpaired two-tailed Student's t-test (n=3-4 mice per group), p*<0.05, p***<0.001, p****<0.0001, ns: not significant.

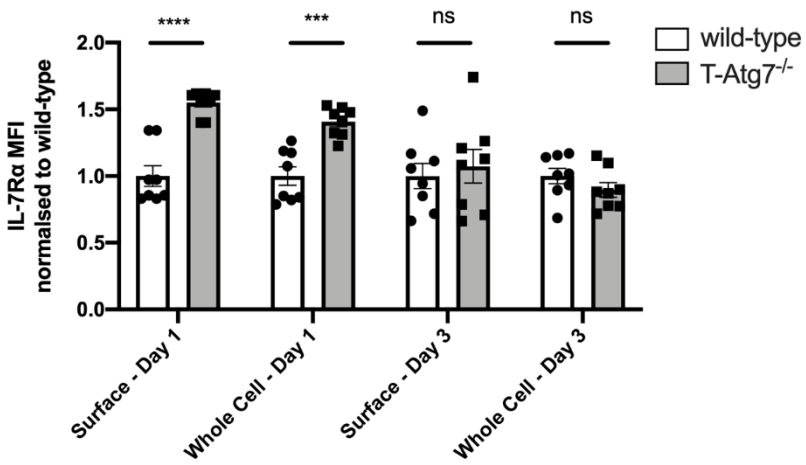


Figure 5.17 IL-7Rα levels in wild-type or T-Atg7$^{-/-}$ CD4+ T cells activated for 1 or 3 days.

Bar graph summarising flow results of both surface and whole-cell IL-7Rα level in splenic CD4+ T cells activated for 1 or 3 days in vitro. Fold change in IL-7Rα geometric mean fluorescence of T-Atg7-/- normalised to wild-type is shown (n=8 mice per group). All values represented as mean ± SEM with unpaired two-tailed Student's t-test, p***<0.001, p****<0.0001, ns: not significant.

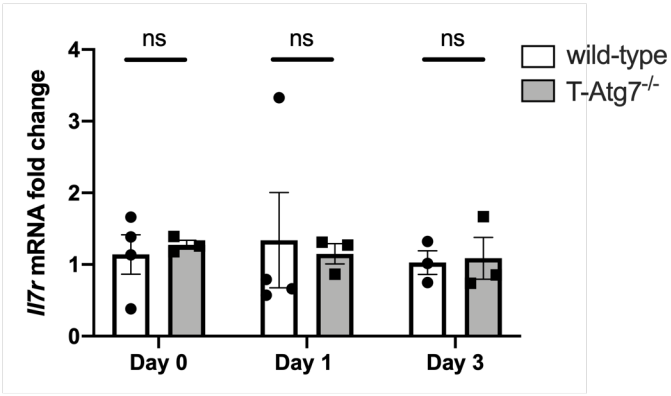


Figure 5.18 Quantification of *Il7ra* mRNA expression in splenic CD4+ T cells without activation, activated for 1 day or 3 days.

The bar graph shows the fold change of *Il7ra* mRNA normalised to wild-type (n = 3-4 mice per group). All values represented as mean ± SEM with unpaired two-tailed Student's t-test, ns: not significant.

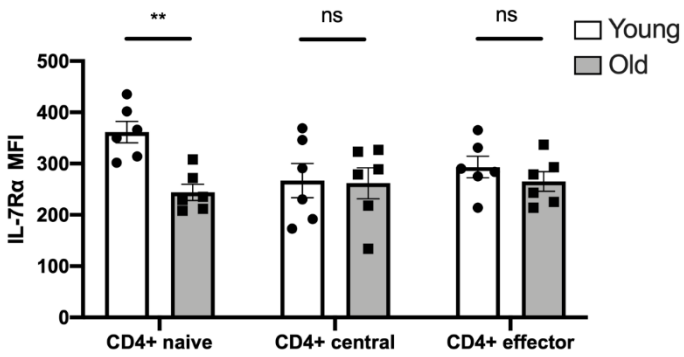


Figure 5.19 IL-7Rα surface level is decreased in naïve CD4+ T cells from aged mice.

Bar graph showing the surface level of IL-7Rα as geometric mean fluorescent intensity (MFI) in naïve CD4+ T cell (CD62L+ CD44^{lo}), central memory CD4+ T cell (CD62L+ CD44^{hi}) or effector CD4+ T cell (CD62L- CD44^{hi}) from old (2 years) and young (3 months) wild-type mice. Quantitative analyses are representative of two independent experiments. All values represented as mean ± SEM with unpaired two-tailed Student's t-test (n=6 mice per group), p**<0.01, ns: not significant.

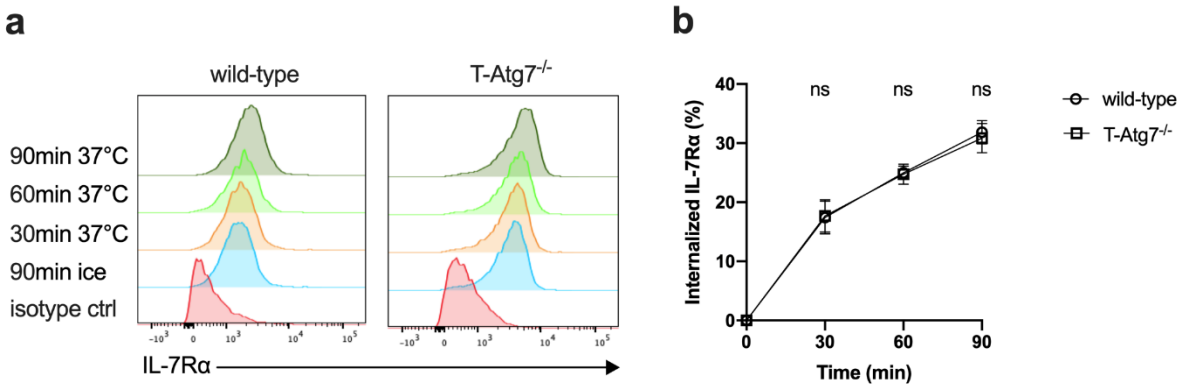


Figure 5.20 The internalisation rate of IL-7Rα is not changed in T-Atg7$^{-/-}$ naïve CD4+ T cells.

The internalisation of surface IL-7Rα on naïve CD4+ T cells was performed with a biotin-based flow cytometric endocytosis assay. a) Representative histograms to show biotin-conjugated IL-7Rα antibody expression. b) Connected scatter plot indicating the percentage of internalised IL-7Rα at 30, 60, and 90 min at 37 °C, n = 6 mice per group. All values represented as mean ± SEM with unpaired two-tailed Student's t-test, ns: not significant.

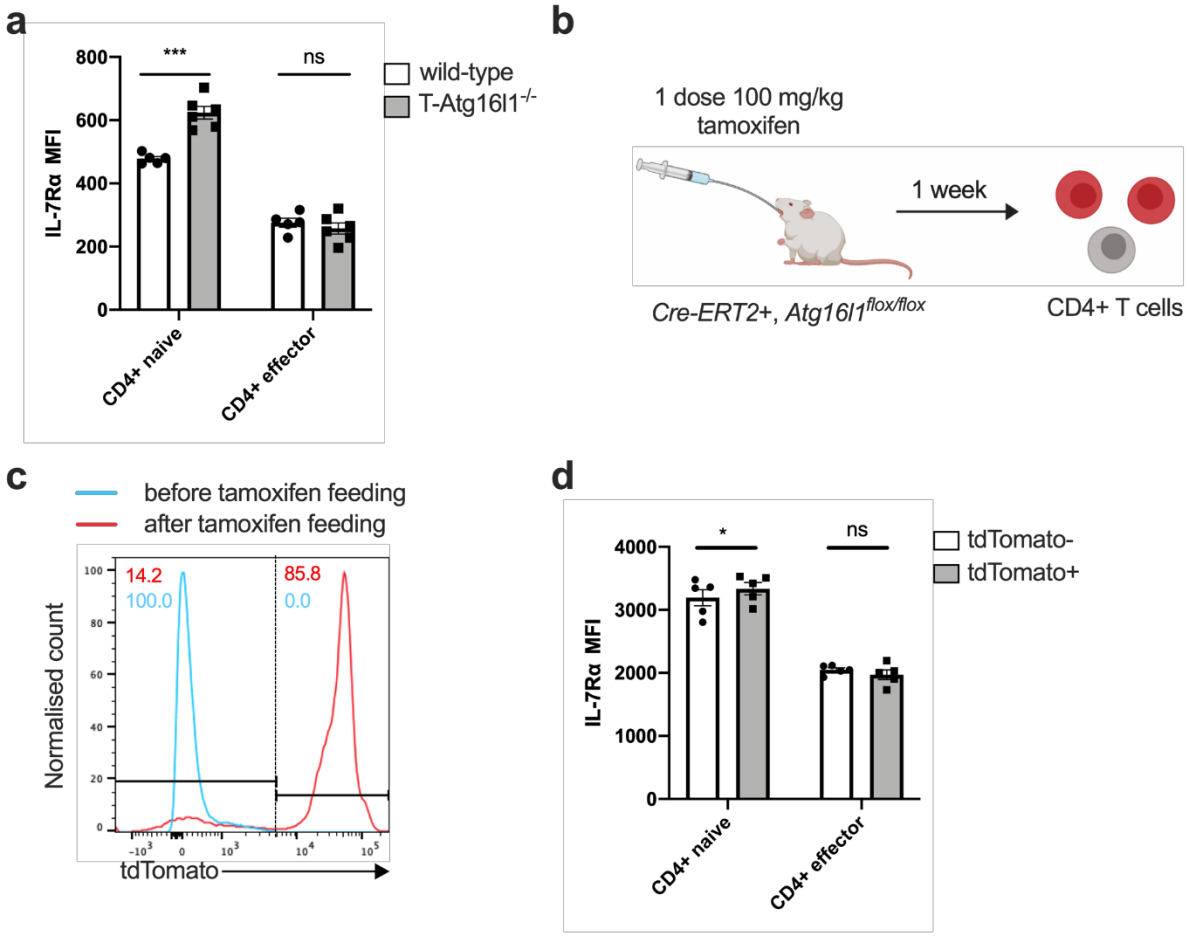


Figure 5.21 IL-7Rα surface level is increased in the constitutive and inducible *Atg16l1*-knockout naïve CD4+ T cells.

a) Bar graph depicting surface IL-7Rα level in different CD4+ subtypes from wild-type and $CD4^{cre}$ *Atg16l1*$^{flox/flox}$ (T-Atg16l1$^{-/-}$) mice, n=5-6 mice per group. All values represented as mean ± SEM with unpaired two-tailed Student's t-test, p***<0.001, ns: not significant. In courtesy of Cristina Dumitru. b) Experimental set-up: *Cre-ERT2*+, *Atg16l1*$^{flox/flox}$ mice were fed with 1 dose 100 mg/kg tamoxifen. After 1 week of reconstitution, mice were culled for analysis. c) Representative histogram to show tdTomato expression gated on total CD4+ T cells before and after tamoxifen feeding. d) Bar graph depicting surface IL-7Rα level in different CD4+ subtypes from *Cre-ERT2*+, *Atg16l1*$^{flox/flox}$ mice fed with 1 dose 100 mg/kg tamoxifen, gated on tdTomato+ (autophagy-deficient) and tdTomato- (autophagy-proficient) populations (n=5 mice per group). All values represented as mean ± SEM with paired two-tailed Student's t-test, p*<0.05, ns: not significant.

5.2.7 IL-2R, but not IL-7R signalling, is impaired in T-Atg7$^{-/-}$ CD4+ T cells

While I confirmed that the accumulation of IL-7Rα in naïve CD4+ T cells is autophagy-dependent, the molecular basis of how it leads to impaired proliferation was still elusive. Both IL-7R and IL-2R share a common gamma-chain (γ_c) to transduce downstream signalling. IL-7R (heterodimer comprised of γ_c and IL-7Rα) is highly expressed on naïve T cells and co-exists with the low-affinity IL-2R (heterodimer comprised of γ_c and IL-2Rβ). During TCR-mediated activation, IL-7Rα is downregulated from the cell surface and IL-2Rα takes over to form high-affinity IL-2R (heterotrimer comprised of γ_c, IL-2Rα and IL-2Rβ). When binding to IL-2, high-affinity IL-2R mediates persistent and robust downstream signalling, which is crucial for the proliferation of CD4+ T cells. It has been reported in regulatory T cells that γ_c has limited availability and pre-associates with excessive IL-7Rα independently of IL-7, which impedes IL-2R signalling. Therefore, I hypothesized that excessive IL-7Rα expression leads to delayed proliferation of T-Atg7$^{-/-}$ CD4+ T cells by a similar mechanism (Figure 5.22).

First, I examined whether the excessive amount of surface IL-7Rα enhances the IL-7R signalling in naïve CD4+ T cells via measuring the level of phosphorylated Stat5 (pStat5), the classical downstream transducer of both IL-7R and IL-2R signalling. However, in response to exogenous IL-7, there was no significant difference in the increase of pStat5 expression between wild-type and autophagy-deficient CD4+ T cells (Figure 5.23). The observation is consistent with a transgenic mouse model, which expresses IL-7Rα refractory to IL-7 induced down-regulation and displays a slightly higher surface level of IL-7Rα[406]. This is probably due to the limited amount of γ_c available for forming the functional IL-7R on the cell surface since IL-7Rα (~4,300 molecules/cell) is more abundant than γ_c (~2,300 molecules/cell) on naïve CD4+ T cells[407].

I further investigated whether IL-2R signalling was impaired in autophagy-deficient CD4+ T cells. Since naïve CD4+ T cells that only express low-affinity IL-2R respond poorly to IL-2, we hypothesized that IL-2R signalling contributes to CD4+ T cell proliferation mainly when IL-2Rα (or CD25), the major component of high-affinity IL-2R, is upregulated[70]. To validate my hypothesis, naïve CD4+ T cells from both genotypes were purified and activated for 24 hours (Figure 5.24a). Flow cytometry analysis indicated that IL-2Rα was upregulated after 24-hour TCR-mediated activation (Figure 5.24b). In the meantime, IL-7Rα was still more abundant on the surface of T-Atg7$^{-/-}$ CD4+ T cells (Figure 5.24c, left). While wild-type CD4+ T cells responded to exogenous IL-2 in a dose-dependent manner, autophagy-deficient T cells showed no change in pStat5 signal (Figure 5.24d and e), indicating that the IL-2R signalling was indeed impaired in T cells that lack autophagy. This was not due to a reduced expression of IL-2R components, since I found no significant difference of the three subunits between wild-type and autophagy-deficient CD4+ T cells (Figure 5.24c).

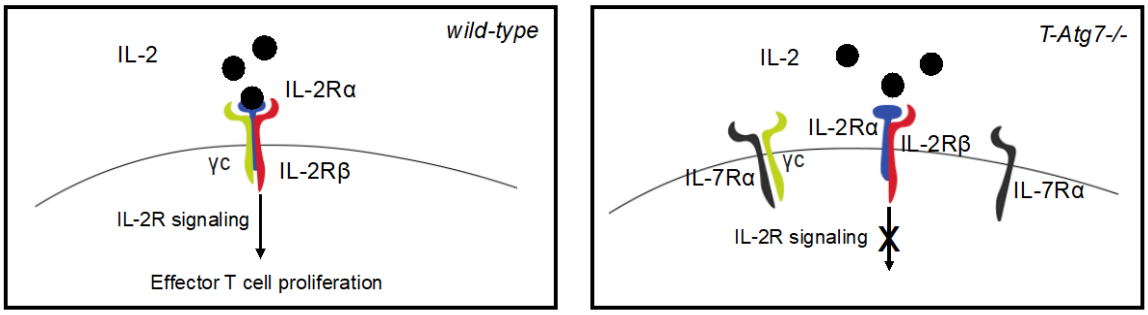


Figure 5.22 Schematic overview of how excessive IL-7Rα may lead to impaired T cell proliferation.

During T cell activation, the IL-2Rα is upregulated on the cell surface, while surface IL-7Rα is decreased. In T-Atg7$^{-/-}$ CD4+ T cells, excessive IL-7Rα sequestrates the common gamma chain (γ_c), a key subunit of both IL-7R and IL-2R, and abrogates the downstream IL-2R signalling which is crucial for the expansion of the effector population.

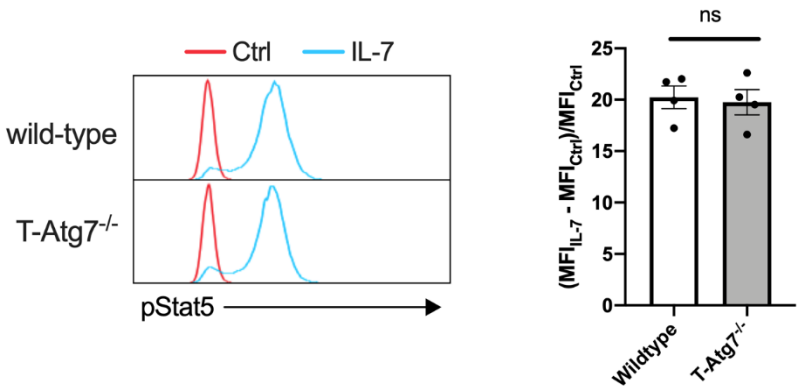


Figure 5.23 The amplitude of IL-7R signalling is not changed in T-Atg7$^{-/-}$ naïve CD4+ T cells.

Histograms (left) of pStat5 level in naive CD4+ T cells from wild-type or T-Atg7$^{-/-}$ mice, stimulated with or without 10 ng/ml murine IL-7. Bar graph (right) depicting the ratio of increase in p-Stat5 signal in response to 10 ng/ml murine IL-7 ($pStat5_{IL\text{-}7} - pStat5_{ctrl}$) to the basal level ($pStat5_{ctrl}$), n=4 mice per group.

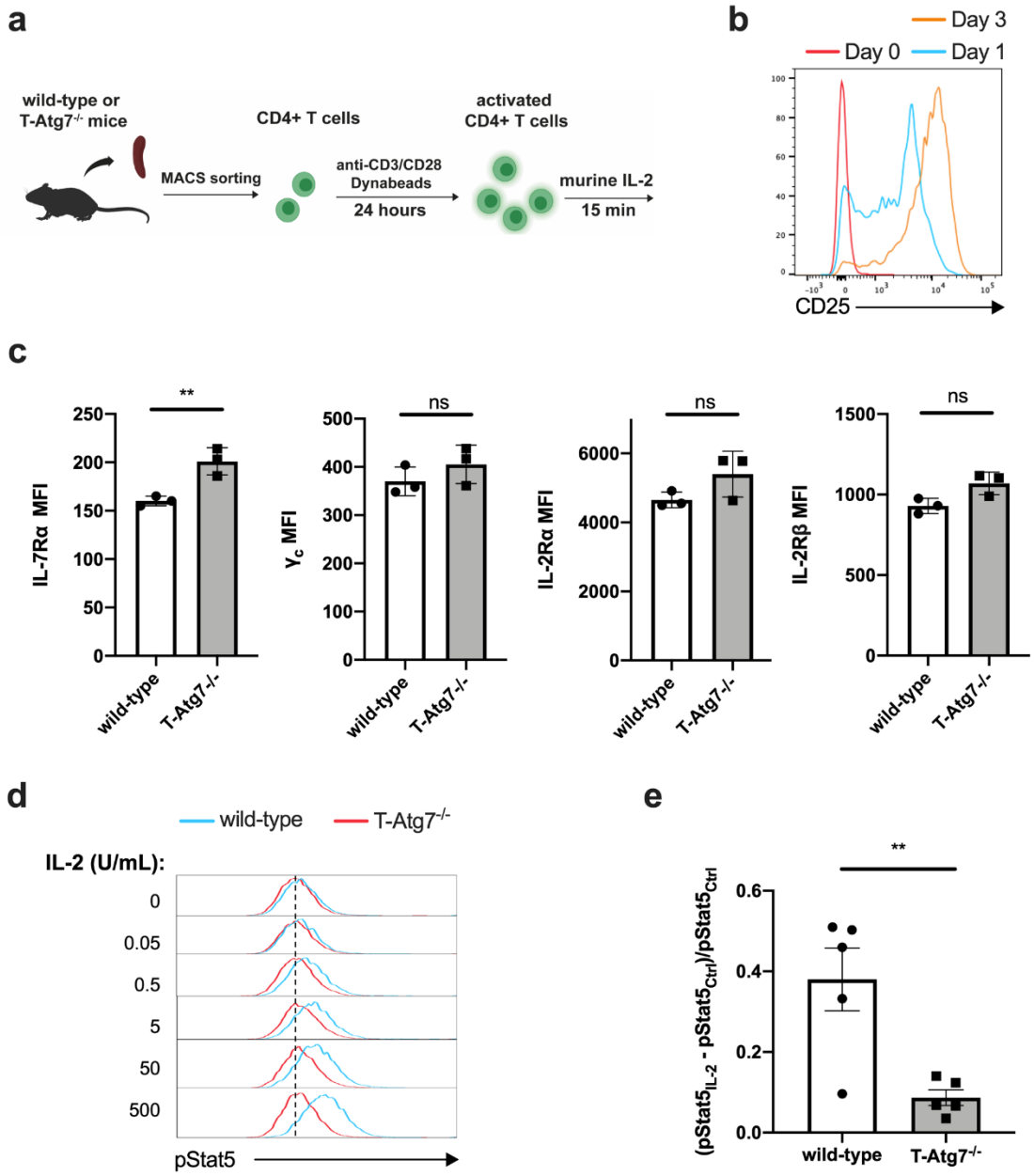


Figure 5.24 IL-2R signalling is impaired in autophagy-deficient CD4+ T cells.

a) Experimental set-up: naïve CD4+ T cells from either wild-type or T-Atg7$^{-/-}$ mice were activated with anti-CD3/CD28 Dynabeads for 24 hours, followed by treatment with murine IL-2 for 15 min. Phosphorylated Stat5 (pStat5) level was measured by flow cytometry. b) Histogram of CD25 level in naive CD4+ T cells or CD4+ T cells activated for 1 or 3 days. c) Histograms of pStat5 level in activated CD4+ T cells from wild-type or T-Atg7$^{-/-}$ mice, stimulated with different doses of murine IL-2. d) Bar graph depicts the ratio of increase in p-Stat5 signal in response to 20 ng/ml murine IL-2 ($pStat5_{IL\text{-}2} - pStat5_{ctrl}$) to the basal level ($pStat5_{ctrl}$), determined from two independent experiments, n=5 mice per group. e) Splenic naïve CD4+ T cells purified from either wild-type or T-Atg7$^{-/-}$ mice were activated with anti-CD3/CD28 Dynabeads for 24 hours. The surface receptor levels were assessed with flow cytometry. Bar graphs depict surface levels of IL-7Rα, IL-2Rα, common gamma chain (γ_c) and IL-2Rβ on activated CD25+ CD4+ T cells (n=3 mice per group). Data are represented as mean ± SEM with unpaired two-tailed Student's t-test, p**<0.01, ns: not significant.

5.2.8 Excessive surface IL-7Rα impairs the assembly of IL-2R via sequestrating γ_c

To further validate that impaired IL-2R signalling in activated T-Atg7$^{-/-}$ CD4+ T cells is due to the disrupted assembly of the cytokine receptor, our collaborators, Professor Michael Dustin and Dr Jesusa Capera, helped me measure the co-localisation of γ_c with either IL-7Rα or IL-2Rα in CD4+ T cells from wild-type and T-Atg7$^{-/-}$ mice. Since IL-2R signalling is polarised at the immune synapse, we incubated the purified CD4+ T cells activated for 1 day on supported lipid bilayers containing ICAM1 and anti-CD3 proteins to mimic the formation of immune synapses with antigen-presenting cells[408]. We then visualised different subunits of the IL-7R and IL-2R at the immune synapse with total internal reflection fluorescence (TIRF) microscopy (Figure 5.25a). As expected, we observed a significantly reduced co-localisation of IL-2Rα and γ_c in T-Atg7$^{-/-}$ CD4+ T cells (Fig. 5.25b, left), indicating an impaired formation of the synaptic IL-2R complex in autophagy-deficient CD4+ T cells. However, we did not see a significant difference in the colocalization of γ_c with IL-7Rα at the immune synapse (Fig. 5.25b, right). We reasoned this could be a consequence of IL-7Rα sequestration in locations other than the immune synapse.

Therefore, we proceeded to see whether the γ_c was more colocalised with IL-7Rα at the whole-cell level in activated T-Atg7$^{-/-}$ CD4+ T cells (Figure 5.26a). Indeed, Pearson's correlation coefficient between γ_c and IL-7Rα was significantly increased in autophagy-deficient cells (Figure 5.26b), which confirmed our hypothesis.

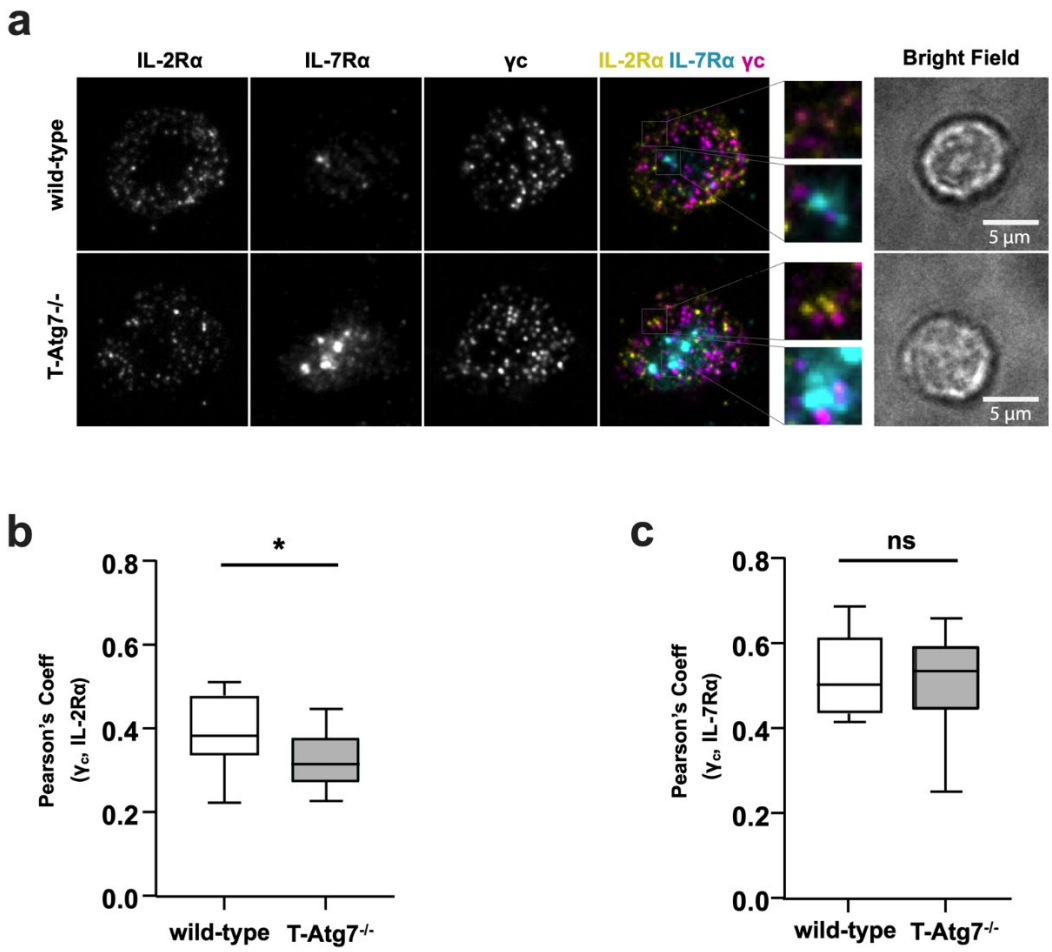


Figure 5.25 Assembly of IL-2R complex is impaired in the immunological synapse of T-Atg7$^{-/-}$ CD4+ T cells.

a) TIRF imaging (left) of IL-7Rα, IL-2Rα and γ_c at the immunological synapse. Naive CD4+ T cells activated for 24 hours were exposed to supported lipid bilayers containing ICAM1 and anti-CD3 proteins, then fixed after a 10 min incubation with 50 U/ml mIL-2. Cytokine receptors were stained for imaging. Square insets show magnification of the co-localisation events. Box graphs (right) show Pearson's correlation coefficients between the IL-2Rα and γ_c (b), and the IL-27α and γ_c (c), n = 15 cells per group. Data are represented as mean ± max and min values, with unpaired two-tailed Student's t-test, p*<0.05. In courtesy of Jesusa Capera.

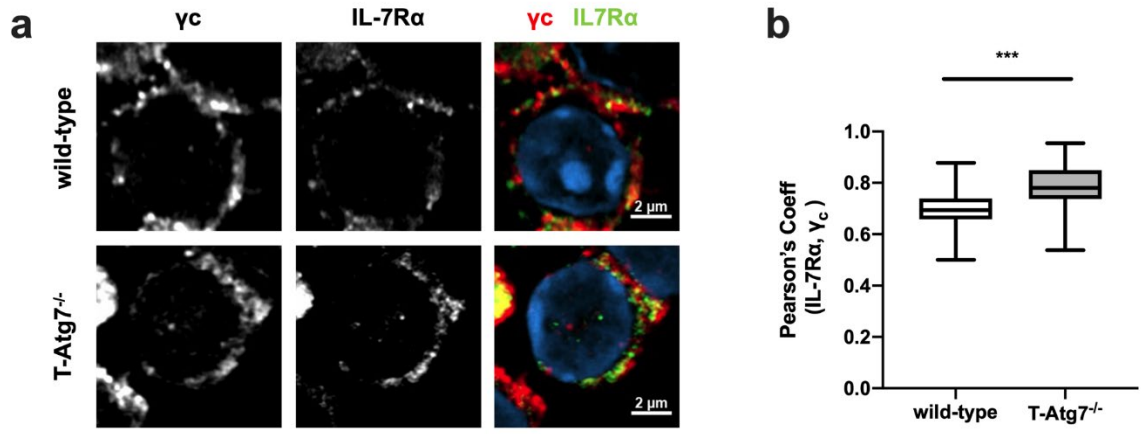


Figure 5.26 γ_c is sequestrated by the excessive IL-7Rα outside of the immunological synapse.

a) Confocal imaging of IL-7Rα and γ_c at the surface of activated CD4+ T cells (with high CD25 expression). b) Box graph (right) shows Pearson's correlation coefficient between the IL-7Rα and γ_c at the cell surface (n=23 cells per group). Data are represented as mean ± max and min values, with unpaired two-tailed Student's t-test, p***<0.001. In collaboration with Mariana Borsa.

5.2.9 Blocking the IL-7R receptor did not rescue the phenotype of impaired proliferation.

We reasoned that a possible way to rescue the proliferation capacity of autophagy-deficient cells was to dissociate the γ_c from IL-7Rα, which could facilitate the assembly of IL-2Rs and recover the IL-2R signalling. Previous studies showed that the rat anti-mouse IL-7Rα clone A7R34 can effectively block IL-7R at its ligand-binding domain both in vitro and in vivo[409]. I hypothesized that the binding of the antibody to IL-7Rα can also block its interaction domain and disrupt the dimerization of the IL-7R receptor.

I performed a titration assay, which showed that IL-7R signalling in naïve T cells can be effectively blocked in vitro even with a concentration of antibody as low as 0.4 μg/ml (Figure 5.27a). Aiming to guarantee a long-term blocking effect, 200 μg/ml of anti-IL-7R antibody was used over a 3-day activation. However, at day 3 post-activation, the proliferation of either wild-type or autophagy-deficient CD4+ T cells was not enhanced when compared to cells treated with the isotype control antibody or left untreated (Figure 5.27b and c). The result indicates that the anti-IL-7Rα antibody may not be able to disrupt the sequestration of γ_c by IL-7Rα. Thus, other alternative methods would need to be implemented to rescue the phenotype of the autophagy-deficient CD4+ T cell, such as engineered IL-2 with a higher affinity to γ_c which may free it from the pre-assembled IL-7R, as ongoing experiments.

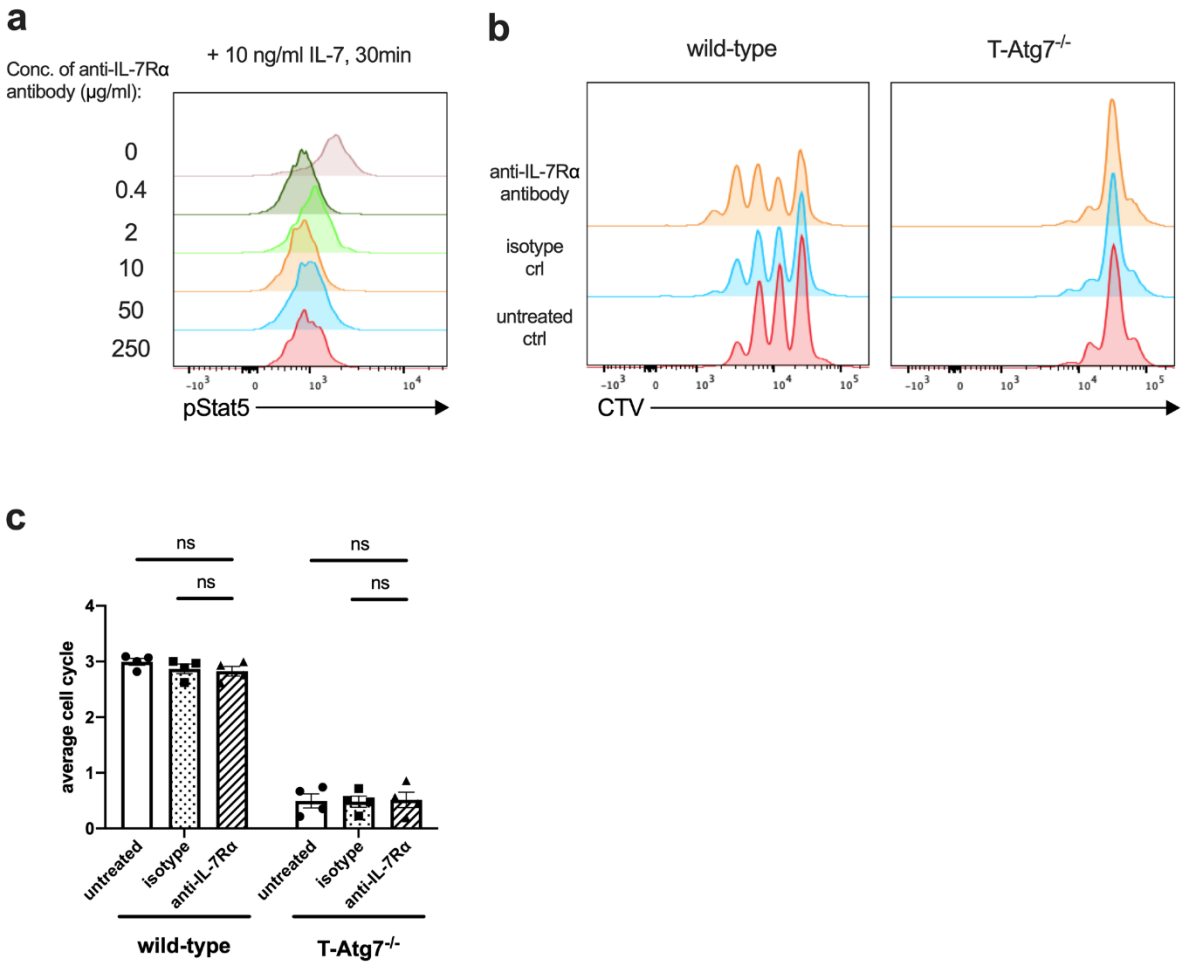


Figure 5.27 Anti-IL-7Rα antibody cannot rescue the impaired proliferation of T-Atg7$^{-/-}$ CD4+ T cells.

a) Histograms of pStat5 level in naive CD4+ T cells from wild-type or T-Atg7$^{-/-}$ mice, treated with 10 ng/ml murine IL-7 for 30 min and pre-incubated with different doses of the anti-IL-7Rα antibody. b) Histograms showing the proliferation profile of CD4+ T cells, from either wild-type or T-Atg7$^{-/-}$ mice, activated for 3 days, with the treatment of 200 µg/ml anti-IL-7Rα antibodies (anti-IL-7Rα), isotype control (isotype) or nothing (untreated). c) Bar graph indicating the average cell cycle of either wild-type or T-Atg7$^{-/-}$ CD4+ T cells activated for 3 days, with the treatment of anti-IL-7Rα antibodies (anti-IL-7Rα), isotype control (isotype) or nothing (untreated) (n=4 mice per group). Data are represented as mean ± SEM with unpaired two-tailed Student's t-test, ns: not significant. In collaboration with Ghada Alsaleh.

Chapter 5: Characterisation of autophagic substrates in activated CD4+ T cells and their role for CD4+ T cell proliferation – Discussion

5.3 Discussion

Our mouse model, which allows the investigation of autophagosomal content by LC3B-proximity biotinylation, showed to be efficient to dissect autophagy targets during T cell activation. Firstly, we performed experiments using pan-T cells, when KLHL6 was identified as a potential autophagosomal cargo that could play a role in T cell proliferation. KLHL6 belongs to Kelch-like gene family proteins[410]. It is a Cullin 3-RING ligase that serves as a tumour suppressor gene in large B-cell lymphoma by restraining the NF-κB signalling[411]. Therefore, I hypothesized that KLHL6 could also inhibit NF-κB signalling in T cells. In this scenario, when T cells receive TCR/CD28-stimuli, its degradation by autophagy could play an important role in promoting T cell activation and proliferation. Other Kelch-like gene family members were shown to either be degraded by autophagy or interact with ATG8s. NF-E2-related factor 2 (NRF2) initiates the expression of cytoprotective genes in response to electrophilic and oxidative stresses as a nuclear transcription factor, while kelch-like ECH-associated protein 1 (KEAP1, or KLHL17) serves as a stress sensor by promoting proteasomal degradation of NRF2[161]. Upon cellular stress, KEAP1 is degraded through autophagy in a p62-dependent manner, which stabilises NRF2 and leads to its accumulation in the nucleus. A new Cullin 3-RING ligase complex containing KBTBD6 and KBTBD7, the other two Kelch-like gene family members, requires the interaction with membrane-bound GABARAPs to mediate the ubiquitination of its substrates[412]. While I confirmed that KLHL6 was degraded by autophagy through overexpressing it in the cell lines, neither dampened NF-κB signalling nor decreased expression of KLHL6 substrates was observed in autophagy-deficient CD4+ T cells. It is possible that the results observed in cell lines in vitro by overexpressing the protein did not reflect what happens in primary T cells, as KLHL6 is much less abundant within the T-cell proteome[413]. Overexpression of KLHL6 may facilitate the formation of protein aggregates due to its misfolding, and boost autophagy to remove them in bulk, which rarely happens in healthy

primary cells[397]. Moreover, the lack of any available antibody to detect KLHL6 directly also compromises the solidity of any conclusion made in the primary cells. These limitations made me decide to look for other autophagosomal candidates that could (1) serve as a proof-of-principle for our mouse model and (2) play a role in T cell proliferation, which could explain the impaired phenotype observed in autophagy-deficient cells, particularly in the first days following activation.

IL-7Rα was also detected as a potential autophagy target in the LC3+ compartment in BafA1-treated pan-T cells. However, we chose not to validate this membrane protein at first, since we reasoned it may be a false-positive candidate due to overlap between autophagy and endocytic pathways. ATG proteins have been widely shown to participate in processes other than macroautophagy, including endosomal microautophagy (eMA), LC3-associated phagocytosis (LAP), LC3-associated endocytosis (LANDO) and LC3-dependent extracellular vesicle loading and secretion (LDELS)[177]. A study in primary human CD8+ T cells showed that IL-7Rα is downregulated from the cell surface through clathrin-mediated endocytosis, then enters early endosomes, late endosomes (or multivesicular bodies, MVBs) and gets degraded by either lysosomes or the proteasome[357]. One may argue that we find IL-7Rα in LC3B+ compartments is due to the crosstalk of its intracellular trafficking with these processes. However, it is unlikely we identified IL-7Rα within vesicles related to LAP or LANDO in our system, since lipidated LC3 is expressed on the cytosolic surface of those vesicles, and the proteinase K digestion in our protocol effectively removes cytosolic proteins. Moreover, our result cannot link IL-7Rα to LDELS, a process independent of lysosomal degradation, as we see a significant accumulation of IL-7Rα in the LC3+ compartment when cells were treated with BafA1, a lysosomal inhibitor. It is possible that eMA might be involved in IL-7Rα degradation, since this receptor was found in MVBs, the vesicular structure related to eMA[312]. During eMA, LC3

proteins are anchored to the limiting membrane of MVBs[177]. Intraluminal budding of the LC3-bound subdomain could lead to IL-7Rα localization into the cisternae of MBVs in the form of intraluminal vesicles (ILVs). In this scenario, MVBs would still fuse with lysosomes, therefore, the biotin-labelled IL-7Rα would be sensitive to BafA1-treatment and could be protected from proteinase K-treatment by the outer membrane of the MVBs. While we have not excluded this possibility experimentally, our data indicate that conventional autophagy plays a major role in IL-7Rα degradation. Indeed, we successfully demonstrated that IL-7Rα was co-localized with WIPI2, an early autophagosomal marker, which has not been linked with MVBs yet. Moreover, IL-7Rα was dramatically upregulated in *Atg7*-knockout CD4+ T cells. However, evidence is accumulating that ATG7 contributes minorly to the microautophagy of cytosolic proteins, and *Atg16l1*-deficient T cells also have upregulated expression of IL-7Rα in our hand[38]. Indeed, MVBs can fuse with autophagosomes to form a hybrid organelle called amphisome, where the autophagy and endocytic machinery converge[414,415]. It could be that IL-7Rα-containing MVBs may rely on the formation of amphisomes for their lysosomal degradation. To address the hypothesis, we will perform the co-staining of IL-7Rα, an autophagosome-specific marker (such as WIPI2) and an MVB-specific marker (such as RAB7) and see whether they are co-localised in CD4+ T cells.

Though I did not find IL-7Rα in the LC3B+ compartment in CD4+ T cells activated for 16 hours, a time point before cell proliferation indicated by other studies, this might be due to the low autophagy level and high heterogeneity of the cells[404]. By contrast, our observation supports that autophagy may contribute to the degradation of IL-7Rα both before and after activation, as IL-7Rα was accumulated in autophagy-deficient CD4+ T cells, and co-localised with autophagosomal markers in autophagy-proficient CD4+ T cells, both pre- and post-activation.

I observed an upregulation of IL-7Rα expression in naïve CD4+ T cells from several autophagy-deficient models. In contrast to our study, T cells lacking *Vps34*, a gene encoding a PI3-kinase involved in the initiation of autophagy, have been reported to downregulate the surface expression of IL-7Rα[312]. This study proposed that a lower level of surface IL-7Rα might be a result of an impaired retromer pathway, which is mediated by VPS34, since they observed no change in autophagic flux but reduced recycling of IL-7Rα from MVBs. On the other hand, in another study using bone marrow chimaera, IL-7Rα expression was found to be higher in *Vps34*-deficient CD4+ T cells compared to autophagy-sufficient counterparts[103]. The authors discussed that reduced IL-7Rα in *Vps34*-knockout mice was a secondary effect of lymphopenia. The latter observation is consistent with our findings, which were also made in a non-lymphopenic environment (found in young mice at 6 weeks of age). Indeed, T cells are major consumers of IL-7 in the periphery. In naïve T cells, surface IL-7R expression is affected by extracellular IL-7 concentrations[356,357]. A decrease in total T cell numbers increases the availability of IL-7 in vivo, therefore downregulating IL-7Rα from the cell surface. When T cells receive TCR/CD28-stimuli, their surface expression of IL-7Rα is rapidly downregulated via degradation and suppressed transcription. However, as our results from proximity labelling and confocal imaging showed, we could still observe IL-7Rα expression in some CD4+ T cells activated for 3 days. The heterogeneous pattern of IL-7Rα expression in the effector population might be linked to the number of cell cycles they have been through, or their cell-intrinsic potential to differentiate into IL-7Rα-dependent memory precursor cells.

Despite the higher IL-7Rα expression found in T-Atg7$^{-/-}$ CD4+ T cells, the downstream IL-7R signalling was not affected. This was probably due to a limited number of γ_c to form functional IL-7R complexes. Besides the magnitude, the duration of IL-7R signalling also affects T cell

homeostasis. In a transgenic mouse model, where T cells express an IL-7 refractory IL-7Rα, T cells exhibit continuous IL-7R signalling [406]. This leads to cytokine-induced cell death and a shift from naïve to effector/memory population, which is more prominent in CD8+ T cells than in their CD4+ counterparts. It mimics precisely the phenotypes of lymphopenia and reduced naïve pool in the T-Atg7$^{-/-}$ mice, implying that IL-7Rα degradation contributes to naïve T cell homeostasis in the absence of autophagy[106].

Our study in conventional CD4+ T cells, together with the previous report in regulatory T cells, has linked an excessive IL-7R expression with impaired IL-2R signalling. However, functional assays are required to confirm a causal link between our proposed molecular mechanism and the observed phenotypes in autophagy-deficient T cells. Although the strategy to free γ_c sequestered by the surplus IL-7Rα with anti-IL-7Rα antibody did not rescue the impaired proliferation of T-Atg7$^{-/-}$ CD4+ T cells, one other possible way is to enhance the assembly of IL-2R and/or its downstream signalling. Engineered IL-2, such as interleukin-2 superkine and neoleukin-2, display higher affinity towards IL-2R subunits, which endows them with the potential to "drag" the γ_c to IL-2α or IL-2β[416,417]. Alternatively, it is possible to try to replicate the phenotype found in autophagy-knock cells via overexpressing IL-7Rα in wild-type naïve CD4+ T cells. For that, a transgenic murine model with forced IL-7Rα expression can be used – the hCD2-IL7R transgenic mouse, whose IL-7Rα is driven by the human CD2 enhance-promoter element[407,418,419]. It has been shown by this model that IL-7Rα expression has an impact on the early development of T cells in the thymus, on the cytotoxic capability of CD8+ T cells and on the survival of regulatory T cells. Our hypothesis could be validated through comparing the proliferation of naïve CD4+ T cells from this mouse model with wild-type CD4+ T cells following TCR/CD28-mediated activation, although the impact on development cannot be excluded. Therefore, inducible overexpression of IL-7Rα or CRISPR targeting of the

endogenous *Il7r* locus in wild-type naïve CD4+ T cells would be better strategies. Although the technique is quite challenging since non-dividing cells naïve primary T cells have a low transfection/transduction rate, the direct delivery of IL-7Rα mRNA into naïve CD4+ T cells through electroporation is a promising solution[420].

Some other molecules were shown to undergo autophagy-mediated degradation during the activation of naïve CD4+ T cells and Th1 cells. CDKN1B/p27Kip1, a cell cyclin-dependent kinase inhibitor, was found to be accumulated in whole-cell proteomics of autophagy-deficient T cells[102]. Further validation indicated that CDKN1B needs to be degraded by autophagy to guarantee the proliferation of naïve CD4+ T cells. Though widely applied to indirectly map autophagosomal content from autophagy-deficient T cells, this method cannot exclude the possibility that cells without autophagy may have synthesized these as new proteins. By purifying autophagosomes with differential centrifugation and subfractionation, Mocholi et al. showed that the turnover of PTPN1, a protein tyrosine phosphatase associated with anergic phenotypes, relies on autophagy in activated Th1 cells[114]. We did not detect either of these molecules in CD4+ T cells activated for either 16 hours or 3 days. We cannot exclude that our method, based on the proximity biotinylation technique, might detect a biased proteome since the biotin-phenol radicals preferentially react with the electron-rich amino acid residues exposed on the surface of the protein. However, we can also be confident that we are analysing an improved purified fraction of autophagosomes compared to previous studies. This allowed us to identify a membrane molecule, IL-7Rα, as a key target of autophagy during CD4+ T cell activation, and at least partially elucidate the defective proliferation phenotype found in autophagy-deficient CD4+ T cells.

Chapter 6: Summary and general discussion

6.1 The application of proximity biotinylation technique to study protein degradation

Autophagy is a conserved physiological pathway that plays crucial roles in the differentiation, maintenance and function of many cell types. Identifying autophagosomal substrates in vivo is particularly important to understand the role of autophagy in health and disease. However, the full spectrum of autophagosomal degraded proteins remains poorly defined. Traditional methods of analysing autophagosomal contents rely on complicated multistep gradient centrifugation. The results are compromised by contamination from other co-purified cellular compartments and by the low reproducibility caused by variation introduced during the differential centrifugation and extensive manipulation. Furthermore, the number of cells required often exceeds what can be obtained from primary material. To avoid this, we are using a method termed "proximity labelling" to selectively tag proteins in autophagosomes with biotin with high specificity and efficiency. (Figure 6.1).

To systemically validate the *Lc3b-APEX2* mouse model, I first confirmed the expression of LC3B-APEX2 chimeric protein, its correct involvement in the autophagic flux, the enzymatic function of APEX2 as well as its localisation in the autophagosomes. To further increase the sensitivity and consistency of the autophagosomal protein detection, I optimised the protocol for purifying autophagosomal cargos in primary cells. Then I performed proximity biotinylation with immortalised mouse embryonic fibroblasts to further confirm the ability of the mouse model to map autophagosomal proteins. Indeed, candidates expected to end up in the autophagosomes were enriched in the following categories: autophagic receptors, autophagy regulators interacting with LC3, autophagy substrates and ATG8 homologs. Moreover, a cell titration experiment indicated that a greater cell number potentially yields more candidates when using the *Lc3b-APEX2* labelling system.

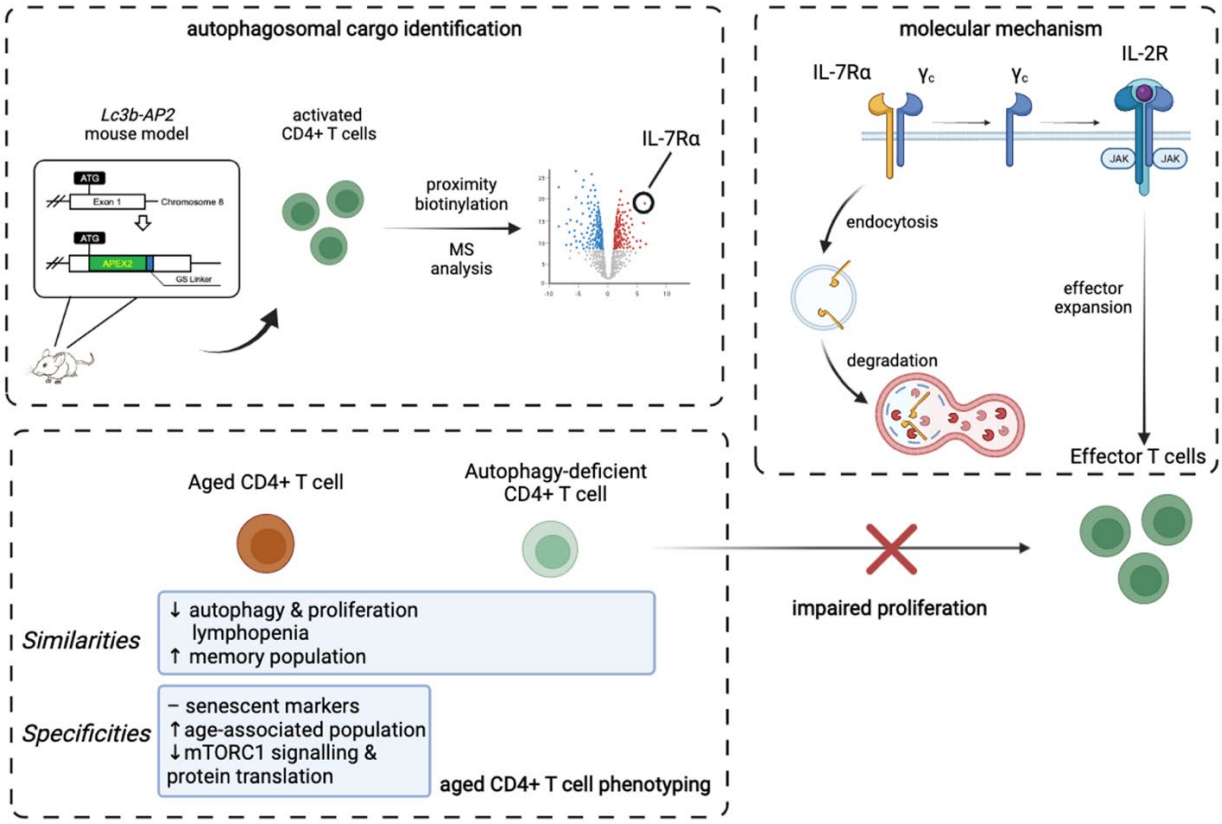


Figure 6.1 Application of *Lc3b-AP2* transgenic mouse model to investigate the molecular mechanism of how autophagy contributes to CD4+ T cell proliferation, and how they age.

CD4+ T cells with compromised autophagy display impaired proliferation upon TCR/CD28-stimuli both in vivo and in vitro, which phenocopies aged CD4+ T cells. To explore what needs to be degraded by autophagy to guarantee T cell proliferation, CD4+ T cells from the *Lc3b-AP2* mouse model were activated and proximity labelled for mass spectrometry (MS) analysis was performed. IL-7Rα was repeatedly identified. Mechanistically, IL-7Rα needs to be degraded by autophagy during CD4+ T cells activation since it can compete for the common gamma chain with IL-2R, whose signalling is indispensable for the expansion of effector T cells.

It is possible to increase the sensitivity of profiling the autophagosomal cargoes in T cells through modifying the mouse model. Here, we tagged the endogenous LC3B with the APEX2 enzyme, currently the most efficient peroxidase for proximity biotinylation. However, the biochemical reaction which transforms biotin phenols into reactive radicals requires H_2O_2, a compound causing oxidative stress in living cells. This step restricts the time window for reaction, as well as its application in vivo due to its toxicity. Recently, to replace APEX, researchers have developed TurboID, a new generation of biotin ligases, to detect the

spatiotemporal dynamics of secretory proteins in living mice[421]. Firstly, TurboID overcomes the issue of the low labelling efficiency of the original BioID. Moreover, a systemic comparison of different engineered peroxidases and biotin ligases for proximity labelling indicates an even better performance of TurboID compared to APEX2. Therefore, making another mouse model that replaces APEX2 with TurboID would probably help to increase the sensitivity of detecting autophagosomal cargoes. Generally, this preprint compares candidates identified through the knock-in strategy versus transient overexpression[422]. In line with the expectation that physiological expression of proteins circumvents the artefacts caused by overexpression, such as mislocalisation and aggregation, tagging endogenous proteins with either of these enzymes increases the sensitivity of the cargo detection[422]. In light of our work and those of our collaborator Christian Behrends, we have started to generate this new mouse model.

The *Lc3b-APEX2* mouse model facilitates an overall identification of proteinaceous substrates of macroautophagy. Moreover, a study that applies the proximity biotinylation system to different autophagy receptors not only addresses the overlapping but distinct selectivity of each receptor but also unravels their roles outside autophagy[45]. Similarly, the ATG8 homologues may vary in their binding preference to autophagy substrates, as well as their expression level on a cell-type basis[146]. Therefore, it would be worthwhile generating a cohort of mouse models bearing the proximity labelling system for each autophagy receptor (ATG8 homologues). Systemic profiling of autophagosomal cargoes in vivo could fill the gap in our knowledge of how autophagy contributes to physiological and pathophysiological processes with their underlying molecular mechanisms, further enabling the discovery of novel therapeutic targets.

The proximity biotinylation technique can also be applied to the identification of substrates degraded by CMA and microautophagy. The substrate selectivity of CMA relies on the recognition of the KFERQ-like motif by chaperone HSC70[46]. By fusing the APEX2 enzyme (or TurboID) with HSC70, substrates of CMA can be labelled with biotin with high spatial resolution. However, since HSC70 also mediates selective microautophagy, to distinguish between these two pathways, CMA needs to be specifically inhibited (such as we did here for macroautophagy by treating with BafA1) followed by quantitative MS[46]. Since the expression of LAMP2 is the rate-limiting step, a common method to specifically inhibit CMA is to silence the *Lamp2a* gene. However, deleting CMA in the long term may lead to homeostatic changes which alter the CMA substrates. Therefore, transient inhibition via small molecules which prevent the multimerization of LAMP2A, or block the channels that translocate the unfolded substrates, provides a better solution. By contrast, the cargoes of microautophagy are more difficult to detect, since the mechanism of its selectivity is largely elusive, and the known molecules involved in microautophagy overlap with macroautophagy and CMA. While it is possible to obtain the list of microautophagy substrates by identifying all proteins in proximity to LC3 and TOLLIP (both are crucial for macroautophagy) or HSC70 (crucial for CMA) and excluding the ones changed with inhibition of both pathways, the method is indirect and requires solid validation[45].

Substrates degraded by the ubiquitin-proteasome system (UPS) can also be mapped by the proximity labelling technique. The conventional protocol in which poly-ubiquitinated proteins are directly immune precipitated and enriched for mass spectrometry analysis yields a large number of false-positive candidates since this post-translational modification also plays non-degradative roles[423]. Instead, the fusion of the proximity labelling enzymes with the E3 ligase, combined with transient inhibition of proteasomal activity, might help identify bona fide

substrates degraded by UPS. The strategy can give rise to a list of biotinylated candidates upregulated upon UPS-inhibition (e.g. MG132, a cell-permeable compound reversibly inhibiting the proteasomal activity) as potential substrates degraded by proteasomes. Moreover, by tagging the proximity labelling enzymes with different E3 ligases, we can obtain an atlas of the selectivity of each E3 ligase.

Overall, with the proximity biotinylation technique, we can systemically understand intracellular degradation pathways and their substrates in primary cells with high specificity. It may vastly improve current clinical treatment approaches that are in development based on protein degradation. For instance, the proteolysis-targeting chimaera (PROTAC) technique is gaining a burgeoning interest in cancer therapies. Mechanistically, PROTAC combines a small molecule binder of a target protein to a moiety recruited by E3 ubiquitin ligase through a chemical linker[424]. The small molecule reduces the distance between target proteins and the E3 ligase complexes, facilitating the ubiquitination of targets and their further proteasomal degradation. However, the design of novel potent PROTACs is hampered by our limited knowledge on choosing an E3 ubiquitin ligase that allows the efficacious degradation of a specific target[424]. To determine optimal target-ligase pairs, we need an atlas of the protein-protein interaction of E3 ubiquitin ligases and their substrates in vivo, which can be achieved with the proximity labelling-based identification of UPS substrates mentioned above. Similarly, autophagy-targeting chimaera (AUTAC), an emerging technique based on selective autophagy, can recruit molecular targets into autophagosomes via directly binding to autophagic receptors or membrane-bound LC3s[425]. Without the need for post-translational modification of target proteins, AUTAC circumvents the issue of PROTAC which requires an optimal target-ligase orientation to enable efficient substrate ubiquitination mediated by PROTACs[426]. By identifying bona fide autophagy substrates in vivo, we would expand the list of target

molecules including large protein complexes and organelles, further extending their application in the treatment of inflammatory, autoimmune and neurodegenerative diseases.

6.2 Phenotypes of CD4+ T cells from aged individuals

My result showed that both CD4+ T cells from aged mice (which have reduced autophagy levels) and autophagy-deficient CD4+ T cells display an impaired proliferation (Figure 6.1). This might be linked with cellular senescence, a term that refers to the irreversible cell cycle arrest state and recapitulates ageing. However, a marker of cellular senescence (SA-β-Gal activity) was not changed compared to their young counterparts. Combined with the result of the other marker ($p16^{INK4a}$) in a previous report, this type of cellular senescence may not be the driver of CD4+ T cells' defect in cell division during ageing[291,427]. Studies using $p16^{INK4a}$-reporter mouse models indicate that the accumulation of senescent cells show tissue-specificity, where their frequencies are higher in livers and skins than in white adipose tissues, lungs and hearts[427,428]. In the meantime, the numbers of senescent cells within the same tissue differ on a cell-type basis. For instance, liver sinusoid endothelial cells (LSECs) undergo more pronounced cellular senescence than tissue-resident macrophages in livers during ageing[428]. Additionally, factors other than extensive replication may contribute to cellular senescence in vivo. Overexpression of growth differentiation factor (GDF) 11 accelerates liver senescence in aged mice through impairing autophagy and lysosomal biogenesis in an mTORC1-dependent mechanism[429]. Besides, endogenous DNA damage caused by reduced DNA repair capability also leads to acceleration of the normal ageing process with enhanced expression of senescence indices[430]. Though it is widely accepted that senescent cells are detrimental to the healthspan, whether each cell type displays the same combination of markers during senescence, how cellular senescence affects their functions, and what are the inducers, remain largely elusive. By mapping the full repertoire of senescent cells in vivo, we can understand the unique pattern of cellular senescence on a cell-type basis and design effective anti-ageing therapies.

Over the lifetime of an individual, some subsets of lymphocytes are significantly increased in frequency during ageing. For CD8+ T cells, these subpopulations, termed age-associated T cells, are typified by the expression or loss of surface markers linked to terminally differentiated and virtual memory phenotypes, as well as co-stimulatory signalling. It may explain their reduced capacity of proliferation. Since it is not clear whether the CD4+ T cells display a similar accumulation of such subpopulations during ageing, I compared the frequency of CD4+ T cells expressing the age-associated surface markers in old and young mice. Similarly, an expansion of these subtypes was also observed in aged CD4+ T cells, hence may be linked with their impaired proliferation. Although these populations have been associated with immune ageing, it remains largely unknown whether they are signs of maladaptation, or the outcome of an adaptation to compensate for a dysregulated immune system. Taking T_{EMRA} as an example, the cell population displayed low proliferative potential and increased production of pro-inflammatory cytokines that are similar to the SASPs in senescent fibroblasts[431,432]. Therefore, T_{EMRA} cells have been considered 'senescent-like' for a long time. Although this cell population tends to accumulate with age, most of these cells are specific for latent viruses, such as cytomegalovirus (CMV)[433]. Moreover, the observation that aged individuals have a much lower incidence of clinical diseases induced by CMV reactivation in comparison to immunosuppressed patients[434]. The evidence further gives rise to the idea that the senescent-like feature of T_{EMRA} is an adaptive mechanism to constrain the inflation of CMV-specific memory T cells while maintaining their anti-viral function[435]. Based on the information, we need to be cautious to conclude that an age-associated population is 'hazardous' and develop interventions to eliminate them.

The level of mTORC1 signalling, an autophagy suppressor, is frequently enhanced in multiple aged tissues. Contrary to what has been reported in other tissues, mTORC1 signalling was significantly decreased in aged CD4+ T cells, consistent with the reduced global protein translational rate, which

is promoted by mTORC1 activation (Figure 6.1)[436]. Taken together, the age-associated decrease of autophagy in T cells was independent of mTORC1 activation, implying an overall disturbance of the anabolic and catabolic signalling networks. Though some previous studies show that inhibition of mTOR can rejuvenate the aged immune system and improve the antigen-specific responses of T cells, no clear evidence supports it that this is mediated via autophagy[120,437]. Based on my observation that mTORC1 signalling was decreased in aged T cells either before or at the effector phase compared to their young counterpart, I suppose that the improvement of T cell function by mTOR inhibition might be due to its effect during the memory formation stage of T cells, or possibly even on other non-T cell types. To effectively boost autophagy in aged T cells and further improve their cellular homeostasis, some mTOR-independent autophagy inducers, may provide an alternative solution that also evades the multiple side effects of mTOR inhibition, like spermidine[106,228,438]. Considering the very few autophagy inducers available to us, it might be worth performing more small molecule screenings on a large scale to unravel more autophagy modulators, which will be beneficial to the development of novel therapies to treat age-related human diseases[439].

Similar to the effect of the 'senescence-related' populations we discussed above, though many molecular and cellular markers are linked with ageing, it is not possible to easily conclude whether a phenotypic change leads to the dysfunction of the aged cells. Some markers are strategies for 'adaptation' rather than maladaptive changes. The formation of protein aggregates has long been considered pathogenetic in several neurodegenerative diseases, as has the accumulation and propagation of amyloid fibrils in the brains of patients with Alzheimer's disease or Parkinson's disease. But new evidence indicates that soluble oligomers formed at the intermediate states of protein aggregates give rise to toxicity[440]. The size of soluble oligomers ranges from 20 to 60 molecules. Their reactive surface can disrupt lipid membranes and the interactions between macromolecules[441,442]. To counteract the

proteotoxicity of oligomers, large protein deposits (e.g. inclusion bodies) are formed to sequestrate the small aggregates and diluted via cell division[443,444]. But they are prone to accumulate in postmitotic cells, like neurons. One evidence comes from the study that the formation of inclusion bodies correlates with decreased neuronal death in a Huntington's disease model[445]. Similarly, the decreased rate of global protein translation may also be beneficial during ageing. The impaired mitochondrial metabolism during ageing leads to a dramatically decreased energy supply[446]. Reducing overall protein translation can help to allocate the limited energy to more essential physiological pathways. Moreover, diminished protein translation during ageing can relieve the burden on the dysregulated proteostasis network and increase the fidelity of protein translation. Several studies support the beneficial effects in prolonging lifespan in nematodes[447-449]. Therefore, it is necessary to unravel the physiological meaning of each biomarker related to ageing and select targets to develop effective anti-ageing interventions[450].

6.3 Applying knowledge of autophagy in T cells to develop novel therapies

Using the *Lc3b-APEX2* mice, I investigated what is degraded through autophagy in activated CD4+ T cells and how its degradation facilitates T cell proliferation (Figure 6.1). I repeatedly detected IL-7Rα and systemically validated it as an autophagosomal cargo in activated CD4+ T cells. I unravelled the molecular mechanism of how excessive IL-7Rα leads to the impaired proliferation of CD4+ T cells. IL-7R and IL-2R compete for the common gamma chain which has limited availability. Therefore, loss of autophagy leads to decreased IL-2R signalling and impaired assembly of IL-2R at the immunological synapse.

Based on our proof-of-principle study in activated CD4+ T cells, the *Lc3b-APEX2* mouse model can further be used to unravel some novel druggable targets of diseases known to be

caused by aberrant autophagy. For instance, inflammatory bowel disease (IBD) is a chronic inflammatory response of the gastrointestinal tract, which is caused by dysregulated immune responses (such as hyperactivation of Th1 and Th17), defective intestinal barrier and dysbiosis[451]. Mutations in several autophagy-related genes, including *Atg16l1*, *Ulk1*, and genes mediating xenophagy, like immunity-related GTPase family M protein 1 (*Irgm1*) and SMAD-specific E3 ubiquitin protein ligase 1 (*Smurf1*), predispose individuals to the pathogenesis of IBD[452-455]. Indeed, boosting autophagy by pharmacological interventions can ameliorate intestinal inflammation in several animal models mimicking IBD[456,457]. Mechanistically, autophagy may play a protective role by dampening the production of pro-inflammatory cytokines and inducing xenophagy to enhance intestinal barriers[451]. However, it remains elusive whether elevating autophagy levels in the long term is beneficial to all cell types involved in the pathogenesis of IBD without side effects. Therefore, a better strategy is to map the autophagosomal cargoes on a cell-type basis in both health and disease contexts and determine the key molecules required to be removed by autophagy to prevent IBD. Once these candidates are identified, selective removal of these using PROTAC or AUTAC can provide more potent and specific effects[458]. The strategy can be further extended to develop treatments for other diseases linked with autophagy dysfunction, such as neurodegenerative disorders, cancers, cardiovascular diseases and ageing[459].

My finding that IL-7Rα is an autophagic substrate in CD4+ T cells may provide an example for the idea above. Many IBD patients not responding to anti-TNF therapy are typified by the homing and infiltration of IL-7R^{hi} T cells into their guts and colons[383]. Moreover, mice with enhanced IL-7Rα-expression in T cells can spontaneously develop chronic colitis, while blockade of IL-7R signalling with anti-IL-7Rα monoclonal antibodies can reduce the inflammation in vivo, indicating IL-7R is a promising therapeutic target[383,460-462]. However,

based on the experience of cancer therapies, the production, storage and administration of humanised monoclonal antibodies are more complicated and costly than small-molecule agents[463]. To efficiently block IL-7R signalling, the endogenous protein degradation system through PROTAC (UPS-mediated) or AUTAC (autophagy-mediated) could be used to promote the removal of IL-7Rα and further optimise IBD therapy.

6.4 Metabolic aspect of T cell activation

Mitophagy, a form of selective autophagy, is one of the main pathways to remove defective and superfluous mitochondria[464]. Except for maintaining mitochondrial homeostasis, mitophagy also controls cellular metabolism during differentiation. For example, it has been reported that mitophagy promotes glycolysis via suppressing mitochondrial-dependent oxidative phosphorylation during macrophage polarisation towards M1 phenotypes[465]. Similarly, mitophagy may govern T cell activation and proliferation since effector T cells rely on glycolysis. However, unexpectedly we did not identify too many mitochondrial proteins as autophagosomal candidates in activated CD4+ T cells. A previous study shows that unlike resting T cells, whose autophagosomes contain numerous mitochondria, activated T cells preferentially degrade cytosolic material through autophagy and tend to exclude mitochondria from autophagosomes[107]. In line with this, T cell activation is accompanied by mitochondrial biogenesis and remodelling of the proteome, which triggers both the salvage pathway and one-carbon metabolism crucial for T cell proliferation and survival[466]. Taken together, T cells may use other strategies, rather than mitophagy, to modulate metabolism during activation.

Activated T cells undergo a dramatic shift in their proteome, which facilitates their functional and metabolic transition. It is likely that autophagy is required to selectively degrade a spectrum of molecules at different time points to lift the brake on T cell proliferation, which is finely tuned

by multiple signalling pathways. Besides, autophagy is crucial for the regulation of cellular metabolism during CD4+ T cell activation, since autophagy-deficient CD4+ T cells display a defective upregulation of ATP production and altered metabolism[107,467].

In general, the modulatory effects of autophagy on T cell metabolism falls into two categories: (1) provision of energy substrates and (2) regulating key components of related signalling pathways. On the one hand, autophagy can break down macromolecules, such as glycogen, lipids and proteins, into their building blocks to fuel T cell activation[468]. Consistent with this hypothesis, phenotypes of the activated CD4+ T cells lacking autophagy, such as impaired ATP production and IL-2 production, are partially rescued by the supplement of methyl pyruvate, an intermediate of glucose metabolism[107]. The observation implies an essential role of autophagy in mobilising energy stores and taking up nutrients. On the other hand, autophagy initiates anabolic pathways in a transcriptional and posttranslational manner. For instance, deletion of *Vps34* in CD4+ T cells reprograms the expression of genes enriched in metabolic pathways transcriptionally, including glycolysis/gluconeogenesis, biosynthesis of amino acids and cAMP signalling[467]. The altered transcription profile of metabolic genes is probably due to secondary effects of compromised autophagy. Moreover, TAX1BP1-mediated autophagy promotes the generation of L-cysteines, which triggers the mTOR signalling pathway and facilitates the transition to anabolism during TCR-mediated activation[109]. Both examples indicate how autophagy indirectly modulates the cellular metabolism of activated T cells, whereas the principal signalling molecules degraded by autophagy still requires further investigation. To study autophagy's direct effect on T cell metabolism, a transient pharmacological inhibition combined with metabolic analysis, either at bulk or single-cell level, can help to decipher the complicated network.

6.5 Autophagic substrates may, in turn, regulate autophagy level

Using the *Lc3b-APEX2* mouse model, I repeatedly detected several proteins as (potential) autophagic substrates, such as KEAP1 and valosin-containing protein (VCP)/p97 in imMEFs, and IL-7Rα in activated CD4+ T cells (alongside CDKN1B, identified by another study)[102]. These autophagic substrates can in turn have an impact on autophagy levels. Here, I will discuss how these autophagic substrates impact on autophagy levels via the following mechanisms respectively: (1) enhancing the expression of autophagic receptors, (2) stabilising the autophagy initiation machinery, and (3) modulating the upstream signalling.

(1) One example is the KEAP1-NRF2 pathway which offers the cell effective protection against oxidative and electrophilic stresses. As a key component of E3 ubiquitin ligase complex, KEAP1 negatively regulates the signalling via promoting the ubiquitination and proteasome-mediated degradation of NRF2 under basal conditions[469]. However, when facing oxidative stress, KEAP1, which bears multiple cysteine residues as sensors, undergoes inactivation due to an alteration in its redox status. It can also be selectively removed by autophagy when binding to phosphorylated p62/SQSTM1[470]. Therefore, the stabilised transcription factor NRF2 translocates into the nucleus and initiates the antioxidant transcription program. The target genes of KEAP1-NRF2 signalling usually bears antioxidant response elements (AREs) in the promoter regions recognised by NRF2[471]. Interestingly, it has been reported that NDP52/CALCOCO2, an autophagic receptor, contains three AREs in its promoter[472]. Further investigation suggests that KEAP1-NRF2 pathway can enhance the expression of NDP52 and trigger the autophagy-mediated clearance of phosphorylated tau in neurons.

(2) Apart from regulating the expression of autophagy receptors, autophagy substrates may also directly promote the initiation of autophagy. In the mass spectrometry result of proximity labelled imMEFs, I repetitively identified VCP/p97 as a biotinylated protein upregulated by BafA1 treatment, thereby a putative autophagy substrate. VCP is a hexameric ATPase conserved in eukaryotic cells. It can bind to various ubiquitinated proteins and promote their proteasome-mediated degradation via providing a pulling force to unfold these substrates[473]. In addition to its role in UPS-mediated degradation, a recent study indicates that VCP can regulate the autophagosome biogenesis in a Beclin-1-dependent manner[474]. It promotes the de-ubiquitination of Beclin-1, thus, stabilising the protein and initiating the nucleation of the autophagosome. Moreover, VCP facilitates the assembly and activity of PI3K complex I, which is crucial for the recruitment of downstream ubiquitin-like conjugation machinery to the autophagosomal membranes[474]. The VCP-mediated enhance of autophagy and the potential autophagy-mediated degradation of VCP may form a negative feedback loop to maintain the homeostasis of cellular autophagy level.

(3) In line with this, the molecules selectively degraded by autophagy in activated T cells can also influence autophagic flux. Another study found that autophagy-mediated degradation of CDKN1B/p27KIP, a CDK inhibitor, is essential for the proliferation of naïve T cells upon TCR/CD28-stimuli[102]. On the other hand, CDKN1B boosts autophagy via an mTOR-dependent mechanism. During prolonged amino acid starvation, CDKN1B is enriched on the surface of lysosomes and inhibits the mTORC1 signalling pathway through interaction with its regulatory machineries[475]. Similarly, the signalling through IL-7Rα, which we have identified as an autophagosomal cargo in CD4+ T cells, also modulates autophagy positively or negatively depending on the

cellular status. In naïve T cells, IL-7, as well as other common gamma chain family cytokines, induces the PI3K-mTOR signalling pathway which inhibits autophagy induction[476]. However, in activated T cells, the common gamma chain signalling enhances autophagy in an mTOR-independent mechanism, since autophagy levels and mTOR signalling are both highly upregulated[37]. In contrast, during the memory formation stage, the weak mTOR tuned by IL-7R signalling activates autophagy and facilitates the development of memory T cells, while a robust mTORC1 signalling induced by IL-2 favours the generation of effector populations[477]. This context-based effect of common gamma chain cytokines on autophagy needs to be taken into consideration if we want to modulate autophagy levels in disease.

In summary, during my PhD, I investigated the ageing phenotypes of CD4+ T cells and how they are linked to autophagy, I generated and validated a novel mouse model which maps the autophagosomal cargoes in primary cells, and found IL-7Rα as a molecule whose degradation is necessary for the proliferation of CD4+ T cells. This research not only provides proof-of-principle for the application of the *Lc3b-AP2* mouse model but also fills a key gap in our knowledge of CD4+ T cell activation. Moreover, our novel mouse model provides an opportunity to study how autophagy mechanistically contributes to disease in which autophagy plays a key role (e.g. neurodegeneration, cancer, diabetes and ageing). The identification of the autophagic cargo in primary cells will facilitate the understanding of pathogenesis of diseases based on CD4+ T cells and the discovery of drug targets to promote or inhibit CD4+ T cell responses.

Bibliography

1 Macian, F. Autophagy in T Cell Function and Aging. *Front Cell Dev Biol* **7**, 213, doi:10.3389/fcell.2019.00213 (2019).

2 Nakatogawa, H., Suzuki, K., Kamada, Y. & Ohsumi, Y. Dynamics and diversity in autophagy mechanisms: lessons from yeast. *Nat Rev Mol Cell Biol* **10**, 458-467, doi:10.1038/nrm2708 (2009).

3 Kuma, A., Komatsu, M. & Mizushima, N. Autophagy-monitoring and autophagy-deficient mice. *Autophagy* **13**, 1619-1628, doi:10.1080/15548627.2017.1343770 (2017).

4 Nascimbeni, A. C. *et al.* ER-plasma membrane contact sites contribute to autophagosome biogenesis by regulation of local PI3P synthesis. *EMBO J* **36**, 2018-2033, doi:10.15252/embj.201797006 (2017).

5 Hamasaki, M. *et al.* Autophagosomes form at ER-mitochondria contact sites. *Nature* **495**, 389-393, doi:10.1038/nature11910 (2013).

6 Nishimura, T. *et al.* Autophagosome formation is initiated at phosphatidylinositol synthase-enriched ER subdomains. *EMBO J* **36**, 1719-1735, doi:10.15252/embj.201695189 (2017).

7 Shirahama-Noda, K., Kira, S., Yoshimori, T. & Noda, T. TRAPPIII is responsible for vesicular transport from early endosomes to Golgi, facilitating Atg9 cycling in autophagy. *J Cell Sci* **126**, 4963-4973, doi:10.1242/jcs.131318 (2013).

8 Martens, S. & Fracchiolla, D. Activation and targeting of ATG8 protein lipidation. *Cell Discov* **6**, 23, doi:10.1038/s41421-020-0155-1 (2020).

9 Oh, S. H., Choi, Y. B., Kim, J. H., Weihl, C. C. & Ju, J. S. Quantification of autophagy flux using LC3 ELISA. *Anal Biochem* **530**, 57-67, doi:10.1016/j.ab.2017.05.003 (2017).

10 Birgisdottir, A. B., Lamark, T. & Johansen, T. The LIR motif - crucial for selective autophagy. *J Cell Sci* **126**, 3237-3247, doi:10.1242/jcs.126128 (2013).

11 Bjorkoy, G. *et al.* p62/SQSTM1 forms protein aggregates degraded by autophagy and has a protective effect on huntingtin-induced cell death. *J Cell Biol* **171**, 603-614, doi:10.1083/jcb.200507002 (2005).

12 Deosaran, E. *et al.* NBR1 acts as an autophagy receptor for peroxisomes. *J Cell Sci* **126**, 939-952, doi:10.1242/jcs.114819 (2013).

13 Geisler, S. *et al.* PINK1/Parkin-mediated mitophagy is dependent on VDAC1 and p62/SQSTM1. *Nat Cell Biol* **12**, 119-131, doi:10.1038/ncb2012 (2010).

14 Chai, Q. *et al.* A Mycobacterium tuberculosis surface protein recruits ubiquitin to trigger host xenophagy. *Nat Commun* **10**, 1973, doi:10.1038/s41467-019-09955-8 (2019).

15 Kirkin, V. *et al.* A role for NBR1 in autophagosomal degradation of ubiquitinated substrates. *Mol Cell* **33**, 505-516, doi:10.1016/j.molcel.2009.01.020 (2009).

16 Hung, Y. H., Chen, L. M., Yang, J. Y. & Yang, W. Y. Spatiotemporally controlled induction of autophagy-mediated lysosome turnover. *Nat Commun* **4**, 2111, doi:10.1038/ncomms3111 (2013).

17 Lazarou, M. *et al.* The ubiquitin kinase PINK1 recruits autophagy receptors to induce mitophagy. *Nature* **524**, 309-314, doi:10.1038/nature14893 (2015).

18 Wild, P. *et al.* Phosphorylation of the autophagy receptor optineurin restricts Salmonella growth. *Science* **333**, 228-233, doi:10.1126/science.1205405 (2011).

19 Lu, K., Psakhye, I. & Jentsch, S. A new class of ubiquitin-Atg8 receptors involved in selective autophagy and polyQ protein clearance. *Autophagy* **10**, 2381-2382, doi:10.4161/15548627.2014.981919 (2014).
20 Tumbarello, D. A. *et al.* The Autophagy Receptor TAX1BP1 and the Molecular Motor Myosin VI Are Required for Clearance of Salmonella Typhimurium by Autophagy. *PLoS Pathog* **11**, e1005174, doi:10.1371/journal.ppat.1005174 (2015).
21 Sarraf, S. A. *et al.* Loss of TAX1BP1-Directed Autophagy Results in Protein Aggregate Accumulation in the Brain. *Mol Cell* **80**, 779-795 e710, doi:10.1016/j.molcel.2020.10.041 (2020).
22 Carling, D., Mayer, F. V., Sanders, M. J. & Gamblin, S. J. AMP-activated protein kinase: nature's energy sensor. *Nat Chem Biol* **7**, 512-518, doi:10.1038/nchembio.610 (2011).
23 Egan, D. F. *et al.* Phosphorylation of ULK1 (hATG1) by AMP-activated protein kinase connects energy sensing to mitophagy. *Science* **331**, 456-461, doi:10.1126/science.1196371 (2011).
24 Kim, J. *et al.* Differential regulation of distinct Vps34 complexes by AMPK in nutrient stress and autophagy. *Cell* **152**, 290-303, doi:10.1016/j.cell.2012.12.016 (2013).
25 Inoki, K., Zhu, T. & Guan, K. L. TSC2 mediates cellular energy response to control cell growth and survival. *Cell* **115**, 577-590, doi:10.1016/s0092-8674(03)00929-2 (2003).
26 Zoncu, R. *et al.* mTORC1 senses lysosomal amino acids through an inside-out mechanism that requires the vacuolar H(+)-ATPase. *Science* **334**, 678-683, doi:10.1126/science.1207056 (2011).
27 Thoreen, C. C. *et al.* A unifying model for mTORC1-mediated regulation of mRNA translation. *Nature* **485**, 109-113, doi:10.1038/nature11083 (2012).
28 Dibble, C. C. & Cantley, L. C. Regulation of mTORC1 by PI3K signaling. *Trends Cell Biol* **25**, 545-555, doi:10.1016/j.tcb.2015.06.002 (2015).
29 Ben-Sahra, I., Howell, J. J., Asara, J. M. & Manning, B. D. Stimulation of de novo pyrimidine synthesis by growth signaling through mTOR and S6K1. *Science* **339**, 1323-1328, doi:10.1126/science.1228792 (2013).
30 Ben-Sahra, I., Hoxhaj, G., Ricoult, S. J. H., Asara, J. M. & Manning, B. D. mTORC1 induces purine synthesis through control of the mitochondrial tetrahydrofolate cycle. *Science* **351**, 728-733, doi:10.1126/science.aad0489 (2016).
31 Duvel, K. *et al.* Activation of a metabolic gene regulatory network downstream of mTOR complex 1. *Mol Cell* **39**, 171-183, doi:10.1016/j.molcel.2010.06.022 (2010).
32 Peterson, T. R. *et al.* mTOR complex 1 regulates lipin 1 localization to control the SREBP pathway. *Cell* **146**, 408-420, doi:10.1016/j.cell.2011.06.034 (2011).
33 Kim, J., Kundu, M., Viollet, B. & Guan, K. L. AMPK and mTOR regulate autophagy through direct phosphorylation of Ulk1. *Nat Cell Biol* **13**, 132-141, doi:10.1038/ncb2152 (2011).
34 Jung, C. H. *et al.* ULK-Atg13-FIP200 complexes mediate mTOR signaling to the autophagy machinery. *Mol Biol Cell* **20**, 1992-2003, doi:10.1091/mbc.E08-12-1249 (2009).
35 Napolitano, G. *et al.* mTOR-dependent phosphorylation controls TFEB nuclear export. *Nat Commun* **9**, 3312, doi:10.1038/s41467-018-05862-6 (2018).
36 Dowling, S. D. & Macian, F. Autophagy and T cell metabolism. *Cancer Lett* **419**, 20-26, doi:10.1016/j.canlet.2018.01.033 (2018).

37 Botbol, Y., Patel, B. & Macian, F. Common gamma-chain cytokine signaling is required for macroautophagy induction during CD4+ T-cell activation. *Autophagy* **11**, 1864-1877, doi:10.1080/15548627.2015.1089374 (2015).
38 Sahu, R. *et al.* Microautophagy of cytosolic proteins by late endosomes. *Dev Cell* **20**, 131-139, doi:10.1016/j.devcel.2010.12.003 (2011).
39 Lee, C., Lamech, L., Johns, E. & Overholtzer, M. Selective Lysosome Membrane Turnover Is Induced by Nutrient Starvation. *Dev Cell* **55**, 289-297 e284, doi:10.1016/j.devcel.2020.08.008 (2020).
40 Krick, R. *et al.* Piecemeal microautophagy of the nucleus requires the core macroautophagy genes. *Mol Biol Cell* **19**, 4492-4505, doi:10.1091/mbc.E08-04-0363 (2008).
41 Seo, A. Y. *et al.* AMPK and vacuole-associated Atg14p orchestrate mu-lipophagy for energy production and long-term survival under glucose starvation. *Elife* **6**, doi:10.7554/eLife.21690 (2017).
42 Uytterhoeven, V. *et al.* Hsc70-4 Deforms Membranes to Promote Synaptic Protein Turnover by Endosomal Microautophagy. *Neuron* **88**, 735-748, doi:10.1016/j.neuron.2015.10.012 (2015).
43 Mukherjee, A., Patel, B., Koga, H., Cuervo, A. M. & Jenny, A. Selective endosomal microautophagy is starvation-inducible in Drosophila. *Autophagy* **12**, 1984-1999, doi:10.1080/15548627.2016.1208887 (2016).
44 Caballero, B. *et al.* Interplay of pathogenic forms of human tau with different autophagic pathways. *Aging Cell* **17**, doi:10.1111/acel.12692 (2018).
45 Zellner, S., Schifferer, M. & Behrends, C. Systematically defining selective autophagy receptor-specific cargo using autophagosome content profiling. *Mol Cell* **81**, 1337-1354 e1338, doi:10.1016/j.molcel.2021.01.009 (2021).
46 Tekirdag, K. & Cuervo, A. M. Chaperone-mediated autophagy and endosomal microautophagy: Joint by a chaperone. *J Biol Chem* **293**, 5414-5424, doi:10.1074/jbc.R117.818237 (2018).
47 Kaushik, S. & Cuervo, A. M. The coming of age of chaperone-mediated autophagy. *Nat Rev Mol Cell Biol* **19**, 365-381, doi:10.1038/s41580-018-0001-6 (2018).
48 Pellicci, D. G., Koay, H. F. & Berzins, S. P. Thymic development of unconventional T cells: how NKT cells, MAIT cells and gammadelta T cells emerge. *Nat Rev Immunol* **20**, 756-770, doi:10.1038/s41577-020-0345-y (2020).
49 Sckisel, G. D. *et al.* Out-of-Sequence Signal 3 Paralyzes Primary CD4(+) T-Cell-Dependent Immunity. *Immunity* **43**, 240-250, doi:10.1016/j.immuni.2015.06.023 (2015).
50 Kim, S. T. *et al.* TCR Mechanobiology: Torques and Tunable Structures Linked to Early T Cell Signaling. *Front Immunol* **3**, 76, doi:10.3389/fimmu.2012.00076 (2012).
51 Liu, B., Chen, W., Evavold, B. D. & Zhu, C. Accumulation of dynamic catch bonds between TCR and agonist peptide-MHC triggers T cell signaling. *Cell* **157**, 357-368, doi:10.1016/j.cell.2014.02.053 (2014).
52 Wang, J. H. & Reinherz, E. L. The structural basis of alphabeta T-lineage immune recognition: TCR docking topologies, mechanotransduction, and co-receptor function. *Immunol Rev* **250**, 102-119, doi:10.1111/j.1600-065X.2012.01161.x (2012).
53 Xu, C. *et al.* Regulation of T cell receptor activation by dynamic membrane binding of the CD3epsilon cytoplasmic tyrosine-based motif. *Cell* **135**, 702-713, doi:10.1016/j.cell.2008.09.044 (2008).
54 Rossjohn, J. *et al.* T cell antigen receptor recognition of antigen-presenting molecules. *Annu Rev Immunol* **33**, 169-200, doi:10.1146/annurev-immunol-032414-112334 (2015).

55 Artyomov, M. N., Lis, M., Devadas, S., Davis, M. M. & Chakraborty, A. K. CD4 and CD8 binding to MHC molecules primarily acts to enhance Lck delivery. *Proc Natl Acad Sci U S A* **107**, 16916-16921, doi:10.1073/pnas.1010568107 (2010).
56 Jain, J., Loh, C. & Rao, A. Transcriptional regulation of the IL-2 gene. *Curr Opin Immunol* **7**, 333-342, doi:10.1016/0952-7915(95)80107-3 (1995).
57 Castellanos, M. C. *et al.* Expression of the leukocyte early activation antigen CD69 is regulated by the transcription factor AP-1. *J Immunol* **159**, 5463-5473 (1997).
58 Macian, F. NFAT proteins: key regulators of T-cell development and function. *Nat Rev Immunol* **5**, 472-484, doi:10.1038/nri1632 (2005).
59 June, C. H., Ledbetter, J. A., Gillespie, M. M., Lindsten, T. & Thompson, C. B. T-cell proliferation involving the CD28 pathway is associated with cyclosporine-resistant interleukin 2 gene expression. *Mol Cell Biol* **7**, 4472-4481, doi:10.1128/mcb.7.12.4472-4481.1987 (1987).
60 Boomer, J. S. & Green, J. M. An enigmatic tail of CD28 signaling. *Cold Spring Harb Perspect Biol* **2**, a002436, doi:10.1101/cshperspect.a002436 (2010).
61 Chen, C. Y. *et al.* Nucleolin and YB-1 are required for JNK-mediated interleukin-2 mRNA stabilization during T-cell activation. *Genes Dev* **14**, 1236-1248 (2000).
62 Seko, Y., Azmi, H., Fariss, R. & Ragheb, J. A. Selective cytoplasmic translocation of HuR and site-specific binding to the interleukin-2 mRNA are not sufficient for CD28-mediated stabilization of the mRNA. *J Biol Chem* **279**, 33359-33367, doi:10.1074/jbc.M312306200 (2004).
63 Shahinian, A. *et al.* Differential T cell costimulatory requirements in CD28-deficient mice. *Science* **261**, 609-612, doi:10.1126/science.7688139 (1993).
64 Denoeud, J. & Moser, M. Role of CD27/CD70 pathway of activation in immunity and tolerance. *J Leukoc Biol* **89**, 195-203, doi:10.1189/jlb.0610351 (2011).
65 Linterman, M. A. *et al.* Roquin differentiates the specialized functions of duplicated T cell costimulatory receptor genes CD28 and ICOS. *Immunity* **30**, 228-241, doi:10.1016/j.immuni.2008.12.015 (2009).
66 Macian, F., Im, S. H., Garcia-Cozar, F. J. & Rao, A. T-cell anergy. *Curr Opin Immunol* **16**, 209-216, doi:10.1016/j.coi.2004.01.013 (2004).
67 Morgan, D. A., Ruscetti, F. W. & Gallo, R. Selective in vitro growth of T lymphocytes from normal human bone marrows. *Science* **193**, 1007-1008, doi:10.1126/science.181845 (1976).
68 Meuer, S. C. *et al.* Triggering of the T3-Ti antigen-receptor complex results in clonal T-cell proliferation through an interleukin 2-dependent autocrine pathway. *Proc Natl Acad Sci U S A* **81**, 1509-1513, doi:10.1073/pnas.81.5.1509 (1984).
69 Liao, W., Lin, J. X. & Leonard, W. J. IL-2 family cytokines: new insights into the complex roles of IL-2 as a broad regulator of T helper cell differentiation. *Curr Opin Immunol* **23**, 598-604, doi:10.1016/j.coi.2011.08.003 (2011).
70 Li, C. & Park, J. H. Assessing IL-2-Induced STAT5 Phosphorylation in Fixed, Permeabilized Foxp3(+) Treg Cells by Multiparameter Flow Cytometry. *STAR Protoc* **1**, 100195, doi:10.1016/j.xpro.2020.100195 (2020).
71 Ross, S. H. & Cantrell, D. A. Signaling and Function of Interleukin-2 in T Lymphocytes. *Annu Rev Immunol* **36**, 411-433, doi:10.1146/annurev-immunol-042617-053352 (2018).
72 Villarino, A. *et al.* Signal transducer and activator of transcription 5 (STAT5) paralog dose governs T cell effector and regulatory functions. *Elife* **5**, doi:10.7554/eLife.08384 (2016).

73 Moriggl, R. *et al.* Stat5 is required for IL-2-induced cell cycle progression of peripheral T cells. *Immunity* **10**, 249-259, doi:10.1016/s1074-7613(00)80025-4 (1999).
74 Liao, W. *et al.* Priming for T helper type 2 differentiation by interleukin 2-mediated induction of interleukin 4 receptor alpha-chain expression. *Nat Immunol* **9**, 1288-1296, doi:10.1038/ni.1656 (2008).
75 Kanai, T. *et al.* Identification of STAT5A and STAT5B target genes in human T cells. *PLoS One* **9**, e86790, doi:10.1371/journal.pone.0086790 (2014).
76 Leung, D. T., Morefield, S. & Willerford, D. M. Regulation of lymphoid homeostasis by IL-2 receptor signals in vivo. *J Immunol* **164**, 3527-3534, doi:10.4049/jimmunol.164.7.3527 (2000).
77 Dooms, H., Wolslegel, K., Lin, P. & Abbas, A. K. Interleukin-2 enhances CD4+ T cell memory by promoting the generation of IL-7R alpha-expressing cells. *J Exp Med* **204**, 547-557, doi:10.1084/jem.20062381 (2007).
78 D'Souza, W. N., Schluns, K. S., Masopust, D. & Lefrancois, L. Essential role for IL-2 in the regulation of antiviral extralymphoid CD8 T cell responses. *J Immunol* **168**, 5566-5572, doi:10.4049/jimmunol.168.11.5566 (2002).
79 D'Souza, W. N. & Lefrancois, L. IL-2 is not required for the initiation of CD8 T cell cycling but sustains expansion. *J Immunol* **171**, 5727-5735, doi:10.4049/jimmunol.171.11.5727 (2003).
80 Carr, J. M. *et al.* CD27 mediates interleukin-2-independent clonal expansion of the CD8+ T cell without effector differentiation. *Proc Natl Acad Sci U S A* **103**, 19454-19459, doi:10.1073/pnas.0609706104 (2006).
81 Lenardo, M. J. Interleukin-2 programs mouse alpha beta T lymphocytes for apoptosis. *Nature* **353**, 858-861, doi:10.1038/353858a0 (1991).
82 Dustin, M. L. & Choudhuri, K. Signaling and Polarized Communication Across the T Cell Immunological Synapse. *Annu Rev Cell Dev Biol* **32**, 303-325, doi:10.1146/annurev-cellbio-100814-125330 (2016).
83 Bachmann, M. F. *et al.* Distinct roles for LFA-1 and CD28 during activation of naive T cells: adhesion versus costimulation. *Immunity* **7**, 549-557, doi:10.1016/s1074-7613(00)80376-3 (1997).
84 Dustin, M. L. & Springer, T. A. T-cell receptor cross-linking transiently stimulates adhesiveness through LFA-1. *Nature* **341**, 619-624, doi:10.1038/341619a0 (1989).
85 Irvine, D. J., Purbhoo, M. A., Krogsgaard, M. & Davis, M. M. Direct observation of ligand recognition by T cells. *Nature* **419**, 845-849, doi:10.1038/nature01076 (2002).
86 Kupfer, A. & Singer, S. J. The specific interaction of helper T cells and antigen-presenting B cells. IV. Membrane and cytoskeletal reorganizations in the bound T cell as a function of antigen dose. *J Exp Med* **170**, 1697-1713, doi:10.1084/jem.170.5.1697 (1989).
87 Huse, M., Lillemeier, B. F., Kuhns, M. S., Chen, D. S. & Davis, M. M. T cells use two directionally distinct pathways for cytokine secretion. *Nat Immunol* **7**, 247-255, doi:10.1038/ni1304 (2006).
88 Poo, W. J., Conrad, L. & Janeway, C. A., Jr. Receptor-directed focusing of lymphokine release by helper T cells. *Nature* **332**, 378-380, doi:10.1038/332378a0 (1988).
89 Sabatos, C. A. *et al.* A synaptic basis for paracrine interleukin-2 signaling during homotypic T cell interaction. *Immunity* **29**, 238-248, doi:10.1016/j.immuni.2008.05.017 (2008).

90 Dustin, M. L. *et al.* A novel adaptor protein orchestrates receptor patterning and cytoskeletal polarity in T-cell contacts. *Cell* **94**, 667-677, doi:10.1016/s0092-8674(00)81608-6 (1998).
91 Grakoui, A. *et al.* The immunological synapse: a molecular machine controlling T cell activation. *Science* **285**, 221-227, doi:10.1126/science.285.5425.221 (1999).
92 Lee, J. *et al.* The Multifaceted Role of Th1, Th9, and Th17 Cells in Immune Checkpoint Inhibition Therapy. *Front Immunol* **12**, 625667, doi:10.3389/fimmu.2021.625667 (2021).
93 Saravia, J., Chapman, N. M. & Chi, H. Helper T cell differentiation. *Cell Mol Immunol* **16**, 634-643, doi:10.1038/s41423-019-0220-6 (2019).
94 Clarke, A. J. & Simon, A. K. Autophagy in the renewal, differentiation and homeostasis of immune cells. *Nat Rev Immunol* **19**, 170-183, doi:10.1038/s41577-018-0095-2 (2019).
95 Valdor, R. & Macian, F. Autophagy and the regulation of the immune response. *Pharmacol Res* **66**, 475-483, doi:10.1016/j.phrs.2012.10.003 (2012).
96 Valdor, R. *et al.* Chaperone-mediated autophagy regulates T cell responses through targeted degradation of negative regulators of T cell activation. *Nat Immunol* **15**, 1046-1054, doi:10.1038/ni.3003 (2014).
97 Jia, W. & He, Y. W. Temporal regulation of intracellular organelle homeostasis in T lymphocytes by autophagy. *J Immunol* **186**, 5313-5322, doi:10.4049/jimmunol.1002404 (2011).
98 Pua, H. H. & He, Y. W. Maintaining T lymphocyte homeostasis: another duty of autophagy. *Autophagy* **3**, 266-267, doi:10.4161/auto.3908 (2007).
99 Pua, H. H. & He, Y. W. Mitophagy in the little lymphocytes: an essential role for autophagy in mitochondrial clearance in T lymphocytes. *Autophagy* **5**, 745-746, doi:10.4161/auto.5.5.8702 (2009).
100 Kovacs, J. R. *et al.* Autophagy promotes T-cell survival through degradation of proteins of the cell death machinery. *Cell Death Differ* **19**, 144-152, doi:10.1038/cdd.2011.78 (2012).
101 Parekh, V. V. *et al.* Impaired autophagy, defective T cell homeostasis, and a wasting syndrome in mice with a T cell-specific deletion of Vps34. *J Immunol* **190**, 5086-5101, doi:10.4049/jimmunol.1202071 (2013).
102 Jia, W. *et al.* Autophagy regulates T lymphocyte proliferation through selective degradation of the cell-cycle inhibitor CDKN1B/p27Kip1. *Autophagy* **11**, 2335-2345, doi:10.1080/15548627.2015.1110666 (2015).
103 Willinger, T. & Flavell, R. A. Canonical autophagy dependent on the class III phosphoinositide-3 kinase Vps34 is required for naive T-cell homeostasis. *Proc Natl Acad Sci U S A* **109**, 8670-8675, doi:10.1073/pnas.1205305109 (2012).
104 Jia, W., Pua, H. H., Li, Q. J. & He, Y. W. Autophagy regulates endoplasmic reticulum homeostasis and calcium mobilization in T lymphocytes. *J Immunol* **186**, 1564-1574, doi:10.4049/jimmunol.1001822 (2011).
105 Pua, H. H., Dzhagalov, I., Chuck, M., Mizushima, N. & He, Y. W. A critical role for the autophagy gene Atg5 in T cell survival and proliferation. *J Exp Med* **204**, 25-31, doi:10.1084/jem.20061303 (2007).
106 Puleston, D. J. *et al.* Autophagy is a critical regulator of memory CD8(+) T cell formation. *Elife* **3**, doi:10.7554/eLife.03706 (2014).
107 Hubbard, V. M. *et al.* Macroautophagy regulates energy metabolism during effector T cell activation. *J Immunol* **185**, 7349-7357, doi:10.4049/jimmunol.1000576 (2010).
108 Yuan, H. X., Xiong, Y. & Guan, K. L. Nutrient sensing, metabolism, and cell growth control. *Mol Cell* **49**, 379-387, doi:10.1016/j.molcel.2013.01.019 (2013).

109 Whang, M. I. *et al.* The Ubiquitin Binding Protein TAX1BP1 Mediates Autophagasome Induction and the Metabolic Transition of Activated T Cells. *Immunity* **46**, 405-420, doi:10.1016/j.immuni.2017.02.018 (2017).
110 Besson, A., Dowdy, S. F. & Roberts, J. M. CDK inhibitors: cell cycle regulators and beyond. *Dev Cell* **14**, 159-169, doi:10.1016/j.devcel.2008.01.013 (2008).
111 Wiede, F. *et al.* T cell protein tyrosine phosphatase attenuates T cell signaling to maintain tolerance in mice. *J Clin Invest* **121**, 4758-4774, doi:10.1172/JCI59492 (2011).
112 Medgyesi, D. *et al.* The protein tyrosine phosphatase PTP1B is a negative regulator of CD40 and BAFF-R signaling and controls B cell autoimmunity. *J Exp Med* **211**, 427-440, doi:10.1084/jem.20131196 (2014).
113 Macian, F. *et al.* Transcriptional mechanisms underlying lymphocyte tolerance. *Cell* **109**, 719-731, doi:10.1016/s0092-8674(02)00767-5 (2002).
114 Mocholi, E. *et al.* Autophagy Is a Tolerance-Avoidance Mechanism that Modulates TCR-Mediated Signaling and Cell Metabolism to Prevent Induction of T Cell Anergy. *Cell Rep* **24**, 1136-1150, doi:10.1016/j.celrep.2018.06.065 (2018).
115 Kabat, A. M. *et al.* The autophagy gene Atg16l1 differentially regulates Treg and TH2 cells to control intestinal inflammation. *Elife* **5**, e12444, doi:10.7554/eLife.12444 (2016).
116 Wei, J. *et al.* Autophagy enforces functional integrity of regulatory T cells by coupling environmental cues and metabolic homeostasis. *Nat Immunol* **17**, 277-285, doi:10.1038/ni.3365 (2016).
117 Amersfoort, J. *et al.* Defective Autophagy in T Cells Impairs the Development of Diet-Induced Hepatic Steatosis and Atherosclerosis. *Front Immunol* **9**, 2937, doi:10.3389/fimmu.2018.02937 (2018).
118 Rivera Vargas, T. *et al.* Selective degradation of PU.1 during autophagy represses the differentiation and antitumour activity of TH9 cells. *Nat Commun* **8**, 559, doi:10.1038/s41467-017-00468-w (2017).
119 Murera, D. *et al.* CD4 T cell autophagy is integral to memory maintenance. *Sci Rep* **8**, 5951, doi:10.1038/s41598-018-23993-0 (2018).
120 Xu, X. *et al.* Autophagy is essential for effector CD8(+) T cell survival and memory formation. *Nat Immunol* **15**, 1152-1161, doi:10.1038/ni.3025 (2014).
121 Chen, M. *et al.* Essential role for autophagy in the maintenance of immunological memory against influenza infection. *Nat Med* **20**, 503-510, doi:10.1038/nm.3521 (2014).
122 Keller, C. W. *et al.* The autophagy machinery restrains iNKT cell activation through CD1D1 internalization. *Autophagy* **13**, 1025-1036, doi:10.1080/15548627.2017.1297907 (2017).
123 Choudhuri, K. *et al.* Polarized release of T-cell-receptor-enriched microvesicles at the immunological synapse. *Nature* **507**, 118-123, doi:10.1038/nature12951 (2014).
124 Feng, Y., He, D., Yao, Z. & Klionsky, D. J. The machinery of macroautophagy. *Cell Res* **24**, 24-41, doi:10.1038/cr.2013.168 (2014).
125 Kim, D. I. *et al.* Probing nuclear pore complex architecture with proximity-dependent biotinylation. *Proc Natl Acad Sci U S A* **111**, E2453-2461, doi:10.1073/pnas.1406459111 (2014).
126 Levine, B. & Kroemer, G. Biological Functions of Autophagy Genes: A Disease Perspective. *Cell* **176**, 11-42, doi:10.1016/j.cell.2018.09.048 (2019).
127 Gatica, D., Lahiri, V. & Klionsky, D. J. Cargo recognition and degradation by selective autophagy. *Nat Cell Biol* **20**, 233-242, doi:10.1038/s41556-018-0037-z (2018).

128 Martins, W. K. *et al.* Autophagy Regulation and Photodynamic Therapy: Insights to Improve Outcomes of Cancer Treatment. *Front Oncol* **10**, 610472, doi:10.3389/fonc.2020.610472 (2020).
129 Rubinsztein, D. C., Codogno, P. & Levine, B. Autophagy modulation as a potential therapeutic target for diverse diseases. *Nat Rev Drug Discov* **11**, 709-730, doi:10.1038/nrd3802 (2012).
130 Mizushima, N. & Levine, B. Autophagy in Human Diseases. *N Engl J Med* **383**, 1564-1576, doi:10.1056/NEJMra2022774 (2020).
131 La Belle Flynn, A. *et al.* Autophagy inhibition elicits emergence from metastatic dormancy by inducing and stabilizing Pfkfb3 expression. *Nat Commun* **10**, 3668, doi:10.1038/s41467-019-11640-9 (2019).
132 Alabi, S. B. & Crews, C. M. Major advances in targeted protein degradation: PROTACs, LYTACs, and MADTACs. *J Biol Chem* **296**, 100647, doi:10.1016/j.jbc.2021.100647 (2021).
133 Mathew, R. *et al.* Functional role of autophagy-mediated proteome remodeling in cell survival signaling and innate immunity. *Mol Cell* **55**, 916-930, doi:10.1016/j.molcel.2014.07.019 (2014).
134 Fellinger, E. & Rez, G. Isolation of pancreatic autophagic vacuoles induced by vinblastine or neutral red. Separation of autophagosomes and autolysosomes by Percoll density gradient centrifugation. *Eur J Cell Biol* **51**, 220-228 (1990).
135 Stromhaug, P. E., Berg, T. O., Fengsrud, M. & Seglen, P. O. Purification and characterization of autophagosomes from rat hepatocytes. *Biochem J* **335 (Pt 2)**, 217-224, doi:10.1042/bj3350217 (1998).
136 Bruckner, A., Polge, C., Lentze, N., Auerbach, D. & Schlattner, U. Yeast two-hybrid, a powerful tool for systems biology. *Int J Mol Sci* **10**, 2763-2788, doi:10.3390/ijms10062763 (2009).
137 Dunham, W. H., Mullin, M. & Gingras, A. C. Affinity-purification coupled to mass spectrometry: basic principles and strategies. *Proteomics* **12**, 1576-1590, doi:10.1002/pmic.201100523 (2012).
138 Qin, W., Cho, K. F., Cavanagh, P. E. & Ting, A. Y. Deciphering molecular interactions by proximity labeling. *Nat Methods* **18**, 133-143, doi:10.1038/s41592-020-01010-5 (2021).
139 Martell, J. D. *et al.* Engineered ascorbate peroxidase as a genetically encoded reporter for electron microscopy. *Nat Biotechnol* **30**, 1143-1148, doi:10.1038/nbt.2375 (2012).
140 Rhee, H. W. *et al.* Proteomic mapping of mitochondria in living cells via spatially restricted enzymatic tagging. *Science* **339**, 1328-1331, doi:10.1126/science.1230593 (2013).
141 Branon, T. C. *et al.* Efficient proximity labeling in living cells and organisms with TurboID. *Nat Biotechnol* **36**, 880-887, doi:10.1038/nbt.4201 (2018).
142 Chou, C. C. *et al.* TDP-43 pathology disrupts nuclear pore complexes and nucleocytoplasmic transport in ALS/FTD. *Nat Neurosci* **21**, 228-239, doi:10.1038/s41593-017-0047-3 (2018).
143 Birendra, K. *et al.* VRK2A is an A-type lamin-dependent nuclear envelope kinase that phosphorylates BAF. *Mol Biol Cell* **28**, 2241-2250, doi:10.1091/mbc.E17-03-0138 (2017).
144 Fu, Y. *et al.* MacroH2A1 associates with nuclear lamina and maintains chromatin architecture in mouse liver cells. *Sci Rep* **5**, 17186, doi:10.1038/srep17186 (2015).
145 Mackmull, M. T. *et al.* Landscape of nuclear transport receptor cargo specificity. *Mol Syst Biol* **13**, 962, doi:10.15252/msb.20177608 (2017).

146 Le Guerroue, F. *et al.* Autophagosomal Content Profiling Reveals an LC3C-Dependent Piecemeal Mitophagy Pathway. *Mol Cell* **68**, 786-796 e786, doi:10.1016/j.molcel.2017.10.029 (2017).
147 Mancias, J. D., Wang, X., Gygi, S. P., Harper, J. W. & Kimmelman, A. C. Quantitative proteomics identifies NCOA4 as the cargo receptor mediating ferritinophagy. *Nature* **509**, 105-109, doi:10.1038/nature13148 (2014).
148 Gao, W. *et al.* Biochemical isolation and characterization of the tubulovesicular LC3-positive autophagosomal compartment. *J Biol Chem* **285**, 1371-1383, doi:10.1074/jbc.M109.054197 (2010).
149 Dengjel, J. *et al.* Identification of autophagosome-associated proteins and regulators by quantitative proteomic analysis and genetic screens. *Mol Cell Proteomics* **11**, M111 014035, doi:10.1074/mcp.M111.014035 (2012).
150 Agrotis, A. *et al.* Human ATG4 autophagy proteases counteract attachment of ubiquitin-like LC3/GABARAP proteins to other cellular proteins. *J Biol Chem* **294**, 12610-12621, doi:10.1074/jbc.AC119.009977 (2019).
151 Hung, V. *et al.* Spatially resolved proteomic mapping in living cells with the engineered peroxidase APEX2. *Nat Protoc* **11**, 456-475, doi:10.1038/nprot.2016.018 (2016).
152 Mizushima, N. & Yoshimori, T. How to interpret LC3 immunoblotting. *Autophagy* **3**, 542-545, doi:10.4161/auto.4600 (2007).
153 Xu, Y. *et al.* Toll-like receptor 4 is a sensor for autophagy associated with innate immunity. *Immunity* **27**, 135-144, doi:10.1016/j.immuni.2007.05.022 (2007).
154 Chandler, C. S. & Ballard, F. J. Multiple biotin-containing proteins in 3T3-L1 cells. *Biochem J* **237**, 123-130, doi:10.1042/bj2370123 (1986).
155 Durkin, M. E., Qian, X., Popescu, N. C. & Lowy, D. R. Isolation of Mouse Embryo Fibroblasts. *Bio Protoc* **3**, doi:10.21769/bioprotoc.908 (2013).
156 Mann, S. S. & Hammarback, J. A. Molecular characterization of light chain 3. A microtubule binding subunit of MAP1A and MAP1B. *J Biol Chem* **269**, 11492-11497 (1994).
157 Zhang, X. *et al.* GRASP55 Senses Glucose Deprivation through O-GlcNAcylation to Promote Autophagosome-Lysosome Fusion. *Dev Cell* **45**, 245-261 e246, doi:10.1016/j.devcel.2018.03.023 (2018).
158 Goeminne, L. J., Gevaert, K. & Clement, L. Peptide-level Robust Ridge Regression Improves Estimation, Sensitivity, and Specificity in Data-dependent Quantitative Label-free Shotgun Proteomics. *Mol Cell Proteomics* **15**, 657-668, doi:10.1074/mcp.M115.055897 (2016).
159 Jin, L. *et al.* A comparative study of evaluating missing value imputation methods in label-free proteomics. *Sci Rep* **11**, 1760, doi:10.1038/s41598-021-81279-4 (2021).
160 Stefely, J. A. *et al.* Mass spectrometry proteomics reveals a function for mammalian CALCOCO1 in MTOR-regulated selective autophagy. *Autophagy* **16**, 2219-2237, doi:10.1080/15548627.2020.1719746 (2020).
161 Taguchi, K. *et al.* Keap1 degradation by autophagy for the maintenance of redox homeostasis. *Proc Natl Acad Sci U S A* **109**, 13561-13566, doi:10.1073/pnas.1121572109 (2012).
162 Hou, W. *et al.* Autophagy promotes ferroptosis by degradation of ferritin. *Autophagy* **12**, 1425-1428, doi:10.1080/15548627.2016.1187366 (2016).
163 Herhaus, L. *et al.* TBK1-mediated phosphorylation of LC3C and GABARAP-L2 controls autophagosome shedding by ATG4 protease. *EMBO Rep* **21**, e48317, doi:10.15252/embr.201948317 (2020).

164 Mavrakis, M., Lippincott-Schwartz, J., Stratakis, C. A. & Bossis, I. mTOR kinase and the regulatory subunit of protein kinase A (PRKAR1A) spatially and functionally interact during autophagosome maturation. *Autophagy* **3**, 151-153, doi:10.4161/auto.3632 (2007).
165 Falcon, B., Noad, J., McMahon, H., Randow, F. & Goedert, M. Galectin-8-mediated selective autophagy protects against seeded tau aggregation. *J Biol Chem* **293**, 2438-2451, doi:10.1074/jbc.M117.809293 (2018).
166 Jia, J. *et al.* Galectins Control mTOR in Response to Endomembrane Damage. *Mol Cell* **70**, 120-135 e128, doi:10.1016/j.molcel.2018.03.009 (2018).
167 Yamano, K., Fogel, A. I., Wang, C., van der Bliek, A. M. & Youle, R. J. Mitochondrial Rab GAPs govern autophagosome biogenesis during mitophagy. *Elife* **3**, e01612, doi:10.7554/eLife.01612 (2014).
168 Sun, A. *et al.* The E3 ubiquitin ligase NEDD4 is an LC3-interactive protein and regulates autophagy. *Autophagy* **13**, 522-537, doi:10.1080/15548627.2016.1268301 (2017).
169 Papadopoulos, C. *et al.* VCP/p97 cooperates with YOD1, UBXD1 and PLAA to drive clearance of ruptured lysosomes by autophagy. *EMBO J* **36**, 135-150, doi:10.15252/embj.201695148 (2017).
170 Corvera, S. & Capocasale, R. J. Enhanced phosphorylation of a coated vesicle polypeptide in response to insulin stimulation of rat adipocytes. *J Biol Chem* **265**, 15963-15969 (1990).
171 Lapuente-Brun, E. *et al.* Supercomplex assembly determines electron flux in the mitochondrial electron transport chain. *Science* **340**, 1567-1570, doi:10.1126/science.1230381 (2013).
172 Deng, Y. *et al.* Rab18 binds PLIN2 and ACSL3 to mediate lipid droplet dynamics. *Biochim Biophys Acta Mol Cell Biol Lipids* **1866**, 158923, doi:10.1016/j.bbalip.2021.158923 (2021).
173 Falguieres, T., Castle, D. & Gruenberg, J. Regulation of the MVB pathway by SCAMP3. *Traffic* **13**, 131-142, doi:10.1111/j.1600-0854.2011.01291.x (2012).
174 Sun, Q., Westphal, W., Wong, K. N., Tan, I. & Zhong, Q. Rubicon controls endosome maturation as a Rab7 effector. *Proc Natl Acad Sci U S A* **107**, 19338-19343, doi:10.1073/pnas.1010554107 (2010).
175 Hu, S. Q. *et al.* Autophagy regulates exosome secretion in rat nucleus pulposus cells via the RhoC/ROCK2 pathway. *Exp Cell Res* **395**, 112239, doi:10.1016/j.yexcr.2020.112239 (2020).
176 Baietti, M. F. *et al.* Syndecan-syntenin-ALIX regulates the biogenesis of exosomes. *Nat Cell Biol* **14**, 677-685, doi:10.1038/ncb2502 (2012).
177 Leidal, A. M. & Debnath, J. Emerging roles for the autophagy machinery in extracellular vesicle biogenesis and secretion. *FASEB Bioadv* **3**, 377-386, doi:10.1096/fba.2020-00138 (2021).
178 Heckmann, B. L. & Green, D. R. LC3-associated phagocytosis at a glance. *J Cell Sci* **132**, doi:10.1242/jcs.222984 (2019).
179 Heckmann, B. L. *et al.* LC3-Associated Endocytosis Facilitates beta-Amyloid Clearance and Mitigates Neurodegeneration in Murine Alzheimer's Disease. *Cell* **178**, 536-551 e514, doi:10.1016/j.cell.2019.05.056 (2019).
180 Mejlvang, J. *et al.* Starvation induces rapid degradation of selective autophagy receptors by endosomal microautophagy. *J Cell Biol* **217**, 3640-3655, doi:10.1083/jcb.201711002 (2018).

181 Leidal, A. M. *et al.* The LC3-conjugation machinery specifies the loading of RNA-binding proteins into extracellular vesicles. *Nat Cell Biol* **22**, 187-199, doi:10.1038/s41556-019-0450-y (2020).
182 Martell, J. D. *et al.* A split horseradish peroxidase for the detection of intercellular protein-protein interactions and sensitive visualization of synapses. *Nat Biotechnol* **34**, 774-780, doi:10.1038/nbt.3563 (2016).
183 Mauvezin, C. & Neufeld, T. P. Bafilomycin A1 disrupts autophagic flux by inhibiting both V-ATPase-dependent acidification and Ca-P60A/SERCA-dependent autophagosome-lysosome fusion. *Autophagy* **11**, 1437-1438, doi:10.1080/15548627.2015.1066957 (2015).
184 Papadopoulos, C. & Meyer, H. Detection and Clearance of Damaged Lysosomes by the Endo-Lysosomal Damage Response and Lysophagy. *Curr Biol* **27**, R1330-R1341, doi:10.1016/j.cub.2017.11.012 (2017).
185 Fedele, A. O. & Proud, C. G. Chloroquine and bafilomycin A mimic lysosomal storage disorders and impair mTORC1 signalling. *Biosci Rep* **40**, doi:10.1042/BSR20200905 (2020).
186 Nakashima, S. *et al.* Vacuolar H+-ATPase inhibitor induces apoptosis via lysosomal dysfunction in the human gastric cancer cell line MKN-1. *J Biochem* **134**, 359-364, doi:10.1093/jb/mvg153 (2003).
187 Cashikar, A. G. & Hanson, P. I. A cell-based assay for CD63-containing extracellular vesicles. *PLoS One* **14**, e0220007, doi:10.1371/journal.pone.0220007 (2019).
188 Oshima, M., Seki, T., Kurauchi, Y., Hisatsune, A. & Katsuki, H. Reciprocal Regulation of Chaperone-Mediated Autophagy/Microautophagy and Exosome Release. *Biol Pharm Bull* **42**, 1394-1401, doi:10.1248/bpb.b19-00316 (2019).
189 Picca, A. *et al.* Extracellular Vesicles and Damage-Associated Molecular Patterns: A Pandora's Box in Health and Disease. *Front Immunol* **11**, 601740, doi:10.3389/fimmu.2020.601740 (2020).
190 Cann, G. M. *et al.* Developmental expression of LC3alpha and beta: absence of fibronectin or autophagy phenotype in LC3beta knockout mice. *Dev Dyn* **237**, 187-195, doi:10.1002/dvdy.21392 (2008).
191 Wirth, M. *et al.* Molecular determinants regulating selective binding of autophagy adapters and receptors to ATG8 proteins. *Nat Commun* **10**, 2055, doi:10.1038/s41467-019-10059-6 (2019).
192 Liu, G. *et al.* Mechanism of adrenergic CaV1.2 stimulation revealed by proximity proteomics. *Nature* **577**, 695-700, doi:10.1038/s41586-020-1947-z (2020).
193 Li, J. *et al.* Cell-Surface Proteomic Profiling in the Fly Brain Uncovers Wiring Regulators. *Cell* **180**, 373-386 e315, doi:10.1016/j.cell.2019.12.029 (2020).
194 Uezu, A. *et al.* Identification of an elaborate complex mediating postsynaptic inhibition. *Science* **353**, 1123-1129, doi:10.1126/science.aag0821 (2016).
195 Dingar, D. *et al.* BioID identifies novel c-MYC interacting partners in cultured cells and xenograft tumors. *J Proteomics* **118**, 95-111, doi:10.1016/j.jprot.2014.09.029 (2015).
196 Simon, A. K., Hollander, G. A. & McMichael, A. Evolution of the immune system in humans from infancy to old age. *Proc Biol Sci* **282**, 20143085, doi:10.1098/rspb.2014.3085 (2015).
197 Campisi, J. & d'Adda di Fagagna, F. Cellular senescence: when bad things happen to good cells. *Nat Rev Mol Cell Biol* **8**, 729-740, doi:10.1038/nrm2233 (2007).
198 Rodier, F. & Campisi, J. Four faces of cellular senescence. *J Cell Biol* **192**, 547-556, doi:10.1083/jcb.201009094 (2011).

199 Salminen, A., Ojala, J. & Kaarniranta, K. Apoptosis and aging: increased resistance to apoptosis enhances the aging process. *Cell Mol Life Sci* **68**, 1021-1031, doi:10.1007/s00018-010-0597-y (2011).
200 Pereira, B. I. *et al.* Senescent cells evade immune clearance via HLA-E-mediated NK and CD8(+) T cell inhibition. *Nat Commun* **10**, 2387, doi:10.1038/s41467-019-10335-5 (2019).
201 Zhou, D., Borsa, M. & Simon, A. K. Hallmarks and detection techniques of cellular senescence and cellular ageing in immune cells. *Aging Cell* **20**, e13316, doi:10.1111/acel.13316 (2021).
202 d'Adda di Fagagna, F. *et al.* A DNA damage checkpoint response in telomere-initiated senescence. *Nature* **426**, 194-198, doi:10.1038/nature02118 (2003).
203 Wang, Y., Sharpless, N. & Chang, S. p16(INK4a) protects against dysfunctional telomere-induced ATR-dependent DNA damage responses. *J Clin Invest* **123**, 4489-4501, doi:10.1172/JCI69574 (2013).
204 Basisty, N. *et al.* A proteomic atlas of senescence-associated secretomes for aging biomarker development. *PLoS Biol* **18**, e3000599, doi:10.1371/journal.pbio.3000599 (2020).
205 Baker, D. J. *et al.* Clearance of p16Ink4a-positive senescent cells delays ageing-associated disorders. *Nature* **479**, 232-236, doi:10.1038/nature10600 (2011).
206 Zhu, Y. *et al.* The Achilles' heel of senescent cells: from transcriptome to senolytic drugs. *Aging Cell* **14**, 644-658, doi:10.1111/acel.12344 (2015).
207 Ayoub, N., Jeyasekharan, A. D., Bernal, J. A. & Venkitaraman, A. R. HP1-beta mobilization promotes chromatin changes that initiate the DNA damage response. *Nature* **453**, 682-686, doi:10.1038/nature06875 (2008).
208 Mah, L. J., El-Osta, A. & Karagiannis, T. C. gammaH2AX: a sensitive molecular marker of DNA damage and repair. *Leukemia* **24**, 679-686, doi:10.1038/leu.2010.6 (2010).
209 Nagelkerke, A. & Span, P. N. Staining Against Phospho-H2AX (gamma-H2AX) as a Marker for DNA Damage and Genomic Instability in Cancer Tissues and Cells. *Adv Exp Med Biol* **899**, 1-10, doi:10.1007/978-3-319-26666-4_1 (2016).
210 Dimri, G. P. *et al.* A biomarker that identifies senescent human cells in culture and in aging skin in vivo. *Proc Natl Acad Sci U S A* **92**, 9363-9367, doi:10.1073/pnas.92.20.9363 (1995).
211 Demaria, M. *et al.* An essential role for senescent cells in optimal wound healing through secretion of PDGF-AA. *Dev Cell* **31**, 722-733, doi:10.1016/j.devcel.2014.11.012 (2014).
212 Rooyackers, O. E., Adey, D. B., Ades, P. A. & Nair, K. S. Effect of age on in vivo rates of mitochondrial protein synthesis in human skeletal muscle. *Proc Natl Acad Sci U S A* **93**, 15364-15369, doi:10.1073/pnas.93.26.15364 (1996).
213 Kerr, J. S. *et al.* Mitophagy and Alzheimer's Disease: Cellular and Molecular Mechanisms. *Trends Neurosci* **40**, 151-166, doi:10.1016/j.tins.2017.01.002 (2017).
214 Schieber, M. & Chandel, N. S. ROS function in redox signaling and oxidative stress. *Curr Biol* **24**, R453-462, doi:10.1016/j.cub.2014.03.034 (2014).
215 Koltover, V. K. Free Radical Timer of Aging: from Chemistry of Free Radicals to Systems Theory of Reliability. *Curr Aging Sci* **10**, 12-17, doi:10.2174/1874609809666161009220822 (2017).
216 Nie, B. *et al.* Age-dependent accumulation of 8-oxoguanine in the DNA and RNA in various rat tissues. *Oxid Med Cell Longev* **2013**, 303181, doi:10.1155/2013/303181 (2013).

217 Bozza, P. T., Bakker-Abreu, I., Navarro-Xavier, R. A. & Bandeira-Melo, C. Lipid body function in eicosanoid synthesis: an update. *Prostaglandins Leukot Essent Fatty Acids* **85**, 205-213, doi:10.1016/j.plefa.2011.04.020 (2011).
218 Gemmink, A., Goodpaster, B. H., Schrauwen, P. & Hesselink, M. K. C. Intramyocellular lipid droplets and insulin sensitivity, the human perspective. *Biochim Biophys Acta Mol Cell Biol Lipids* **1862**, 1242-1249, doi:10.1016/j.bbalip.2017.07.010 (2017).
219 Lopez-Otin, C., Blasco, M. A., Partridge, L., Serrano, M. & Kroemer, G. The hallmarks of aging. *Cell* **153**, 1194-1217, doi:10.1016/j.cell.2013.05.039 (2013).
220 Childs, B. G. *et al.* Senescent intimal foam cells are deleterious at all stages of atherosclerosis. *Science* **354**, 472-477, doi:10.1126/science.aaf6659 (2016).
221 Marschallinger, J. *et al.* Lipid-droplet-accumulating microglia represent a dysfunctional and proinflammatory state in the aging brain. *Nat Neurosci* **23**, 194-208, doi:10.1038/s41593-019-0566-1 (2020).
222 Hipp, M. S., Kasturi, P. & Hartl, F. U. The proteostasis network and its decline in ageing. *Nat Rev Mol Cell Biol* **20**, 421-435, doi:10.1038/s41580-019-0101-y (2019).
223 Liang, V. *et al.* Altered proteostasis in aging and heat shock response in C. elegans revealed by analysis of the global and de novo synthesized proteome. *Cell Mol Life Sci* **71**, 3339-3361, doi:10.1007/s00018-014-1558-7 (2014).
224 Kirstein-Miles, J., Scior, A., Deuerling, E. & Morimoto, R. I. The nascent polypeptide-associated complex is a key regulator of proteostasis. *EMBO J* **32**, 1451-1468, doi:10.1038/emboj.2013.87 (2013).
225 Stout, G. J. *et al.* Insulin/IGF-1-mediated longevity is marked by reduced protein metabolism. *Mol Syst Biol* **9**, 679, doi:10.1038/msb.2013.35 (2013).
226 Walther, D. M. *et al.* Widespread Proteome Remodeling and Aggregation in Aging C. elegans. *Cell* **161**, 919-932, doi:10.1016/j.cell.2015.03.032 (2015).
227 Costa-Mattioli, M. & Walter, P. The integrated stress response: From mechanism to disease. *Science* **368**, doi:10.1126/science.aat5314 (2020).
228 Zhang, H. *et al.* Polyamines Control eIF5A Hypusination, TFEB Translation, and Autophagy to Reverse B Cell Senescence. *Mol Cell* **76**, 110-125 e119, doi:10.1016/j.molcel.2019.08.005 (2019).
229 Johnson, S. C., Rabinovitch, P. S. & Kaeberlein, M. mTOR is a key modulator of ageing and age-related disease. *Nature* **493**, 338-345, doi:10.1038/nature11861 (2013).
230 van Heesch, S. *et al.* The Translational Landscape of the Human Heart. *Cell* **178**, 242-260 e229, doi:10.1016/j.cell.2019.05.010 (2019).
231 Carrard, G., Dieu, M., Raes, M., Toussaint, O. & Friguet, B. Impact of ageing on proteasome structure and function in human lymphocytes. *Int J Biochem Cell Biol* **35**, 728-739, doi:10.1016/s1357-2725(02)00356-4 (2003).
232 Chondrogianni, N., Georgila, K., Kourtis, N., Tavernarakis, N. & Gonos, E. S. 20S proteasome activation promotes life span extension and resistance to proteotoxicity in Caenorhabditis elegans. *FASEB J* **29**, 611-622, doi:10.1096/fj.14-252189 (2015).
233 Nguyen, N. N. *et al.* Proteasome beta5 subunit overexpression improves proteostasis during aging and extends lifespan in Drosophila melanogaster. *Sci Rep* **9**, 3170, doi:10.1038/s41598-019-39508-4 (2019).
234 Arensman, M. D. & Eng, C. H. Self-Digestion for Lifespan Extension: Enhanced Autophagy Delays Aging. *Mol Cell* **71**, 485-486, doi:10.1016/j.molcel.2018.08.002 (2018).

235 Simonsen, A. *et al.* Promoting basal levels of autophagy in the nervous system enhances longevity and oxidant resistance in adult Drosophila. *Autophagy* **4**, 176-184, doi:10.4161/auto.5269 (2008).
236 Hughes, A. L. & Gottschling, D. E. An early age increase in vacuolar pH limits mitochondrial function and lifespan in yeast. *Nature* **492**, 261-265, doi:10.1038/nature11654 (2012).
237 Sun, Y. *et al.* Lysosome activity is modulated by multiple longevity pathways and is important for lifespan extension in C. elegans. *Elife* **9**, doi:10.7554/eLife.55745 (2020).
238 Kaushik, S. *et al.* Loss of autophagy in hypothalamic POMC neurons impairs lipolysis. *EMBO Rep* **13**, 258-265, doi:10.1038/embor.2011.260 (2012).
239 Menzies, F. M., Fleming, A. & Rubinsztein, D. C. Compromised autophagy and neurodegenerative diseases. *Nat Rev Neurosci* **16**, 345-357, doi:10.1038/nrn3961 (2015).
240 Cheon, S. Y., Kim, H., Rubinsztein, D. C. & Lee, J. E. Autophagy, Cellular Aging and Age-related Human Diseases. *Exp Neurobiol* **28**, 643-657, doi:10.5607/en.2019.28.6.643 (2019).
241 Leidal, A. M., Levine, B. & Debnath, J. Autophagy and the cell biology of age-related disease. *Nat Cell Biol* **20**, 1338-1348, doi:10.1038/s41556-018-0235-8 (2018).
242 Alsaleh, G. *et al.* Autophagy in T cells from aged donors is maintained by spermidine and correlates with function and vaccine responses. *Elife* **9**, doi:10.7554/eLife.57950 (2020).
243 Stranks, A. J. *et al.* Autophagy Controls Acquisition of Aging Features in Macrophages. *J Innate Immun* **7**, 375-391, doi:10.1159/000370112 (2015).
244 Matecic, M. *et al.* A microarray-based genetic screen for yeast chronological aging factors. *PLoS Genet* **6**, e1000921, doi:10.1371/journal.pgen.1000921 (2010).
245 Toth, M. L. *et al.* Longevity pathways converge on autophagy genes to regulate life span in Caenorhabditis elegans. *Autophagy* **4**, 330-338, doi:10.4161/auto.5618 (2008).
246 Komatsu, M. *et al.* Loss of autophagy in the central nervous system causes neurodegeneration in mice. *Nature* **441**, 880-884, doi:10.1038/nature04723 (2006).
247 Masiero, E. & Sandri, M. Autophagy inhibition induces atrophy and myopathy in adult skeletal muscles. *Autophagy* **6**, 307-309, doi:10.4161/auto.6.2.11137 (2010).
248 de Haan, G. & Lazare, S. S. Aging of hematopoietic stem cells. *Blood* **131**, 479-487, doi:10.1182/blood-2017-06-746412 (2018).
249 Mortensen, M. *et al.* The autophagy protein Atg7 is essential for hematopoietic stem cell maintenance. *J Exp Med* **208**, 455-467, doi:10.1084/jem.20101145 (2011).
250 Pyo, J. O. *et al.* Overexpression of Atg5 in mice activates autophagy and extends lifespan. *Nat Commun* **4**, 2300, doi:10.1038/ncomms3300 (2013).
251 Ulgherait, M., Rana, A., Rera, M., Graniel, J. & Walker, D. W. AMPK modulates tissue and organismal aging in a non-cell-autonomous manner. *Cell Rep* **8**, 1767-1780, doi:10.1016/j.celrep.2014.08.006 (2014).
252 Hansen, M. *et al.* A role for autophagy in the extension of lifespan by dietary restriction in C. elegans. *PLoS Genet* **4**, e24, doi:10.1371/journal.pgen.0040024 (2008).
253 Melendez, A. *et al.* Autophagy genes are essential for dauer development and life-span extension in C. elegans. *Science* **301**, 1387-1391, doi:10.1126/science.1087782 (2003).
254 Jia, K. & Levine, B. Autophagy is required for dietary restriction-mediated life span extension in C. elegans. *Autophagy* **3**, 597-599, doi:10.4161/auto.4989 (2007).

255 Hars, E. S. *et al.* Autophagy regulates ageing in C. elegans. *Autophagy* **3**, 93-95, doi:10.4161/auto.3636 (2007).
256 Lapierre, L. R. *et al.* The TFEB orthologue HLH-30 regulates autophagy and modulates longevity in Caenorhabditis elegans. *Nat Commun* **4**, 2267, doi:10.1038/ncomms3267 (2013).
257 Harrison, D. E. *et al.* Rapamycin fed late in life extends lifespan in genetically heterogeneous mice. *Nature* **460**, 392-395, doi:10.1038/nature08221 (2009).
258 Wilkinson, J. E. *et al.* Rapamycin slows aging in mice. *Aging Cell* **11**, 675-682, doi:10.1111/j.1474-9726.2012.00832.x (2012).
259 Eisenberg, T. *et al.* Induction of autophagy by spermidine promotes longevity. *Nat Cell Biol* **11**, 1305-1314, doi:10.1038/ncb1975 (2009).
260 Huang, R. *et al.* Deacetylation of nuclear LC3 drives autophagy initiation under starvation. *Mol Cell* **57**, 456-466, doi:10.1016/j.molcel.2014.12.013 (2015).
261 Lee, I. H. *et al.* A role for the NAD-dependent deacetylase Sirt1 in the regulation of autophagy. *Proc Natl Acad Sci U S A* **105**, 3374-3379, doi:10.1073/pnas.0712145105 (2008).
262 Fang, E. F. *et al.* NAD(+) augmentation restores mitophagy and limits accelerated aging in Werner syndrome. *Nat Commun* **10**, 5284, doi:10.1038/s41467-019-13172-8 (2019).
263 Mouchiroud, L. *et al.* The NAD(+)/Sirtuin Pathway Modulates Longevity through Activation of Mitochondrial UPR and FOXO Signaling. *Cell* **154**, 430-441, doi:10.1016/j.cell.2013.06.016 (2013).
264 Zhang, H. *et al.* NAD(+) repletion improves mitochondrial and stem cell function and enhances life span in mice. *Science* **352**, 1436-1443, doi:10.1126/science.aaf2693 (2016).
265 Mitchell, S. J. *et al.* Nicotinamide Improves Aspects of Healthspan, but Not Lifespan, in Mice. *Cell Metab* **27**, 667-676 e664, doi:10.1016/j.cmet.2018.02.001 (2018).
266 Escobar, K. A., Cole, N. H., Mermier, C. M. & VanDusseldorp, T. A. Autophagy and aging: Maintaining the proteome through exercise and caloric restriction. *Aging Cell* **18**, e12876, doi:10.1111/acel.12876 (2019).
267 Ravikumar, B., Duden, R. & Rubinsztein, D. C. Aggregate-prone proteins with polyglutamine and polyalanine expansions are degraded by autophagy. *Hum Mol Genet* **11**, 1107-1117, doi:10.1093/hmg/11.9.1107 (2002).
268 Rocchi, A. *et al.* A Becn1 mutation mediates hyperactive autophagic sequestration of amyloid oligomers and improved cognition in Alzheimer's disease. *PLoS Genet* **13**, e1006962, doi:10.1371/journal.pgen.1006962 (2017).
269 Kumsta, C. *et al.* The autophagy receptor p62/SQST-1 promotes proteostasis and longevity in C. elegans by inducing autophagy. *Nat Commun* **10**, 5648, doi:10.1038/s41467-019-13540-4 (2019).
270 Aparicio, R., Rana, A. & Walker, D. W. Upregulation of the Autophagy Adaptor p62/SQSTM1 Prolongs Health and Lifespan in Middle-Aged Drosophila. *Cell Rep* **28**, 1029-1040 e1025, doi:10.1016/j.celrep.2019.06.070 (2019).
271 Demontis, F. & Perrimon, N. FOXO/4E-BP signaling in Drosophila muscles regulates organism-wide proteostasis during aging. *Cell* **143**, 813-825, doi:10.1016/j.cell.2010.10.007 (2010).
272 Duran, J., Gruart, A., Garcia-Rocha, M., Delgado-Garcia, J. M. & Guinovart, J. J. Glycogen accumulation underlies neurodegeneration and autophagy impairment in Lafora disease. *Hum Mol Genet* **23**, 3147-3156, doi:10.1093/hmg/ddu024 (2014).
273 Singh, R. *et al.* Autophagy regulates lipid metabolism. *Nature* **458**, 1131-1135, doi:10.1038/nature07976 (2009).

274 Xiao, B. *et al.* Superoxide drives progression of Parkin/PINK1-dependent mitophagy following translocation of Parkin to mitochondria. *Cell Death Dis* **8**, e3097, doi:10.1038/cddis.2017.463 (2017).
275 Riffelmacher, T., Richter, F. C. & Simon, A. K. Autophagy dictates metabolism and differentiation of inflammatory immune cells. *Autophagy* **14**, 199-206, doi:10.1080/15548627.2017.1362525 (2018).
276 Swanson, K. V., Deng, M. & Ting, J. P. The NLRP3 inflammasome: molecular activation and regulation to therapeutics. *Nat Rev Immunol* **19**, 477-489, doi:10.1038/s41577-019-0165-0 (2019).
277 Goronzy, J. J., Fang, F., Cavanagh, M. M., Qi, Q. & Weyand, C. M. Naive T cell maintenance and function in human aging. *J Immunol* **194**, 4073-4080, doi:10.4049/jimmunol.1500046 (2015).
278 Quinn, K. M. *et al.* Age-Related Decline in Primary CD8(+) T Cell Responses Is Associated with the Development of Senescence in Virtual Memory CD8(+) T Cells. *Cell Rep* **23**, 3512-3524, doi:10.1016/j.celrep.2018.05.057 (2018).
279 Miller, C. H. *et al.* Eomes identifies thymic precursors of self-specific memory-phenotype CD8(+) T cells. *Nat Immunol* **21**, 567-577, doi:10.1038/s41590-020-0653-1 (2020).
280 Sosinowski, T. *et al.* CD8alpha+ dendritic cell trans presentation of IL-15 to naive CD8+ T cells produces antigen-inexperienced T cells in the periphery with memory phenotype and function. *J Immunol* **190**, 1936-1947, doi:10.4049/jimmunol.1203149 (2013).
281 Tripathi, P. *et al.* IL-4 and IL-15 promotion of virtual memory CD8(+) T cells is determined by genetic background. *Eur J Immunol* **46**, 2333-2339, doi:10.1002/eji.201646404 (2016).
282 Henson, S. M. *et al.* KLRG1 signaling induces defective Akt (ser473) phosphorylation and proliferative dysfunction of highly differentiated CD8+ T cells. *Blood* **113**, 6619-6628, doi:10.1182/blood-2009-01-199588 (2009).
283 Acuto, O. & Michel, F. CD28-mediated co-stimulation: a quantitative support for TCR signalling. *Nat Rev Immunol* **3**, 939-951, doi:10.1038/nri1248 (2003).
284 Goodwin, R. G. *et al.* Molecular and biological characterization of a ligand for CD27 defines a new family of cytokines with homology to tumor necrosis factor. *Cell* **73**, 447-456, doi:10.1016/0092-8674(93)90133-b (1993).
285 Plunkett, F. J. *et al.* The loss of telomerase activity in highly differentiated CD8+CD28-CD27- T cells is associated with decreased Akt (Ser473) phosphorylation. *J Immunol* **178**, 7710-7719, doi:10.4049/jimmunol.178.12.7710 (2007).
286 Voehringer, D., Koschella, M. & Pircher, H. Lack of proliferative capacity of human effector and memory T cells expressing killer cell lectinlike receptor G1 (KLRG1). *Blood* **100**, 3698-3702, doi:10.1182/blood-2002-02-0657 (2002).
287 Voehringer, D. *et al.* Viral infections induce abundant numbers of senescent CD8 T cells. *J Immunol* **167**, 4838-4843, doi:10.4049/jimmunol.167.9.4838 (2001).
288 Tessmer, M. S. *et al.* KLRG1 binds cadherins and preferentially associates with SHIP-1. *Int Immunol* **19**, 391-400, doi:10.1093/intimm/dxm004 (2007).
289 Haynes, L., Linton, P. J. & Swain, S. L. Age-related changes in CD4 T cells of T cell receptor transgenic mice. *Mech Ageing Dev* **93**, 95-105, doi:10.1016/s0047-6374(96)01826-x (1997).
290 Stephenson, L. M. *et al.* Identification of Atg5-dependent transcriptional changes and increases in mitochondrial mass in Atg5-deficient T lymphocytes. *Autophagy* **5**, 625-635, doi:10.4161/auto.5.5.8133 (2009).

291 Liu, J. Y. *et al.* Cells exhibiting strong p16 (INK4a) promoter activation in vivo display features of senescence. *Proc Natl Acad Sci U S A* **116**, 2603-2611, doi:10.1073/pnas.1818313116 (2019).
292 Lee, P. P. *et al.* A critical role for Dnmt1 and DNA methylation in T cell development, function, and survival. *Immunity* **15**, 763-774, doi:10.1016/s1074-7613(01)00227-8 (2001).
293 Strutt, T. M., McKinstry, K. K., Kuang, Y., Bradley, L. M. & Swain, S. L. Memory CD4+ T-cell-mediated protection depends on secondary effectors that are distinct from and superior to primary effectors. *Proc Natl Acad Sci U S A* **109**, E2551-2560, doi:10.1073/pnas.1205894109 (2012).
294 Barnden, M. J., Allison, J., Heath, W. R. & Carbone, F. R. Defective TCR expression in transgenic mice constructed using cDNA-based alpha- and beta-chain genes under the control of heterologous regulatory elements. *Immunol Cell Biol* **76**, 34-40, doi:10.1046/j.1440-1711.1998.00709.x (1998).
295 Bhattacharyya, N. D. & Feng, C. G. Regulation of T Helper Cell Fate by TCR Signal Strength. *Front Immunol* **11**, 624, doi:10.3389/fimmu.2020.00624 (2020).
296 Feil, R., Wagner, J., Metzger, D. & Chambon, P. Regulation of Cre recombinase activity by mutated estrogen receptor ligand-binding domains. *Biochem Biophys Res Commun* **237**, 752-757, doi:10.1006/bbrc.1997.7124 (1997).
297 Ruzankina, Y. *et al.* Deletion of the developmentally essential gene ATR in adult mice leads to age-related phenotypes and stem cell loss. *Cell Stem Cell* **1**, 113-126, doi:10.1016/j.stem.2007.03.002 (2007).
298 Li, M. *et al.* Age related human T cell subset evolution and senescence. *Immun Ageing* **16**, 24, doi:10.1186/s12979-019-0165-8 (2019).
299 Covre, L. P., De Maeyer, R. P. H., Gomes, D. C. O. & Akbar, A. N. The role of senescent T cells in immunopathology. *Aging Cell* **19**, e13272, doi:10.1111/acel.13272 (2020).
300 Kovaiou, R. D. *et al.* Age-related differences in phenotype and function of CD4+ T cells are due to a phenotypic shift from naive to memory effector CD4+ T cells. *Int Immunol* **17**, 1359-1366, doi:10.1093/intimm/dxh314 (2005).
301 Homann, D., Teyton, L. & Oldstone, M. B. Differential regulation of antiviral T-cell immunity results in stable CD8+ but declining CD4+ T-cell memory. *Nat Med* **7**, 913-919, doi:10.1038/90950 (2001).
302 Henson, S. M. & Akbar, A. N. KLRG1--more than a marker for T cell senescence. *Age (Dordr)* **31**, 285-291, doi:10.1007/s11357-009-9100-9 (2009).
303 Zhang, H. & Simon, A. K. Polyamines reverse immune senescence via the translational control of autophagy. *Autophagy* **16**, 181-182, doi:10.1080/15548627.2019.1687967 (2020).
304 Pieren, D. K. J., Smits, N. A. M., van de Garde, M. D. B. & Guichelaar, T. Response kinetics reveal novel features of ageing in murine T cells. *Sci Rep* **9**, 5587, doi:10.1038/s41598-019-42120-1 (2019).
305 Ron-Harel, N. *et al.* Defective respiration and one-carbon metabolism contribute to impaired naive T cell activation in aged mice. *Proc Natl Acad Sci U S A* **115**, 13347-13352, doi:10.1073/pnas.1804149115 (2018).
306 Debacq-Chainiaux, F., Erusalimsky, J. D., Campisi, J. & Toussaint, O. Protocols to detect senescence-associated beta-galactosidase (SA-betagal) activity, a biomarker of senescent cells in culture and in vivo. *Nat Protoc* **4**, 1798-1806, doi:10.1038/nprot.2009.191 (2009).
307 Jewell, J. L., Russell, R. C. & Guan, K. L. Amino acid signalling upstream of mTOR. *Nat Rev Mol Cell Biol* **14**, 133-139, doi:10.1038/nrm3522 (2013).

308 Kimball, S. R., Vary, T. C. & Jefferson, L. S. Age-dependent decrease in the amount of eukaryotic initiation factor 2 in various rat tissues. *Biochem J* **286 (Pt 1)**, 263-268, doi:10.1042/bj2860263 (1992).
309 Ward, W. & Richardson, A. Effect of age on liver protein synthesis and degradation. *Hepatology* **14**, 935-948, doi:10.1002/hep.1840140529 (1991).
310 Olzmann, J. A. & Carvalho, P. Dynamics and functions of lipid droplets. *Nat Rev Mol Cell Biol* **20**, 137-155, doi:10.1038/s41580-018-0085-z (2019).
311 Zechner, R., Madeo, F. & Kratky, D. Cytosolic lipolysis and lipophagy: two sides of the same coin. *Nat Rev Mol Cell Biol* **18**, 671-684, doi:10.1038/nrm.2017.76 (2017).
312 McLeod, I. X., Zhou, X., Li, Q. J., Wang, F. & He, Y. W. The class III kinase Vps34 promotes T lymphocyte survival through regulating IL-7Ralpha surface expression. *J Immunol* **187**, 5051-5061, doi:10.4049/jimmunol.1100710 (2011).
313 Fulop, T. *et al.* Cellular signaling in the aging immune system. *Curr Opin Immunol* **29**, 105-111, doi:10.1016/j.coi.2014.05.007 (2014).
314 Li, G. *et al.* Decline in miR-181a expression with age impairs T cell receptor sensitivity by increasing DUSP6 activity. *Nat Med* **18**, 1518-1524, doi:10.1038/nm.2963 (2012).
315 Stefanova, I. *et al.* TCR ligand discrimination is enforced by competing ERK positive and SHP-1 negative feedback pathways. *Nat Immunol* **4**, 248-254, doi:10.1038/ni895 (2003).
316 Luo, Y., Xu, W., Li, G. & Cui, W. Weighing In on mTOR Complex 2 Signaling: The Expanding Role in Cell Metabolism. *Oxid Med Cell Longev* **2018**, 7838647, doi:10.1155/2018/7838647 (2018).
317 Almeida, L., Lochner, M., Berod, L. & Sparwasser, T. Metabolic pathways in T cell activation and lineage differentiation. *Semin Immunol* **28**, 514-524, doi:10.1016/j.smim.2016.10.009 (2016).
318 Remmerie, A. & Scott, C. L. Macrophages and lipid metabolism. *Cell Immunol* **330**, 27-42, doi:10.1016/j.cellimm.2018.01.020 (2018).
319 Martinez-Lopez, N. *et al.* Autophagy in the CNS and Periphery Coordinate Lipophagy and Lipolysis in the Brown Adipose Tissue and Liver. *Cell Metab* **23**, 113-127, doi:10.1016/j.cmet.2015.10.008 (2016).
320 Kaushik, S. & Cuervo, A. M. Degradation of lipid droplet-associated proteins by chaperone-mediated autophagy facilitates lipolysis. *Nat Cell Biol* **17**, 759-770, doi:10.1038/ncb3166 (2015).
321 Oeckinghaus, A. & Ghosh, S. The NF-kappaB family of transcription factors and its regulation. *Cold Spring Harb Perspect Biol* **1**, a000034, doi:10.1101/cshperspect.a000034 (2009).
322 Moorthy, A. K., Huang, D. B., Wang, V. Y., Vu, D. & Ghosh, G. X-ray structure of a NF-kappaB p50/RelB/DNA complex reveals assembly of multiple dimers on tandem kappaB sites. *J Mol Biol* **373**, 723-734, doi:10.1016/j.jmb.2007.08.039 (2007).
323 Lawrence, T. The nuclear factor NF-kappaB pathway in inflammation. *Cold Spring Harb Perspect Biol* **1**, a001651, doi:10.1101/cshperspect.a001651 (2009).
324 Zhang, Q., Lenardo, M. J. & Baltimore, D. 30 Years of NF-kappaB: A Blossoming of Relevance to Human Pathobiology. *Cell* **168**, 37-57, doi:10.1016/j.cell.2016.12.012 (2017).
325 Christian, F., Smith, E. L. & Carmody, R. J. The Regulation of NF-kappaB Subunits by Phosphorylation. *Cells* **5**, doi:10.3390/cells5010012 (2016).
326 Wang, D. & Baldwin, A. S., Jr. Activation of nuclear factor-kappaB-dependent transcription by tumor necrosis factor-alpha is mediated through phosphorylation of

RelA/p65 on serine 529. *J Biol Chem* **273**, 29411-29416, doi:10.1074/jbc.273.45.29411 (1998).
327 Wang, D., Westerheide, S. D., Hanson, J. L. & Baldwin, A. S., Jr. Tumor necrosis factor alpha-induced phosphorylation of RelA/p65 on Ser529 is controlled by casein kinase II. *J Biol Chem* **275**, 32592-32597, doi:10.1074/jbc.M001358200 (2000).
328 Charpentier, J. C. *et al.* Macropinocytosis drives T cell growth by sustaining the activation of mTORC1. *Nat Commun* **11**, 180, doi:10.1038/s41467-019-13997-3 (2020).
329 Gan, P., Gao, Z., Zhao, X. & Qi, G. Surfactin inducing mitochondria-dependent ROS to activate MAPKs, NF-kappaB and inflammasomes in macrophages for adjuvant activity. *Sci Rep* **6**, 39303, doi:10.1038/srep39303 (2016).
330 Silva, A., Cornish, G., Ley, S. C. & Seddon, B. NF-kappaB signaling mediates homeostatic maturation of new T cells. *Proc Natl Acad Sci U S A* **111**, E846-855, doi:10.1073/pnas.1319397111 (2014).
331 Rao, S., Gerondakis, S., Woltring, D. & Shannon, M. F. c-Rel is required for chromatin remodeling across the IL-2 gene promoter. *J Immunol* **170**, 3724-3731, doi:10.4049/jimmunol.170.7.3724 (2003).
332 Schmitz, M. L. & Krappmann, D. Controlling NF-kappaB activation in T cells by costimulatory receptors. *Cell Death Differ* **13**, 834-842, doi:10.1038/sj.cdd.4401845 (2006).
333 Saibil, S. D. *et al.* CD4+ and CD8+ T cell survival is regulated differentially by protein kinase Ctheta, c-Rel, and protein kinase B. *J Immunol* **178**, 2932-2939, doi:10.4049/jimmunol.178.5.2932 (2007).
334 Liu, T., Zhang, L., Joo, D. & Sun, S. C. NF-kappaB signaling in inflammation. *Signal Transduct Target Ther* **2**, doi:10.1038/sigtrans.2017.23 (2017).
335 Knudson, K. M. *et al.* NFkappaB-Pim-1-Eomesodermin axis is critical for maintaining CD8 T-cell memory quality. *Proc Natl Acad Sci U S A* **114**, E1659-E1667, doi:10.1073/pnas.1608448114 (2017).
336 Helenius, M., Hanninen, M., Lehtinen, S. K. & Salminen, A. Changes associated with aging and replicative senescence in the regulation of transcription factor nuclear factor-kappa B. *Biochem J* **318 (Pt 2)**, 603-608, doi:10.1042/bj3180603 (1996).
337 Korhonen, P., Helenius, M. & Salminen, A. Age-related changes in the regulation of transcription factor NF-kappa B in rat brain. *Neurosci Lett* **225**, 61-64, doi:10.1016/s0304-3940(97)00190-0 (1997).
338 Bregegere, F., Milner, Y. & Friguet, B. The ubiquitin-proteasome system at the crossroads of stress-response and ageing pathways: a handle for skin care? *Ageing Res Rev* **5**, 60-90, doi:10.1016/j.arr.2005.09.002 (2006).
339 Bernard, D. *et al.* Involvement of Rel/nuclear factor-kappaB transcription factors in keratinocyte senescence. *Cancer Res* **64**, 472-481, doi:10.1158/0008-5472.can-03-0005 (2004).
340 Bektas, A. *et al.* Age-associated changes in basal NF-kappaB function in human CD4+ T lymphocytes via dysregulation of PI3 kinase. *Aging (Albany NY)* **6**, 957-974, doi:10.18632/aging.100705 (2014).
341 Hara, T. *et al.* Identification of IL-7-producing cells in primary and secondary lymphoid organs using IL-7-GFP knock-in mice. *J Immunol* **189**, 1577-1584, doi:10.4049/jimmunol.1200586 (2012).
342 Lin, J. X. & Leonard, W. J. The Common Cytokine Receptor gamma Chain Family of Cytokines. *Cold Spring Harb Perspect Biol* **10**, doi:10.1101/cshperspect.a028449 (2018).

343 Kabata, H. *et al.* Targeted deletion of the TSLP receptor reveals cellular mechanisms that promote type 2 airway inflammation. *Mucosal Immunol* **13**, 626-636, doi:10.1038/s41385-020-0266-x (2020).
344 Sharfe, N., Dadi, H. K. & Roifman, C. M. JAK3 protein tyrosine kinase mediates interleukin-7-induced activation of phosphatidylinositol-3' kinase. *Blood* **86**, 2077-2085 (1995).
345 Suzuki, K. *et al.* Janus kinase 3 (Jak3) is essential for common cytokine receptor gamma chain (gamma(c))-dependent signaling: comparative analysis of gamma(c), Jak3, and gamma(c) and Jak3 double-deficient mice. *Int Immunol* **12**, 123-132, doi:10.1093/intimm/12.2.123 (2000).
346 Hennighausen, L. & Robinson, G. W. Interpretation of cytokine signaling through the transcription factors STAT5A and STAT5B. *Genes Dev* **22**, 711-721, doi:10.1101/gad.1643908 (2008).
347 Venkitaraman, A. R. & Cowling, R. J. Interleukin-7 induces the association of phosphatidylinositol 3-kinase with the alpha chain of the interleukin-7 receptor. *Eur J Immunol* **24**, 2168-2174, doi:10.1002/eji.1830240935 (1994).
348 Crawley, J. B. *et al.* T cell proliferation in response to interleukins 2 and 7 requires p38MAP kinase activation. *J Biol Chem* **272**, 15023-15027, doi:10.1074/jbc.272.23.15023 (1997).
349 Barata, J. T., Cardoso, A. A. & Boussiotis, V. A. Interleukin-7 in T-cell acute lymphoblastic leukemia: an extrinsic factor supporting leukemogenesis? *Leuk Lymphoma* **46**, 483-495, doi:10.1080/10428190400027852 (2005).
350 Cui, G. *et al.* IL-7R-Dependent Phosphatidylinositol 3-Kinase Competes with the STAT5 Signal to Modulate T Cell Development and Homeostasis. *J Immunol* **204**, 844-857, doi:10.4049/jimmunol.1900456 (2020).
351 Grenningloh, R. *et al.* Ets-1 maintains IL-7 receptor expression in peripheral T cells. *J Immunol* **186**, 969-976, doi:10.4049/jimmunol.1002099 (2011).
352 Kerdiles, Y. M. *et al.* Foxo1 links homing and survival of naive T cells by regulating L-selectin, CCR7 and interleukin 7 receptor. *Nat Immunol* **10**, 176-184, doi:10.1038/ni.1689 (2009).
353 Park, J. H. *et al.* 'Coreceptor tuning': cytokine signals transcriptionally tailor CD8 coreceptor expression to the self-specificity of the TCR. *Nat Immunol* **8**, 1049-1059, doi:10.1038/ni1512 (2007).
354 Park, J. H. *et al.* Suppression of IL7Ralpha transcription by IL-7 and other prosurvival cytokines: a novel mechanism for maximizing IL-7-dependent T cell survival. *Immunity* **21**, 289-302, doi:10.1016/j.immuni.2004.07.016 (2004).
355 Chandele, A. *et al.* Formation of IL-7Ralphahigh and IL-7Ralphalow CD8 T cells during infection is regulated by the opposing functions of GABPalpha and Gfi-1. *J Immunol* **180**, 5309-5319, doi:10.4049/jimmunol.180.8.5309 (2008).
356 Henriques, C. M., Rino, J., Nibbs, R. J., Graham, G. J. & Barata, J. T. IL-7 induces rapid clathrin-mediated internalization and JAK3-dependent degradation of IL-7Ralpha in T cells. *Blood* **115**, 3269-3277, doi:10.1182/blood-2009-10-246876 (2010).
357 Faller, E. M., Ghazawi, F. M., Cavar, M. & MacPherson, P. A. IL-7 induces clathrin-mediated endocytosis of CD127 and subsequent degradation by the proteasome in primary human CD8 T cells. *Immunol Cell Biol* **94**, 196-207, doi:10.1038/icb.2015.80 (2016).
358 Faller, E. M., Sugden, S. M., McVey, M. J., Kakal, J. A. & MacPherson, P. A. Soluble HIV Tat protein removes the IL-7 receptor alpha-chain from the surface of

resting CD8 T cells and targets it for degradation. *J Immunol* **185**, 2854-2866, doi:10.4049/jimmunol.0902207 (2010).
359 Peschon, J. J. *et al.* Early lymphocyte expansion is severely impaired in interleukin 7 receptor-deficient mice. *J Exp Med* **180**, 1955-1960, doi:10.1084/jem.180.5.1955 (1994).
360 von Freeden-Jeffry, U. *et al.* Lymphopenia in interleukin (IL)-7 gene-deleted mice identifies IL-7 as a nonredundant cytokine. *J Exp Med* **181**, 1519-1526, doi:10.1084/jem.181.4.1519 (1995).
361 Osborne, L. C. *et al.* Impaired CD8 T cell memory and CD4 T cell primary responses in IL-7R alpha mutant mice. *J Exp Med* **204**, 619-631, doi:10.1084/jem.20061871 (2007).
362 Kondo, M., Weissman, I. L. & Akashi, K. Identification of clonogenic common lymphoid progenitors in mouse bone marrow. *Cell* **91**, 661-672, doi:10.1016/s0092-8674(00)80453-5 (1997).
363 Clark, M. R., Mandal, M., Ochiai, K. & Singh, H. Orchestrating B cell lymphopoiesis through interplay of IL-7 receptor and pre-B cell receptor signalling. *Nat Rev Immunol* **14**, 69-80, doi:10.1038/nri3570 (2014).
364 Diefenbach, A., Colonna, M. & Koyasu, S. Development, differentiation, and diversity of innate lymphoid cells. *Immunity* **41**, 354-365, doi:10.1016/j.immuni.2014.09.005 (2014).
365 Vonarbourg, C. & Diefenbach, A. Multifaceted roles of interleukin-7 signaling for the development and function of innate lymphoid cells. *Semin Immunol* **24**, 165-174, doi:10.1016/j.smim.2012.03.002 (2012).
366 Boudil, A. *et al.* IL-7 coordinates proliferation, differentiation and Tcra recombination during thymocyte beta-selection. *Nat Immunol* **16**, 397-405, doi:10.1038/ni.3122 (2015).
367 Yuan, J. S., Kousis, P. C., Suliman, S., Visan, I. & Guidos, C. J. Functions of notch signaling in the immune system: consensus and controversies. *Annu Rev Immunol* **28**, 343-365, doi:10.1146/annurev.immunol.021908.132719 (2010).
368 Shitara, S. *et al.* IL-7 produced by thymic epithelial cells plays a major role in the development of thymocytes and TCRgammadelta+ intraepithelial lymphocytes. *J Immunol* **190**, 6173-6179, doi:10.4049/jimmunol.1202573 (2013).
369 Yu, Q. *et al.* Cytokine signal transduction is suppressed in preselection double-positive thymocytes and restored by positive selection. *J Exp Med* **203**, 165-175, doi:10.1084/jem.20051836 (2006).
370 Sinclair, C., Saini, M., Schim van der Loeff, I., Sakaguchi, S. & Seddon, B. The long-term survival potential of mature T lymphocytes is programmed during development in the thymus. *Sci Signal* **4**, ra77, doi:10.1126/scisignal.2002246 (2011).
371 Rathmell, J. C., Farkash, E. A., Gao, W. & Thompson, C. B. IL-7 enhances the survival and maintains the size of naive T cells. *J Immunol* **167**, 6869-6876, doi:10.4049/jimmunol.167.12.6869 (2001).
372 Cieri, N. *et al.* IL-7 and IL-15 instruct the generation of human memory stem T cells from naive precursors. *Blood* **121**, 573-584, doi:10.1182/blood-2012-05-431718 (2013).
373 Jacobs, S. R., Michalek, R. D. & Rathmell, J. C. IL-7 is essential for homeostatic control of T cell metabolism in vivo. *J Immunol* **184**, 3461-3469, doi:10.4049/jimmunol.0902593 (2010).
374 Lawson, B. R. *et al.* Interleukin-7 is required for CD4(+) T cell activation and autoimmune neuroinflammation. *Clin Immunol* **161**, 260-269, doi:10.1016/j.clim.2015.08.007 (2015).

375 Xue, H. H. *et al.* IL-2 negatively regulates IL-7 receptor alpha chain expression in activated T lymphocytes. *Proc Natl Acad Sci U S A* **99**, 13759-13764, doi:10.1073/pnas.212214999 (2002).
376 Alves, N. L., van Leeuwen, E. M., Derks, I. A. & van Lier, R. A. Differential regulation of human IL-7 receptor alpha expression by IL-7 and TCR signaling. *J Immunol* **180**, 5201-5210, doi:10.4049/jimmunol.180.8.5201 (2008).
377 Kaech, S. M. *et al.* Selective expression of the interleukin 7 receptor identifies effector CD8 T cells that give rise to long-lived memory cells. *Nat Immunol* **4**, 1191-1198, doi:10.1038/ni1009 (2003).
378 Oliveira, M. L., Akkapeddi, P., Ribeiro, D., Melao, A. & Barata, J. T. IL-7R-mediated signaling in T-cell acute lymphoblastic leukemia: An update. *Adv Biol Regul* **71**, 88-96, doi:10.1016/j.jbior.2018.09.012 (2019).
379 Alsadeq, A. *et al.* IL7R is associated with CNS infiltration and relapse in pediatric B-cell precursor acute lymphoblastic leukemia. *Blood* **132**, 1614-1617, doi:10.1182/blood-2018-04-844209 (2018).
380 Lee, L. F. *et al.* Anti-IL-7 receptor-alpha reverses established type 1 diabetes in nonobese diabetic mice by modulating effector T-cell function. *Proc Natl Acad Sci U S A* **109**, 12674-12679, doi:10.1073/pnas.1203795109 (2012).
381 Churchman, S. M. & Ponchel, F. Interleukin-7 in rheumatoid arthritis. *Rheumatology (Oxford)* **47**, 753-759, doi:10.1093/rheumatology/ken053 (2008).
382 Krzystek-Korpacka, M. *et al.* Elevated systemic interleukin-7 in patients with colorectal cancer and individuals at high risk of cancer: association with lymph node involvement and tumor location in the right colon. *Cancer Immunol Immunother* **66**, 171-179, doi:10.1007/s00262-016-1933-3 (2017).
383 Belarif, L. *et al.* IL-7 receptor influences anti-TNF responsiveness and T cell gut homing in inflammatory bowel disease. *J Clin Invest* **129**, 1910-1925, doi:10.1172/JCI121668 (2019).
384 Sortino, O. *et al.* IL-7 treatment supports CD8+ mucosa-associated invariant T-cell restoration in HIV-1-infected patients on antiretroviral therapy. *AIDS* **32**, 825-828, doi:10.1097/QAD.0000000000001760 (2018).
385 Sheikh, V. *et al.* Administration of interleukin-7 increases CD4 T cells in idiopathic CD4 lymphocytopenia. *Blood* **127**, 977-988, doi:10.1182/blood-2015-05-645077 (2016).
386 Harel, A. *et al.* Successful treatment of progressive multifocal leukoencephalopathy with recombinant interleukin-7 and maraviroc in a patient with idiopathic CD4 lymphocytopenia. *J Neurovirol* **24**, 652-655, doi:10.1007/s13365-018-0657-x (2018).
387 Thampy, L. K. *et al.* Restoration of T Cell function in multi-drug resistant bacterial sepsis after interleukin-7, anti-PD-L1, and OX-40 administration. *PLoS One* **13**, e0199497, doi:10.1371/journal.pone.0199497 (2018).
388 Kim, H. R., Hong, M. S., Dan, J. M. & Kang, I. Altered IL-7Ralpha expression with aging and the potential implications of IL-7 therapy on CD8+ T-cell immune responses. *Blood* **107**, 2855-2862, doi:10.1182/blood-2005-09-3560 (2006).
389 Passtoors, W. M. *et al.* IL7R gene expression network associates with human healthy ageing. *Immun Ageing* **12**, 21, doi:10.1186/s12979-015-0048-6 (2015).
390 Okoye, A. A. *et al.* Effect of IL-7 Therapy on Naive and Memory T Cell Homeostasis in Aged Rhesus Macaques. *J Immunol* **195**, 4292-4305, doi:10.4049/jimmunol.1500609 (2015).
391 Finkbeiner, E., Haindl, M., Raman, N. & Muller, S. SUMO routes ribosome maturation. *Nucleus* **2**, 527-532, doi:10.4161/nucl.2.6.17604 (2011).

392 Walther, Z. & Hall, J. L. The uni chromosome of Chlamydomonas: histone genes and nucleosome structure. *Nucleic Acids Res* **23**, 3756-3763, doi:10.1093/nar/23.18.3756 (1995).
393 Melo, S. A. *et al.* Glypican-1 identifies cancer exosomes and detects early pancreatic cancer. *Nature* **523**, 177-182, doi:10.1038/nature14581 (2015).
394 Olga, K., Yulia, B. & Vassilios, P. The Functions of Mitochondrial 2',3'-Cyclic Nucleotide-3'-Phosphodiesterase and Prospects for Its Future. *Int J Mol Sci* **21**, doi:10.3390/ijms21093217 (2020).
395 Wang, Z. *et al.* SIRT3-mediated deacetylation of PRDX3 alleviates mitochondrial oxidative damage and apoptosis induced by intestinal ischemia/reperfusion injury. *Redox Biol* **28**, 101343, doi:10.1016/j.redox.2019.101343 (2020).
396 Kalvari, I. *et al.* iLIR: A web resource for prediction of Atg8-family interacting proteins. *Autophagy* **10**, 913-925, doi:10.4161/auto.28260 (2014).
397 Zhang, Y. B. *et al.* Protein aggregation during overexpression limited by peptide extensions with large net negative charge. *Protein Expr Purif* **36**, 207-216, doi:10.1016/j.pep.2004.04.020 (2004).
398 Bertocci, B. *et al.* Klhl6 Deficiency Impairs Transitional B Cell Survival and Differentiation. *J Immunol* **199**, 2408-2420, doi:10.4049/jimmunol.1700708 (2017).
399 Singh, M. *et al.* Lymphoma Driver Mutations in the Pathogenic Evolution of an Iconic Human Autoantibody. *Cell* **180**, 878-894 e819, doi:10.1016/j.cell.2020.01.029 (2020).
400 Huber, L. A. *et al.* Rab8, a small GTPase involved in vesicular traffic between the TGN and the basolateral plasma membrane. *J Cell Biol* **123**, 35-45, doi:10.1083/jcb.123.1.35 (1993).
401 Pridans, C. *et al.* Identification of Pax5 target genes in early B cell differentiation. *J Immunol* **180**, 1719-1728, doi:10.4049/jimmunol.180.3.1719 (2008).
402 Jia, W., Yao, Z., Zhao, J., Guan, Q. & Gao, L. New perspectives of physiological and pathological functions of nucleolin (NCL). *Life Sci* **186**, 1-10, doi:10.1016/j.lfs.2017.07.025 (2017).
403 Wang, C. W. & Lee, S. C. The ubiquitin-like (UBX)-domain-containing protein Ubx2/Ubxd8 regulates lipid droplet homeostasis. *J Cell Sci* **125**, 2930-2939, doi:10.1242/jcs.100230 (2012).
404 Cano-Gamez, E. *et al.* Single-cell transcriptomics identifies an effectorness gradient shaping the response of CD4(+) T cells to cytokines. *Nat Commun* **11**, 1801, doi:10.1038/s41467-020-15543-y (2020).
405 Loi, M. *et al.* Macroautophagy Proteins Control MHC Class I Levels on Dendritic Cells and Shape Anti-viral CD8(+) T Cell Responses. *Cell Rep* **15**, 1076-1087, doi:10.1016/j.celrep.2016.04.002 (2016).
406 Kimura, M. Y. *et al.* IL-7 signaling must be intermittent, not continuous, during CD8(+) T cell homeostasis to promote cell survival instead of cell death. *Nat Immunol* **14**, 143-151, doi:10.1038/ni.2494 (2013).
407 Waickman, A. T. *et al.* The Cytokine Receptor IL-7Ralpha Impairs IL-2 Receptor Signaling and Constrains the In Vitro Differentiation of Foxp3(+) Treg Cells. *iScience* **23**, 101421, doi:10.1016/j.isci.2020.101421 (2020).
408 Wuest, S. C. *et al.* A role for interleukin-2 trans-presentation in dendritic cell-mediated T cell activation in humans, as revealed by daclizumab therapy. *Nat Med* **17**, 604-609, doi:10.1038/nm.2365 (2011).
409 Mai, H. L. *et al.* IL-7 receptor blockade following T cell depletion promotes long-term allograft survival. *J Clin Invest* **124**, 1723-1733, doi:10.1172/JCI66287 (2014).

410 Dhanoa, B. S., Cogliati, T., Satish, A. G., Bruford, E. A. & Friedman, J. S. Update on the Kelch-like (KLHL) gene family. *Hum Genomics* **7**, 13, doi:10.1186/1479-7364-7-13 (2013).
411 Choi, J. *et al.* Loss of KLHL6 promotes diffuse large B-cell lymphoma growth and survival by stabilizing the mRNA decay factor roquin2. *Nat Cell Biol* **20**, 586-596, doi:10.1038/s41556-018-0084-5 (2018).
412 Genau, H. M. *et al.* CUL3-KBTBD6/KBTBD7 ubiquitin ligase cooperates with GABARAP proteins to spatially restrict TIAM1-RAC1 signaling. *Mol Cell* **57**, 995-1010, doi:10.1016/j.molcel.2014.12.040 (2015).
413 Howden, A. J. M. *et al.* Quantitative analysis of T cell proteomes and environmental sensors during T cell differentiation. *Nat Immunol* **20**, 1542-1554, doi:10.1038/s41590-019-0495-x (2019).
414 Sanchez-Wandelmer, J. & Reggiori, F. Amphisomes: out of the autophagosome shadow? *EMBO J* **32**, 3116-3118, doi:10.1038/emboj.2013.246 (2013).
415 Tooze, S. A., Abada, A. & Elazar, Z. Endocytosis and autophagy: exploitation or cooperation? *Cold Spring Harb Perspect Biol* **6**, a018358, doi:10.1101/cshperspect.a018358 (2014).
416 Silva, D. A. *et al.* De novo design of potent and selective mimics of IL-2 and IL-15. *Nature* **565**, 186-191, doi:10.1038/s41586-018-0830-7 (2019).
417 Levin, A. M. *et al.* Exploiting a natural conformational switch to engineer an interleukin-2 'superkine'. *Nature* **484**, 529-533, doi:10.1038/nature10975 (2012).
418 Yu, Q., Erman, B., Park, J. H., Feigenbaum, L. & Singer, A. IL-7 receptor signals inhibit expression of transcription factors TCF-1, LEF-1, and RORgammat: impact on thymocyte development. *J Exp Med* **200**, 797-803, doi:10.1084/jem.20032183 (2004).
419 Peng, Y. Forced expression of IL-7R promotes CD8 T cell cytotoxicity to self antigen. *PLoS One* **12**, e0188112, doi:10.1371/journal.pone.0188112 (2017).
420 Abu-Shah, E. *et al.* A tissue-like platform for studying engineered quiescent human T-cells' interactions with dendritic cells. *Elife* **8**, doi:10.7554/eLife.48221 (2019).
421 Kim, K. E. *et al.* Dynamic tracking and identification of tissue-specific secretory proteins in the circulation of live mice. *Nat Commun* **12**, 5204, doi:10.1038/s41467-021-25546-y (2021).
422 Stockhammer, A., Benz, L. S., Freund, C., Kuropka, B. & Bottanelli, F. When less is more-Endogenous tagging with TurboID increases the sensitivity of proximity labelling-based experiments. doi:10.1101/2021.11.19.469212 (2021).
423 Akutsu, M., Dikic, I. & Bremm, A. Ubiquitin chain diversity at a glance. *J Cell Sci* **129**, 875-880, doi:10.1242/jcs.183954 (2016).
424 Sakamoto, K. M. *et al.* Protacs: chimeric molecules that target proteins to the Skp1-Cullin-F box complex for ubiquitination and degradation. *Proc Natl Acad Sci U S A* **98**, 8554-8559, doi:10.1073/pnas.141230798 (2001).
425 Takahashi, D. & Arimoto, H. Selective autophagy as the basis of autophagy-based degraders. *Cell Chem Biol* **28**, 1061-1071, doi:10.1016/j.chembiol.2021.05.006 (2021).
426 Smith, B. E. *et al.* Differential PROTAC substrate specificity dictated by orientation of recruited E3 ligase. *Nat Commun* **10**, 131, doi:10.1038/s41467-018-08027-7 (2019).
427 Omori, S. *et al.* Generation of a p16 Reporter Mouse and Its Use to Characterize and Target p16(high) Cells In Vivo. *Cell Metab* **32**, 814-828 e816, doi:10.1016/j.cmet.2020.09.006 (2020).

428 Grosse, L. *et al.* Defined p16(High) Senescent Cell Types Are Indispensable for Mouse Healthspan. *Cell Metab* **32**, 87-99 e86, doi:10.1016/j.cmet.2020.05.002 (2020).
429 Sun, J. *et al.* Growth differentiation factor 11 accelerates liver senescence through the inhibition of autophagy. *Aging Cell*, e13532, doi:10.1111/acel.13532 (2021).
430 Yousefzadeh, M. J. *et al.* Tissue specificity of senescent cell accumulation during physiologic and accelerated aging of mice. *Aging Cell* **19**, e13094, doi:10.1111/acel.13094 (2020).
431 Akbar, A. N., Henson, S. M. & Lanna, A. Senescence of T Lymphocytes: Implications for Enhancing Human Immunity. *Trends Immunol* **37**, 866-876, doi:10.1016/j.it.2016.09.002 (2016).
432 Tchkonia, T., Zhu, Y., van Deursen, J., Campisi, J. & Kirkland, J. L. Cellular senescence and the senescent secretory phenotype: therapeutic opportunities. *J Clin Invest* **123**, 966-972, doi:10.1172/JCI64098 (2013).
433 Newell, E. W., Sigal, N., Bendall, S. C., Nolan, G. P. & Davis, M. M. Cytometry by time-of-flight shows combinatorial cytokine expression and virus-specific cell niches within a continuum of CD8+ T cell phenotypes. *Immunity* **36**, 142-152, doi:10.1016/j.immuni.2012.01.002 (2012).
434 Rowshani, A. T., Bemelman, F. J., van Leeuwen, E. M., van Lier, R. A. & ten Berge, I. J. Clinical and immunologic aspects of cytomegalovirus infection in solid organ transplant recipients. *Transplantation* **79**, 381-386, doi:10.1097/01.tp.0000148239.00384.f0 (2005).
435 Goronzy, J. J. & Weyand, C. M. Successful and Maladaptive T Cell Aging. *Immunity* **46**, 364-378, doi:10.1016/j.immuni.2017.03.010 (2017).
436 Laplante, M. & Sabatini, D. M. mTOR signaling in growth control and disease. *Cell* **149**, 274-293, doi:10.1016/j.cell.2012.03.017 (2012).
437 Mannick, J. B. *et al.* mTOR inhibition improves immune function in the elderly. *Sci Transl Med* **6**, 268ra179, doi:10.1126/scitranslmed.3009892 (2014).
438 Lamming, D. W., Ye, L., Sabatini, D. M. & Baur, J. A. Rapalogs and mTOR inhibitors as anti-aging therapeutics. *J Clin Invest* **123**, 980-989, doi:10.1172/JCI64099 (2013).
439 Zinecker, H. & Simon, A. K. Autophagy takes it all – Autophagy inducers target immune aging. *accepted in DMM* (2021).
440 Sengupta, U., Nilson, A. N. & Kayed, R. The Role of Amyloid-beta Oligomers in Toxicity, Propagation, and Immunotherapy. *EBioMedicine* **6**, 42-49, doi:10.1016/j.ebiom.2016.03.035 (2016).
441 Lashuel, H. A., Hartley, D., Petre, B. M., Walz, T. & Lansbury, P. T., Jr. Neurodegenerative disease: amyloid pores from pathogenic mutations. *Nature* **418**, 291, doi:10.1038/418291a (2002).
442 Anguiano, M., Nowak, R. J. & Lansbury, P. T., Jr. Protofibrillar islet amyloid polypeptide permeabilizes synthetic vesicles by a pore-like mechanism that may be relevant to type II diabetes. *Biochemistry* **41**, 11338-11343, doi:10.1021/bi020314u (2002).
443 Kim, Y. E. *et al.* Soluble Oligomers of PolyQ-Expanded Huntingtin Target a Multiplicity of Key Cellular Factors. *Mol Cell* **63**, 951-964, doi:10.1016/j.molcel.2016.07.022 (2016).
444 Ramdzan, Y. M. *et al.* Huntingtin Inclusions Trigger Cellular Quiescence, Deactivate Apoptosis, and Lead to Delayed Necrosis. *Cell Rep* **19**, 919-927, doi:10.1016/j.celrep.2017.04.029 (2017).

445 Arrasate, M., Mitra, S., Schweitzer, E. S., Segal, M. R. & Finkbeiner, S. Inclusion body formation reduces levels of mutant huntingtin and the risk of neuronal death. *Nature* **431**, 805-810, doi:10.1038/nature02998 (2004).
446 Bratic, I. & Trifunovic, A. Mitochondrial energy metabolism and ageing. *Biochim Biophys Acta* **1797**, 961-967, doi:10.1016/j.bbabio.2010.01.004 (2010).
447 Hansen, M. *et al.* Lifespan extension by conditions that inhibit translation in Caenorhabditis elegans. *Aging Cell* **6**, 95-110, doi:10.1111/j.1474-9726.2006.00267.x (2007).
448 Pan, K. Z. *et al.* Inhibition of mRNA translation extends lifespan in Caenorhabditis elegans. *Aging Cell* **6**, 111-119, doi:10.1111/j.1474-9726.2006.00266.x (2007).
449 Syntichaki, P., Troulinaki, K. & Tavernarakis, N. eIF4E function in somatic cells modulates ageing in Caenorhabditis elegans. *Nature* **445**, 922-926, doi:10.1038/nature05603 (2007).
450 Panda, P. K. *et al.* Chemical Screening Approaches Enabling Drug Discovery of Autophagy Modulators for Biomedical Applications in Human Diseases. *Front Cell Dev Biol* **7**, 38, doi:10.3389/fcell.2019.00038 (2019).
451 Merkley, S. D., Chock, C. J., Yang, X. O., Harris, J. & Castillo, E. F. Modulating T Cell Responses via Autophagy: The Intrinsic Influence Controlling the Function of Both Antigen-Presenting Cells and T Cells. *Front Immunol* **9**, 2914, doi:10.3389/fimmu.2018.02914 (2018).
452 Hampe, J. *et al.* A genome-wide association scan of nonsynonymous SNPs identifies a susceptibility variant for Crohn disease in ATG16L1. *Nat Genet* **39**, 207-211, doi:10.1038/ng1954 (2007).
453 Henckaerts, L. *et al.* Genetic variation in the autophagy gene ULK1 and risk of Crohn's disease. *Inflamm Bowel Dis* **17**, 1392-1397, doi:10.1002/ibd.21486 (2011).
454 McCarroll, S. A. *et al.* Deletion polymorphism upstream of IRGM associated with altered IRGM expression and Crohn's disease. *Nat Genet* **40**, 1107-1112, doi:10.1038/ng.215 (2008).
455 Barrett, J. C. *et al.* Genome-wide association defines more than 30 distinct susceptibility loci for Crohn's disease. *Nat Genet* **40**, 955-962, doi:10.1038/ng.175 (2008).
456 Matsuda, C. *et al.* Therapeutic effect of a new immunosuppressive agent, everolimus, on interleukin-10 gene-deficient mice with colitis. *Clin Exp Immunol* **148**, 348-359, doi:10.1111/j.1365-2249.2007.03345.x (2007).
457 Macias-Ceja, D. C. *et al.* Stimulation of autophagy prevents intestinal mucosal inflammation and ameliorates murine colitis. *Br J Pharmacol* **174**, 2501-2511, doi:10.1111/bph.13860 (2017).
458 Takahashi, D. *et al.* AUTACs: Cargo-Specific Degraders Using Selective Autophagy. *Mol Cell* **76**, 797-810 e710, doi:10.1016/j.molcel.2019.09.009 (2019).
459 Klionsky, D. J. *et al.* Autophagy in major human diseases. *EMBO J* **40**, e108863, doi:10.15252/embj.2021108863 (2021).
460 Watanabe, M. *et al.* Interleukin 7 transgenic mice develop chronic colitis with decreased interleukin 7 protein accumulation in the colonic mucosa. *J Exp Med* **187**, 389-402, doi:10.1084/jem.187.3.389 (1998).
461 Yamazaki, M. *et al.* Mucosal T cells expressing high levels of IL-7 receptor are potential targets for treatment of chronic colitis. *J Immunol* **171**, 1556-1563, doi:10.4049/jimmunol.171.3.1556 (2003).
462 Okada, E. *et al.* IL-7 exacerbates chronic colitis with expansion of memory IL-7Rhigh CD4+ mucosal T cells in mice. *Am J Physiol Gastrointest Liver Physiol* **288**, G745-754, doi:10.1152/ajpgi.00276.2004 (2005).

463 Imai, K. & Takaoka, A. Comparing antibody and small-molecule therapies for cancer. *Nat Rev Cancer* **6**, 714-727, doi:10.1038/nrc1913 (2006).
464 Lou, G. *et al.* Mitophagy and Neuroprotection. *Trends Mol Med* **26**, 8-20, doi:10.1016/j.molmed.2019.07.002 (2020).
465 Esteban-Martinez, L. *et al.* Programmed mitophagy is essential for the glycolytic switch during cell differentiation. *EMBO J* **36**, 1688-1706, doi:10.15252/embj.201695916 (2017).
466 Ron-Harel, N. *et al.* Mitochondrial Biogenesis and Proteome Remodeling Promote One-Carbon Metabolism for T Cell Activation. *Cell Metab* **24**, 104-117, doi:10.1016/j.cmet.2016.06.007 (2016).
467 Yang, G. *et al.* Autophagy-related protein PIK3C3/VPS34 controls T cell metabolism and function. *Autophagy* **17**, 1193-1204, doi:10.1080/15548627.2020.1752979 (2021).
468 Singh, R. & Cuervo, A. M. Autophagy in the cellular energetic balance. *Cell Metab* **13**, 495-504, doi:10.1016/j.cmet.2011.04.004 (2011).
469 Baird, L. & Yamamoto, M. The Molecular Mechanisms Regulating the KEAP1-NRF2 Pathway. *Mol Cell Biol* **40**, doi:10.1128/MCB.00099-20 (2020).
470 Ichimura, Y. *et al.* Phosphorylation of p62 activates the Keap1-Nrf2 pathway during selective autophagy. *Mol Cell* **51**, 618-631, doi:10.1016/j.molcel.2013.08.003 (2013).
471 Raghunath, A. *et al.* Antioxidant response elements: Discovery, classes, regulation and potential applications. *Redox Biol* **17**, 297-314, doi:10.1016/j.redox.2018.05.002 (2018).
472 Jo, C. *et al.* Nrf2 reduces levels of phosphorylated tau protein by inducing autophagy adaptor protein NDP52. *Nat Commun* **5**, 3496, doi:10.1038/ncomms4496 (2014).
473 van den Boom, J. & Meyer, H. VCP/p97-Mediated Unfolding as a Principle in Protein Homeostasis and Signaling. *Mol Cell* **69**, 182-194, doi:10.1016/j.molcel.2017.10.028 (2018).
474 Hill, S. M. *et al.* VCP/p97 regulates Beclin-1-dependent autophagy initiation. *Nat Chem Biol* **17**, 448-455, doi:10.1038/s41589-020-00726-x (2021).
475 Nowosad, A. *et al.* p27 controls Ragulator and mTOR activity in amino acid-deprived cells to regulate the autophagy-lysosomal pathway and coordinate cell cycle and cell growth. *Nat Cell Biol* **22**, 1076-1090, doi:10.1038/s41556-020-0554-4 (2020).
476 McLeod, I. X., Saxena, R., Carico, Z. & He, Y. W. Class I PI3K Provide Lipid Substrate in T Cell Autophagy Through Linked Activity of Inositol Phosphatases. *Front Cell Dev Biol* **9**, 709398, doi:10.3389/fcell.2021.709398 (2021).
477 Xu, A. *et al.* Prosurvival IL-7-Stimulated Weak Strength of mTORC1-S6K Controls T Cell Memory via Transcriptional FOXO1-TCF1-Id3 and Metabolic AMPKalpha1-ULK1-ATG7 Pathways. *J Immunol*, doi:10.4049/jimmunol.2100452 (2021).